CP3-Origins-2013-040 DNRF90, DIAS-2013-40
FERMILAB-PUB-13-484-T, FTUAM-13-28
IFIC/13-76, IFT-UAM/CSIC-13-106
MITP/13-067, YITP-13-114

Review of lattice results concerning low energy particle physics

November 1, 2013

FLAG Working Group

S. Aoki[1], Y. Aoki[2,3], C. Bernard[4], T. Blum[2,5], G. Colangelo[6], M. Della Morte[7], S. Dürr[8], A. X. El Khadra[9], H. Fukaya[1]0, R. Horsley[11], T. Kaneko[12], A. Jüttner[13], J. Laiho[⋆14], L. Lellouch[15,16], H. Leutwyler[6], V. Lubicz[17,18], E. Lunghi[19], S. Necco[6], T. Onogi[10], C. Pena[20], C. T. Sachrajda[13], S. R. Sharpe[21], J. Shigemitsu[22], S. Simula[17], R. Sommer[23], R. S. Van de Water[24], A. Vladikas[25], U. Wenger[6], H. Wittig[26]

Abstract

We review lattice results related to pion, kaon, D- and B-meson physics with the aim of making them easily accessible to the particle physics community. More specifically, we report on the determination of the light-quark masses, the form factor $f_+(0)$, arising in semileptonic $K \to \pi$ transition at zero momentum transfer, as well as the decay constant ratio f_K/f_π of decay constants and its consequences for the CKM matrix elements V_{us} and V_{ud}. Furthermore, we describe the results obtained on the lattice for some of the low-energy constants of $SU(2)_L \times SU(2)_R$ and $SU(3)_L \times SU(3)_R$ Chiral Perturbation Theory and review the determination of the B_K parameter of neutral kaon mixing. The inclusion of heavy-quark quantities significantly expands the FLAG scope with respect to the previous review. Therefore, for this review, we focus on D- and B-meson decay constants, form factors, and mixing parameters, since these are most relevant for the determination of CKM matrix elements and the global CKM unitarity-triangle fit.

[1] Yukawa Institute for Theoretical Physics, Kyoto University, Kitashirakawa Oiwakecho, Sakyo-ku, Kyoto 606-8502, Japan
[2] Kobayashi-Maskawa Institute for the Origin of Particles and the Universe (KMI), Nagoya University, Nagoya 464-8602, Japan
[3] RIKEN BNL Research Center, Brookhaven National Laboratory, Upton, NY 11973, USA
[4] Department of Physics, Washington University, Saint Louis, MO 63130, USA
[5] Physics Department, University of Connecticut, Storrs, CT 06269-3046, USA and
[6] Albert Einstein Center for Fundamental Physics, Institut für theoretische Physik, Universität Bern, Sidlerstr. 5, 3012 Switzerland
[7] CP3-Origins & Danish IAS, University of Southern Denmark, Campusvej 55, DK-5230 Odense M, Denmark and IFIC (CSIC), c/ Catedrático José Beltrán, 2. E-46980, Paterna, Spain
[8] Bergische Universität Wuppertal, Gaußstraße 20, 42119 Wuppertal, Germany and Jülich Supercomputing Center, Forschungszentrum Jülich, 52425 Jülich, Germany
[9] Department of Physics, University of Illinois, Urbana, IL 61801, USA
[10] Department of Physics, Osaka University, Toyonaka, Osaka 560-0043 Japan
[11] School of Physics, University of Edinburgh, Edinburgh EH9 3JZ, UK
[12] High Energy Accelerator Research Organization (KEK), Ibaraki 305-0801, Japan
[13] School of Physics & Astronomy, University of Southampton, SO17 1BJ, UK
[14] SUPA, Department of Physics and Astronomy, University of Glasgow, Glasgow, G12 8QQ, United Kingdom
[15] Aix-Marseille Université, CNRS, CPT, UMR 7332, 13288 Marseille, France
[16] Université de Toulon, CNRS, CPT, UMR 7332, 83957 La Garde, France
[17] Dipartimento di Matematica e Fisica, Università Roma Tre, Via della Vasca Navale 84, 00146 Rome, Italy
[18] INFN, Sezione di Roma Tre, Via della Vasca Navale 84, 00146 Rome, Italy
[19] Physics Department, Indiana University, Bloomington, IN 47405, USA
[20] Instituto de Física Teórica UAM/CSIC and Departamento de Física Teórica, Universidad Autónoma de Madrid, Cantoblanco 28049 Madrid, Spain
[21] Physics Department, University of Washington, Seattle, WA 98195-1560, USA
[22] Department of Physics, The Ohio State University, Columbus, OH 43210, USA
[23] NIC @ DESY, Platanenallee 6, 15738 Zeuthen, Germany
[24] Fermi National Accelerator Laboratory, Batavia, IL 60510, USA
[25] INFN, Sezione di Tor Vergata, c/o Dipartimento di Fisica, Università di Roma Tor Vergata, Via della Ricerca Scientifica 1, 00133 Rome, Italy
[26] PRISMA Cluster of Excellence, Institut für Kernphysik and Helmholtz Institute Mainz, University of Mainz, 55099 Mainz, Germany

[⋆] Present address: Department of Physics, Syracuse University, Syracuse, New York, USA

Contents

1 Introduction

Flavour physics provides an important opportunity for exploring the limits of the Standard Model of particle physics and for constraining possible extensions of theories that go beyond it. As the LHC explores a new energy frontier and as experiments continue to extend the precision frontier, the importance of flavour physics will grow, both in terms of searches for signatures of new physics through precision measurements and in terms of attempts to unravel the theoretical framework behind direct discoveries of new particles. A major theoretical limitation consists in the precision with which strong interaction effects can be quantified. Large-scale numerical simulations of lattice QCD allow for the computation of these effects from first principles. The scope of the Flavour Lattice Averaging Group (FLAG) is to review the current status of lattice results for a variety of physical quantities in low-energy physics. Set up in November 2007[1], it comprises experts in Lattice Field Theory and Chiral Perturbation Theory. Our aim is to provide an answer to the frequently posed question "What is currently the best lattice value for a particular quantity?", in a way which is readily accessible to non-lattice-experts. This is generally not an easy question to answer; different collaborations use different lattice actions (discretizations of QCD) with a variety of lattice spacings and volumes, and with a range of masses for the $u-$ and $d-$quarks. Not only are the systematic errors different, but also the methodology used to estimate these uncertainties varies between collaborations. In the present work we summarize the main features of each of the calculations and provide a framework for judging and combining the different results. Sometimes it is a single result which provides the "best" value; more often it is a combination of results from different collaborations. Indeed, the consistency of values obtained using different formulations adds significantly to our confidence in the results.

The first edition of the FLAG review was published in 2011 [1]. It was limited to lattice results related to pion and kaon physics: light-quark masses (u-, d- and s-flavours), the form factor $f_+(0)$ arising in semileptonic $K \to \pi$ transitions at zero momentum transfer and the decay constant ratio f_K/f_π, as well as their implications for the CKM matrix elements V_{us} and V_{ud}. Furthermore, results were reported for some of the low-energy constants of $SU(2)_L \otimes SU(2)_R$ and $SU(3)_L \otimes SU(3)_R$ Chiral Perturbation Theory and the B_K parameter of neutral kaon mixing. Results for all of these quantities have been updated in the present paper. Moreover, the scope of the present review has been extended by including lattice results related to D- and B-meson physics. We focus on B- and D-meson decay constants, form factors, and mixing parameters, which are most relevant for the determination of CKM matrix elements and the global CKM unitarity-triangle fit. Last but not least, the present status of lattice results on the QCD coupling α_s is currently also being reviewed by a working group of FLAG and will be included in the next update. Bottom- and charm-quark masses, though important parametric inputs to Standard-Model calculations, have not been covered in the present edition. They will be included in a future FLAG report.

Our plan is to continue providing FLAG updates, in the form of a peer reviewed paper, roughly on a biannual basis. This effort is supplemented by our more frequently updated website http://itpwiki.unibe.ch/flag, where figures as well as pdf-files for the individual sections can be downloaded. The papers reviewed in the present edition have appeared before the closing date 30 April 2013.

[1] The original group had been set up in the framework of a European Network on Flavour Physics (Flavianet).

Finally, we draw attention to a particularly important point. As stated above, our aim is to make lattice QCD results easily accessible to non-lattice-experts and we are well aware that it is likely that some readers will only consult the present paper and not the original lattice literature. We consider it very important that this paper is not the only one which gets cited when the lattice results which are discussed and analyzed here are quoted. Readers who find the review and compilations offered in this paper useful are therefore kindly requested to also cite the original sources. The bibliography at the end of this paper should make this task easier. Indeed we hope that the bibliography will be one of the most widely used elements of the whole paper.

This review is organized as follows. In the remainder of Sec. 1 we summarize the composition and rules of FLAG, describe the goals of the FLAG effort and general issues that arise in modern lattice calculations. For the reader's convenience, Table 1 summarizes the main results (averages and estimates) of the present review. In Sec. 2 we explain our general methodology for evaluating the robustness of lattice results which have appeared in the literature. We also describe the procedures followed for combining results from different collaborations in a single average or estimate (see Sec. 2.2 for our use of these terms). The rest of the paper consists in sections, each of which is dedicated to a single (or groups of closely connected) physical quantity(ies). Each of these sections is accompanied by an Appendix with explicatory notes.

1.1 FLAG enlargement

Upon completion of the first review, it was decided to extend the project by adding new physical quantities and co-authors. FLAG became more representative of the lattice community, both in terms of the geographical location of its members and the lattice collaborations to which they belong. At the time a parallel effort had been carried out [2, 3]; the two efforts have now merged in order to provide a single source of information on lattice results to the particle-physics community.

The experience gained in managing the activities of a medium-sized group of co-authors taught us that it was necessary to have a more formal structure and a set of rules by which all concerned had to abide, in order to make the inner workings of FLAG function smoothly. The collaboration presently consists of an Advisory Board (AB), an Editorial Board (EB), and seven Working Groups (WG). The rôle of the Advisory Board is that of general supervision and consultation. Its members may interfere at any point in the process of drafting the paper, expressing their opinion and offering advice. They also give their approval of the final version of the preprint before it is rendered public. The Editorial Board coordinates the activities of FLAG, sets priorities and intermediate deadlines, and takes care of the editorial work needed to amalgamate the sections written by the individual working groups into a uniform and coherent review. The working groups concentrate on writing up the review of the physical quantities for which they are responsible, which is subsequently circulated to the whole collaboration for criticisms and suggestions.

Quantity	Sect.	■	$N_f=2+1+1$	■	$N_f=2+1$	■	$N_f=2$
m_s(MeV)	3.3			3	93.8(2.4)	2	101(3)
m_{ud}(MeV)	3.3			3	3.42(9)	1	3.6(2)
m_s/m_{ud}	3.3			3	27.5(4)	1	28.1(1.2)
m_d(MeV)	3.4				4.68(14)(7)		4.8(15)(17)
m_u(MeV)	3.4				2.16(9)(7)		2.40(15)(17)
m_u/m_d	3.4				0.46(2)(2)		0.50(2)(3)
$f_+^{K\pi}(0)$	4.3			1	0.9667(23)(33)	1	0.9560(57)(62)
f_{K^+}/f_{π^+}	4.3	1	1.195(3)(4)	4	1.192(5)	1	1.205(6)(17)
f_K(MeV)	4.6			3	156.3(0.8)	1	158.1(2.5)
f_π(MeV)	4.6			3	130.2(1.4)		
Σ(MeV)	5.1			2	265(17)	1	270(7)
F_π/F	5.1	1	1.0760(28)	2	1.0620(34)	1	1.0733(73)
$\bar{\ell}_3$	5.1	1	3.70(27)	3	2.77(1.27)	1	3.45(26)
$\bar{\ell}_4$	5.1	1	4.67(10)	3	3.95(35)	1	4.59(26)
$\hat{B}_K$	6.2			4	0.766(10)	1	0.729(25)(17)
$B_K^{\overline{\rm MS}}$(2 GeV)	6.2			4	0.560(7)	1	0.533(18)(12)
f_D(MeV)	7.1			2	209.2(3.3)	1	212(8)
f_{D_s}(MeV)	7.1			2	248.6(2.7)	1	248(6)
f_{D_s}/f_D	7.1			2	1.187(12)	1	1.17(5)
$f_+^{D\pi}(0)$	7.2			1	0.666(29)		
$f_+^{DK}(0)$	7.2			1	0.747(19)		
f_B(MeV)	8.1			3	190.5(4.2)	1	197(10)
f_{B_s}(MeV)	8.1			3	227.7(4.5)	1	234(6)
f_{B_s}/f_B	8.1			2	1.202(22)	1	1.19(5)
$f_{B_d}\sqrt{\hat{B}_{B_d}}$(MeV)	8.2			1	216(15)		
$f_{B_s}\sqrt{\hat{B}_{B_s}}$(MeV)	8.2			1	266(18)		
$\hat{B}_{B_d}$	8.2			1	1.27(10)		
$\hat{B}_{B_s}$	8.2			1	1.33(10)		
ξ	8.2			1	1.268(63)		
$\hat{B}_{B_s}/\hat{B}_{B_d}$	8.2			1	1.06(11)		
$\Delta\zeta^{B\pi}$(ps^{-1})	8.3			2	2.16(50)		
$f_+^{B\pi}(q^2)$: $a_0^{\rm BCL}$	8.3			2	0.453(33)		
$a_1^{\rm BCL}$				2	$-0.43(33)$		
$a_2^{\rm BCL}$				2	0.9(3.9)		
$\mathcal{F}^{B\to D^*}(1)$	8.3			1	0.9017(51)(156)		
$R(D)$	8.3			1	0.316(12)(7)		

Table 1: Summary of the main results of this review, grouped in terms of N_f, the number of dynamical quark flavours in lattice simulations. Quark masses and the quark condensate are given in the $\overline{\rm MS}$ scheme at running scale $\mu = 2\,$GeV; the other quantities listed are specified in the quoted sections. The columns marked ■ indicate the number of results that enter our averages for each quantity. We emphasize that these numbers only give a very rough indication of how thoroughly the quantity in question has been explored on the lattice and recommend to consult the detailed tables and figures in the relevant section for more significant information.

The most important internal FLAG rules are the following:

- members of the AB have a 4-year mandate (to avoid a simultaneous change of all members, some of the current members of the AB will have a shorter mandate);
- the composition of the AB reflects the main geographical areas in which lattice collaborations are active: one member comes from America, one from Asia/Oceania and one from Europe ;
- the mandate of regular members is not limited in time, but we expect that a certain turnover will occur naturally;
- whenever a replacement becomes necessary this has to keep, and possibly improve, the balance in FLAG;
- in all working groups the three members must belong to three different lattice collaborations;[2]
- a paper is in general not reviewed (nor colour-coded, as described in the next section) by one of its authors;
- lattice collaborations not represented in FLAG will be asked to check whether the colour coding of their calculation is correct.

The current list of FLAG members and their Working Group assignments is:

- Advisory Board (AB): S. Aoki, C. Bernard, C. Sachrajda
- Editorial Board (EB): G. Colangelo, H. Leutwyler, A. Vladikas, U. Wenger
- Working Groups (WG)
  (each WG coordinator is listed first):
  - Quark masses: L. Lellouch, T. Blum, V. Lubicz
  - V_{us}, V_{ud}: A. Jüttner, T. Kaneko, S. Simula
  - LEC: S. Dürr, H. Fukaya, S. Necco
  - B_K: H. Wittig, J. Laiho, S. Sharpe
  - $f_{B_{(s)}}$, $f_{D_{(s)}}$, B_B: A. El Khadra, Y. Aoki, M. Della Morte
  - $B_{(s)}$, D semileptonic and radiative decays: R. Van de Water, E. Lunghi, C. Pena, J. Shigemitsu
  - α_s: R. Sommer, R. Horsley, T. Onogi

1.2 General issues and summary of the main results

The present review aims at two distinct goals:

a. offer a **description** of the work done on the lattice concerning low energy particle physics;

b. draw **conclusions** on the basis of that work, which summarize the results obtained for the various quantities of physical interest.

The core of the information about the work done on the lattice is presented in the form of tables, which not only list the various results, but also describe the quality of the data that underlie them. We consider it important that this part of the review represents a generally accepted description of the work done. For this reason, we explicitly specify the quality

[2] The WG on semileptonic D and B decays has currently four members, but only three of them belong to lattice collaborations.

requirements used and provide sufficient details in the appendices so that the reader can verify the information given in the tables.

The conclusions drawn on the basis of the available lattice results, on the other hand, are the responsibility of FLAG alone. We aim at staying on the conservative side and in several cases reach conclusions which are more cautious than what a plain average of the available lattice results would give, in particular when this is dominated by a single lattice result. An additional issue occurs when only one lattice result is available for a given quantity. In such cases one does not have the same degree of confidence in results and errors as one has when there is agreement among many different calculations using different approaches. Since this degree of confidence cannot be quantified, it is not reflected in the quoted errors, but should be kept in mind by the reader. At present, the issue of having only a single result occurs much more often in heavy-quark physics or in the lattice determinations of α_s, than in light-quark physics. We are confident that the heavy-quark and α_s calculations will soon reach the state that pertains in light-quark physics.

Several general issues concerning the present review are thoroughly discussed in Sect. 1.1 of our initial paper [1] and we encourage the reader to consult the relevant pages. In the remainder of the present section, we focus on a few important points.

Each discretization has its merits, but also its shortcomings. For the topics covered already in the first edition of the FLAG review, we have by now a remarkably broad data base, and for most quantities lattice calculations based on totally different discretizations are now available. This is illustrated by the dense population of the tables and figures shown in the first part of this review. Those calculations which do satisfy our quality criteria indeed lead to consistent results, confirming universality within the accuracy reached. In our opinion, the consistency between independent lattice results, obtained with different discretizations, methods, and simulation parameters, is an important test of lattice QCD, and observing such consistency then also provides further evidence that systematic errors are fully under control.

In the sections dealing with heavy quarks and with α_s, the situation is not the same. Since the b-quark mass cannot be resolved with current lattice spacings, all lattice methods for treating b quarks use effective field theory at some level. This introduces additional complications not present in the light-quark sector. An overview of the issues specific to heavy-quark quantities is given in the introduction of Sec. 8. For B and D meson leptonic decay constants, there already exist a good number of different independent calculations that use different heavy-quark methods, but there are only one or two independent calculations of semileptonic B and D meson form factors and B meson mixing parameters. For α_s, most lattice methods involve a range of scales that need to be resolved and controlling the systematic error over a large range of scales is more demanding. The issues specific to determinations of the strong coupling will be discussed in detail in a new section which will be included in the next update of the review.

The lattice spacings reached in recent simulations go down to 0.05 fm or even smaller. In that region, growing autocorrelation times may slow down the sampling of the configurations [4–8]. Many groups check for autocorrelations in a number of observables, including the topological charge, for which a rapid growth of the autocorrelation time is observed if the lattice spacing becomes small. In the following, we assume that the continuum limit can be reached by extrapolating the existing simulations.

Lattice simulations of QCD currently involve at most four dynamical quark flavours. Moreover, most of the data concern simulations for which the masses of the two lightest quarks are set equal. This is indicated by the notation $N_f = 2 + 1 + 1$ which, in this case, denotes a lattice calculation with four dynamical quark flavours and $m_u = m_d \neq m_s \neq m_c$. Note that calculations with $N_f = 2$ dynamical flavours often include strange valence quarks interacting with gluons, so that bound states with the quantum numbers of the kaons can be studied, albeit neglecting strange sea quark fluctuations. The quenched approximation ($N_f = 0$), in which the sea quarks are treated as a mean field, is no longer used in modern lattice simulations. Accordingly, we will review results obtained with $N_f = 2$, $N_f = 2+1$, and $N_f = 2+1+1$, but omit earlier results with $N_f = 0$. On the other hand, the dependence of the QCD coupling constant α_s on the number of flavours is a theoretical issue of considerable interest, and we will therefore include results obtained for gluodynamics in the upcoming α_s section. We stress, however, that only results with $N_f \geq 3$ will be used to determine the physical value of α_s.

The remarkable recent progress in the precision of lattice calculations is due to improved algorithms, better computing resources and, last but not least, conceptual developments, such as improved actions which reduce lattice artifacts, actions which preserve (remnants of) chiral symmetry, understanding finite-size effects, non-perturbative renormalization, etc. A concise characterization of the various discretizations that underlie the results reported in the present review is given in Appendix A.1.

Lattice simulations are performed at fixed values of the bare QCD parameters (gauge coupling and quark masses) and physical quantities with mass dimensions (e.g. quark masses, decay constants ...) are computed in units of the lattice spacing; i.e. they are dimensionless. Their conversion to physical units requires knowledge of the lattice spacing at the fixed values of the bare QCD parameters of the simulations. This is achieved by requiring agreement between the lattice calculation and experimental measurement of a known quantity, which "sets the scale" of a given simulation. A few details on this procedure are provided in Appendix A.2.

Several of the results covered by this review, such as quark masses, the gauge coupling, and B-parameters, are quantities defined in a given renormalization scheme and scale. The schemes employed are often chosen because of their specific merits when combined with the lattice regularization. For a brief discussion of their properties, see Appendix A.3. The conversion of the results, obtained in these so-called intermediate schemes, to more familiar regularization schemes, such as the $\overline{\rm MS}$-scheme, is done with the aid of perturbation theory. It must be stressed that the renormalization scales accessible by the simulations are subject to limitations, naturally arising in Field Theory computations at finite UV and small non-zero IR cutoff. Typically, such scales are of the order of the UV cutoff, or $\Lambda_{\rm QCD}$, depending on the chosen scheme. To safely match to $\overline{\rm MS}$, a scheme defined in perturbation theory, Renormalization Group (RG) running to higher scales is performed, either perturbatively, or non-perturbatively (the latter using finite-size scaling techniques).

Because of limited computing resources, lattice simulations are often performed at unphysically heavy pion masses, although results at the physical point have recently become available. Further, numerical simulations must be done at finite lattice spacing. In order to obtain physical results, lattice data are generated at a sequence of pion masses and a sequence of lattice spacings, and then extrapolated to $M_\pi \approx 135$ MeV and $a \to 0$. To control the associated systematic uncertainties, these extrapolations are guided by effective theory. For light-quark actions, the lattice-spacing dependence is described by Symanzik's effective theory [9, 10]; for heavy quarks, this can be extended and/or supplemented by other effective theories such as Heavy-Quark Effective Theory (HQET). The pion-mass dependence can be parameterized with Chiral Perturbation Theory (χPT), which takes into account the Nambu-

Goldstone nature of the lowest excitations that occur in the presence of light quarks; similarly one can use Heavy-Light Meson Chiral Perturbation Theory (HMχPT) to extrapolate quantities involving mesons composed of one heavy (b or c) and one light quark. One can combine Symanzik's effective theory with χPT to simultaneously extrapolate to the physical pion mass and continuum; in this case, the form of the effective theory depends on the discretization. See Appendix A.4 for a brief description of the different variants in use and some useful references.

2 Quality criteria

The essential characteristics of our approach to the problem of rating and averaging lattice quantities reported by different collaborations have been outlined in our first publication [1]. Our aim is to help the reader assess the reliability of a particular lattice result without necessarily studying the original article in depth. This is a delicate issue, which may make things appear simpler than they are. However, it safeguards against the common practice of using lattice results and drawing physics conclusions from them, without a critical assessment of the quality of the various calculations. We believe that despite the risks, it is important to provide some compact information about the quality of a calculation. However, the importance of the accompanying detailed discussion of the results presented in the bulk of the present review cannot be underestimated.

2.1 Systematic errors and colour-coding

In Ref. [1], we identified a number of sources of systematic errors, for which a systematic improvement is possible, and assigned one of three coloured symbols to each calculation: green star, amber disc or red square. The appearance of a red tag, even in a single source of systematic error of a given lattice result, disqualified it from the global averaging. Since results with green and amber tags entered the averages, and since this policy has been retained in the present edition, we have decided to substitute the amber disc by a green unfilled circle. Thus the new colour coding is as follows:

★ the systematic error has been estimated in a satisfactory manner and convincingly shown to be under control;

○ a reasonable attempt at estimating the systematic error has been made, although this could be improved;

■ no or a clearly unsatisfactory attempt at estimating the systematic error has been made.

We stress once more that only results without a red tag in the systematic errors are averaged in order to provide a given FLAG estimate.

The precise criteria used in determining the colour coding is unavoidably time-dependent; as lattice calculations become more accurate the standards against which they are measured become tighter. For quantities related to the light-quark sector, which have been dealt with in the first edition of the FLAG review [1], some of the quality criteria have remained the same, while others have been tightened up. We will compare them to those of Ref. [1], case-by-case, below. For the newly introduced physical quantities, related to heavy quark physics, the adoption of new criteria was necessary. This is due to the fact that, in most cases, the discretization of the heavy quark action follows a very different approach to that of light flavours. Moreover, the two Working Groups dedicated to heavy flavours have opted for a somewhat different rating of the extrapolation of lattice results to the continuum limit.

Finally, the strong coupling being in a class of its own, as far as methods for its computation are concerned, led to the introduction of dedicated rating criteria for it.

Of course any colour coding has to be treated with caution; we repeat that the criteria are subjective and evolving. Sometimes a single source of systematic error dominates the systematic uncertainty and it is more important to reduce this uncertainty than to aim for green stars for other sources of error. In spite of these caveats we hope that our attempt to introduce quality measures for lattice results will prove to be a useful guide. In addition we would like to stress that the agreement of lattice results obtained using different actions and procedures evident in many of the tables presented below provides further validation.

For a coherent assessment of the present situation, the quality of the data plays a key role, but the colour coding cannot be carried over to the figures. On the other hand, simply showing all data on equal footing would give the misleading impression that the overall consistency of the information available on the lattice is questionable. As a way out, the figures do indicate the quality in a rudimentary way:

■ results included in the average;
□ results that are not included in the average but pass all quality criteria;
□ all other results.

The reason for not including a given result in the average is not always the same: the paper may fail one of the quality criteria, may not be published, be superseded by other results or not offer a complete error budget. Symbols other than squares are used to distinguish results with specific properties and are always explained in the caption.

2.1.1 Light-quark physics

The colour code used in the tables is specified as follows:

- Chiral extrapolation:
  ★ $M_{\pi,\mathrm{min}} < 200$ MeV
  ○ $200 \text{ MeV} \le M_{\pi,\mathrm{min}} \le 400$ MeV
  ■ $400 \text{ MeV} < M_{\pi,\mathrm{min}}$
  It is assumed that the chiral extrapolation is done with at least a three-point analysis; otherwise this will be explicitly mentioned. Note that, compared to Ref. [1], chiral extrapolations are now treated in a somewhat more stringent manner and the cutoff between green star and green open circle (formerly amber disc), previously set at 250 MeV, is now lowered to 200 MeV.

- Continuum extrapolation:
  ★ 3 or more lattice spacings, at least 2 points below 0.1 fm
  ○ 2 or more lattice spacings, at least 1 point below 0.1 fm
  ■ otherwise
  It is assumed that the action is $O(a)$-improved (i.e. the discretization errors vanish quadratically with the lattice spacing); otherwise this will be explicitly mentioned. Moreover, for non-improved actions an additional lattice spacing is required. This criterion is the same as the one adopted in Ref. [1].

- Finite-volume effects:
  ★ $M_{\pi,\mathrm{min}}L > 4$ or at least 3 volumes
  ○ $M_{\pi,\mathrm{min}}L > 3$ and at least 2 volumes
  ■ otherwise

These ratings apply to calculations in the p-regime and it is assumed that $L_{\min} \geq 2$ fm; otherwise this will be explicitly mentioned and a red square will be assigned.

- Renormalization (where applicable):
  ★ non-perturbative
  ○ 1-loop perturbation theory or higher with a reasonable estimate of truncation errors
  ■ otherwise
  In Ref. [1], we assigned a red square to all results which were renormalized at 1-loop in perturbation theory. We now feel that this is too restrictive, since the error arising from renormalization constants, calculated in perturbation theory at 1-loop, is often estimated conservatively and reliably.
- Running (where applicable):
  For scale-dependent quantities, such as quark masses or B_K, it is essential that contact with continuum perturbation theory can be established. Various different methods are used for this purpose (cf. Appendix A.3): Regularization-independent Momentum Subtraction (RI/MOM), Schrödinger functional, direct comparison with (resummed) perturbation theory. Irrespective of the particular method used, the uncertainty associated with the choice of intermediate renormalization scales in the construction of physical observables must be brought under control. This is best achieved by performing comparisons between non-perturbative and perturbative running over a reasonably broad range of scales. These comparisons were initially only made in the Schrödinger functional (SF) approach, but are now also being performed in RI/MOM schemes. We mark the data for which information about non-perturbative running checks is available and give some details, but do not attempt to translate this into a colour-code.

The pion mass plays an important rôle in the criteria relevant for chiral extrapolation and finite volume. For some of the regularizations used, however, it is not a trivial matter to identify this mass. In the case of twisted-mass fermions, discretization effects give rise to a mass difference between charged and neutral pions even when the up- and down-quark masses are equal, with the charged pion being the heavier of the two. The discussion of the twisted-mass results presented in the following sections assumes that the artificial isospin-breaking effects which occur in this regularization are under control. In addition, we assume that mass of the charged pion may be used when evaluating the chiral extrapolation and finite volume criteria. In the case of staggered fermions, discretization effects give rise to several light states with the quantum numbers of the pion.[3] The mass splitting among these "taste" partners represents a discretization effect of $\mathcal{O}(a^2)$, which can be significant at big lattice spacings but shrinks as the spacing is reduced. In the discussion of the results obtained with staggered quarks given in the following sections, we assume that these artefacts are under control. When evaluating the chiral extrapolation criteria, we conservatively identify $M_{\pi,\min}$ with the root mean square (RMS) of the mass of all taste partners. These masses are also used in sections 4 and 6 when evaluating the finite volume criteria, while in sections 3, 5, 7 and 8, a more stringent finite volume criterion is applied: $M_{\pi,\min}$ is identified with the mass of the lightest state.

[3] We refer the interested reader to a number of good reviews on the subject [11–15].

2.1.2 Heavy-quark physics

This subsection discusses the criteria adopted for the heavy-quark quantities included in this review, characterized by non-zero charm and bottom quantum numbers. There are several different approaches to treating heavy quarks on the lattice, each with their own issues and considerations. In general all b-quark methods rely on the use of Effective Field Theory (EFT) at some point in the computation, either via direct simulation of the EFT, use of the EFT to estimate the size of cutoff errors, or use of the EFT to extrapolate from the simulated lattice quark mass up to the physical b-quark mass. Some simulations of charm-quark quantities use the same heavy-quark methods as for bottom quarks, but there are also computations that use improved light-quark actions to simulate charm quarks. Hence, with some methods and for some quantities, truncation effects must be considered together with discretization errors. With other methods, discretization errors are more severe for heavy-quark quantities than for the corresponding light-quark quantities.

In order to address these complications, we add a new heavy-quark treatment category to the ratings system. The purpose of this criterion is to provide a guideline for the level of action and operator improvement needed in each approach to make reliable calculations possible, in principle. In addition, we replace the rating criteria for the continuum extrapolations of Sec. 2.1.1 with a new empirical approach based on the size of observed discretization errors in the lattice simulation data. This accounts for the fact that whether discretization and truncation effects in a given calculation are sufficiently small as to be controllable depends not only on the range of lattice spacings used in the simulations, but also on the simulated heavy-quark masses and on the level of action and operator improvement. For the other categories, we adopt the same strict criteria as in Sec. 2.1.1, with one minor modification, as explained below.

- Heavy-quark treatment:
  A description of the different approaches to treating heavy quarks on the lattice is given in Appendix A.1.3 including a discussion of the associated discretization, truncation, and matching errors. For truncation errors we use HQET power counting throughout, since this review is focused on heavy quark quantities involving B and D mesons. Here we describe the criteria for how each approach must be implemented in order to receive an acceptable (✓) rating for both the heavy quark actions and the weak operators. Heavy-quark implementations without the level of improvement described below are rated not acceptable (■). The matching is evaluated together with renormalization, using the renormalization criteria described in Sec. 2.1.1. We emphasize that the heavy-quark implementations rated as acceptable and described below have been validated in a variety of ways, such as via phenomenological agreement with experimental measurements, consistency between independent lattice calculations, and numerical studies of truncation errors. These tests are summarized in Sec. 8.

  Relativistic heavy quark actions:
  ✓ at least tree-level $O(a)$ improved action and weak operators
  This is similar to the requirements for light quark actions. All current implementations of relativistic heavy quark actions satisfy these criteria.

  NRQCD:
  ✓ tree-level matched through $O(1/m_h)$ and improved through $O(a^2)$
  The current implementations of NRQCD satisfy these criteria, and also include tree-level

corrections of $O(1/m_h^2)$ in the action.

HQET:

✓ matched through $O(1/m_h)$ with discretization errors starting at $O(a^2)$

The current implementation of HQET by the ALPHA collaboration satisfies these criteria with an action and weak operators that are nonperturbatively matched through $O(1/m_h)$. Calculations that exclusively use a static limit action do not satisfy theses criteria, since the static limit action, by definition, does not include $1/m_h$ terms. However for SU(3)-breaking ratios such as ξ and f_{B_s}/f_B truncation errors start at $O((m_s - m_d)/m_h)$. We therefore consider lattice calculations of such ratios that use a static limit action to still have controllable truncation errors.

Light-quark actions for heavy quarks:

✓ discretization errors starting at $O(a^2)$ or higher

This applies to calculations that use the tmWilson action, a nonperturbatively improved Wilson action, or the HISQ action for charm quark quantities. It also applies to calculations that use these light quark actions in the charm region and above together with either the static limit or with an HQET inspired extrapolation to obtain results at the physical b quark mass. In these cases, the continuum extrapolation criteria must be applied to the entire range of heavy quark masses used in the calculation.

- Continuum extrapolation:
  First we introduce the following definitions:

$$D(a) = \frac{Q(a) - Q(0)}{Q(a)}\,, \tag{1}$$

where $Q(a)$ denotes the central value of quantity Q obtained at lattice spacing a and $Q(0)$ denotes the continuum extrapolated value. $D(a)$ is a measure of how far the continuum extrapolated result is from the lattice data. We evaluate this quantity on the smallest lattice spacing used in the calculation, $a_{\rm min}$.

$$\delta(a) = \frac{Q(a) - Q(0)}{\sigma_Q}\,, \tag{2}$$

where σ_Q is the combined statistical and systematic (due to the continuum extrapolation) error. $\delta(a)$ is a measure of how well the continuum extrapolated result agrees with the lattice data within the statistical and systematic errors of the calculation. Again, we evaluate this quantity on the smallest lattice spacing used in the calculation, $a_{\rm min}$.

★ (i) Three or more lattice spacings, and
(ii) $a^2_{\rm max}/a^2_{\rm min} \geq 2$, and
(iii) $D(a_{\rm min}) \leq 2\%$, and
(iv) $\delta(a_{\rm min}) \leq 1$

○ (i) Two or more lattice spacings, and
(ii) $a^2_{\rm max}/a^2_{\rm min} \geq 1.4$, and
(iii) $D(a_{\rm min}) \leq 10\%$, and
(iv) $\delta(a_{\rm min}) \leq 2$

■ otherwise

For the time being, these new criteria for the quality of the continuum extrapolation have only been adopted for the heavy-quark quantities, but their use may be extended to all FLAG quantities in future reviews.

- Finite-volume:
  ★ $M_{\pi,\min}L \gtrsim 3.7$ or 2 volumes at fixed parameters
  ○ $M_{\pi,\min}L \gtrsim 3$
  ■ otherwise
  Here the boundary between green star and open circle is slightly relaxed compared to that in Sec. 2.1.1 to account for the fact that heavy-quark quantities are less sensitive to this systematic error than light-quark quantities. A ★ rating requires an estimate of the finite volume error either by analyzing data on two or more physical volumes (with all other parameters fixed) or by using finite volume chiral perturbation theory. In the case of staggered sea quarks, $M_{\pi,\min}$ refers to the lightest (taste Goldstone) pion mass.

2.2 Averages and estimates

For many observables there are enough independent lattice calculations of good quality that it makes sense to average them and propose such an *average* as the best current lattice number. In order to decide whether this is true for a certain observable, we rely on the colour coding. We restrict the averages to data for which the colour code does not contain any red tags. In some cases, the averaging procedure nevertheless leads to a result which in our opinion does not cover all uncertainties. This is related to the fact that procedures for estimating errors and the resulting conclusions necessarily have an element of subjectivity, and would vary between groups even with the same data set. In order to stay on the conservative side, we may replace the average by an *estimate*, which we consider as a fair assessment of the knowledge acquired on the lattice at present. This estimate is not obtained with a prescribed mathematical procedure, but is based on a critical analysis of the available information.

There are two other important criteria which also play a role in this respect, but which cannot be colour coded, because a systematic improvement is not possible. These are: *i)* the publication status, and *ii)* the number of flavours N_f. As far as the former criterion is concerned, we adopt the following policy: we average only results which have been published in peer reviewed journals, *i.e.* they have been endorsed by referee(s). The only exception to this rule consists in obvious updates of previously published results, typically presented in conference proceedings. Such updates, which supersede the corresponding results in the published papers, are included in the averages. Nevertheless, all results are listed and their publication status is identified by the following symbols:

- Publication status:
  A published or plain update of published results
  P preprint
  C conference contribution

Note that updates of earlier results rely, at least partially, on the same gauge field configuration ensembles. For this reason, we do not average updates with earlier results. In the present edition, the publication status on April 30, 2013 is relevant. If the paper appeared in print before September 30, 2013, this is accounted for in the bibliography, but does not affect the averages. These will be updated only in the final version of the review.

In this review we present results from simulations with $N_f = 2$, $N_f = 2+1$, and $N_f = 2+1+1$. We are not aware of an *a priori* way to quantitatively estimate the difference between results produced in simulations with a different number of dynamical quarks. We therefore average results at fixed N_f separately; averages of calculations with different N_f will not be provided.

To date, no significant differences between results with different values of N_f have been observed. In the future, as the accuracy and the control over systematic effects in lattice calculations will increase, it will hopefully be possible to see a difference between $N_f = 2$ and $N_f = 2+1$ calculations and so determine the size of the Zweig-rule violations related to strange quark loops. This is a very interesting issue *per se*, and one which can be quantitatively addressed only with lattice calculations.

2.3 Averaging procedure and error analysis

In [1], the FLAG averages and their errors were estimated through the following procedure: Having added in quadrature statistical and systematic errors for each individual result, we obtained their weighted χ^2 average. This was our central value. If the fit was of good quality ($\chi^2_{\rm min}/dof \leq 1$), we calculated the net uncertainty δ from $\chi^2 = \chi^2_{\rm min}+1$; otherwise, we inflated the result obtained in this way by the factor $S = \sqrt(\chi^2/dof)$. Whenever this χ^2 minimization procedure resulted in a total error which was smaller than the smallest systematic error of any individual lattice result, we assigned the smallest systematic error of that result to the total systematic error in the average.

One of the problems arising when forming such averages is that not all of the data sets are independent; in fact, some rely on the same ensembles. In particular, the same gauge field configurations, produced with a given fermion descretization, are often used by different research teams with different valence quark lattice actions, obtaining results which are not really independent. In the present paper we have modified our averaging procedure, in order to account for such correlations. To start with, we examine error budgets for individual calculations and look for potentially correlated uncertainties. Specific problems encountered in connection with correlations between different data sets are commented in the text. If there is any reason to believe that a source of error is correlated between two calculations, a 100% correlation is assumed. We then obtain the central value from a χ^2 weighted average, evaluated by adding statistical and systematic errors in quadrature (just as in Ref. [1]): for a set of individual measurements x_i with error σ_i and correlation matrix C_{ij}, the central value is given by:

$$\begin{aligned} x_{\rm average} &= \sum_i x_i \omega_i \\ \omega_i &= \frac{\sigma_i^{-2}}{\sum_j \sigma_j^{-2}} \ . \end{aligned} \tag{3}$$

The error is obtained by constructing the covariance matrix for the set of correlated lattice results, using the prescription by Schmelling [16]:

$$\sigma^2_{\rm average} = \sum_{i,j} \omega_i \omega_j C_{ij} \ . \tag{4}$$

When necessary, the statistical and systematic error bars are stretched by a factor S, as specified in the previous paragraph.

3 Masses of the light quarks

Quark masses are fundamental parameters of the Standard Model. An accurate determination of these parameters is important for both phenomenological and theoretical applications. The charm and bottom masses, for instance, enter the theoretical expressions of several cross sections and decay rates in heavy-quark expansions. The up-, down- and strange-quark masses govern the amount of explicit chiral symmetry breaking in QCD. From a theoretical point of view, the values of quark masses provide information about the flavour structure of physics beyond the Standard Model. The Review of Particle Physics of the Particle Data Group contains a review of quark masses [17], which covers light as well as heavy flavours. The present summary only deals with the light-quark masses (those of the up, down and strange quarks), but discusses the lattice results for these in more detail.

Quark masses cannot be measured directly with experiment because quarks cannot be isolated, as they are confined inside hadrons. On the other hand, quark masses are free parameters of the theory and, as such, cannot be obtained on the basis of purely theoretical considerations. Their values can only be determined by comparing the theoretical prediction for an observable, which depends on the quark mass of interest, with the corresponding experimental value. What makes light-quark masses particularly difficult to determine is the fact that they are very small (for the up and down) or small (for the strange) compared to typical hadronic scales. Thus, their impact on typical hadronic observables is minute and it is difficult to isolate their contribution accurately.

Fortunately, the spontaneous breaking of $SU(3)_L \otimes SU(3)_R$ chiral symmetry provides observables which are particularly sensitive to the light-quark masses: the masses of the resulting Nambu-Goldstone bosons (NGB), i.e. pions, kaons and etas. Indeed, the Gell-Mann-Oakes-Renner relation [18] predicts that the squared mass of a NGB is directly proportional to the sum of the masses of the quark and antiquark which compose it, up to higher-order mass corrections. Moreover, because these NGBs are light and are composed of only two valence particles, their masses have a particularly clean statistical signal in lattice-QCD calculations. In addition, the experimental uncertainties on these meson masses are negligible.

Three flavour QCD has four free parameters: the strong coupling, α_s (alternatively $\Lambda_{\rm QCD}$) and the up, down and strange quark masses, m_u, m_d and m_s. However, present day lattice calculations are often performed in the isospin limit, and the up and down quark masses (especially those in the sea) usually get replaced by a single parameter: the isospin averaged up- and down-quark mass, $m_{ud} = \frac{1}{2}(m_u + m_d)$. A lattice determination of these parameters requires two steps:

1. Calculations of three experimentally measurable quantities are used to fix the three bare parameters. As already discussed, NGB masses are particularly appropriate for fixing the light-quark masses. Another observable, such as the mass of a member of the baryon octet, can be used to fix the overall scale. It is important to note that until recently, most calculations were performed at values of m_{ud} which were still substantially larger than its physical value, typically four times as large. Reaching the physical up- and down-quark mass point required a significant extrapolation. This situation is changing fast. The PACS-CS [19–21] and BMW [22, 23] calculations were performed with masses all the way down to their physical value (and even below in the case of BMW), albeit in very small volumes for PACS-CS. More recently, MILC [24] and RBC/UKQCD [25] have also extended their simulations almost down to the physical point, by considering pions with

$M_\pi \gtrsim 170\,\mathrm{MeV}$.[4] Regarding the strange quark, modern simulations can easily include them with masses that bracket its physical value, and only interpolations are needed.

2. Renormalizations of these bare parameters must be performed to relate them to the corresponding cutoff-independent, renormalized parameters.[5] These are short distance calculations, which may be performed perturbatively. Experience shows that one-loop calculations are unreliable for the renormalization of quark masses: usually at least two loops are required to have trustworthy results. Therefore, it is best to perform the renormalizations nonperturbatively to avoid potentially large perturbative uncertainties due to neglected higher-order terms. However we will include in our averages one-loop results which carry a solid estimate of the systematic uncertainty due to the truncation of the series.

Of course, in quark mass ratios the renormalization factor cancels, so that this second step is no longer relevant.

3.1 Contributions from the electromagnetic interaction

As mentioned in Section 2.1, the present review relies on the hypothesis that, at low energies, the Lagrangian $\mathcal{L}_{\mathrm{QCD}} + \mathcal{L}_{\mathrm{QED}}$ describes nature to a high degree of precision. Moreover, we assume that, at the accuracy reached by now and for the quantities discussed here, the difference between the results obtained from simulations with three dynamical flavours and full QCD is small in comparison with the quoted systematic uncertainties. This will soon no longer be the case. The electromagnetic (e.m.) interaction, on the other hand, cannot be ignored. Quite generally, when comparing QCD calculations with experiment, radiative corrections need to be applied. In lattice simulations, where the QCD parameters are fixed in terms of the masses of some of the hadrons, the electromagnetic contributions to these masses must be accounted for.[6]

The electromagnetic interaction plays a crucial role in determinations of the ratio m_u/m_d, because the isospin-breaking effects generated by this interaction are comparable to those from $m_u \neq m_d$ (see Subsection 3.4). In determinations of the ratio m_s/m_{ud}, the electromagnetic interaction is less important, but at the accuracy reached, it cannot be neglected. The reason is that, in the determination of this ratio, the pion mass enters as an input parameter. Because M_π represents a small symmetry breaking effect, it is rather sensitive to the perturbations generated by QED.

We distinguish the physical mass M_P, $P \in \{\pi^+, \pi^0, K^+, K^0\}$, from the mass $\hat{M}_P$ within QCD alone. The e.m. self-energy is the difference between the two, $M_P^\gamma \equiv M_P - \hat{M}_P$. Because the self-energy of the Nambu-Goldstone bosons diverges in the chiral limit, it is convenient

[4] In the case of MILC, we are referring to the staggered root-mean-squared average mass of the taste partners (see discussion in Section 2.1). The mass of the corresponding taste-Goldstone-pion in these simulations is the physical value.

[5] Throughout this review, the quark masses m_u, m_d and m_s refer to the $\overline{\mathrm{MS}}$ scheme at running scale $\mu = 2\,\mathrm{GeV}$ and the numerical values are given in MeV units.

[6] Since the decomposition of the sum $\mathcal{L}_{\mathrm{QCD}} + \mathcal{L}_{\mathrm{QED}}$ into two parts is not unique, specifying the QCD part requires a convention. In order to give results for the quark masses in the Standard Model at scale $\mu = 2\,\mathrm{GeV}$, on the basis of a calculation done within QCD, it is convenient to match the two theories at that scale. We use this convention throughout the present review. Note that a different convention is used in the analysis of the precision measurements carried out in low energy pion physics (e.g. [26]). When comparing lattice results with experiment, it is important to fix the QCD parameters in accordance with the convention used in the analysis of the experimental data (for a more detailed discussion, see [27–30]).

to replace it by the contribution of the e.m. interaction to the *square* of the mass,

$$\Delta_P^\gamma \equiv M_P^2 - \hat{M}_P^2 = 2\, M_P M_P^\gamma + O(e^4)\,. \tag{5}$$

The main effect of the e.m. interaction is an increase in the mass of the charged particles, generated by the photon cloud that surrounds them. The self-energies of the neutral ones are comparatively small, particularly for the Nambu-Goldstone bosons, which do not have a magnetic moment. Dashen's theorem [31] confirms this picture, as it states that, to leading order (LO) of the chiral expansion, the self-energies of the neutral NGBs vanish, while the charged ones obey $\Delta_{K^+}^\gamma = \Delta_{\pi^+}^\gamma$. It is convenient to express the self-energies of the neutral particles as well as the mass difference between the charged and neutral pions within QCD in units of the observed mass difference, $\Delta_\pi \equiv M_{\pi^+}^2 - M_{\pi^0}^2$:

$$\Delta_{\pi^0}^\gamma \equiv \epsilon_{\pi^0}\, \Delta_\pi\,, \quad \Delta_{K^0}^\gamma \equiv \epsilon_{K^0}\, \Delta_\pi\,, \quad \hat{M}_{\pi^+}^2 - \hat{M}_{\pi^0}^2 \equiv \epsilon_m\, \Delta_\pi\,. \tag{6}$$

In this notation, the self-energies of the charged particles are given by

$$\Delta_{\pi^+}^\gamma = (1 + \epsilon_{\pi^0} - \epsilon_m)\, \Delta_\pi\,, \qquad \Delta_{K^+}^\gamma = (1 + \epsilon + \epsilon_{K^0} - \epsilon_m)\, \Delta_\pi\,, \tag{7}$$

where the dimensionless coefficient ϵ parameterizes the violation of Dashen's theorem,[7]

$$\Delta_{K^+}^\gamma - \Delta_{K^0}^\gamma - \Delta_{\pi^+}^\gamma + \Delta_{\pi^0}^\gamma \equiv \epsilon\, \Delta_\pi\,. \tag{8}$$

Any determination of the light-quark masses based on a calculation of the masses of π^+, K^+ and K^0 within QCD requires an estimate for the coefficients ϵ, ϵ_{π^0}, ϵ_{K^0} and ϵ_m.

The first determination of the self-energies on the lattice was carried out by Duncan, Eichten and Thacker [33]. Using the quenched approximation, they arrived at $M_{K^+}^\gamma - M_{K^0}^\gamma = 1.9\,\text{MeV}$. Actually, the parameterization of the masses given in that paper yields an estimate for all but one of the coefficients introduced above (since the mass splitting between the charged and neutral pions in QCD is neglected, the parameterization amounts to setting $\epsilon_m = 0$ ab initio). Evaluating the differences between the masses obtained at the physical value of the electromagnetic coupling constant and at $e = 0$, we obtain $\epsilon = 0.50(8)$, $\epsilon_{\pi^0} = 0.034(5)$ and $\epsilon_{K^0} = 0.23(3)$. The errors quoted are statistical only: an estimate of lattice systematic errors is not possible from the limited results of [33]. The result for ϵ indicates that the violation of Dashen's theorem is sizeable: according to this calculation, the nonleading contributions to the self-energy difference of the kaons amount to 50% of the leading term. The result for the self-energy of the neutral pion cannot be taken at face value, because it is small, comparable to the neglected mass difference $\hat{M}_{\pi^+} - \hat{M}_{\pi^0}$. To illustrate this, we note that the numbers quoted above are obtained by matching the parameterization with the physical masses for π^0, K^+ and K^0. This gives a mass for the charged pion that is too high by 0.32 MeV. Tuning the parameters instead such that M_{π^+} comes out correctly, the result for the self-energy of the neutral pion becomes larger: $\epsilon_{\pi^0} = 0.10(7)$ where, again, the error is statistical only.

In an update of this calculation by the RBC collaboration [34] (RBC 07), the electromagnetic interaction is still treated in the quenched approximation, but the strong interaction is simulated with $N_f = 2$ dynamical quark flavours. The quark masses are fixed with the physical

[7]Sometimes, e.g. in [32], the violation of Dashen's theorem is given in terms of a different quantity, $\bar{\epsilon} \equiv (\Delta_{K^+}^\gamma - \Delta_{K^0}^\gamma)/(\Delta_{\pi^+}^\gamma - \Delta_{\pi^0}^\gamma) - 1$. This parameter is related to ϵ used here through $\epsilon = (1 - \epsilon_m)\bar{\epsilon}$. Given the value of ϵ_m (see (9)), these two quantities differ by only 4%.

masses of π^0, K^+ and K^0. The outcome for the difference in the electromagnetic self-energy of the kaons reads $M^\gamma_{K^+} - M^\gamma_{K^0} = 1.443(55)\,\mathrm{MeV}$. This corresponds to a remarkably small violation of Dashen's theorem. Indeed, a recent extension of this work to $N_f = 2+1$ dynamical flavours [32] leads to a significantly larger self-energy difference: $M^\gamma_{K^+} - M^\gamma_{K^0} = 1.87(10)\,\mathrm{MeV}$, in good agreement with the estimate of Eichten et al. Expressed in terms of the coefficient ϵ that measures the size of the violation of Dashen's theorem, it corresponds to $\epsilon = 0.5(1)$.

The input for the electromagnetic corrections used by MILC is specified in [35]. In their analysis of the lattice data, ϵ_{π^0}, ϵ_{K^0} and ϵ_m are set equal to zero. For the remaining coefficient, which plays a crucial role in determinations of the ratio m_u/m_d, the very conservative range $\epsilon = 1 \pm 1$ was used in MILC 04 [36], while in more recent work, in particular in MILC 09 [15] and MILC 09A [37], this input is replaced by $\epsilon = 1.2 \pm 0.5$, as suggested by phenomenological estimates for the corrections to Dashen's theorem [38, 39]. Results of an evaluation of the electromagnetic self-energies based on $N_f = 2 + 1$ dynamical quarks in the QCD sector and on the quenched approximation in the QED sector are also reported by MILC [40–42]. Their preliminary result is $\bar{\epsilon} = 0.65(7)(14)(10)$, where the first error is statistical, the second systematic, and the third a separate systematic for the combined chiral and continuum extrapolation. The estimate of the systematic error does not yet include finite-volume effects. With the estimate for ϵ_m given in (9), this result corresponds to $\epsilon = 0.62(7)(14)(10)$. Similar preliminary results were previously reported by the BMW collaboration in conference proceedings [43, 44].

The RM123 collaboration employs a new technique to compute e.m. shifts in hadron masses in two-flavour QCD: the effects are included at leading order in the electromagnetic coupling α through simple insertions of the fundamental electromagnetic interaction in quark lines of relevant Feynman graphs [45]. They find $\epsilon = 0.79(18)(18)$ where the first error is statistical and the second is the total systematic error resulting from chiral, finite-volume, discretization, quenching and fitting errors all added in quadrature.

The effective Lagrangian that governs the self-energies to next-to-leading order (NLO) of the chiral expansion was set up in [46]. The estimates in [38, 39] are obtained by replacing QCD with a model, matching this model with the effective theory and assuming that the effective coupling constants obtained in this way represent a decent approximation to those of QCD. For alternative model estimates and a detailed discussion of the problems encountered in models based on saturation by resonances, see [47–49]. In the present review of the information obtained on the lattice, we avoid the use of models altogether.

There is an indirect phenomenological determination of ϵ, which is based on the decay $\eta \to 3\pi$ and does not rely on models. The result for the quark mass ratio Q, defined in (24) and obtained from a dispersive analysis of this decay, implies $\epsilon = 0.70(28)$ (see Section 3.4). While the values found in older lattice calculations [32–34] are a little less than one standard deviation lower, the most recent determinations [40–45, 50], though still preliminary, are in excellent agreement with this result and have significantly smaller error bars. However, even in the more recent calculations, e.m. effects are treated in the quenched approximation. Thus, we choose to quote $\epsilon = 0.7(3)$, which is essentially the $\eta \to 3\pi$ result and covers generously the range of post 2010 lattice results. Note that this value has an uncertainty which is reduced by about 40% compared to the result quoted in the first edition of the FLAG review [1].

We add a few comments concerning the physics of the self-energies and then specify the estimates used as an input in our analysis of the data. The Cottingham formula [51] represents the self-energy of a particle as an integral over electron scattering cross sections; elastic as well as inelastic reactions contribute. For the charged pion, the term due to elastic scattering, which involves the square of the e.m. form factor, makes a substantial contribution. In the case of the π^0, this term is absent, because the form factor vanishes on account of charge conjugation invariance. Indeed, the contribution from the form factor to the self-energy of the π^+ roughly reproduces the observed mass difference between the two particles. Furthermore, the numbers given in [52–54] indicate that the inelastic contributions are significantly smaller than the elastic contributions to the self-energy of the π^+. The low energy theorem of Das, Guralnik, Mathur, Low and Young [55] ensures that, in the limit $m_u, m_d \to 0$, the e.m. self-energy of the π^0 vanishes, while the one of the π^+ is given by an integral over the difference between the vector and axial-vector spectral functions. The estimates for ϵ_{π^0} obtained in [33] are consistent with the suppression of the self-energy of the π^0 implied by chiral SU(2)×SU(2). In our opinion, $\epsilon_{\pi^0} = 0.07(7)$ is a conservative estimate for this coefficient. The self-energy of the K^0 is suppressed less strongly, because it remains different from zero if m_u and m_d are taken massless and only disappears if m_s is turned off as well. Note also that, since the e.m. form factor of the K^0 is different from zero, the self-energy of the K^0 does pick up an elastic contribution. The lattice result for ϵ_{K^0} indicates that the violation of Dashen's theorem is smaller than in the case of ϵ. In the following, we use $\epsilon_{K^0} = 0.3(3)$.

Finally, we consider the mass splitting between the charged and neutral pions in QCD. This effect is known to be very small, because it is of second order in $m_u - m_d$. There is a parameter-free prediction, which expresses the difference $\hat{M}^2_{\pi^+} - \hat{M}^2_{\pi^0}$ in terms of the physical masses of the pseudoscalar octet and is valid to NLO of the chiral perturbation series. Numerically, the relation yields $\epsilon_m = 0.04$ [56], indicating that this contribution does not play a significant role at the present level of accuracy. We attach a conservative error also to this coefficient: $\epsilon_m = 0.04(2)$. The lattice result for the self-energy difference of the pions, reported in [32], $M^\gamma_{\pi^+} - M^\gamma_{\pi^0} = 4.50(23)\,\text{MeV}$, agrees with this estimate: expressed in terms of the coefficient ϵ_m that measures the pion mass splitting in QCD, the result corresponds to $\epsilon_m = 0.04(5)$. The corrections of next-to-next-to-leading order (NNLO) have been worked out [57], but the numerical evaluation of the formulae again meets with the problem that the relevant effective coupling constants are not reliably known.

In summary, we use the following estimates for the e.m. corrections:

$$\epsilon = 0.7(3)\,, \quad \epsilon_{\pi^0} = 0.07(7)\,, \quad \epsilon_{K^0} = 0.3(3)\,, \quad \epsilon_m = 0.04(2)\,. \tag{9}$$

While the range used for the coefficient ϵ affects our analysis in a significant way, the numerical values of the other coefficients only serve to set the scale of these contributions. The range given for ϵ_{π^0} and ϵ_{K^0} may be overly generous, but because of the exploratory nature of the lattice determinations, we consider it advisable to use a conservative estimate.

Treating the uncertainties in the four coefficients as statistically independent and adding errors in quadrature, the numbers in equation (9) yield the following estimates for the e.m. self-energies,

$$\begin{aligned} &M^\gamma_{\pi^+} = 4.7(3)\,\text{MeV}\,, \quad M^\gamma_{\pi^0} = 0.3(3)\,\text{MeV}\,, \quad M^\gamma_{\pi^+} - M^\gamma_{\pi^0} = 4.4(1)\,\text{MeV}\,,\\ &M^\gamma_{K^+} = 2.5(5)\,\text{MeV}\,, \quad M^\gamma_{K^0} = 0.4(4)\,\text{MeV}\,, \quad M^\gamma_{K^+} - M^\gamma_{K^0} = 2.1(4)\,\text{MeV}\,, \end{aligned} \tag{10}$$

and for the pion and kaon masses occurring in the QCD sector of the Standard Model,

$$\begin{aligned} &\hat{M}_{\pi^+} = 134.8(3)\,\text{MeV}\,, \quad \hat{M}_{\pi^0} = 134.6(3)\,\text{MeV}\,, \quad \hat{M}_{\pi^+} - \hat{M}_{\pi^0} = 0.2(1)\,\text{MeV}\,,\\ &\hat{M}_{K^+} = 491.2(5)\,\text{MeV}\,, \quad \hat{M}_{K^0} = 497.2(4)\,\text{MeV}\,, \quad \hat{M}_{K^+} - \hat{M}_{K^0} = -6.1(4)\,\text{MeV}\,. \end{aligned} \tag{11}$$

The self-energy difference between the charged and neutral pion involves the same coefficient ϵ_m that describes the mass difference in QCD – this is why the estimate for $M^{\gamma}_{\pi^+} - M^{\gamma}_{\pi^0}$ is so sharp.

3.2 Pion and kaon masses in the isospin limit

As mentioned above, most of the lattice calculations concerning the properties of the light mesons are performed in the isospin limit of QCD ($m_u - m_d \to 0$ at fixed $m_u + m_d$). We denote the pion and kaon masses in that limit by $\overline{M}_\pi$ and $\overline{M}_K$, respectively. Their numerical values can be estimated as follows. Since the operation $u \leftrightarrow d$ interchanges π^+ with π^- and K^+ with K^0, the expansion of the quantities $\hat{M}^2_{\pi^+}$ and $\frac{1}{2}(\hat{M}^2_{K^+} + \hat{M}^2_{K^0})$ in powers of $m_u - m_d$ only contains even powers. As shown in [58], the effects generated by $m_u - m_d$ in the mass of the charged pion are strongly suppressed: the difference $\hat{M}^2_{\pi^+} - \overline{M}_\pi^2$ represents a quantity of $O[(m_u - m_d)^2(m_u + m_d)]$ and is therefore small compared to the difference $\hat{M}^2_{\pi^+} - \hat{M}^2_{\pi^0}$, for which an estimate was given above. In the case of $\frac{1}{2}(\hat{M}^2_{K^+} + \hat{M}^2_{K^0}) - \overline{M}_K^2$, the expansion does contain a contribution at NLO, determined by the combination $2L_8 - L_5$ of low energy constants, but the lattice results for that combination show that this contribution is very small, too. Numerically, the effects generated by $m_u - m_d$ in $\hat{M}^2_{\pi^+}$ and in $\frac{1}{2}(\hat{M}^2_{K^+} + \hat{M}^2_{K^0})$ are negligible compared to the uncertainties in the electromagnetic self-energies. The estimates for these given in equation (11) thus imply

$$\overline{M}_\pi = \hat{M}_{\pi^+} = 134.8(3)\,\text{MeV} \;, \qquad \overline{M}_K = \sqrt{\frac{1}{2}(\hat{M}^2_{K^+} + \hat{M}^2_{K^0})} = 494.2(4)\,\text{MeV} \;. \tag{12}$$

This shows that, for the convention used above to specify the QCD sector of the Standard Model, and within the accuracy to which this convention can currently be implemented, the mass of the pion in the isospin limit agrees with the physical mass of the neutral pion: $\overline{M}_\pi - M_{\pi^0} = -0.2(3)$ MeV.

3.3 Lattice determination of m_s and m_{ud}

We now turn to a review of the lattice calculations of the light-quark masses and begin with m_s, the isospin averaged up- and down-quark mass, m_{ud}, and their ratio. Most groups quote only m_{ud}, not the individual up- and down-quark masses. We then discuss the ratio m_u/m_d and the individual determination of m_u and m_d.

Quark masses have been calculated on the lattice since the mid nineties. However early calculations were performed in the quenched approximation, leading to unquantifiable systematics. Thus in the following, we only review modern, unquenched calculations, which include the effects of light sea-quarks.

Tables 2 and 3 list the results of $N_f = 2$ and $N_f = 2+1$ lattice calculations of m_s and m_{ud}. These results are given in the $\overline{\text{MS}}$ scheme at 2 GeV, which is standard nowadays, though some groups are starting to quote results at higher scales (e.g. [25]). The tables also show the colour-coding of the calculations leading to these results. The corresponding results for m_s/m_{ud} are given in Table 4. As indicated earlier in this review, we treat $N_f = 2$ and $N_f = 2+1$ calculations separately. The latter include the effects of a strange sea-quark, but the former do not.

3.3.1 $N_f = 2$ lattice calculations

We begin with $N_f = 2$ calculations. A quick inspection of Table 2 indicates that only the most recent calculations, ALPHA 12 [59] and ETM 10B [60], control all systematic effects– the special case of Dürr 11 [61] is discussed below. Only ALPHA 12 [59], ETM 10B [60] and ETM 07 [62] really enter the chiral regime, with pion masses down to about 270 MeV for ALPHA and ETM. Because this pion mass is still quite far from the physical pion mass, ALPHA 12 refrain from determining m_{ud} and give only m_s. All the other calculations have significantly more massive pions, the lightest being about 430 MeV, in the calculation by CP-PACS 01 [63]. Moreover, the latter calculation is performed on very coarse lattices, with lattice spacings $a \geq 0.11$ fm and only one-loop perturbation theory is used to renormalize the results.

ETM 10B's [60] calculation of m_{ud} and m_s is an update of the earlier twisted-mass determination of ETM 07 [62]. In particular, they have added ensembles with a larger volume and three new lattice spacings, $a = 0.054, 0.067$ and 0.098 fm, allowing for a continuum extrapolation. In addition, it presents analyses performed in $SU(2)$ and $SU(3)$ χPT.

The new ALPHA 12 [59] calculation of m_s is an update of ALPHA 05 [64], which pushes computations to finer lattices and much lighter pion masses. It also importantly includes a determination of the lattice spacing with the decay constant F_K, whereas ALPHA 05 converted results to physical units using the scale parameter r_0 [65], defined via the force between static quarks. In particular, the conversion relied on measurements of r_0/a by QCDSF/UKQCD 04 [66] which differ significantly from the new determination by ALPHA 12. As in ALPHA 05, in ALPHA 12 both nonperturbative running and nonperturbative renormalization are performed in a controlled fashion, using Schrödinger functional methods.

The conclusion of our analysis of $N_f = 2$ calculations is that the results of ALPHA 12 [59] and ETM 10B [60] (which update and extend ALPHA 05 [64] and ETM 07 [62], respectively), are the only ones to date which satisfy our selection criteria. Thus we average those two results for m_s, obtaining 101(3) MeV. Regarding m_{ud}, for which only ETM 10B [60] gives a value, we do not offer an average but simply quote ETM's number. Because ALPHA's result induces an increase by 7% of our earlier average for m_s [1] while m_{ud} remains unchanged, our average for m_s/m_{ud} also increases by 7%. For the latter, however, we retain the percent error quoted by ETM, who directly estimates this ratio, and add it in quadrature to the percent error on ALPHA's m_s. Thus, we quote as our estimates:

$$N_f = 2: \quad m_s = 101(3)\,\text{MeV}\,, \quad m_{ud} = 3.6(2)\,\text{MeV}\,, \quad \frac{m_s}{m_{ud}} = 28.1(1.2)\,. \tag{13}$$

The errors on these results are 3%, 6% and 4% respectively. The error is smaller in the ratio than one would get from combining the errors on m_{ud} and m_s, because statistical and systematic errors cancel in ETM's result for this ratio, most notably those associated with renormalization and the setting of the scale. It is worth noting that thanks to ALPHA 12 [59], the total error on m_s has reduced significantly, from 7% in the last edition of our report to 3% now. It is also interesting to remark that ALPHA 12's [59] central value for m_s is about 1 σ larger than that of ETM 10B [60] and nearly 2 σ larger than our present $N_f = 2+1$ determination given in (14). Moreover, this larger value for m_s increases our $N_f = 2$ determination of m_s/m_{ud}, making it larger than ETM 10B's direct measurement, though compatible within errors.

We have not discussed yet the precise results of Dürr 11 [61] which satisfy our selection criteria. This is because Dürr 11 pursue an approach which is sufficiently different

Collaboration	Ref.	publication status	chiral extrapolation	continuum extrapolation	finite volume	renormalization	running	m_{ud}	m_s
ALPHA 12	[59]	A	○	★	★	★	a, b		102(3)(1)
Dürr 11‡	[61]	A	○	★	○	–	–	3.52(10)(9)	97.0(2.6)(2.5)
ETM 10B	[60]	A	○	★	○	★	c	3.6(1)(2)	95(2)(6)
JLQCD/TWQCD 08A	[67]	A	○	■	■	★	–	$4.452(81)(38)(^{+0}_{-227})$	–
RBC 07†	[34]	A	■	■	★	★	–	4.25(23)(26)	119.5(5.6)(7.4)
ETM 07	[62]	A	○	■	○	★	–	3.85(12)(40)	105(3)(9)
QCDSF/ UKQCD 06	[68]	A	■	★	■	★	–	4.08(23)(19)(23)	111(6)(4)(6)
SPQcdR 05	[69]	A	■	○	○	★	–	$4.3(4)(^{+1.1}_{-0.0})$	$101(8)(^{+25}_{-0})$
ALPHA 05	[64]	A	■	○	★	★	a		97(4)(18)§
QCDSF/ UKQCD 04	[66]	A	■	★	■	★	–	4.7(2)(3)	119(5)(8)
JLQCD 02	[70]	A	■	■	○	■	–	$3.223(^{+46}_{-69})$	$84.5(^{+12.0}_{-1.7})$
CP-PACS 01	[63]	A	■	■	★	■	–	$3.45(10)(^{+11}_{-18})$	$89(2)(^{+2}_{-6})^\star$

‡ What is calculated is $m_c/m_s = 11.27(30)(26)$. m_s is then obtained using lattice and phenomenological determinations of m_c which rely on perturbation theory. Finally, m_{ud} is determined from m_s using BMW 10A, 10B's $N_f = 2+1$ result for m_s/m_{ud} [22, 23]. Since m_c/m_s is renormalization group invariant in QCD, the renormalization and running of the quark masses enter indirectly through that of m_c, a mass that we do not review here.

† The calculation includes quenched e.m. effects.

§ The data used to obtain the bare value of m_s are from UKQCD/QCDSF 04 [66].

⋆ This value of m_s was obtained using the kaon mass as input. If the ϕ meson mass is used instead, the authors find $m_s = 90^{+5}_{-11}$.

a The masses are renormalized and run nonperturbatively up to a scale of 100 GeV in the $N_f = 2$ SF scheme. In this scheme, nonperturbative and NLO running for the quark masses are shown to agree well from 100 GeV all the way down to 2 GeV [64].

b The running and renormalization results of [64] are improved in [59] with higher statistical and systematic accuracy.

c The masses are renormalized nonperturbatively at scales $1/a \sim 2 \div 3$ GeV in the $N_f = 2$ RI/MOM scheme. In this scheme, nonperturbative and N^{3}LO running for the quark masses are shown to agree from 4 GeV down 2 GeV to better than 3% [71].

Table 2: $N_f = 2$ lattice results for the masses m_{ud} and m_s (MeV, running masses in the $\overline{\rm MS}$ scheme at scale 2 GeV). The significance of the colours is explained in Sec. 2. If information about nonperturbative running is available, this is indicated in the column "running", with details given at the bottom of the table.

from the one of other calculations that we prefer not to include it in an average at this stage. Following HPQCD 09A, 10 [72, 73], the observable which they actually compute is $m_c/m_s = 11.27(30)(26)$, with an accuracy of 3.5%. This result is about 1.5 combined standard deviations below ETM 10B's [60] result $m_c/m_s = 12.0(3)$. m_s is subsequently obtained using lattice and phenomenological determinations of m_c which rely on perturbation theory. The value of the charm-quark mass which they use is an average of those determinations, which they estimate to be $m_c(2\,\text{GeV}) = 1.093(13)\,\text{GeV}$, with a 1.2% total uncertainty. Note that this value is consistent with the PDG 12 [74] average $m_c(2\,\text{GeV}) = 1.094(21)\,\text{GeV}$, though the latter has a larger 2.0% uncertainty. Dürr 11's value of m_c leads to $m_s = 97.0(2.6)(2.5)$ MeV given in Table 2, which has a total error of 3.7%. The use of the PDG 12 value for m_c [74] would lead to a very similar result. The result for m_s is perfectly compatible with our estimate given in (13) and has a comparable error bar. To determine m_{ud}, Dürr 11 combine their result for m_s with the $N_f = 2+1$ calculation of m_s/m_{ud} of BMW 10A, 10B [22, 23] discussed below. They obtain $m_{ud} = 3.52(10)(9)$ MeV with a total uncertainty of less than 4%, which is again fully consistent with our estimate of (13) and its uncertainty.

3.3.2 $N_f = 2+1$ lattice calculations

We turn now to $N_f = 2+1$ calculations. These and the corresponding results are summarized in Tables 3 and 4. Somewhat paradoxically, these calculations are more mature than those with $N_f = 2$. This is thanks, in large part, to the head start and sustained effort of MILC, who have been performing $N_f = 2+1$ rooted staggered fermion calculations for the past ten or so years. They have covered an impressive range of parameter space, with lattice spacings which, today, go down to 0.045 fm and valence pion masses down to approximately 180 MeV [37]. The most recent updates, MILC 10A [75] and MILC 09A [37], include significantly more data and use two-loop renormalization. Since these data sets subsume those of their previous calculations, these latest results are the only ones that must be kept in any world average.

Since our last report [1] the situation for $N_f = 2+1$ determinations of light quarks has undergone some evolution. There are new computations by RBC/UKQCD 12 [25], PACS-CS 12 [76] and Laiho 11 [77]. Furthermore, the results of BMW 10A, 10B [22, 23] have been published and can now be included in our averages.

The RBC/UKQCD 12 [25] computation improves on the one of RBC/UKQCD 10A [78] in a number of ways. In particular it involves a new simulation performed at a rather coarse lattice spacing of 0.144 fm, but with unitary pion masses down to 171(1) MeV and valence pion masses down to 143(1) MeV in a volume of $(4.6\,\mathrm{fm})^3$, compared respectively to 290 MeV, 225 MeV and $(2.7\,\mathrm{fm})^3$ in RBC/UKQCD 10A. This provides them with a significantly better control over the extrapolation to physical M_π and to the infinite-volume limit. As before, they perform nonperturbative renormalization and running in RI/SMOM schemes. The only weaker point of the calculation comes from the fact that two of their three lattice spacings are larger than 0.1 fm and correspond to different discretizations, while the finest is only 0.085 fm, making it difficult to convincingly claim full control over the continuum limit. This is mitigated by the fact that the scaling violations which they observe on their coarsest lattice are for many quantities small, around 5%.

The Laiho 11 results [77] are based on MILC staggered ensembles at the lattice spacings 0.15, 0.09 and 0.06 fm, on which they propagate domain wall quarks. Moreover they work in volumes of up to $(4.8\,\mathrm{fm})^3$. These features give them full control over the continuum and infinite-volume extrapolations. Their lightest RMS sea pion mass is 280 MeV and their valence pions have masses down to 210 MeV. The fact that their sea pions do not enter deeply into the chiral regime penalizes somewhat their extrapolation to physical M_π. Moreover, to renormalize the quark masses, they use one-loop perturbation theory for $Z_A/Z_S - 1$ which they combine with Z_A determined nonperturbatively from the axial-vector Ward identity. Although they conservatively estimate the uncertainty associated with the procedure to be 5%, which is the size of their largest one-loop correction, this represents a weaker point of this calculation.

The new PACS-CS 12 [76] calculation represents an important extension of the collaboration's earlier 2010 computation [21], which already probed pion masses down to $M_\pi \simeq 135$ MeV, i.e. down to the physical mass point. This was achieved by reweighting the simulations performed in PACS-CS 08 [19] at $M_\pi \simeq 160$ MeV. If adequately controlled, this procedure eliminates the need to extrapolate to the physical mass point and, hence, the cor-

Collaboration	Ref.	publication status	chiral extrapolation	continuum extrapolation	finite volume	renormalization	running	m_{ud}	m_s
RBC/UKQCD 12$^{\ominus}$	[25]	A	★	○	★	★	a	3.37(9)(7)(1)(2)	92.3(1.9)(0.9)(0.4)(0.8)
PACS-CS 12*	[76]	A	★	■	■	★	b	3.12(24)(8)	83.60(0.58)(2.23)
Laiho 11	[77]	C	○	★	★	○	–	3.31(7)(20)(17)	94.2(1.4)(3.2)(4.7)
BMW 10A, 10B^{+}	[22, 23]	A	★	★	★	★	c	3.469(47)(48)	95.5(1.1)(1.5)
PACS-CS 10	[21]	A	★	■	■	★	b	2.78(27)	86.7(2.3)
MILC 10A	[75]	C	○	★	★	○	–	3.19(4)(5)(16)	–
HPQCD 10*	[72]	A	○	★	★	–	–	3.39(6)	92.2(1.3)
RBC/UKQCD 10A	[78]	A	○	○	★	★	a	3.59(13)(14)(8)	96.2(1.6)(0.2)(2.1)
Blum 10†	[32]	A	○	■	○	★	–	3.44(12)(22)	97.6(2.9)(5.5)
PACS-CS 09	[20]	A	★	■	■	★	b	2.97(28)(3)	92.75(58)(95)
HPQCD 09A$^{\oplus}$	[73]	A	○	★	★	–	–	3.40(7)	92.4(1.5)
MILC 09A	[37]	C	○	★	★	○	–	3.25 (1)(7)(16)(0)	89.0(0.2)(1.6)(4.5)(0.1)
MILC 09	[15]	A	○	★	★	○	–	3.2(0)(1)(2)(0)	88(0)(3)(4)(0)
PACS-CS 08	[19]	A	★	■	■	■	–	2.527(47)	72.72(78)
RBC/UKQCD 08	[79]	A	○	■	★	★	–	3.72(16)(33)(18)	107.3(4.4)(9.7)(4.9)
CP-PACS/ JLQCD 07	[80]	A	■	★	★	■	–	$3.55(19)(^{+56}_{-20})$	$90.1(4.3)(^{+16.7}_{-4.3})$
HPQCD 05	[81]	A	○	○	○	○	–	3.2(0)(2)(2)(0)‡	87(0)(4)(4)(0)‡
MILC 04, HPQCD/ MILC/UKQCD 04	[36, 82]	A	○	○	○	■	–	2.8(0)(1)(3)(0)	76(0)(3)(7)(0)

$^{\ominus}$ The results are given in the $\overline{\rm MS}$ scheme at 3 instead of 2 GeV: $m_{ud}^{\overline{\rm MS}}(3\,{\rm GeV}) = 3.05(8)(6)(1)(2)$ MeV, $m_s^{\overline{\rm MS}}(3\,{\rm GeV}) = 83.5(1.7)(0.8)(0.4)(0.7)$ MeV, where the errors are statistical, chiral, finite-volume and from the perturbative matching. We run them down to 2 GeV using numerically integrated four-loop running [83, 84] with $N_f = 3$ and with the values of $\alpha_s(M_Z)$, m_b and m_c taken from [74]. The running factor is 1.106. At three loops it is only 0.2% smaller. We therefore neglect the small uncertainty associated with this conversion.

* The calculation includes e.m. and $m_u \neq m_d$ effects through reweighting.

$^{+}$ The fermion action used is tree-level improved.

* What is calculated is $m_c(m_c) = 1.273(6)$ GeV, using lattice results and perturbation theory. m_s is then obtained by combing this result with HPQCD 09A's $m_c/m_s = 11.85(16)$ [73]. Finally, m_{ud} is determined from m_s with the MILC 09 result for m_s/m_{ud}. Since m_c/m_s is renormalization group invariant in QCD, the renormalization and running of the quark masses enter indirectly through that of m_c, a mass that we do not review here.

† The calculation includes quenched e.m. effects.

$^{\oplus}$ What is calculated is $m_c/m_s = 11.85(16)$. m_s is then obtained by combing this result with the determination $m_c(m_c) = 1.268(9)$ GeV from [85]. Finally, m_{ud} is determined from m_s with the MILC 09 result for m_s/m_{ud}.

‡ The bare numbers are those of MILC 04. The masses are simply rescaled, using the ratio of the two-loop to one-loop renormalization factors.

a The masses are renormalized nonperturbatively at a scale of 2 GeV in a couple of $N_f = 3$ RI/SMOM schemes. A careful study of perturbative matching uncertainties has been performed by comparing results in the two schemes in the region of 2 GeV to 3 GeV [78].

b The masses are renormalized and run nonperturbatively up to a scale of 40 GeV in the $N_f = 3$ SF scheme. In this scheme, nonperturbative and NLO running for the quark masses are shown to agree well from 40 GeV all the way down to 3 GeV[21].

c The masses are renormalized and run nonperturbatively up to a scale of 4 GeV in the $N_f = 3$ RI/MOM scheme. In this scheme, nonperturbative and N^{3}LO running for the quark masses are shown to agree from 6 GeV down to 3 GeV to better than 1% [23].

Table 3: $N_f = 2 + 1$ lattice results for the masses m_{ud} and m_s (see Table 2 for notation).

responding systematic error. The new calculation now applies similar reweighting techniques to include electromagnetic and $m_u \neq m_d$ isospin-breaking effects directly at the physical pion mass. It technically adds to Blum 10 [32] and BMW's preliminary results of [43, 44] by including these effects not only for valence but also for sea-quarks, as is also done in [86]. Further, as in PACS-CS 10 [21], renormalization of quark masses is implemented nonperturbatively, through the Schrödinger functional method [87]. As it stands, the main drawback

Collaboration	Ref.	N_f	publication status	chiral extrapolation	continuum extrapolation	finite volume	m_s/m_{ud}
RBC/UKQCD 12$^{\ominus}$	[25]	2+1	A	★	○	★	27.36(39)(31)(22)
PACS-CS 12*	[76]	2+1	A	★	■	■	26.8(2.0)
Laiho 11	[77]	2+1	C	○	★	★	28.4(0.5)(1.3)
BMW 10A, 10B^{+}	[22, 23]	2+1	A	★	★	★	27.53(20)(8)
RBC/UKQCD 10A	[78]	2+1	A	○	○	★	26.8(0.8)(1.1)
Blum 10†	[32]	2+1	A	○	■	○	28.31(0.29)(1.77)
PACS-CS 09	[20]	2+1	A	★	■	■	31.2(2.7)
MILC 09A	[37]	2+1	C	○	★	★	27.41(5)(22)(0)(4)
MILC 09	[15]	2+1	A	○	★	★	27.2(1)(3)(0)(0)
PACS-CS 08	[19]	2+1	A	★	■	■	28.8(4)
RBC/UKQCD 08	[79]	2+1	A	○	■	★	28.8(0.4)(1.6)
MILC 04, HPQCD/ MILC/UKQCD 04	[36, 82]	2+1	A	○	○	○	27.4(1)(4)(0)(1)
ETM 10B	[60]	2	A	○	★	○	27.3(5)(7)
RBC 07†	[34]	2	A	■	■	★	28.10(38)
ETM 07	[62]	2	A	○	■	○	27.3(0.3)(1.2)
QCDSF/UKQCD 06	[68]	2	A	■	★	■	27.2(3.2)

$^{\ominus}$ The errors are statistical, chiral and finite-volume.
* The calculation includes e.m. and $m_u \neq m_d$ effects through reweighting.
$^{+}$ The fermion action used is tree-level improved.
† The calculation includes quenched e.m. effects.

Table 4: Lattice results for the ratio m_s/m_{ud}.

of the calculation, which makes the inclusion of its results in a world average of lattice results inappropriate at this stage, is that for the lightest quark mass the volume is very small, corresponding to $LM_\pi \simeq 2.0$, a value for which finite-volume effects will be difficult to control. Another problem is that the calculation was performed at a single lattice spacing, forbidding a continuum extrapolation. Further, it is unclear at this point what might be the systematic errors associated with the reweighting procedure.

As shown by the colour-coding in Tables 3 and 4, the BMW 10A, 10B [22, 23] calculation is still the only one to have addressed all sources of systematic effects while reaching the physical up- and down-quark mass by *interpolation* instead of by extrapolation. Moreover, their calculation was performed at five lattice spacings ranging from 0.054 to 0.116 fm, with full nonperturbative renormalization and running and in volumes of up to $(6\text{ fm})^3$ guaranteeing that the continuum limit, renormalization and infinite-volume extrapolation are controlled. It does neglect, however, isospin-breaking effects, which are small on the scale of their error bars.

Finally we come to another calculation which satisfies our selection criteria, HPQCD 10 [72] (which updates HPQCD 09A [73]). The strange-quark mass is computed using a precise determination of the charm-quark mass, $m_c(m_c) = 1.273(6)$ GeV [72, 85], whose accuracy is better than 0.5%, and a calculation of the quark-mass ratio $m_c/m_s = 11.85(16)$ [73], which achieves a precision slightly above 1%. The determination of m_s via the ratio m_c/m_s displaces the problem of lattice renormalization in the computation of m_s to one of renormalization in

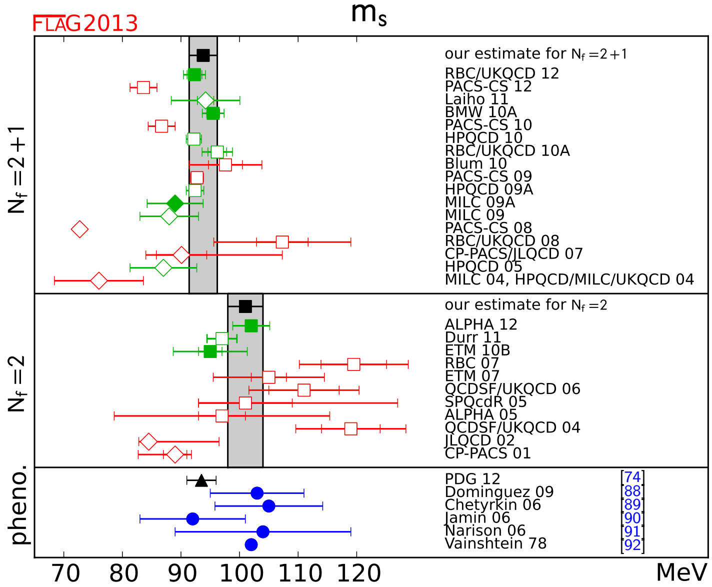

Figure 1: Mass of the strange quark ($\overline{\rm MS}$ scheme , running scale 2 GeV). The central and top panels show the lattice results listed in tables 2 and 3. For comparison, the bottom panel collects a few sum rule results and also indicates the current PDG estimate. Diamonds represent results based on perturbative renormalization, while squares indicate that, in the relation between the lattice regularized and renormalized $\overline{\rm MS}$ masses, nonperturbative effects are accounted for. The black squares and the grey bands represent our estimates (13) and (14). The significance of the colours is explained in section 2.

the continuum for the determination of m_c. To calculate m_{ud} HPQCD 10 [72] use the MILC 09 determination of the quark-mass ratio m_s/m_{ud} [15].

The high precision quoted by HPQCD 10 on the strange-quark mass relies in large part on the precision reached in the determination of the charm-quark mass [72, 85]. This calculation uses an approach based on the lattice determination of moments of charm-quark pseudoscalar, vector and axial-vector correlators. These moments are then combined with four-loop results from continuum perturbation theory to obtain a determination of the charm-quark mass in the $\overline{\rm MS}$ scheme . In the preferred case, in which pseudoscalar correlators are used for the analysis, there are no lattice renormalization factors required, since the corresponding axial-vector current is partially conserved in the staggered lattice formalism.

Instead of combining the result for m_c/m_s of [73] with m_c from [72], one can use it with the PDG 12 [74] average $m_c(m_c) = 1.275(25)\,\text{GeV}$, whose error is four times as large as the one obtained by HPQCD 10. If one does so, one obtains $m_s = 92.3(2.2)$ in lieu of the value $m_s = 92.2(1.3)$ given in Table 3, thereby nearly doubling HPQCD 10's error. Though we plan to do so in the future, we have not yet performed a review of lattice determinations of m_c. Thus, as for the results of Dürr 11 [61] in the $N_f = 2$ case, we postpone its inclusion in our final averages until we have performed an independent analysis of m_c, emphasizing that this

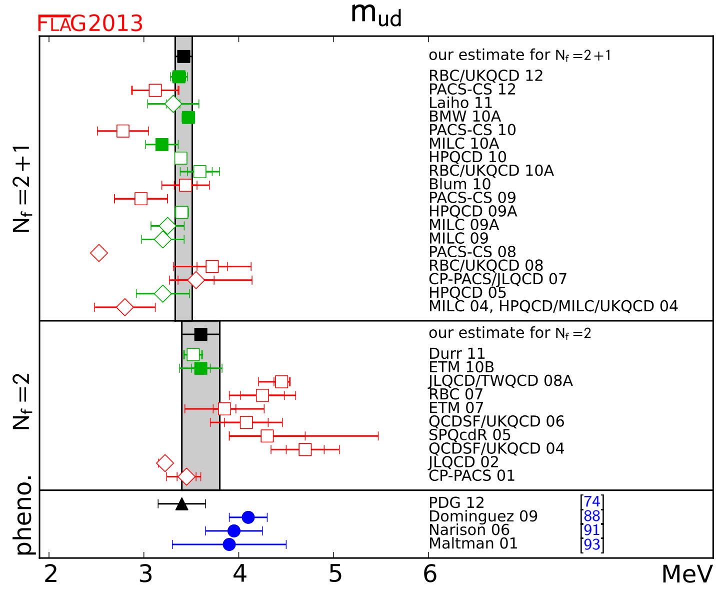

Figure 2: Mean mass of the two lightest quarks, $m_{ud} = \frac{1}{2}(m_u + m_d)$ (for details see Fig. 1).

novel strategy for computing the light-quark masses may very well turn out to be the best way to determine them.

This discussion leaves us with three results for our final average for m_s, those of MILC 09A [37], BMW 10A, 10B [22, 23] and RBC/UKQCD 12 [25], and the result of HPQCD 10 [72] as an important cross-check. Thus, we first check that the three other results which will enter our final average are consistent with HPQCD 10's result. To do this we implement the averaging procedure described in Sect. 2.2 on all four results. This yields $m_s = 93.0(1.0)$ MeV with a $\chi^2/dof = 3.0/3 = 1.0$, indicating overall consistency. Note that in making this average, we have accounted for correlations in the small statistical errors of HPQCD 10 and MILC 09A. Omitting HPQCD 10 in our final average results in an increase by 50% of the average's uncertainty and by 0.8 σ of its central value. Thus, we obtain $m_s = 93.8(1.5)$ MeV with a $\chi^2/dof = 2.26/2 = 1.13$. When repeating the exercise for m_{ud}, we replace MILC 09A by the more recent analysis reported in MILC 10A [75]. A fit of all four results yields $m_{ud} = 3.41(5)$ MeV with a $\chi^2/dof = 2.6/3 = 0.9$ and including only the same three as above gives $m_{ud} = 3.42(6)$ MeV with a $\chi^2/dof = 2.4/2 = 1.2$. Here the results are barely distinguishable, indicating full compatibility of all four results. Note that the outcome of the averaging procedure amounts to a determination of m_s and m_{ud} of 1.6%. and 1.8%, respectively.

The heavy sea-quarks affect the determination of the light-quark masses only through contributions of order $1/m_c^2$, which moreover are suppressed by the Okubo-Zweig-Iizuka-rule. We expect these contributions to be small, but do not know of a reliable quantitative evaluation. The problem originates in the fact that the relation between the parameters of QCD_3 and those of full QCD can currently be analyzed only in the framework of perturbation theory. The β- and γ-functions, which control the renormalization of the coupling constants and quark masses, respectively, are known to four loops [83, 84, 94, 95]. The precision achieved in this framework for the decoupling of the t- and b-quarks is excellent, but the c-quark is not heavy enough: at the percent level, the corrections of order $1/m_c^2$ cannot be neglected and the decoupling formulae of perturbation theory do not provide a reliable evaluation, because the scale $m_c(m_c) \simeq 1.28\,\mathrm{GeV}$ is too low for these formulae to be taken at face value. Consequently, the accuracy to which it is possible to identify the running masses of the light quarks of full QCD in terms of those occurring in QCD_3 is limited. For this reason, it is preferable to characterize the masses m_u, m_d, m_s in terms of QCD_4, where the connection with full QCD is under good control. The role of the c-quarks in the determination of the light-quark masses will soon be studied in detail – some simulations with 2+1+1 dynamical quarks have already been carried out [24, 96].

A crude upper bound on the size of the effects due to the neglected heavy quarks can be established within the $N_f = 2+1$ simulations themselves, without invoking perturbation theory. In [97] it is found that when the scale is set by M_Ξ, the result for M_Λ agrees well with experiment within the 2.3% accuracy of the calculation. Because of the very strong correlations between the statistical and systematic errors of these two masses, we expect the uncertainty in the difference $M_\Xi - M_\Lambda$ to also be of order 2%. To leading order in the chiral expansion this mass difference is proportional to $m_s - m_{ud}$. Barring accidental cancellations, we conclude that the agreement of $N_f = 2+1$ calculations with experiment suggests an upper bound on the sensitivity of m_s to heavy sea-quarks of order 2%.

Taking this uncertainty into account yields the following averages:

$$N_f = 2+1: \qquad m_{ud} = 3.42(6)(7)\ \mathrm{MeV}\,, \qquad m_s = 93.8(1.5)(1.9)\ \mathrm{MeV} \tag{14}$$

where the first error comes from the averaging of the lattice results, and the second is the one that we add to account for the neglect of sea effects from the charm and more massive quarks. This corresponds to determinations of m_{ud} and m_s with a precision of and 2.6% and 2.7%, respectively. These estimates represent the conclusions we draw from the information gathered on the lattice until now. They are shown as vertical bands in Figures 1 and 2, together with the $N_f = 2$ results (13).

In the ratio m_s/m_{ud}, one of the sources of systematic error – the uncertainties in the renormalization factors – drops out. Also, we can compare the lattice results with the leading-order formula of χPT,

$$\frac{m_s}{m_{ud}} \overset{\text{LO}}{=} \frac{\hat{M}^2_{K^+} + \hat{M}^2_{K^0} - \hat{M}^2_{\pi^+}}{\hat{M}^2_{\pi^+}}\,, \tag{15}$$

which relates the quantity m_s/m_{ud} to a ratio of meson masses in QCD. Expressing these in terms of the physical masses and the four coefficients introduced in (6)-(8), linearizing the result with respect to the corrections and inserting the observed mass values, we obtain

$$\frac{m_s}{m_{ud}} \overset{\text{LO}}{=} 25.9 - 0.1\,\epsilon + 1.9\,\epsilon_{\pi^0} - 0.1\,\epsilon_{K^0} - 1.8\,\epsilon_m\,. \tag{16}$$

If the coefficients ϵ, ϵ_{π^0}, ϵ_{K^0} and ϵ_m are set equal to zero, the right hand side reduces to the value $m_s/m_{ud} = 25.9$ that follows from Weinberg's leading-order formulae for m_u/m_d and m_s/m_d [98], in accordance with the fact that these do account for the e.m. interaction at leading order, but neglect the mass difference between the charged and neutral pions in QCD. Inserting the estimates (9), the LO prediction becomes

$$\frac{m_s}{m_{ud}} \overset{\text{LO}}{=} 25.9(1)\,. \tag{17}$$

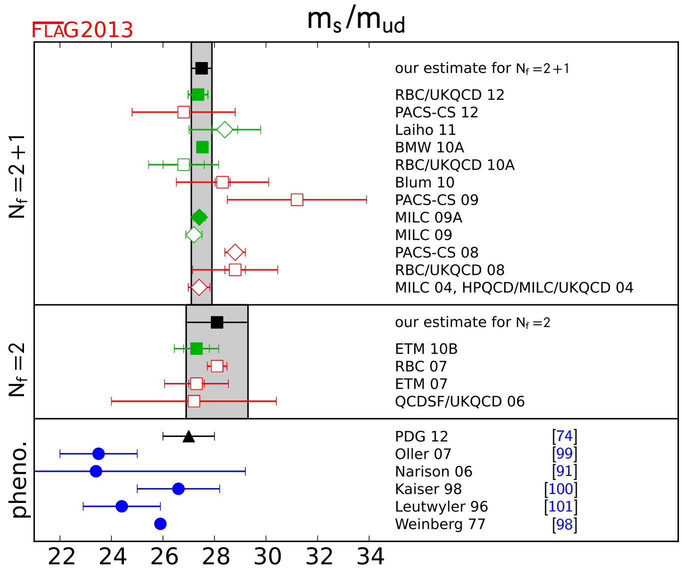

Figure 3: Results for the ratio m_s/m_{ud}. The upper part indicates the lattice results listed in Table 4. The lower part shows results obtained from χPT and sum rules, together with the current PDG estimate.

The quoted uncertainty does not include an estimate for the higher-order contributions, but only accounts for the error bars in the coefficients, which is dominated by the one in the estimate given for ϵ_{π^0}. The result shows that, despite the high accuracy reached in lattice determinations of the ratio m_s/m_{ud}, the uncertainties due to the electromagnetic corrections are still subdominant, but no longer irrelevant.

The lattice results in Table 4, which satisfy our selection criteria, indicate that the corrections generated by the nonleading terms of the chiral perturbation series are remarkably small, in the range 3–10%. Despite the fact that the SU(3)-flavour-symmetry breaking effects in the Nambu-Goldstone boson masses are very large ($M_K^2 \simeq 13\, M_\pi^2$), the mass spectrum of the pseudoscalar octet obeys the SU(3)×SU(3) formula (15) very well.

Our average for m_s/m_{ud} is based on the results of MILC 09A, BMW 10A, 10B and RBC/UKQCD 12 – the value quoted by HPQCD 10 does not represent independent information as it relies on the result for m_s/m_{ud} obtained by the MILC collaboration. Averaging these results according to the precription of Section 2.3 gives $m_s/m_{ud} = 27.46(15)$ with $\chi^2/dof = 0.2/2$. The fit is dominated by MILC 09A and BMW 10A, 10B. Since the errors associated with renormalization drop out in the ratio, the uncertainties are even smaller than in the case of the quark masses themselves: the above number for m_s/m_{ud} amounts to an accuracy of 0.5%.

At this level of precision, the uncertainties in the electromagnetic and strong isospin-breaking corrections are not completely negligible. The error estimate in the LO result (17) indicates the expected order of magnitude. The uncertainties in m_s and m_{ud} associated with the heavy sea-quarks cancel at least partly. In view of this, we ascribe a total 1.5% uncertainty to these two sources of error. Thus, we are convinced that our final estimate,

$$N_f = 2+1: \qquad \frac{m_s}{m_{ud}} = 27.46(15)(41)\,, \tag{18}$$

is on the conservative side, with a total 1.5% uncertainty. It is also fully consistent with the ratio computed from our individual quark masses in (14), $m_s/m_{ud} = 27.6(6)$, which has a larger 2.2% uncertainty. In (18) the first error comes from the averaging of the lattice results, and the second is the one that we add to account for the neglect of isospin-breaking and heavy sea-quark effects.

The lattice results show that the LO prediction of χPT in (17) receives only small corrections from higher orders of the chiral expansion: according to (18), these generate a shift of $5.7 \pm 1.5\%$. Our estimate does therefore not represent a very sharp determination of the higher-order contributions.

The ratio m_s/m_{ud} can also be extracted from the masses of the neutral Nambu-Goldstone bosons: neglecting effects of order $(m_u - m_d)^2$ also here, the leading-order formula reads $m_s/m_{ud} \overset{\rm LO}{=} \frac{3}{2}\hat{M}_\eta^2/\hat{M}_\pi^2 - \frac{1}{2}$. Numerically, this gives $m_s/m_{ud} \overset{\rm LO}{=} 24.2$. The relation has the advantage that the e.m. corrections are expected to be much smaller here, but it is more difficult to calculate the η-mass on the lattice. The comparison with (18) shows that, in this case, the contributions of NLO are somewhat larger: $14 \pm 2\%$.

3.4 Lattice determination of m_u and m_d

The determination of m_u and m_d separately requires additional input. MILC 09A [37] uses the mass difference between K^0 and K^+, from which they subtract electromagnetic effects using Dashen's theorem with corrections, as discussed in Section 3.1. The up- and down-sea-quarks remain degenerate in their calculation, fixed to the value of m_{ud} obtained from M_{π^0}.

To determine m_u/m_d, BMW 10A, 10B [22, 23] follow a slightly different strategy. They obtain this ratio from their result for m_s/m_{ud} combined with a phenomenological determination of the isospin-breaking quark-mass ratio $Q = 22.3(8)$, defined below in (24), from $\eta \to 3\pi$ decays [30] (the decay $\eta \to 3\pi$ is very sensitive to QCD isospin-breaking but fairly insensitive to QED isospin-breaking). As discussed in Section 3.5, the central value of the e.m. parameter ϵ in (9) is taken from the same source.

RM123 11 [102] actually uses the e.m. parameter $\epsilon = 0.7(5)$ from the first edition of the FLAG review [1]. However they estimate the effects of strong isospin-breaking at first nontrivial order, by inserting the operator $\frac{1}{2}(m_u - m_d)\int(\bar{u}u - \bar{d}d)$ into correlation functions, while performing the gauge averages in the isospin limit. Applying these techniques, they obtain $(\hat{M}^2_{K^0} - \hat{M}^2_{K^+})/(m_d - m_u) = 2.57(8)\,\mathrm{MeV}$. Combining this result with the phenomenological $(\hat{M}^2_{K^0} - \hat{M}^2_{K^+}) = 6.05(63) \times 10^3$ determined with the above value of ϵ, they get $(m_d - m_u) = 2.35(8)(24)\,\mathrm{MeV}$, where the first error corresponds to the lattice statistical and systematic uncertainties combined in quadrature, while the second arises from the uncertainty on ϵ. Note that below we quote results from RM123 11 for m_u, m_d and m_u/m_d. As described in Table 5, we obtain them by combining RM123 11's result for $(m_d - m_u)$ with ETM 10B's result for m_{ud}.

Collaboration	Ref.	publication status	chiral extrapolation	continuum extrapolation	finite volume	renormalization	running	m_u	m_d	m_u/m_d
PACS-CS 12⋆	[76]	A	★	■	■	★	*a*	2.57(26)(7)	3.68(29)(10)	0.698(51)
Laiho 11	[77]	C	○	★	★	○	–	1.90(8)(21)(10)	4.73(9)(27)(24)	0.401(13)(45)
HPQCD 10‡	[72]	A	○	★	★	★	–	2.01(14)	4.77(15)	
BMW 10A, 10B+	[22, 23]	A	★	★	★	★	*b*	2.15(03)(10)	4.79(07)(12)	0.448(06)(29)
Blum 10†	[32]	A	○	■	○	★	–	2.24(10)(34)	4.65(15)(32)	0.4818(96)(860)
MILC 09A	[37]	C	○	★	★	○	–	1.96(0)(6)(10)(12)	4.53(1)(8)(23)(12)	0.432(1)(9)(0)(39)
MILC 09	[15]	A	○	★	★	○	–	1.9(0)(1)(1)(1)	4.6(0)(2)(2)(1)	0.42(0)(1)(0)(4)
MILC 04, HPQCD/ MILC/UKQCD 04	[36, 82]	A	○	○	○	■	–	1.7(0)(1)(2)(2)	3.9(0)(1)(4)(2)	0.43(0)(1)(0)(8)
RM123 13	[45]	A	○	★	○	★	*c*	2.40(15)(17)	4.80 (15)(17)	0.50(2)(3)
RM123 11⊕	[102]	A	○	★	○	★	*c*	*2.43(11)(23)*	*4.78(11)(23)*	*0.51(2)(4)*
Dürr 11*	[61]	A	○	★	○	–	–	2.18(6)(11)	4.87(14)(16)	
RBC 07†	[34]	A	■	■	★	★	–	3.02(27)(19)	5.49(20)(34)	0.550(31)

⋆ The calculation includes e.m. and $m_u \neq m_d$ effects through reweighting.
‡ Values obtained by combining the HPQCD 10 result for m_s with the MILC 09 results for m_s/m_{ud} and m_u/m_d.
+ The fermion action used is tree-level improved.
* Values obtained by combining the Dürr 11 result for m_s with the BMW 10A, 10B results for m_s/m_{ud} and m_u/m_d.
⊕ m_u, m_d and m_u/m_d are obtained by combining the result of RM123 11 for $(m_d - m_u)$ [102] with $m_{ud} = 3.6(2)$ MeV from ETM 10B. $(m_d - m_u) = 2.35(8)(24)$ MeV in [102] was obtained assuming $\epsilon = 0.7(5)$ [1] and $\epsilon_m = \epsilon_{\pi^0} = \epsilon_{K^0} = 0$. In the quoted results, the first error corresponds to the lattice statistical and systematic errors combined in quadrature, while the second arises from the uncertainties associated with ϵ.
† The calculation includes quenched e.m. effects.
a The masses are renormalized and run nonperturbatively up to a scale of 100 GeV in the $N_f = 2$ SF scheme. In this scheme, nonperturbative and NLO running for the quark masses are shown to agree well from 100 GeV all the way down to 2 GeV [64].
b The masses are renormalized and run nonperturbatively up to a scale of 4 GeV in the $N_f = 3$ RI/MOM scheme. In this scheme, nonperturbative and N^{3}LO running for the quark masses are shown to agree from 6 GeV down to 3 GeV to better than 1% [23].
c The masses are renormalized nonperturbatively at scales $1/a \sim 2 \div 3$ GeV in the $N_f = 2$ RI/MOM scheme. In this scheme, nonperturbative and N^{3}LO running for the quark masses are shown to agree from 4 GeV down 2 GeV to better than 3% [71].

Table 5: Lattice results for m_u, m_d (MeV) and for the ratio m_u/m_d. The values refer to the $\overline{\rm MS}$ scheme at scale 2 GeV. The upper part of the table lists results obtained with $N_f = 2+1$, while the lower part presents calculations with $N_f = 2$.

Instead of subtracting electromagnetic effects using phenomenology, RBC 07 [34] and Blum 10 [32] actually include a quenched electromagnetic field in their calculation. This means that their results include corrections to Dashen's theorem, albeit only in the presence of quenched electromagnetism. Since the up- and down-quarks in the sea are treated as degenerate, very small isospin corrections are neglected, as in MILC's calculation.

PACS-CS 12 [76] takes the inclusion of isospin-breaking effects one step further. Using reweighting techniques, it also includes electromagnetic and $m_u - m_d$ effects in the sea.

Lattice results for m_u, m_d and m_u/m_d are summarized in Table 5. In order to discuss them, we consider the LO formula

$$\frac{m_u}{m_d} \overset{\rm LO}{=} \frac{\hat{M}^2_{K^+} - \hat{M}^2_{K^0} + \hat{M}^2_{\pi^+}}{\hat{M}^2_{K^0} - \hat{M}^2_{K^+} + \hat{M}^2_{\pi^+}} \,. \tag{19}$$

Using equations (6)–(8) to express the meson masses in QCD in terms of the physical ones and linearizing in the corrections, this relation takes the form

$$\frac{m_u}{m_d} \overset{\rm LO}{=} 0.558 - 0.084\,\epsilon - 0.02\,\epsilon_{\pi^0} + 0.11\,\epsilon_m \,. \tag{20}$$

Inserting the estimates (9) and adding errors in quadrature, the LO prediction becomes

$$\frac{m_u}{m_d} \overset{\rm LO}{=} 0.50(3) \,. \tag{21}$$

Again, the quoted error exclusively accounts for the errors attached to the estimates (9) for the epsilons – contributions of nonleading order are ignored. The uncertainty in the leading-order prediction is dominated by the one in the coefficient ϵ, which specifies the difference between the meson squared-mass splittings generated by the e.m. interaction in the kaon and pion multiplets. The reduction in the error on this coefficient since the previous review [1] results in a reduction of a factor of a little less than 2 in the uncertainty on the LO value of m_u/m_d given in (21).

It is interesting to compare the assumptions made or results obtained by the different collaborations for the violation of Dashen's theorem. The input used in MILC 09A is $\epsilon = 1.2(5)$ [37], while the $N_f = 2$ computation of RM123 13 finds $\epsilon = 0.79(18)(18)$ [45]. As discussed in Section 3.5, the value of Q used by BMW 10A, 10B [22, 23] gives $\epsilon = 0.70(28)$ at NLO (see (31)). On the other hand, RBC 07 [34] and Blum 10 [32] obtain the results $\epsilon = 0.13(4)$ and $\epsilon = 0.5(1)$. Note that PACS-CS 12 [76] do not provide results which allow us to determine ϵ directly. However, using their result for m_u/m_d, together with (20), and neglecting NLO terms, one finds $\epsilon = -1.6(6)$, which is difficult to reconcile with what is known from phenomenology (see Sections 3.1 and 3.5). Since the values assumed or obtained for ϵ differ, it does not come as a surprise that the determinations of m_u/m_d are different.

These values of ϵ are also interesting because they allow us to estimate the chiral corrections to the LO prediction (21) for m_u/m_d. Indeed, evaluating the relation (20) for the values of ϵ given above, and neglecting all other corrections in this equation, yields the LO values $(m_u/m_d)^{\rm LO} = 0.46(4)$, 0.547(3), 0.52(1), 0.50(2), 0.49(2) for MILC 09A, RBC 07, Blum 10, BMW 10A, 10B and RM123 13, respectively. However, in comparing these numbers to the nonperturbative results of Table 5 one must be careful not to double count the uncertainty arising from ϵ. One way to obtain a sharp comparison is to consider the ratio of the results of Table 5 to the LO values $(m_u/m_d)^{\rm LO}$, in which the uncertainty from ϵ cancels to good accuracy. Here we will assume for simplicity that they cancel completely and will drop all uncertainties related to ϵ. For $N_f = 2$ we consider RM123 13 [45], which updates RM123 11 and has no red dots. Since the uncertainties common to ϵ and m_u/m_d are not explicitly given in [45], we have to estimate them. For that we use the leading-order result for m_u/m_d, computed with RM123 13's value for ϵ. Its error bar is the contribution of the uncertainty on ϵ to $(m_u/m_d)^{\rm LO}$. To good approximation this contribution will be the same for the value of m_u/m_d computed in [45]. Thus, we subtract it in quadrature from RM123 13's result in Table 5 and compute $(m_u/m_d)/(m_u/m_d)^{\rm LO}$, dropping uncertainties related to ϵ. We find

$(m_u/m_d)/(m_u/m_d)^{\rm LO} = 1.02(6)$. This result suggests that chiral corrections in the case of $N_f = 2$ are negligible. For the two most accurate $N_f = 2+1$ calculations, those of MILC 09A and BMW 10A, 10B, this ratio of ratios is 0.94(2) and 0.90(1), respectively. Though these two numbers are not fully consistent within our rough estimate of the errors, they indicate that higher-order corrections to (21) are negative and about 8% when $N_f = 2+1$. In the following, we will take them to be -8(4)%. The fact that these corrections are seemingly larger and of opposite sign than in the $N_f = 2$ case is not understood at this point. It could be an effect associated with the quenching of the strange quark. It could also be due to the fact that the RM123 13 calculation does not probe deeply enough into the chiral regime–it has $M_\pi \gtrsim 270\,\mathrm{MeV}$–to pick up on important chiral corrections. Of course, being less than a two standard deviation effect, it may be that there is no problem at all and that differences from the LO result are actually small.

Given the exploratory nature of the RBC 07 calculation, its results do not allow us to draw solid conclusions about the e.m. contributions to m_u/m_d for $N_f = 2$. As discussed in Section 3.3.2, the $N_f = 2+1$ results of Blum 10 and PACS-CS 12 do not pass our selection criteria either. We therefore resort to the phenomenological estimates of the electromagnetic self-energies discussed in Section 3.1, which are validated by recent, preliminary lattice results.

Since RM123 13 [45] includes a lattice estimate of e.m. corrections, for the $N_f = 2$ final results we simply quote the values of m_u, m_d, and m_u/m_d from RM123 13 given in Table 5:

$$N_f = 2: \quad m_u = 2.40(23)\,\mathrm{MeV}\,, \quad m_d = 4.80(23)\,\mathrm{MeV}\,, \quad \frac{m_u}{m_d} = 0.50(4)\,, \tag{22}$$

with errors of roughly 10%, 5% and 8%, respectively. In these results, the errors are obtained by combining the lattice statistical and systematic errors in quadrature.

For $N_f = 2+1$ there is to date no final, published computation of e.m. corrections. Thus, we take the LO estimate for m_u/m_d of (21) and use the -8(4)% obtained above as an estimate of the size of the corrections from higher orders in the chiral expansion. This gives $m_u/m_d = 0.46(3)$. The two individual masses can then be worked out from the estimate (14) for their mean. Therefore, for $N_f = 2+1$ we obtain:

$$N_f = 2+1: \quad m_u = 2.16(9)(7)\,\mathrm{MeV}\,, \quad m_d = 4.68(14)(7)\,\mathrm{MeV}\,, \quad \frac{m_u}{m_d} = 0.46(2)(2)\,. \tag{23}$$

In these results, the first error represents the lattice statistical and systematic errors, combined in quadrature, while the second arises from the uncertainties associated with e.m. corrections of (9). The estimates in (23) have uncertainties of order 5%, 3% and 7%, respectively.

Naively propagating errors to the end, we obtain $(m_u/m_d)_{N_f=2}/(m_u/m_d)_{N_f=2+1} = 1.09(10)$. If instead of (22) we use the results from RM123 11, modified by the e.m. corrections in (9), as was done in our previous review, we obtain $(m_u/m_d)_{N_f=2}/(m_u/m_d)_{N_f=2+1} = 1.11(7)(1)$, confirming again the strong cancellation of e.m. uncertainties in the ratio. The $N_f = 2$ and $2+1$ results are compatible at the 1 to 1.5 σ level.

It is interesting to note that in the results above, the errors are no longer dominated by the uncertainties in the input used for the electromagnetic corrections, though these are still significant at the level of precision reached in the $N_f = 2+1$ results. This is due to the reduction in the error on ϵ discussed in Section 3.1. Nevertheless, the comparison of equations (21) and (23) indicates that more than half of the difference between the prediction $m_u/m_d = 0.558$ obtained from Weinberg's mass formulae [98] and the result for m_u/m_d obtained on the lattice stems from electromagnetism, the higher orders in the chiral perturbation generating a comparable correction.

In view of the fact that a *massless up-quark* would solve the strong CP-problem, many authors have considered this an attractive possibility, but the results presented above exclude this possibility: the value of m_u in (23) differs from zero by 20 standard deviations. We conclude that nature solves the strong CP-problem differently. This conclusion relies on lattice calculations of kaon masses and on the phenomenological estimates of the e.m. self-energies discussed in Section 3.1. The uncertainties therein currently represent the limiting factor in determinations of m_u and m_d. As demonstrated in [32–34, 40–44, 50], lattice methods can be used to calculate the e.m. self-energies. Further progress on the determination of the light-quark masses hinges on an improved understanding of the e.m. effects.

3.5 Estimates for R and Q

The quark-mass ratios

$$R \equiv \frac{m_s - m_{ud}}{m_d - m_u} \quad \text{and} \quad Q^2 \equiv \frac{m_s^2 - m_{ud}^2}{m_d^2 - m_u^2} \tag{24}$$

compare SU(3)-breaking with isospin-breaking. The quantity Q is of particular interest because of a low energy theorem [103], which relates it to a ratio of meson masses,

$$Q_M^2 \equiv \frac{\hat{M}_K^2}{\hat{M}_\pi^2} \cdot \frac{\hat{M}_K^2 - \hat{M}_\pi^2}{\hat{M}_{K^0}^2 - \hat{M}_{K^+}^2}\,, \qquad \hat{M}_\pi^2 \equiv \tfrac{1}{2}(\hat{M}_{\pi^+}^2 + \hat{M}_{\pi^0}^2)\,, \qquad \hat{M}_K^2 \equiv \tfrac{1}{2}(\hat{M}_{K^+}^2 + \hat{M}_{K^0}^2)\,. \tag{25}$$

Chiral symmetry implies that the expansion of Q_M^2 in powers of the quark masses (i) starts with Q^2 and (ii) does not receive any contributions at NLO:

$$Q_M \overset{\text{NLO}}{=} Q\,. \tag{26}$$

Inserting the estimates for the mass ratios m_s/m_{ud}, and m_u/m_d given for $N_f = 2$ in equations (13) and (22) respectively, we obtain

$$R = 40.7(3.7)(2.2)\,, \qquad Q = 24.3(1.4)(0.6)\ , \tag{27}$$

where the errors have been propagated naively and the e.m. uncertainty has been separated out, as discussed in the third paragraph after (21). Thus, the meaning of the errors is the same as in (23). These numbers agree within errors with those reported in [45] where values for m_s and m_{ud} are taken from ETM 10B [60].

For $N_f = 2 + 1$, we use equations (18) and (23) and obtain

$$R = 35.8(1.9)(1.8)\,, \qquad Q = 22.6(7)(6)\ , \tag{28}$$

where the meaning of the errors is the same as above. The $N_f = 2$ and $N_f = 2+1$ results are compatible within 2σ, even taking the correlations between e.m. effects into account.

It is interesting to use these results to study the size of chiral corrections in the relations of R and Q to their expressions in terms of meson masses. To investigate this issue, we use χPT to express the quark-mass ratios in terms of the pion and kaon masses in QCD and then again use equations (6)–(8) to relate the QCD masses to the physical ones. Linearizing in the corrections, this leads to

$$R \stackrel{\text{LO}}{=} R_M = 43.9 - 10.8\,\epsilon + 0.2\,\epsilon_{\pi^0} - 0.2\,\epsilon_{K^0} - 10.7\,\epsilon_m\,, \tag{29}$$

$$Q \stackrel{\text{NLO}}{=} Q_M = 24.3 - 3.0\,\epsilon + 0.9\,\epsilon_{\pi^0} - 0.1\,\epsilon_{K^0} + 2.6\,\epsilon_m\,. \tag{30}$$

While the first relation only holds to LO of the chiral perturbation series, the second remains valid at NLO, on account of the low energy theorem mentioned above. The first terms on the right hand side represent the values of R and Q obtained with the Weinberg leading-order formulae for the quark-mass ratios [98]. Inserting the estimates (9), we find that the e.m. corrections lower the Weinberg values to $R_M = 36.7(3.3)$ and $Q_M = 22.3(9)$, respectively.

Comparison of R_M and Q_M with the full results quoted above gives a handle on higher-order terms in the chiral expansion. Indeed, the ratios R_M/R and Q_M/Q give NLO and NNLO (and higher) corrections to the relations $R \stackrel{\text{LO}}{=} R_M$ and $Q \stackrel{\text{NLO}}{=} Q_M$, respectively. The uncertainties due to the use of the e.m. corrections of (9) are highly correlated in the numerators and denominators of these ratios, and we make the simplifying assumption that they cancel in the ratio. Thus, for $N_f = 2$ we evaluate (29) and (30) using $\epsilon = 0.79(18)(18)$ from RM123 13 [45] and the other corrections from (9), dropping all uncertainties. We divide them by the results for R and Q in (27), omitting the uncertainties due to e.m. We obtain $R_M/R \simeq 0.88(8)$ and $Q_M/Q \simeq 0.91(5)$. We proceed analogously for $N_f = 2+1$, using $\epsilon = 0.70(3)$ from (9) and R and Q from (28), and find $R_M/R \simeq 1.02(5)$ and $Q_M/Q \simeq 0.99(3)$. The chiral corrections appear to be small for $N_f = 2+1$, especially those in the relation of Q to Q_M. This is less true for $N_f = 2$, where the NNLO and higher corrections to $Q = Q_M$ could be significant. However, as for other quantities which depend on m_u/m_d, this difference is not significant.

As mentioned in Section 3.1, there is a phenomenological determination of Q based on the decay $\eta \to 3\pi$ [104, 105]. The key point is that the transition $\eta \to 3\pi$ violates isospin-conservation. The dominating contribution to the transition amplitude stems from the mass difference $m_u - m_d$. At NLO of χPT, the QCD part of the amplitude can be expressed in a parameter free manner in terms of Q. It is well-known that the electromagnetic contributions to the transition amplitude are suppressed (a thorough recent analysis is given in [106]). This implies that the result for Q is less sensitive to the electromagnetic uncertainties than the value obtained from the masses of the Nambu-Goldstone bosons. For a recent update of this determination and for further references to the literature, we refer to [107]. Using dispersion theory to pin down the momentum-dependence of the amplitude, the observed decay rate implies $Q = 22.3(8)$ (since the uncertainty quoted in [107] does not include an estimate for all sources of error, we have retained the error estimate given in [101], which is twice as large). The formulae for the corrections of NNLO are available also in this case [108] – the poor knowledge of the effective coupling constants, particularly of those that are relevant for the dependence on the quark masses, is currently the limiting factor encountered in the application of these formulae.

As was to be expected, the central value of Q obtained from η-decay agrees exactly with the central value obtained from the low energy theorem: we have used that theorem to estimate the coefficient ϵ, which dominates the e.m. corrections. Using the numbers for ϵ_m, ϵ_{π^0} and ϵ_{K^0} in (9) and adding the corresponding uncertainties in quadrature to those in the phenomenological result for Q, we obtain

$$\epsilon \overset{\text{NLO}}{=} 0.70(28)\,. \tag{31}$$

The estimate (9) for the size of the coefficient ϵ is taken from here, as it is confirmed by the most recent, preliminary lattice determinations [40–45].

Our final results for the masses m_u, m_d, m_{ud}, m_s and the mass ratios m_u/m_d, m_s/m_{ud}, R, Q are collected in Tables 6 and 7. We separate m_u, m_d, m_u/m_d, R and Q from m_{ud}, m_s and m_s/m_{ud}, because the latter are completely dominated by lattice results while the former still include some phenomenological input.

N_f	m_{ud}	m_s	m_s/m_{ud}
2+1	3.42(6)(7)	93.8(1.5)(1.9)	27.46(15)(41)
2	3.6(2)	101(3)	28.1(1.2)

Table 6: Our estimates for the strange and the average up-down quark masses in the $\overline{\text{MS}}$ scheme at running scale $\mu = 2\,\text{GeV}$ for $N_f = 3$. Numerical values are given in MeV. In the results presented here, the first error is the one which we obtain by applying the averaging procedure of Section 2.2 to the relevant lattice results. We have added an uncertainty to the $N_f = 2+1$ results, which is associated with the neglect of heavy sea-quark and isospin-breaking effects, as discussed around (14) and (18). This uncertainty is not included in the $N_f = 2$ results, as it should be smaller than the uncontrolled systematic associated with the neglect of strange sea-quark effects.

N_f	m_u	m_d	m_u/m_d	R	Q
2+1	2.16(11)	4.68(14)(7)	0.46(2)(2)	35.8(1.9)(1.8)	22.6(7)(6)
2	2.40(23)	4.80(23)	0.50(4)	40.7(3.7)(2.2)	24.3(1.4)(0.6)

Table 7: Our estimates for the masses of the two lightest quarks and related, strong isospin-breaking ratios. Again, the masses refer to the $\overline{\text{MS}}$ scheme at running scale $\mu = 2\,\text{GeV}$ for $N_f = 3$ and the numerical values are given in MeV. In the results presented here, the first error is the one that comes from lattice computations while the second for $N_f = 2+1$ is associated with the phenomenological estimate of e.m. contributions, as discussed after (23). The second error on the $N_f = 2$ results for R and Q is also an estimate of the e.m. uncertainty, this time associated with the lattice computation of [45], as explained after (27). We present these results in a separate table, because they are less firmly established than those in Table 6. For $N_f = 2+1$ they still include information coming from phenomenology, in particular on e.m. corrections, and for $N_f = 2$ the e.m. contributions are computed neglecting the feedback of sea-quarks on the photon field.

4 Leptonic and semileptonic kaon and pion decay and $|V_{ud}|$ and $|V_{us}|$

This section summarizes state of the art lattice calculations of the leptonic kaon and pion decay constants and kaon the semileptonic decay form factor and provides an analysis in view of the Standard Model. With respect to the previous edition of the FLAG review [1] the data in this section has been updated, correlations of lattice data are now taken into account in all the analysis and a subsection on the individual decay constants f_K and f_π (rather than only the ratio) has been included. Furthermore, when combining lattice data with experimental results we now take into account the strong SU(2) isospin correction in chiral perturbation theory for the ratio of leptonic decay constants f_K/f_π.

4.1 Experimental information concerning $|V_{ud}|$, $|V_{us}|$, $f_+(0)$ and $f_{K^\pm}/f_{\pi^\pm}$

The following review relies on the fact that precision experimental data on kaon decays very accurately determine the product $|V_{us}|f_+(0)$ and the ratio $|V_{us}/V_{ud}|f_{K^\pm}/f_{\pi^\pm}$ [109]:

$$|V_{us}|f_+(0) = 0.2163(5)\,, \qquad \left|\frac{V_{us}}{V_{ud}}\right|\frac{f_{K^\pm}}{f_{\pi^\pm}} = 0.2758(5)\,. \tag{32}$$

Here and in the following $f_{K^\pm}$ and $f_{\pi^\pm}$ are the isospin-broken decay constants, respectively, in QCD (the electromagnetic effects have already been subtracted in the experimental analysis using chiral perturbation theory). We will refer to the decay constants in the SU(2) isospin-symmetric limit as f_K and f_π. $|V_{ud}|$ and $|V_{us}|$ are elements of the Cabibbo-Kobayashi-Maskawa matrix and $f_+(t)$ represents one of the form factors relevant for the semileptonic decay $K^0 \to \pi^-\ell\,\nu$, which depends on the momentum transfer t between the two mesons. What matters here is the value at $t = 0$: $f_+(0) \equiv f_+^{K^0\pi^-}(t)\big|_{t\to 0}$. The pion and kaon decay constants are defined by[8]

$$\langle 0|\,\bar{d}\gamma_\mu\gamma_5\,u|\pi^+(p)\rangle = i\,p_\mu f_{\pi^+}\,, \qquad \langle 0|\,\bar{s}\gamma_\mu\gamma_5\,u|K^+(p)\rangle = i\,p_\mu f_{K^+}\,.$$

In this normalization, $f_{\pi^\pm} \simeq 130$ MeV, $f_{K^\pm} \simeq 155$ MeV.

The measurement of $|V_{ud}|$ based on superallowed nuclear β transitions has now become remarkably precise. The result of the update of Hardy and Towner [112], which is based on 20 different superallowed transitions, reads[9]

$$|V_{ud}| = 0.97425(22)\,. \tag{33}$$

The matrix element $|V_{us}|$ can be determined from semiinclusive τ decays [119–122]. Separating the inclusive decay $\tau \to \text{hadrons} + \nu$ into nonstrange and strange final states, e.g.

[8]The pion decay constant represents a QCD matrixelement – in the full Standard Model, the one-pion state is not a meaningful notion: the correlation function of the charged axial current does not have a pole at $p^2 = M_{\pi^+}^2$, but a branch cut extending from $M_{\pi^+}^2$ to ∞. The analytic properties of the correlation function and the problems encountered in the determination of f_π are thoroughly discussed in [110]. The "experimental" value of f_π depends on the convention used when splitting the sum $\mathcal{L}_{\rm QCD} + \mathcal{L}_{\rm QED}$ into two parts (compare section 3.1). The lattice determinations of f_π do not yet reach the accuracy where this is of significance, but at the precision claimed by the Particle Data Group [111], the numerical value does depend on the convention used [27–29, 110].

[9]It is not a trivial matter to perform the data analysis at this precision. In particular, isospin-breaking effects need to be properly accounted for [113–117]. For a review of recent work on this issue, we refer to [118].

HFAG 12 [123] obtain

$$|V_{us}| = 0.2173(22)\,. \tag{34}$$

Maltman et al. [121, 124, 125] and Gamiz et al. [126, 127] arrive at very similar values.

In principle, τ decay offers a clean measurement of $|V_{us}|$, but a number of open issues yet remain to be clarified. In particular, the value of $|V_{us}|$ as determined from inclusive τ decays differs from the result one obtains from assuming three-flavour SM-unitarity by more than three standard deviations [123]. It is important to understand this apparent tension better. The most interesting possibility is that τ decay involves new physics, but more work both on the theoretical (see e.g.[128–131]) and experimental side is required.

The experimental results in equation (32) are for the semileptonic decay of a neutral kaon into a negatively charged pion and the charged pion and kaon leptonic decays, respectively, in QCD. In the case of the semileptonic decays the corrections for strong and electromagnetic isospin breaking in chiral perturbation theory at NLO have allowed for averaging the different experimentally measured isospin channels [109]. This is quite a convenient procedure as long as lattice QCD does not include strong or QED isospin-breaking effects. Lattice results for f_K/f_π are typically quoted for QCD with (squared) pion and kaon masses of $M_\pi^2 = M_{\pi^0}^2$ and $M_K^2 = \frac{1}{2}\left(M_{K^\pm}^2 + M_{K^0}^2 - M_{\pi^\pm}^2 + M_{\pi^0}^2\right)$ for which the leading strong and electromagnetic isospin violations cancel. While progress is being made for including strong and electromagnetic isospin breaking in the simulations (e.g. [19, 86, 102, 132]), for now contact to experimental results is made by correcting leading SU(2) isospin breaking guided by chiral perturbation theory.

In the following we will start by presenting the lattice results for isospin-symmetric QCD. For any Standard Model analysis based on these results we then utilize chiral perturbation theory to correct for the leading isospin-breaking effects.

4.2 Lattice results for $f_+(0)$ and f_K/f_π

The traditional way of determining $|V_{us}|$ relies on using theory for the value of $f_+(0)$, invoking the Ademollo-Gatto theorem [143]. Since this theorem only holds to leading order of the expansion in powers of m_u, m_d and m_s, theoretical models are used to estimate the corrections. Lattice methods have now reached the stage where quantities like $f_+(0)$ or f_K/f_π can be determined to good accuracy. As a consequence, the uncertainties inherent in the theoretical estimates for the higher order effects in the value of $f_+(0)$ do not represent a limiting factor any more and we shall therefore not invoke those estimates. Also, we will use the experimental results based on nuclear β decay and τ decay exclusively for comparison – the main aim of the present review is to assess the information gathered with lattice methods and to use it for testing the consistency of the SM and its potential to provide constraints for its extensions.

The database underlying the present review of the semileptonic form factor and the ratio of decay constants is listed in Tables 8 and 9. The properties of the lattice data play a crucial role for the conclusions to be drawn from these results: range of M_π, size of LM_π, continuum extrapolation, extrapolation in the quark masses, finite size effects, etc. The key features of the various data sets are characterized by means of the colour code specified in section 2.1. More detailed information on individual computations are compiled in appendix B.2.

The quantity $f_+(0)$ represents a matrix element of a strangeness changing null plane charge, $f_+(0) = (K|Q^{us}|\pi)$. The vector charges obey the commutation relations of the Lie algebra of SU(3), in particular $[Q^{us}, Q^{su}] = Q^{uu-ss}$. This relation implies the sum rule

Collaboration	Ref.	N_f	publication status	chiral extrapolation	continuum extrapolation	finite volume errors	$f_+(0)$
MILC 12	[133]	2+1	P	○	○	★	0.9667(23)(33)
JLQCD 12	[134]	2+1	C	○	■	★	0.959(6)(5)
JLQCD 11	[135]	2+1	C	○	■	★	0.964(6)
RBC/UKQCD 10	[136]	2+1	A	○	■	★	$0.9599(34)(^{+31}_{-47})(14)$
RBC/UKQCD 07	[137]	2+1	A	○	■	★	0.9644(33)(34)(14)
ETM 10D	[138]	2	C	○	★	○	$0.9544(68)_{stat}$
ETM 09A	[139]	2	A	○	○	○	0.9560(57)(62)
QCDSF 07	[140]	2	C	■	■	★	$0.9647(15)_{stat}$
RBC 06	[141]	2	A	■	■	★	0.968(9)(6)
JLQCD 05	[142]	2	C	■	■	★	0.967(6), 0.952(6)

Table 8: Colour code for the data on $f_+(0)$.

$\sum_n |(K|Q^{us}|n)|^2 - \sum_n |(K|Q^{su}|n)|^2 = 1$. Since the contribution from the one-pion intermediate state to the first sum is given by $f_+(0)^2$, the relation amounts to an exact representation for this quantity [144]:

$$f_+(0)^2 = 1 - \sum_{n\neq\pi} |(K|Q^{us}|n)|^2 + \sum_n |(K|Q^{su}|n)|^2 \,. \tag{35}$$

While the first sum on the right extends over nonstrange intermediate states, the second runs over exotic states with strangeness ± 2 and is expected to be small compared to the first.

The expansion of $f_+(0)$ in SU(3) chiral perturbation theory in powers of m_u, m_d and m_s starts with $f_+(0) = 1 + f_2 + f_4 + \ldots$ [56]. Since all of the low energy constants occurring in f_2 can be expressed in terms of M_π, M_K, M_η and f_π [145], the NLO correction is known. In the language of the sum rule (35), f_2 stems from nonstrange intermediate states with three mesons. Like all other nonexotic intermediate states, it lowers the value of $f_+(0)$: $f_2 = -0.023$ when using the experimental value of f_π as input. The corresponding expressions have also been derived in quenched or partially quenched (staggered) chiral perturbation theory [133, 146]. At the same order in the SU(2) expansion [147], $f_+(0)$ is parameterized in terms of M_π and two *a priori* unknown parameters. The latter can be determined from the dependence of the lattice results on the masses of the quarks. Note that any calculation that relies on the χPT formula for f_2 is subject to the uncertainties inherent in NLO results: instead of using the physical value of the pion decay constant f_π, one may, for instance, work with the constant f_0 that occurs in the effective Lagrangian and represents the value of f_π in the chiral limit. Although trading f_π for f_0 in the expression for the NLO term affects the result only at NNLO, it may make a significant numerical difference in calculations where the latter are not explicitly accounted for (the lattice results concerning the value of the ratio f_π/f_0 are reviewed in section 5.2).

Collaboration	Ref.	N_f	publication status	chiral extrapolation	continuum extrapolation	finite volume errors	f_K/f_π	$f_{K^\pm}/f_{\pi^\pm}$
HPQCD 13A	[148]	2+1+1	P	★	○	★		1.1916(15)(16)
MILC 13A	[149]	2+1+1	A	★	○	★		1.1947(26)(37)
MILC 11	[24]	2+1+1	C	○	○	○		$1.1872(42)^{\dagger}_{\rm stat.}$
ETM 10E	[150]	2+1+1	C	○	○	○	$1.224(13)_{\rm stat}$	
RBC/UKQCD 12	[25]	2+1	A	★	○	★	1.199(12)(14)	
Laiho 11	[77]	2+1	C	○	○	○		$1.202(11)(9)(2)(5)^{\dagger\dagger}$
MILC 10	[151]	2+1	C	○	★	★		$1.197(2)(^{+3}_{-7})$
JLQCD/TWQCD 10	[152]	2+1	C	○	■	★	1.230(19)	
RBC/UKQCD 10A	[78]	2+1	A	○	○	★	1.204(7)(25)	
PACS-CS 09	[20]	2+1	A	★	■	■	1.333(72)	
BMW 10	[153]	2+1	A	★	★	★	1.192(7)(6)	
JLQCD/TWQCD 09A	[154]	2+1	C	○	■	■	$1.210(12)_{\rm stat}$	
MILC 09A	[37]	2+1	C	○	★	★		$1.198(2)(^{+6}_{-8})$
MILC 09	[15]	2+1	A	○	★	★		$1.197(3)(^{+6}_{-13})$
Aubin 08	[155]	2+1	C	○	○	○		1.191(16)(17)
PACS-CS 08, 08A	[19, 156]	2+1	A	★	■	■	1.189(20)	
RBC/UKQCD 08	[79]	2+1	A	○	■	★	1.205(18)(62)	
HPQCD/UKQCD 07	[157]	2+1	A	○	★	○	1.189(2)(7)	
NPLQCD 06	[158]	2+1	A	○	■	■	$1.218(2)(^{+11}_{-24})$	
MILC 04	[36]	2+1	A	○	○	○		1.210(4)(13)
BGR 11	[159]	2	A	★	■	■	1.215(41)	
ETM 10D	[138]	2	C	○	★	○	$1.190(8)_{\rm stat}$	
ETM 09	[160]	2	A	○	★	○	1.210(6)(15)(9)	
QCDSF/UKQCD 07	[161]	2	C	○	○	★	1.21(3)	

† Result with statistical error only from polynomial interpolation to the physical point. †† This work is the continuation of Aubin 08.

Table 9: Colour code for the data on the ratio of decay constants: f_K/f_π is the pure QCD SU(2)-symmetric ratio and $f_{K^\pm}/f_{\pi^\pm}$ is in pure QCD with the SU(2) isospin breaking applied after simulation.

The lattice results shown in the left panel of Figure 4 indicate that the higher order contributions $\Delta f \equiv f_+(0) - 1 - f_2$ are negative and thus amplify the effect generated by f_2. This confirms the expectation that the exotic contributions are small. The entries in the lower part of the left panel represent various model estimates for f_4. In [166] the symmetry breaking effects are estimated in the framework of the quark model. The more recent calculations are more sophisticated, as they make use of the known explicit expression for the $K_{\ell 3}$ form factors to NNLO in χPT [165, 167]. The corresponding formula for f_4 accounts for the chiral logarithms occurring at NNLO and is not subject to the ambiguity mentioned above.[10] The numerical result, however, depends on the model used to estimate the low energy constants occurring in f_4 [162–165]. The figure indicates that the most recent numbers obtained in this

[10] Fortran programs for the numerical evaluation of the form factor representation in [165] are available on request from Johan Bijnens.

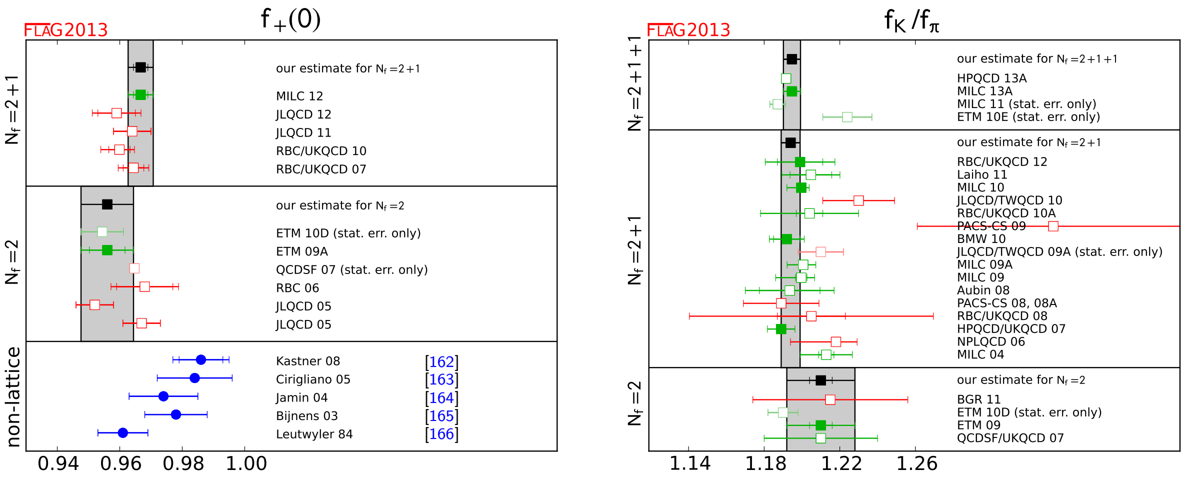

Figure 4: Comparison of lattice results (squares) for $f_+(0)$ and f_K/f_π with various model estimates based on χPT (blue circles). The black squares and grey bands indicate our estimates. The significance of the colours is explained in section 2.

way correspond to a positive rather than a negative value for Δf. We note that MILC 12 [133] have made an attempt at determining some of the low energy constants appearing in f_4 from lattice data.

4.3 Direct determination of $f_+(0)$ and $f_{K^\pm}/f_{\pi^\pm}$

All lattice results for the form factor and the ratio of decay constants that we summarize here (Tables 8 and 9) have been computed in isospin-symmetric QCD. The reason for this unphysical parameter choice is that simulations of SU(2) isospin-breaking effects in lattice QCD, while ultimately the cleanest way for predicting these effects, are still rare and in their infancy [32, 33, 40, 43, 102]. In the meantime one relies either on chiral perturbation theory [36, 56] to estimate the correction to the isospin limit or one mimicks the breaking in the valence quark sector by making a suitable choice of the physical point to which the lattice data is extrapolated. Aubin 08, MILC and Laiho 11 for example extrapolate their simulation results for the kaon decay constant to the physical value of the *up*-quark mass (the results for the pion decay constant are extrapolated to the value of the average light-quark mass $\hat{m}$). This then defines their prediction for $f_{K^\pm}/f_{\pi^\pm}$. As long as the majority of collaborations present their final results in the isospin-symmetric limit (as we will see this comprises the majority of results which qualify for inclusion into a FLAG average) we prefer to provide the overview of world data in Figure 4 in this limit. To this end we compute the isospin-symmetric ratio f_K/f_π for Aubin 08, MILC and Laiho 11 using NLO chiral perturbation theory [56, 168] where

$$\frac{f_K}{f_\pi} = \frac{1}{\sqrt{\delta_{\mathrm{SU}(2)}+1}}\,\frac{f_{K^\pm}}{f_{\pi^\pm}}\,, \tag{36}$$

and where [168] ,

$$\delta_{\mathrm{SU}(2)} \approx \sqrt{3}\,\epsilon_{\mathrm{SU}(2)}\left[-\frac{4}{3}\left(f_{K^\pm}/f_{\pi^\pm}-1\right)+\frac{2}{3(4\pi)^2 f_0^2}\left(M_K^2-M_\pi^2-M_\pi^2\ln\frac{M_K^2}{M_\pi^2}\right)\right]. \tag{37}$$

We use as input $\epsilon_{\rm SU(2)} = \sqrt{3}/4/R$ with the FLAG result for R of equation (28), $F_0 = f_0/\sqrt{2} =$ 80(20) MeV, M_π = 135 MeV and M_K = 495 MeV (we decided to choose a conservative uncertainty on f_0 in order to reflect the magnitude of potential higher order corrections) and obtain for example

	$f_{K^\pm}/f_{\pi^\pm}$	$\delta_{\rm SU(2)}$	f_K/f_π
Aubin 08	1.202(11)(9)(2)(5)	-0.0044(8)	1.205(11)(2)(9)(2)(5)
MILC 10	1.197(2)($^{+3}_{-7}$)	-0.0043(7)	1.200(2)(2)($^{+3}_{-7}$)
Laiho 11	1.191(16)(17)	-0.0041(9)	1.193(16)(2)(17)

(and similarly also for all other $N_f = 2+1$ and $N_f = 2+1+1$ results where applicable). In the last column the first error is statistical and the second is the one from the isospin correction (the remaining errors are quoted in the same order as in the original data). For $N_f = 2$ a dedicated study of the strong-isospin correction in lattice QCD does exist. The result of the RM123 collaboration [102] amounts to $\delta_{\rm SU(2)} = -0.0078(7)$ and we will later use this result for the correction in the case of $N_f = 2$. We note that this value for the strong-isospin correction is incompatible with the above results based on SU(3) chiral perturbation theory. One would not expect the strange sea-quark contribution to be responsible for such a large effect. Whether higher order effects in chiral perturbation theory or other sources are responsible still needs to be understood. To remain on the conservative side we attach the difference between the two- and three-flavour result as an additional uncertainty to the result based on chiral perturbation theory. For the further analysis we add both errors in quadrature.

The plots in Figure 4 illustrate our compilation of data for $f_+(0)$ and f_K/f_π. In both cases the lattice data are largely consistent even when comparing simulations with different N_f. We now proceed to form the corresponding averages, separately for the data with $N_f = 2+1+1$, $N_f = 2+1$ and $N_f = 2$ dynamical flavours and in the following will refer to these averages as the "direct" determinations.

For $f_+(0)$ there are currently two computational strategies: MILC 12 uses the Ward identity relating the $K \to \pi$ form factor to the matrix element $\langle \pi|S|K\rangle$ of the flavour-changing scalar current. Peculiarities of the staggered fermion discretisation (see [133]) which MILC is using makes this the favoured choice. The other collaborations are instead computing the vector current matrix element $\langle \pi|V_\mu|K\rangle$. All simulations in Table 8 are for unphysically heavy quark masses and therefore the lattice data needs to be extrapolated to the physical pion and kaon masses corresponding to the $K^0 \to \pi^-$ channel. MILC [169] report that simulations with $N_f = 2+1+1$ staggered fermions at the physical point are under way. With the mass extrapolation being a dominating source of systematic uncertainty this class of simulations will allow for a new quality of predictions. We note that all state of the art computations of $f_+(0)$ are using partially twisted boundary conditions which allow to determine the form factor results directly at the relevant kinematical point $q^2 = 0$ [170, 171].

The colour code in Table 8 shows that for $f_+(0)$, presently only the result of ETM (we will be using ETM 09A [139]) and the MILC collaboration with $N_f = 2$ and $N_f = 2+1$ dynamical flavours of fermions, respectively, are without a red tag and we quote their results:

$$\begin{aligned} f_+(0) &= 0.9667(23)(33)\,, \qquad && (\text{direct}, N_f = 2+1), \qquad (38)\\ f_+(0) &= 0.9560(57)(62)\,, \qquad && (\text{direct}, N_f = 2). \end{aligned}$$

The brackets indicate the statistical and systematic errors, respectively. MILC's result is from simulations reaching down to a lightest RMS pion mass of about 380 MeV (the lightest valence pion mass for one of their ensembles is about 260 MeV). Their combined chiral and continuum extrapolation (scaling study from results for two lattice spacings) is based on NLO staggered chiral perturbation theory supplemented by the continuum NNLO expression [165] and a phenomenological parameterisation of the breaking of the Ademollo-Gatto theorem at finite lattice spacing inherent in their approach. The p^4 low energy constants entering the NNLO expression have been fixed in terms of external input [57].

The ETM collaboration which uses the twisted-mass discretization provides a comprehensive study of the systematics by presenting results for three lattice spacings [172] and simulating at light pion masses (down to $M_\pi = 260$ MeV). This allows to constrain the chiral extrapolation, using both SU(3) [145] and SU(2) [147] chiral perturbation theory. Moreover, a rough estimate for the size of the effects due to quenching the strange quark is given, based on the comparison of the result for $N_f = 2$ dynamical quark flavours [160] with the one in the quenched approximation, obtained earlier by the SPQcdR collaboration [173]. We note for completeness that ETM extrapolate their lattice results to the point corresponding to M_K^2 and M_π^2 as defined at the end of Section 4.1. At the current level of precision though this is expected to be a tiny effect.

In the case of the ratio of decay constants the data sets that meet the criteria formulated in the introduction are MILC 13A [149] with $N_f = 2+1+1$, MILC 10 [151], BMW 10 [153], HPQCD/UKQCD 07 [157] and RBC/UKQCD 12 [25] (which is an update of RBC/UKQCD 10A [78]) with $N_f = 2+1$ and ETM 09 [160] with $N_f = 2$ dynamical flavours. MILC 13A have determined the ratio of decay constants from a comprehensive set of ensembles for four values of the lattice spacing and with the Goldstone pion mass tuned to the physical point which at least on their finest lattice agrees roughly with the RMS pion mass (the difference in mass between different *pion species* originates from staggered taste-splitting). Supplementary simulations with slightly heavier Goldstone pion mass allow to extract the result for the physical value of the light-quark masses from a fit. In a second step the data is extrapolated to the continuum limit and eventually the ratio $f_{K^\pm}/f_{\pi^\pm}$ is extracted. Concerning simulations with $N_f = 2+1$, MILC 10 and HPQCD/UKQCD 07 are based on staggered fermions, BMW 10 has used improved Wilson fermions and RBC/UKQCD 12's result is based on the domain wall formulation. For $N_f = 2$ ETM has simulated twisted-mass fermions. In contrast to MILC 13A all these latter simulations are for unphysically heavy quark masses (corresponding to smallest pion masses in the range 240-260MeV in the case of MILC 10, HPQCD/UKQCD 07 and ETM 09 and around 170MeV for RBC/UKQCD 12) and therefore slightly more sophisticated extrapolations needed to be controlled. Various ansätze for the mass and cutoff dependence comprising SU(2) and SU(3) chiral perturbation theory or simply polynomials were used and compared in order to estimate the model dependence.

We now provide the FLAG average for these data. While BMW 10 and RBC/UKQCD 12 are entirely independent computations, subsets of the MILC gauge ensembles used by MILC 10 and HPQCD/UKQCD 07 are the same. MILC 10 is certainly based on a larger and more advanced set of gauge configurations than HPQCD/UQKCD 07. This allows them for a more reliable estimation of systematic effects. In this situation we consider only their statistical but not their systematic uncertainties to be correlated. For $N_f = 2+1+1$ and $N_f = 2$ the FLAG averages are just the results by MILC 13A and ETM 09, respectively. They are shown as vertical grey bands in the r.h.s. panel of Figure 4. For the purpose of this plot only, the isospin correction has been removed from the MILC 13A result along the lines laid out earlier.

For the average indicated in the case of $N_f = 2+1$ we take the original data of BMW 10, HPQCD/UKQCD 07 and RBC/UKQCD 12 and use the MILC 10 result as computed above. The resulting fit is of good quality, with $f_K/f_\pi = 1.194(4)$ and $\chi^2/dof = 0.4$. The systematic errors of the individual data sets are larger for MILC 10, BMW 10, HPQCD/UKQCD 07 and RBC/UKQCD 12, respectively, and following again the prescription of section 2.3 we replace the error by the smallest one of these leading to $f_K/f_\pi = 1.194(5)$ for $N_f = 2+1$.

Before determining the average for $f_{K^\pm}/f_{\pi^\pm}$ which should be used for applications to Standard Model phenomenology we apply the isospin correction individually to all those results which have been published in the isospin-symmetric limit, i.e. BMW 10, HPQCD/UKQCD07 and RBC/UKQCD 12. To this end we invert Equation (36) and use

$$\delta_{\rm SU(2)} \approx \sqrt{3}\,\epsilon_{\rm SU(2)} \Big[-\tfrac{4}{3}(f_K/f_\pi - 1) + \tfrac{2}{3(4\pi)^2 f_0^2}\big(M_K^2 - M_\pi^2 - M_\pi^2 \ln \tfrac{M_K^2}{M_\pi^2}\big)\Big]\,. \tag{39}$$

The results are:

	f_K/f_π	$\delta_{\rm SU(2)}$	$f_{K^\pm}/f_{\pi^\pm}$
HPQCD/UKQCD 07	1.189(2)(7)	-0.0040(7)	1.187(2) (2)(7)
BMW 10	1.192(7)(6)	-0.0041(7)	1.190(7) (2)(6)
RBC/UKQCD 12	1.199(12)(14)	-0.0043(9)	1.196(12)(2)(14)

As before, in the last column the first error is statistical and the second error is due to the isospin correction. Using these results we obtain

$$\begin{aligned} f_{K^\pm}/f_{\pi^\pm} &= 1.195(3)(4), && (\text{direct},\ N_f = 2+1+1)\,,\\ f_{K^\pm}/f_{\pi^\pm} &= 1.192(5), && (\text{direct},\ N_f = 2+1)\,,\\ f_{K^\pm}/f_{\pi^\pm} &= 1.205(6)(17)\,, && (\text{direct},\ N_f = 2)\,, \end{aligned} \tag{40}$$

for QCD with broken isospin.

It is instructive to convert the above results for $f_+(0)$ and $f_{K^\pm}/f_{\pi^\pm}$ into a corresponding range for the CKM matrix elements $|V_{ud}|$ and $|V_{us}|$, using the relations (32). Consider first the results for $N_f = 2+1$. The range for $f_+(0)$ in (38) is mapped into the interval $|V_{us}| = 0.2238(11)$, depicted as a horizontal green band in Figure 5, while the one for $f_{K^\pm}/f_{\pi^\pm}$ in (40) is converted into $|V_{us}|/|V_{ud}| = 0.2314(11)$, shown as a tilted green band. The smaller green ellipse is the intersection of these two bands. More precisely, it represents the 68% likelihood contour, obtained by treating the above two results as independent measurements. Values of $|V_{us}|$, $|V_{ud}|$ in the region enclosed by this contour are consistent with the lattice data for $N_f = 2+1$, within one standard deviation. In particular, the plot shows that the nuclear β decay result for $|V_{ud}|$ is in good agreement with these data. We note that with respect to the previous edition of the FLAG review the reanalysis including new results has moved the ellipse representing QCD with $N_f = 2+1$ slightly down and to the left.

Repeating the exercise for $N_f = 2$ leads to the larger blue ellipse. The figure indicates a slight tension between the $N_f = 2$ and $N_f = 2+1$ results, which, at the current level of precision is not visible if considering the $N_f = 2$ and $N_f = 2+1$ results for $f_+(0)$ and $f_{K^\pm}/f_{\pi^\pm}$ in Figure 4 on their own. It remains to be seen if this is a first indication of the effect of quenching the strange quark.

In the case of $N_f = 2+1+1$ no result for $f_+(0)$ exists to date. We have therefore only plotted the corresponding band for $|V_{us}|$ from $f_{K^\pm}/f_{\pi^\pm}$.

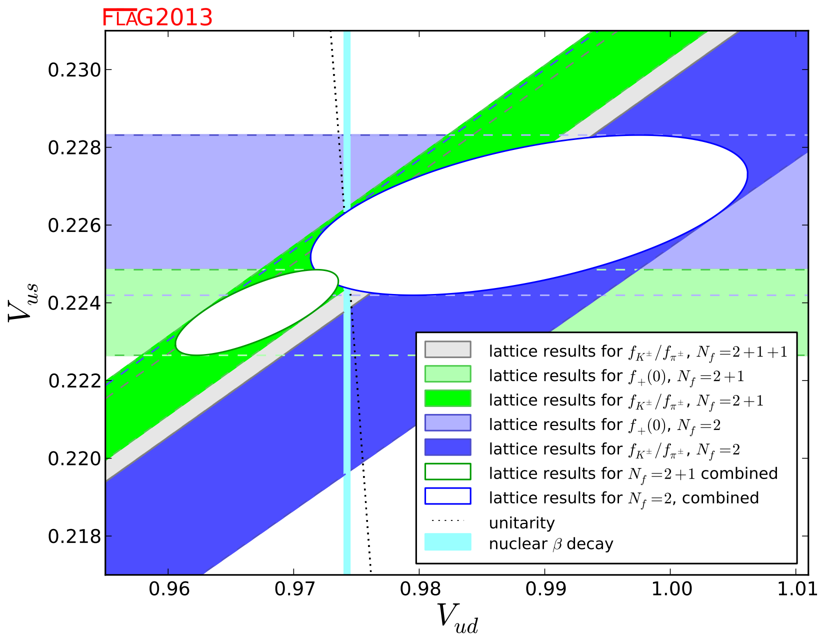

Figure 5: The plot compares the information for $|V_{ud}|$, $|V_{us}|$ obtained on the lattice with the experimental result extracted from nuclear β transitions. The dotted arc indicates the correlation between $|V_{ud}|$ and $|V_{us}|$ that follows if the three-flavour CKM-matrix is unitary.

4.4 Testing the Standard Model

In the Standard Model, the CKM matrix is unitary. In particular, the elements of the first row obey

$$|V_u|^2 \equiv |V_{ud}|^2 + |V_{us}|^2 + |V_{ub}|^2 = 1\,. \tag{41}$$

The tiny contribution from $|V_{ub}|$ is known much better than needed in the present context: $|V_{ub}| = 4.15(49)\cdot 10^{-3}$ [74]. In the following, we first discuss the evidence for the validity of the relation (41) and only then use it to analyze the lattice data within the Standard Model.

In Figure 5, the correlation between $|V_{ud}|$ and $|V_{us}|$ imposed by the unitarity of the CKM matrix is indicated by a dotted arc (more precisely, in view of the uncertainty in $|V_{ub}|$, the correlation corresponds to a band of finite width, but the effect is too small to be seen here). The plot shows that the data for $N_f = 2+1$ are in good agreement with this constraint. Numerically, the outcome for the sum of the squares of the first row of the CKM matrix reads $|V_u|^2 = 0.985(13)$. The Standard Model thus passes a nontrivial test that exclusively involves lattice data and well-established kaon decay branching ratios. Combining the lattice results for $f_+(0)$ and $f_{K^\pm}/f_{\pi^\pm}$ in (38) and (40) with the β decay value of $|V_{ud}|$ quoted in (33), the test sharpens considerably: the lattice result for $f_+(0)$ leads to $|V_u|^2 = 0.9992(6)$, while the one for $f_{K^\pm}/f_{\pi^\pm}$ implies $|V_u|^2 = 1.0000(6)$, thus confirming CKM unitarity at the permille level.

Repeating the analysis for $N_f = 2$, we find $|V_u|^2 = 1.029(35)$ with the lattice data alone. The number is somewhat larger than 1, in accordance with the fact that the dotted curve passes just outside the blue contour. Moreover, it only concerns the comparison of the $N_f = 2$

Collaboration	Ref.	N_f	from	$\vert V_{us}\vert$
MILC 13A	[149]	$2+1+1$	$f_{K^\pm}/f_{\pi^\pm}$	0.2249(6)(7)
MILC 12	[133]	$2+1$	$f_+(0)$	0.2238(7)(8)
MILC 10	[151]	$2+1$	$f_{K^\pm}/f_{\pi^\pm}$	0.2249(5)(9)
RBC/UKQCD 10A	[78]	$2+1$	$f_{K^\pm}/f_{\pi^\pm}$	0.2246(22)(25)
BMW 10	[153]	$2+1$	$f_{K^\pm}/f_{\pi^\pm}$	0.2259(13)(11)
HPQCD/UKQCD 07	[157]	$2+1$	$f_{K^\pm}/f_{\pi^\pm}$	0.2264(5)(13)
ETM 09	[160]	2	$f_{K^\pm}/f_{\pi^\pm}$	0.2231(11)(31)
ETM 09A	[139]	2	$f_+(0)$	0.2263(14)(15)

Table 10: Values of $|V_{us}|$ obtained from lattice determinations of $f_+(0)$ or $f_{K^\pm}/f_{\pi^\pm}$ with CKM unitarity. The first (second) number in brackets represents the statistical (systematic) error.

results for $f_+(0)$ with those for $f_{K^\pm}/f_{\pi^\pm}$. Taken by themselves, these results are perfectly consistent with the value of $|V_{ud}|$ found in nuclear β decay: combining this value with the data on $f_+(0)$ yields $|V_u|^2 = 1.0004(10)$, combining it with the data on $f_{K^\pm}/f_{\pi^\pm}$ gives $|V_u|^2 = 0.9989(16)$.

Note that the above tests also offer a check of the basic hypothesis that underlies our analysis: we are assuming that the weak interaction between the quarks and the leptons is governed by the same Fermi constant as the one that determines the strength of the weak interaction among the leptons and determines the lifetime of the muon. In certain modifications of the Standard Model, this is not the case. In those models it need not be true that the rates of the decays $\pi \to \ell\nu$, $K \to \ell\nu$ and $K \to \pi\ell\nu$ can be used to determine the matrix elements $|V_{ud}f_\pi|$, $|V_{us}f_K|$ and $|V_{us}f_+(0)|$, respectively and that $|V_{ud}|$ can be measured in nuclear β decay. The fact that the lattice data are consistent with unitarity and with the value of $|V_{ud}|$ found in nuclear β decay indirectly also checks the equality of the Fermi constants.

4.5 Analysis within the Standard Model

The Standard Model implies that the CKM matrix is unitary. The precise experimental constraints quoted in (32) and the unitarity condition (41) then reduce the four quantities $|V_{ud}|, |V_{us}|, f_+(0), f_{K^\pm}/f_{\pi^\pm}$ to a single unknown: any one of these determines the other three within narrow uncertainties.

Figure 6 shows that the results obtained for $|V_{us}|$ and $|V_{ud}|$ from the data on $f_{K^\pm}/f_{\pi^\pm}$ (squares) are quite consistent with the determinations via $f_+(0)$ (triangles). In order to calculate the corresponding average values, we restrict ourselves to those determinations that we have considered best in section 4.3. The corresponding results for $|V_{us}|$ are listed in Table 10 (the error in the experimental numbers used to convert the values of $f_+(0)$ and $f_{K^\pm}/f_{\pi^\pm}$ into values for $|V_{us}|$ is included in the statistical error).

We consider the fact that the results from the five $N_f = 2+1$ data sets MILC 12 [133], RBC/UKQCD 12 [25], BMW 10 [153], MILC 10 [151] and HPQCD/UKQCD 07 [157] are

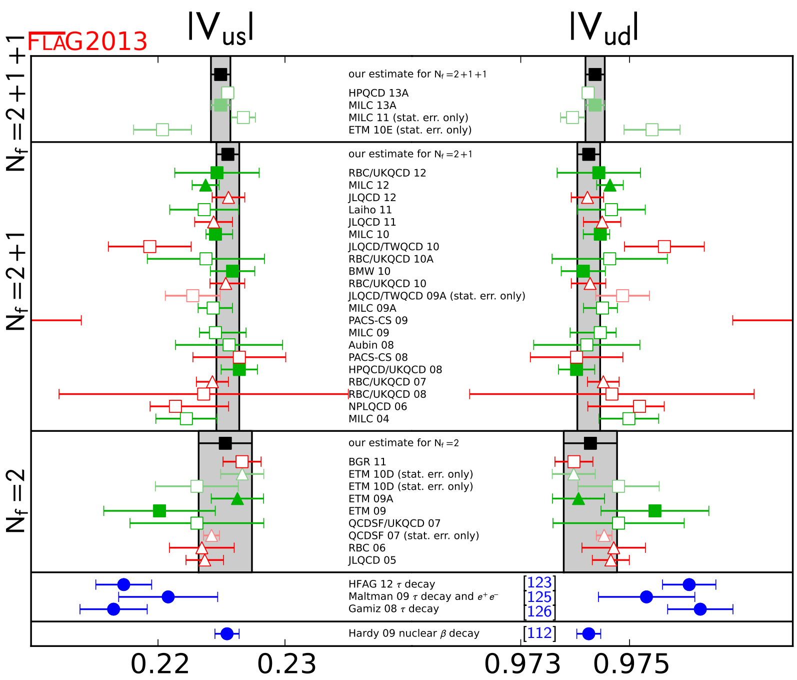

⋆ Estimates obtained from an analysis of the lattice data within the Standard Model, see section 4.5.

Figure 6: Results for $|V_{us}|$ and $|V_{ud}|$ that follow from the lattice data for $f_+(0)$ (triangles) and $f_{K^\pm}/f_{\pi^\pm}$ (squares), on the basis of the assumption that the CKM matrix is unitary. The black squares and the grey bands represent our estimates, obtained by combining these two different ways of measuring $|V_{us}|$ and $|V_{ud}|$ on a lattice. For comparison, the figure also indicates the results obtained if the data on nuclear β decay and τ decay are analyzed within the Standard Model.

consistent with each other to be an important reliability test of the lattice work. Applying the prescription of section 2.3, where we consider MILC 10, MILC 12 and HPQCD/UKQCD 07 as mutually statistically correlated since analysis starts from partly the same set of gauge-ensembles, we arrive at $|V_{us}| = 0.2249(8)$ with $\chi^2/dof = 0.9$. This result is indicated on the left hand side of Fig. 6 by the narrow vertical band. The broader band shows the corresponding value for $N_f = 2$, $|V_{us}| = 0.2253(21)$, with $\chi^2/dof = 0.9$, where we have considered ETM 09 and ETM 09A as statistically correlated. The figure shows that the result obtained for the data with $N_f = 2$ is perfectly consistent with the one found for $N_f = 2 + 1$.

Alternatively, we can solve the relations for $|V_{ud}|$ instead of $|V_{us}|$. Again, the result $|V_{ud}| = 0.97438(18)$ which follows from the lattice data with $N_f = 2+1$ is perfectly consistent with the value $|V_{ud}| = 0.97427(49)$ obtained from those with $N_f = 2$. The reduction of the uncertainties in the result for $|V_{ud}|$ due to CKM unitarity is to be expected from Figure 5: the unitarity condition reduces the region allowed by the lattice results to a nearly vertical interval.

Next, we determine the value of $f_+(0)$ that follows from the lattice data within the Standard Model. Using CKM unitarity to convert the lattice determinations of $f_{K^\pm}/f_{\pi^\pm}$ into corresponding values for $f_+(0)$ and then combining these with the direct determinations of $f_+(0)$, we find $f_+(0) = 0.9624(36)$ from the data with $N_f = 2+1$ and $f_+(0) = 0.9595(90)$ for $N_f = 2$.

Finally, we work out the analogous Standard Model fits for $f_{K^\pm}/f_{\pi^\pm}$, converting the direct determinations of $f_+(0)$ into corresponding values for $f_{K^\pm}/f_{\pi^\pm}$ and combining the outcome with the direct determinations of that quantity. The results read $f_{K^\pm}/f_{\pi^\pm} = 1.194(4)$ for $N_f = 2+1$ and $f_{K^\pm}/f_{\pi^\pm} = 1.192(12)$ for $N_f = 2$, respectively.

	Ref.	$\lvert V_{us}\rvert$	$\lvert V_{ud}\rvert$	$f_+(0)$	$f_{K^\pm}/f_{\pi^\pm}$
$N_f = 2+1$		0.2249(8)	0.97438(18)	0.9624(36)	1.194(4)
$N_f = 2$		0.2253(21)	0.97427(49)	0.9595(90)	1.192(12)
β decay	[112]	0.22544(95)	0.97425(22)	0.9595(46)	1.1919(57)
τ decay	[126]	0.2165(26)	0.9763(6)	0.999(12)	1.244(16)
τ decay	[125]	0.2208(39)	0.9753(9)	0.980(18)	1.218(23)

Table 11: The upper half of the table shows our final results for $|V_{us}|$, $|V_{ud}|$, $f_+(0)$ and $f_{K^\pm}/f_{\pi^\pm}$, which are obtained by analyzing the lattice data within the Standard Model. For comparison, the lower half lists the values that follow if the lattice results are replaced by the experimental results on nuclear β decay and τ decay, respectively.

The results obtained by analyzing the lattice data in the framework of the Standard Model are collected in the upper half of Table 11. In the lower half of this table, we list the analogous results, found by working out the consequences of CKM-unitarity for the experimental values of $|V_{ud}|$ and $|V_{us}|$ obtained from nuclear β decay and τ decay, respectively. The comparison shows that the lattice result for $|V_{ud}|$ not only agrees very well with the totally independent determination based on nuclear β transitions, but is also remarkably precise. On the other hand, the values of $|V_{ud}|$, $f_+(0)$ and $f_{K^\pm}/f_{\pi^\pm}$ which follow from the τ decay data if the Standard Model is assumed to be valid, are not in good agreement with the lattice results for these quantities. The disagreement is reduced considerably if the analysis of the τ data is supplemented with experimental results on electroproduction [125]: the discrepancy then amounts to little more than one standard deviation.

4.6 Direct determination of f_K and f_π

It is useful for flavour physics to provide not only the lattice average of f_K/f_π, but also the average of the decay constant f_K. Indeed, the $\Delta S = 2$ hadronic matrix element for neutral kaon mixing is generally parameterized by M_K, f_K and the kaon bag parameter B_K. The knowledge of both f_K and B_K is therefore crucial for a precise theoretical determination of the CP-violation parameter ϵ_K and for the constraint on the apex of the CKM unitarity triangle.

The case of the decay constant f_π is somehow different, since the experimental value of this quantity is often used for setting the scale in lattice QCD (see Appendix A.2). However, the physical scale can be set in different ways, namely by using as input the mass of the Ωbaryon (m_Ω) or the Υ-meson spectrum (ΔM_Υ), which are less sensitive to the uncertainties of the chiral extrapolation in the light-quark mass with respect to f_π. In such cases the value of the decay constant f_π becomes a direct prediction of the lattice QCD simulations. It is therefore interesting to provide also the average of the decay constant f_π, obtained when the physical scale is set through another hadron observable, in order to check the consistency of different scale setting procedures.

Our compilation of the values of f_π and f_K with the corresponding colour code is presented in Table 12. With respect to the case of f_K/f_π we have added two columns indicating which quantity is used to set the physical scale and the possible use of a renormalization constant for the axial current. Indeed, for several lattice formulations the use of the nonsinglet axial-vector Ward identity allows to avoid the use of any renormalization constant.

One can see that the determinations of f_π and f_K suffer from larger uncertainties with respect to the ones of the ratio f_K/f_π, which is less sensitive to various systematic effects (including the uncertainty of a possible renormalization constant) and, moreover, is not so exposed to the uncertainties of the procedure used to set the physical scale.

According to the FLAG rules three data sets can form the average of f_π and f_K for $N_f = 2+1$: RBC/UKQCD 12 [25] (update of RBC/UKQCD 10A), HPQCD/UKQCD 07 [157] and MILC 10 [151], which is the latest update of the MILC program. [11] We consider HPQCD/UKQCD 07 and MILC 10 as statistically correlated and use the prescription of 2.3 to form an average. For $N_f = 2$ the average cannot be formed for f_π, and only one data set (ETM 09) satisfies the FLAG rules in the case of f_K.

Thus, our estimates (in the isospin-symmetric limit of QCD) read

$$f_\pi = 130.2\ (1.4)\ \text{MeV} \qquad (N_f = 2+1), \tag{42}$$

$$\begin{aligned} f_K &= 156.3\ (0.8)\ \text{MeV} \qquad (N_f = 2+1), \\ f_K &= 158.1\ (2.5)\ \text{MeV} \qquad (N_f = 2). \end{aligned} \tag{43}$$

The lattice results of Table 12 and our estimates (42-43) are reported in Fig. 7. The latter ones compare positively within the errors with the latest experimental determinations of f_π and f_K from the PDG:

$$f_\pi^{(PDG)} = 130.41\ (0.20)\ \text{MeV} \quad , \quad f_K^{(PDG)} = 156.1\ (0.8)\ \text{MeV}\ , \tag{44}$$

which, we recall, do not correspond however to pure QCD results in the isospin-symmetric limit. Moreover the values of f_π and f_K quoted by the PDG are obtained assuming Eq. (32) for the value of $|V_{ud}|$ and adopting the RBC-UKQCD 07 result for $f_+(0)$.

[11] Since the MILC result is obtained for a charged kaon, we remove the isospin-breaking effect according to the formula $f_K = f_{K^+}(1-\delta_{\mathrm{SU}(2)}/2)$, valid at NLO in ChPT, with $\delta_{SU(2)}$ for MILC 10 computed using eq. (37).

Collaboration	Ref.	N_f	publication status	chiral extrapolation	continuum extrapolation	finite volume errors	renormalisation	physical scale	SU(2) breaking	f_π	f_K
HPQCD 13A	[148]	2+1+1	P	★	○	★	na	f_π	✓	–	155.37(20)(28)
ETM 10E	[150]	2+1+1	C	○	○	○	na	f_π		–	160(2)
RBC/UKQCD 12	[25]	2+1	A	★	○	★	NPR	m_Ω		127(3)(3)	152(3)(2)
Laiho 11	[77]	2+1	C	○	○	○	na	†	✓	130.53(87)(210)	156.8(1.0)(1.7)
MILC 10	[151]	2+1	C	○	★	★	na	†	✓	129.2(4)(14)	–
MILC 10	[151]	2+1	C	○	★	★	na	f_π	✓	–	$156.1(4)(^{+6}_{-9})$
JLQCD/TWQCD 10	[152]	2+1	C	○	■	★	na	m_Ω		$118.5(3.6)_{\rm stat}$	$145.8(2.7)_{\rm stat}$
RBC/UKQCD 10A	[78]	2+1	A	○	○	★	NPR	m_Ω		124(2)(5)	149(2)(3)
PACS-CS 09	[20]	2+1	A	★	■	■	NPR	m_Ω		124.6(8.6)(0.9)	166.1(3.4)(1.2)
JLQCD/TWQCD 09A	[154]	2+1	C	○	■	■	na	f_π		–	$157.3(5.5)_{\rm stat}$
MILC 09A	[37]	2+1	C	○	★	★	na	ΔM_Υ	✓	128.0(0.3)(2.9)	153.8(0.3)(3.9)
MILC 09A	[37]	2+1	C	○	★	★	na	f_π	✓	–	156.2(0.3)(1.1)
MILC 09	[15]	2+1	A	○	★	★	na	ΔM_Υ	✓	$128.3(0.5)(^{+2.4}_{-3.5})$	$154.3(0.4)(^{+2.1}_{-3.4})$
MILC 09	[15]	2+1	A	○	★	★	na	f_π	✓		$156.5(0.4)(^{+1.0}_{-2.7})$
Aubin 08	[155]	2+1	C	○	○	○	na	ΔM_Υ	✓	129.1(1.9)(4.0)	153.9(1.7)(4.4)
PACS-CS 08, 08A	[19, 156]	2+1	A	★	■	■	1lp	m_Ω		$134.0(4.2)_{\rm stat}$	$159.4(3.1)_{\rm stat}$
RBC/UKQCD 08	[79]	2+1	A	○	■	★	NPR	m_Ω		124.1(3.6)(6.9)	149.6(3.6)(6.3)
HPQCD/UKQCD 07	[157]	2+1	A	○	★	○	na	ΔM_Υ		132(2)	157(2)
MILC 04	[36]	2+1	A	○	○	○	na	ΔM_Υ	✓	129.5(0.9)(3.5)	156.6(1.0)(3.6)
TWQCD 11	[174]	2	P	★	■	■	na	r_0^*		127.3(1.7)(2.0)**	–
ETM 09	[160]	2	A	○	★	○	na	f_π		–	158.1(0.8)(2.0)(1.1)††
JLQCD/TWQCD 08A	[67]	2	A	○	■	■	na	r_0		$119.6(3.0)(^{+6.5}_{-1.0})$**	–

The label "na" indicates the lattice calculations which do not require the use of any renormalization constant for the axial current, while the label "NPR" ("1lp") signals the use of a renormalization constant calculated nonperturbatively (at one-loop order in perturbation theory).

† The ratios of lattice spacings within the ensembles were determined using the quantity r_1. The conversion to physical units was made basing on ref. [175] and we note that such a determination depends on the experimental value of the pion decay constant

†† Errors are (stat+chiral)$(a \neq 0)$(finite size).

* The ratio f_π/M_π was used as experimental input to fix the light-quark mass.

** $L_{\rm min} < 2$fm in these simulations.

Table 12: Colour code for the lattice data on f_π and f_K together with information on the way the lattice spacing was converted to physical units and on whether or not an isospin-breaking correction has been applied (using chiral perturbation theory) to the quoted result. The numerical values are listed in MeV units.

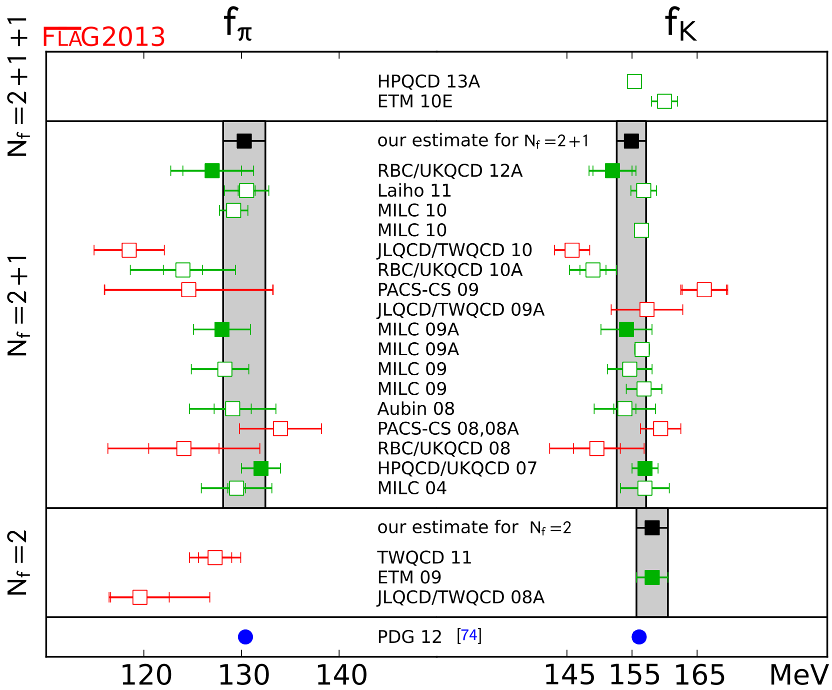

Figure 7: Values of f_π and f_K. The black squares and grey bands indicate our estimates (42) and (43). The blue dots represent the experimental values quoted by the PDG (44).

5 Low-energy constants

In the study of the quark-mass dependence of QCD observables calculated on the lattice it is common practice to invoke Chiral Perturbation Theory (χPT). For a given quantity this framework predicts the nonanalytic quark-mass dependence and it provides symmetry relations among different observables. These relations are best expressed with the help of a set of linearly independent and universal (i.e. process-independent) low-energy constants (LECs), which appear as coefficients of the polynomial terms (in m_q or M_π^2) in different observables. If one expands around the SU(2) chiral limit, in the Chiral Effective Lagrangian there appear two LECs at order p^2

$$F \equiv F_\pi \Big|_{m_u,m_d\to 0}\,, \qquad B \equiv \frac{\Sigma}{F^2} \quad \text{where} \quad \Sigma \equiv -\langle \bar{u}u\rangle \Big|_{m_u,m_d\to 0}\,, \tag{45}$$

and seven at order p^4, indicated by $\bar{\ell}_i$ with $i = 1, \ldots, 7$. In the analysis of the SU(3) chiral limit there are also just two LECs at order p^2

$$F_0 \equiv F_\pi \Big|_{m_u,m_d,m_s\to 0}\,, \qquad B_0 \equiv \frac{\Sigma_0}{F_0^2} \quad \text{where} \quad \Sigma_0 \equiv -\langle \bar{u}u\rangle \Big|_{m_u,m_d,m_s\to 0}\,, \tag{46}$$

but ten at order p^4, indicated by the capital letter $L_i(\mu)$ with $i = 1, \ldots, 10$. These constants are independent of the quark masses[12], but they become scale dependent after renormalization (sometimes a superscript r is added). The SU(2) constants $\bar{\ell}_i$ are scale independent, since they are defined at $\mu = M_\pi$ (as indicated by the bar). For the precise definition of these constants and their scale dependence we refer the reader to [56, 58].

First of all, lattice calculations can be used to test if chiral symmetry is indeed broken as $\mathrm{SU}(N_f)_L \times \mathrm{SU}(N_f)_R \to \mathrm{SU}(N_f)_{L+R}$ by measuring nonzero chiral condensates and by verifying the validity of the GMOR relation $M_\pi^2 \propto m$ close to the chiral limit. If the chiral extrapolation of quantities calculated on the lattice is made with the help of χPT, apart from determining the observable at the physical value of the quark masses one also obtains the relevant LECs. This is a very important by-product for two reasons:

1. All LECs up to order p^4 (with the exception of B and B_0, since only the product of these times the quark masses can be estimated from phenomenology) have either been determined by comparison to experiment or estimated theoretically. A lattice determination of the better known ones thus provides a test of the χPT approach.
2. The less well known LECs are those which describe the quark-mass dependence of observables – these cannot be determined from experiment, and therefore the lattice provides unique quantitative information. This information is essential for improving phenomenological χPT predictions in which these LECs play a role.

We stress that this program is based on the nonobvious assumption that χPT is valid in the region of masses used in the lattice simulations under consideration.

The fact that, at large volume, the finite-size effects, which occur if a system undergoes spontaneous symmetry breakdown, are controlled by the Nambu-Goldstone modes, was first noted in solid state physics, in connection with magnetic systems [176, 177]. As pointed out

[12] More precisely, they are independent of the 2 or 3 light quark masses which are explicitly considered in the respective framework. However, all low-energy constants depend on the masses of the remaining quarks s, c, b, t or c, b, t in the SU(2) and SU(3) framework, respectively.

in [178] in the context of QCD, the thermal properties of such systems can be studied in a systematic and model-independent manner by means of the corresponding effective field theory, provided the temperature is low enough. While finite volumes are not of physical interest in particle physics, lattice simulations are necessarily carried out in a finite box. As shown in [179–181], the ensuing finite-size effects can also be studied on the basis of the effective theory – χPT in the case of QCD – provided the simulation is close enough to the continuum limit, the volume is sufficiently large and the explicit breaking of chiral symmetry generated by the quark masses is sufficiently small. Indeed, χPT represents also a useful tool for the analysis of the finite-size effects in lattice simulations.

In the following two subsections we summarize the lattice results for the SU(2) and SU(3) LECs, respectively. In either case we first discuss the $O(p^2)$ constants and then proceed to their $O(p^4)$ counterparts. The $O(p^2)$ LECs are determined from the chiral extrapolation of masses and decay constants or, alternatively, from a finite-size study of correlators in the ϵ-regime. At order p^4 some LECs affect two-point functions while other appear only in three- or four-point functions; the latter need to be determined from form factors or scattering amplitudes. The χPT analysis of the (non-lattice) phenomenological quantities is nowadays[13] based on $O(p^6)$ formulae. At this level the number of LECs explodes and we will not discuss any of these. We will, however, discuss how comparing different orders and different expansions (in particular x versus ξ-expansion, see below) can help to assess the theoretical uncertainties of the LECs determined on the lattice.

5.1 SU(2) Low-Energy Constants

5.1.1 Quark-mass dependence of pseudoscalar masses and decay constants

The expansions[14] of M_π^2 and F_π in powers of the quark mass are known to next-to-next-to-leading order in the SU(2) chiral effective theory. In the isospin limit, $m_u = m_d = m$, the explicit expressions may be written in the form [182]

$$
\begin{aligned}
M_\pi^2 &= M^2\left\{1-\frac{1}{2}x\ln\frac{\Lambda_3^2}{M^2}+\frac{17}{8}x^2\left(\ln\frac{\Lambda_M^2}{M^2}\right)^2+x^2k_M+O(x^3)\right\}, \qquad (47)\\
F_\pi &= F\left\{1+x\ln\frac{\Lambda_4^2}{M^2}-\frac{5}{4}x^2\left(\ln\frac{\Lambda_F^2}{M^2}\right)^2+x^2k_F+O(x^3)\right\}.
\end{aligned}
$$

Here the expansion parameter is given by

$$
x=\frac{M^2}{(4\pi F)^2}, \qquad M^2=2Bm=\frac{2\Sigma m}{F^2}, \qquad (48)
$$

but there is another option as discussed below. The scales Λ_3, Λ_4 are related to the effective coupling constants $\bar\ell_3, \bar\ell_4$ of the chiral Lagrangian at running scale $M_\pi \equiv M_\pi^{\rm phys}$ by

$$
\bar\ell_n=\ln\frac{\Lambda_n^2}{M_\pi^2}, \qquad n=1,...,7. \qquad (49)
$$

[13]Some of the $O(p^6)$ formulae presented below have been derived in an unpublished note by three of us (GC, SD and HL) and Jürg Gasser. We thank him for allowing us to publish them here.

[14]Here and in the following, we stick to the notation used in the papers where the χPT formulae were established, i.e. we work with $F_\pi \equiv f_\pi/\sqrt{2} = 92.2(1)$ MeV and $F_K \equiv f_K/\sqrt{2}$. The occurrence of different normalization conventions is not convenient, but avoiding it by reformulating the formulae in terms of f_π, f_K is not a good way out. Since we are using different symbols, confusion cannot arise.

Note that in Eq. (47) the logarithms are evaluated at M^2, not at M_π^2. The coupling constants k_M, k_F in Eq. (47) are mass-independent. The scales of the squared logarithms can be expressed in terms of the $O(p^4)$ coupling constants as

$$\begin{aligned}
\ln \frac{\Lambda_M^2}{M^2} &= \frac{1}{51}\left(28 \ln \frac{\Lambda_1^2}{M^2} + 32 \ln \frac{\Lambda_2^2}{M^2} - 9 \ln \frac{\Lambda_3^2}{M^2} + 49\right), \qquad (50)\\
\ln \frac{\Lambda_F^2}{M^2} &= \frac{1}{30}\left(14 \ln \frac{\Lambda_1^2}{M^2} + 16 \ln \frac{\Lambda_2^2}{M^2} + 6 \ln \frac{\Lambda_3^2}{M^2} - 6 \ln \frac{\Lambda_4^2}{M^2} + 23\right).
\end{aligned}$$

Hence by analyzing the quark-mass dependence of M_π^2 and F_π with Eq. (47), possibly truncated at NLO, one can determine[15] the $O(p^2)$ LECs B and F, as well as the $O(p^4)$ LECs $\bar{\ell}_3$ and $\bar{\ell}_4$. The quark condensate in the chiral limit is given by $\Sigma = F^2 B$. With precise enough data at several small enough pion masses, one could in principle also determine Λ_M, Λ_F and k_M, k_F. To date this is not yet possible. The results for the LO and NLO constants will be presented in Sec. 5.1.6.

Alternatively, one can invert Eq. (47) and express M^2 and F as an expansion in

$$\xi \equiv \frac{M_\pi^2}{16\pi^2 F_\pi^2} , \qquad (51)$$

and the corresponding expressions then take the form

$$\begin{aligned}
M^2 &= M_\pi^2 \left\{1 + \frac{1}{2}\xi \ln \frac{\Lambda_3^2}{M_\pi^2} - \frac{5}{8}\xi^2 \left(\ln \frac{\Omega_M^2}{M_\pi^2}\right)^2 + \xi^2 c_M + O(\xi^3)\right\}, \qquad (52)\\
F &= F_\pi \left\{1 - \xi \ln \frac{\Lambda_4^2}{M_\pi^2} - \frac{1}{4}\xi^2 \left(\ln \frac{\Omega_F^2}{M_\pi^2}\right)^2 + \xi^2 c_F + O(\xi^3)\right\}.
\end{aligned}$$

The scales of the quadratic logarithms are determined by $\Lambda_1, \ldots, \Lambda_4$ through

$$\begin{aligned}
\ln \frac{\Omega_M^2}{M_\pi^2} &= \frac{1}{15}\left(28 \ln \frac{\Lambda_1^2}{M_\pi^2} + 32 \ln \frac{\Lambda_2^2}{M_\pi^2} - 33 \ln \frac{\Lambda_3^2}{M_\pi^2} - 12 \ln \frac{\Lambda_4^2}{M_\pi^2} + 52\right), \qquad (53)\\
\ln \frac{\Omega_F^2}{M_\pi^2} &= \frac{1}{3}\left(-7 \ln \frac{\Lambda_1^2}{M_\pi^2} - 8 \ln \frac{\Lambda_2^2}{M_\pi^2} + 18 \ln \frac{\Lambda_4^2}{M_\pi^2} - \frac{29}{2}\right).
\end{aligned}$$

5.1.2 Two-point correlation functions in the epsilon-regime

The finite-size effects encountered in lattice calculations can be used to determine some of the LECs of QCD. In order to illustrate this point, we focus on the two lightest quarks, take the isospin limit $m_u = m_d = m$ and consider a box of size L_s in the three space directions and size L_t in the time direction. If m is sent to zero at fixed box size, chiral symmetry is restored. The behaviour of the various observables in the symmetry-restoration region is controlled by the parameter $\mu \equiv m\,\Sigma\,V$, where $V = L_s^3 L_t$ is the four-dimensional volume of the box. Up to a sign and a factor of two, the parameter μ represents the minimum of the classical action that belongs to the leading-order effective Lagrangian of QCD.

[15] Notice that one could analyze the quark-mass dependence entirely in terms of the parameter M^2 defined in Eq. (48) and determine equally well all other LECs. Using the determination of the quark masses described in Sec. 3 one can then extract B or Σ.

For $\mu \gg 1$, the system behaves qualitatively as if the box was infinitely large. In that region, the p-expansion, which counts $1/L_s$, $1/L_t$ and M as quantities of the same order, is adequate. In view of $\mu = \frac{1}{2}F^2M^2V$, this region includes configurations with $ML \gtrsim 1$, where the finite-size effects due to pion loop diagrams are suppressed by the factor e^{-ML}.

If μ is comparable to or smaller than 1, however, the chiral perturbation series must be reordered. The ϵ-expansion achieves this by counting $1/L_s, 1/L_t$ as quantities of $O(\epsilon)$, while the quark mass m is booked as a term of $O(\epsilon^4)$. This ensures that the symmetry-restoration parameter μ represents a term of order $O(\epsilon^0)$, so that the manner in which chiral symmetry is restored can be worked out.

As an example, we consider the correlator of the axial charge carried by the two lightest quarks, $q(x) = \{u(x), d(x)\}$. The axial current and the pseudoscalar density are given by

$$A^i_\mu(x) = \bar{q}(x)\tfrac{1}{2}\tau^i\,\gamma_\mu\gamma_5\,q(x)\,, \qquad P^i(x) = \bar{q}(x)\tfrac{1}{2}\tau^i\,\mathrm{i}\gamma_5\,q(x)\,, \tag{54}$$

where τ^1, τ^2, τ^3, are the Pauli matrices in flavour space. In Euclidean space, the correlators of the axial charge and of the space integral over the pseudoscalar density are given by

$$\begin{aligned} \delta^{ik}C_{AA}(t) &= L_s^3 \int d^3\vec{x}\,\langle A^i_4(\vec{x},t)A^k_4(0)\rangle\,, \\ \delta^{ik}C_{PP}(t) &= L_s^3 \int d^3\vec{x}\,\langle P^i(\vec{x},t)P^k(0)\rangle\,. \end{aligned} \tag{55}$$

χPT yields explicit finite-size scaling formulae for these quantities [181, 183, 184]. In the ϵ-regime, the expansion starts with

$$\begin{aligned} C_{AA}(t) &= \frac{F^2L_s^3}{L_t}\left[a_A + \frac{L_t}{F^2L_s^3}\,b_A\,h_1\!\left(\frac{t}{L_t}\right) + O(\epsilon^4)\right], \\ C_{PP}(t) &= \Sigma^2L_s^6\left[a_P + \frac{L_t}{F^2L_s^3}\,b_P\,h_1\!\left(\frac{t}{L_t}\right) + O(\epsilon^4)\right], \end{aligned} \tag{56}$$

where the coefficients a_A, b_A, a_P, b_P stand for quantities of $O(\epsilon^0)$. They can be expressed in terms of the variables L_s, L_t and m and involve only the two leading low-energy constants F and Σ. In fact, at leading order only the combination $\mu = m\,\Sigma\,L_s^3L_t$ matters, the correlators are t-independent and the dependence on μ is fully determined by the structure of the groups involved in the SSB pattern. In the case of SU(2)×SU(2) → SU(2), relevant for QCD in the symmetry restoration region with two light quarks, the coefficients can be expressed in terms of Bessel functions. The t-dependence of the correlators starts showing up at $O(\epsilon^2)$, in the form of a parabola, viz. $h_1(\tau) = \frac{1}{2}\left[\left(\tau - \frac{1}{2}\right)^2 - \frac{1}{12}\right]$. Explicit expressions for a_A, b_A, a_P, b_P can be found in [181, 183, 184], where some of the correlation functions are worked out to NNLO. By matching the finite-size scaling of correlators computed on the lattice with these predictions one can extract F and Σ. A way to deal with the numerical challenges genuine to the ϵ-regime has been described [185].

The fact that the representation of the correlators to NLO is not "contaminated" by higher-order unknown LECs, makes the ϵ-regime potentially convenient for a clean extraction of the LO couplings. The determination of these LECs is then affected by different systematic uncertainties with respect to the standard case; simulations in this regime yield complementary information which can serve as a valuable cross-check to get a comprehensive picture of the low-energy properties of QCD.

The effective theory can also be used to study the distribution of the topological charge in QCD [186] and the various quantities of interest may be defined for a fixed value of this charge. The expectation values and correlation functions then not only depend on the symmetry restoration parameter μ, but also on the topological charge ν. The dependence on these two variables can explicitly be calculated. It turns out that the two-point correlation functions considered above retain the form (56), but the coefficients a_A, b_A, a_P, b_P now depend on the topological charge as well as on the symmetry restoration parameter (see [187–189] for explicit expressions).

A specific issue with ϵ-regime calculations is the scale setting. Ideally one would perform a p-regime study with the same bare parameters to measure a hadronic scale (e.g. the proton mass). In the literature, sometimes a gluonic scale (e.g. r_0) is used to avoid such expenses. Obviously the issues inherent in scale setting are aggravated if the ϵ-regime simulation is restricted to a fixed sector of topological charge.

It is important to stress that in the ϵ-expansion higher-order finite-volume corrections might be significant, and the physical box size (in fm) should still be large in order to keep these contributions under control. The criteria for the chiral extrapolation and finite-volume effects are obviously different with respect to the p-regime. For these reasons we have to adjust the colour coding defined in Sect. 2.1 (see 5.1.6 for more details).

Recently, the effective theory has been extended to the "mixed regime" where some quarks are in the p-regime and some in the ϵ-regime [190, 191]. In [192] a technique is proposed to smoothly connect the p- and ϵ-regimes. In [193] the issue is reconsidered with a counting rule which is essentially the same as in the p-regime. In this new scheme, the theory remains IR finite even in the chiral limit, while the chiral-logarithmic effects are kept present.

5.1.3 Energy levels of the QCD Hamiltonian in a box and δ-regime

At low temperature, the properties of the partition function are governed by the lowest eigenvalues of the Hamiltonian. In the case of QCD, the lowest levels are due to the Nambu-Goldstone bosons and can be worked out with χPT [194]. In the chiral limit the level pattern follows the one of a quantum-mechanical rotator, i.e. $E_\ell = \ell(\ell+1)/(2\,\Theta)$ with $\ell = 0, 1, 2, \ldots$. For a cubic spatial box and to leading order in the expansion in inverse powers of the box size L_s, the moment of inertia is fixed by the value of the pion decay constant in the chiral limit, i.e. $\Theta = F^2 L_s^3$.

In order to analyze the dependence of the levels on the quark masses and on the parameters that specify the size of the box, a reordering of the chiral series is required, the so-called δ-expansion; the region where the properties of the system are controlled by this expansion is referred to as the δ-regime. Evaluating the chiral perturbation series in this regime, one finds that the expansion of the partition function goes in even inverse powers of FL_s, that the rotator formula for the energy levels holds up to NNLO and the expression for the moment of inertia is now also known up to and including terms of order $(FL_s)^{-4}$ [195–197]. Since the level spectrum is governed by the value of the pion decay constant in the chiral limit, an evaluation of this spectrum on the lattice can be used to measure F. More generally, the evaluation of various observables in the δ-regime offers an alternative method for a determination of some of the low-energy constants occurring in the effective Lagrangian. At present, however, the numerical results obtained in this way [198, 199] are not yet competitive with those found in the p- or ϵ-regimes.

5.1.4 Other methods for the extraction of the Low-Energy Constants

An observable that can be used to extract the LECs is the topological susceptibility

$$\chi_t = \int d^4x \, \langle \omega(x)\omega(0) \rangle, \tag{57}$$

where $\omega(x)$ is the topological charge density,

$$\omega(x) = \frac{1}{32\pi^2} \epsilon^{\mu\nu\rho\sigma} \mathrm{Tr} \left[F_{\mu\nu}(x) F_{\rho\sigma}(x) \right]. \tag{58}$$

At infinite volume, the expansion of χ_t in powers of the quark masses starts with [200]

$$\chi_t = \overline{m}\, \Sigma \left\{ 1 + O(m) \right\}, \qquad \overline{m} \equiv \left(\frac{1}{m_u} + \frac{1}{m_d} + \frac{1}{m_s} + \ldots \right)^{-1}. \tag{59}$$

The condensate Σ can thus be extracted from the properties of the topological susceptibility close to the chiral limit. The behaviour at finite volume, in particular in the region where the symmetry is restored, is discussed in [184]. The dependence on the vacuum angle θ and the projection on sectors of fixed ν have been studied in [186]. For a discussion of the finite-size effects at NLO, including the dependence on θ, we refer to [189, 201].

The role that the topological susceptibility plays in attempts to determine whether there is a large paramagnetic suppression when going from the $N_f = 2$ to the $N_f = 2+1$ theory has been highlighted in Ref. [202]. And the potential usefulness of higher moments of the topological charge distribution to determine LECs has been investigated in [203].

Another method for computing the quark condensate has been proposed in [204], where it is shown that starting from the Banks-Casher relation [205] one may extract the condensate from suitable (renormalizable) spectral observables, for instance the number of Dirac operator modes in a given interval. For those spectral observables higher-order corrections can be systematically computed in terms of the chiral effective theory. A recent paper based on this strategy is ETM 13 [206]. As an aside let us remark that corrections to the Banks-Casher relation that come from a finite quark mass, a finite four-dimensional volume and (with Wilson-type fermions) a finite lattice spacing can be parameterized in a properly extended version of the chiral framework [207].

An alternative strategy is based on the fact that at LO in the ϵ-expansion the partition function in a given topological sector ν is equivalent to the one of a chiral Random Matrix Theory (RMT) [208–211]. In RMT it is possible to extract the probability distributions of individual eigenvalues [212–214] in terms of two dimensionless variables $\zeta = \lambda\Sigma V$ and $\mu = m\Sigma V$, where λ represents the eigenvalue of the massless Dirac operator and m is the sea quark mass. More recently this approach has been extended to the Hermitian (Wilson) Dirac operator [215] which is easier to study in numerical simulations. Hence, if it is possible to match the QCD low-lying spectrum of the Dirac operator to the RMT predictions, then one may extract[16] the chiral condensate Σ. One issue with this method is that for the distributions of individual eigenvalues higher-order corrections are still not known in the effective theory, and this may introduce systematic effects which are hard[17] to control. Another open question

[16] By introducing an imaginary isospin chemical potential, the framework can be extended such that the low-lying spectrum of the Dirac operator is also sensitive to the pseudoscalar decay constant F at LO [216].

[17] Higher-order systematic effects in the matching with RMT have been investigated in [217, 218].

is that, while it is clear how the spectral density is renormalized [219], this is not the case for the individual eigenvalues, and one relies on assumptions. There have been many lattice studies [220–224] which investigate the matching of the low-lying Dirac spectrum with RMT. In this review the results of the LECs obtained in this way[18] are not included.

5.1.5 Pion form factors

The scalar and vector form factors of the pion are defined by the matrix elements

$$\begin{aligned} \langle\pi^i(p_2)|\,\bar q\,q\,|\pi^j(p_1)\rangle &= \delta^{ij}F_S^\pi(t)\,, \\ \langle\pi^i(p_2)|\,\bar q\,\tfrac{1}{2}\tau^k\gamma^\mu q\,|\pi^j(p_1)\rangle &= \mathrm{i}\,\epsilon^{ikj}(p_1^\mu+p_2^\mu)F_V^\pi(t)\,, \end{aligned} \tag{60}$$

where the operators contain only the lightest two quark flavours, i.e. τ^1, τ^2, τ^3 are the Pauli matrices, and $t\equiv(p_1-p_2)^2$ denotes the momentum transfer.

The vector form factor has been measured by several experiments for timelike as well as for spacelike values of t. The scalar form factor is not directly measurable, but it can be evaluated theoretically from data on the $\pi\pi$ and πK phase shifts [225] by means of analyticity and unitarity, i.e. in a model-independent way. Lattice calculations can be compared with data or model-independent theoretical evaluations at any given value of t. At present, however, most lattice studies concentrate on the region close to $t=0$ and on the evaluation of the slope and curvature which are defined as

$$\begin{aligned} F_V^\pi(t) &= 1+\tfrac{1}{6}\langle r^2\rangle_V^\pi t+c_V\,t^2+\dots\ , \\ F_S^\pi(t) &= F_S^\pi(0)\left[1+\tfrac{1}{6}\langle r^2\rangle_S^\pi t+c_S\,t^2+\dots\right]\ . \end{aligned} \tag{61}$$

The slopes are related to the mean-square vector and scalar radii which are the quantities on which most experiments and lattice calculations concentrate.

In chiral perturbation theory, the form factors are known at NNLO [226]. The corresponding formulae are available in fully analytical form and are compact enough that they can be used for the chiral extrapolation of the data (as done, for example in [227, 228]). The expressions for the scalar and vector radii and for the $c_{S,V}$ coefficients at two-loop level read

$$\begin{aligned} \langle r^2\rangle_S^\pi &= \frac{1}{(4\pi F_\pi)^2}\left\{6\ln\frac{\Lambda_4^2}{M_\pi^2}-\frac{13}{2}-\frac{29}{3}\,\xi\left(\ln\frac{\Omega_{r_S}^2}{M_\pi^2}\right)^2+6\xi\,k_{r_S}+O(\xi^2)\right\}\,, \\ \langle r^2\rangle_V^\pi &= \frac{1}{(4\pi F_\pi)^2}\left\{\ln\frac{\Lambda_6^2}{M_\pi^2}-1+2\,\xi\left(\ln\frac{\Omega_{r_V}^2}{M_\pi^2}\right)^2+6\xi\,k_{r_V}+O(\xi^2)\right\}\,, \\ c_S &= \frac{1}{(4\pi F_\pi M_\pi)^2}\left\{\frac{19}{120}+\xi\left[\frac{43}{36}\left(\ln\frac{\Omega_{c_S}^2}{M_\pi^2}\right)^2+k_{c_S}\right]\right\}\,, \\ c_V &= \frac{1}{(4\pi F_\pi M_\pi)^2}\left\{\frac{1}{60}+\xi\left[\frac{1}{72}\left(\ln\frac{\Omega_{c_V}^2}{M_\pi^2}\right)^2+k_{c_V}\right]\right\}\,, \end{aligned} \tag{62}$$

[18] The results for Σ and F lie in the same range as the determinations reported in Tables 13 and 14.

where

$$\begin{aligned}
\ln\frac{\Omega_{r_S}^2}{M_\pi^2} &= \frac{1}{29}\left(31\,\ln\frac{\Lambda_1^2}{M_\pi^2}+34\,\ln\frac{\Lambda_2^2}{M_\pi^2}-36\,\ln\frac{\Lambda_4^2}{M_\pi^2}+\frac{145}{24}\right)\,, \\
\ln\frac{\Omega_{r_V}^2}{M_\pi^2} &= \frac{1}{2}\left(\ln\frac{\Lambda_1^2}{M_\pi^2}-\ln\frac{\Lambda_2^2}{M_\pi^2}+\ln\frac{\Lambda_4^2}{M_\pi^2}+\ln\frac{\Lambda_6^2}{M_\pi^2}-\frac{31}{12}\right)\,, \\
\ln\frac{\Omega_{c_S}^2}{M_\pi^2} &= \frac{43}{63}\left(11\,\ln\frac{\Lambda_1^2}{M_\pi^2}+14\,\ln\frac{\Lambda_2^2}{M_\pi^2}+18\,\ln\frac{\Lambda_4^2}{M_\pi^2}-\frac{6041}{120}\right)\,, \\
\ln\frac{\Omega_{c_V}^2}{M_\pi^2} &= \frac{1}{72}\left(2\ln\frac{\Lambda_1^2}{M_\pi^2}-2\ln\frac{\Lambda_2^2}{M_\pi^2}-\ln\frac{\Lambda_6^2}{M_\pi^2}-\frac{26}{30}\right)\,,
\end{aligned} \tag{63}$$

and k_{r_S}, k_{r_V} and k_{c_S}, k_{c_V} are independent of the quark masses. Their expression in terms of the ℓ_i and of the $O(p^6)$ constants c_M, c_F is known but will not be reproduced here.

The difference between the quark-line connected and the full (i.e. containing the connected and the disconnected piece) scalar pion form factor has been investigated by means of Chiral Perturbation Theory in [229]. It is expected that the technique used can be applied to a large class of observables relevant in QCD-phenomenology.

As a point of practical interest let us remark that there are no finite-volume correction formulae for the mean-square radii $\langle r^2\rangle_{V,S}$ and the curvatures $c_{V,S}$. The lattice data for $F_{V,S}(t)$ need to be corrected, point by point in t, for finite-volume effects. In fact, if a given t is realized through several inequivalent p_1-p_2 combinations, the level of agreement after the correction has been applied is indicative of how well higher-order effects are under control.

5.1.6 Lattice determinations

In this section we summarize the lattice results for the SU(2) couplings in a set of tables (13–16) and figures (8–10). The tables present our usual colour coding which summarizes the main aspects related to the treatment of the systematic errors of the various calculations.

A delicate issue in the lattice determination of chiral LECs (in particular at NLO) which cannot be reflected by our colour coding is a reliable assessment of the theoretical error that comes from the chiral expansion. We add a few remarks on this point:

1. Using *both* the x and the ξ expansion is a good way to test how the ambiguity of the chiral expansion (at a given order) affects the numerical values of the LECs that are determined from a particular set of data. For instance, to determine $\bar\ell_4$ (or Λ_4) from lattice data for F_π as a function of the quark mass, one may compare the fits based on the parameterization $F_\pi = F\{1+x\ln(\Lambda_4^2/M^2)\}$ [see Eq. (47)] with those obtained from $F_\pi = F/\{1-\xi\ln(\Lambda_4^2/M_\pi^2)\}$ [see Eq. (52)]. The difference between the two results provides an estimate of the uncertainty due to the truncation of the chiral series. Which central value one chooses is in principle arbitrary, but we find it advisable to use the one obtained with the ξ expansion[19], in particular because it makes the comparison with phenomenological determinations (where it is standard practice to use the ξ expansion) more meaningful.

[19] There are theoretical arguments suggesting that the ξ expansion is preferable to the x expansion, based on the observation that the coefficients in front of the squared logs in (47) are somewhat larger than in (52). This can be traced to the fact that a part of every formula in the x expansion is concerned with locating the position of the pion pole (at the previous order) while in the ξ expansion the knowledge of this position is built in exactly. Numerical evidence supporting this view is presented in [67].

2. Alternatively one could try to estimate the influence of higher chiral orders by reshuffling irrelevant higher-order terms. For instance, in the example mentioned above one might use $F_\pi = F/\{1 - x\ln(\Lambda_4^2/M^2)\}$ as a different functional form at NLO. Another way to establish such an estimate is through introducing by hand "analytical" higher-order terms (e.g. "analytical NNLO" as done, in the past, by MILC [15]). In principle it would be preferable to include all NNLO terms or none, such that the structure of the chiral expansion is preserved at any order (this is what ETM [230] and JLQCD/TWQCD [67] have done for SU(2) χPT and MILC for SU(3) χPT [37]). There are different opinions in the field as to whether it is advisable to include terms to which the data are not sensitive. In case one is willing to include external (typically: non-lattice) information, the use of priors is a theoretically well founded option (e.g. priors for NNLO LECs if one is interested in LECs at LO/NLO).
3. Another issue concerns the s-quark mass dependence of the LECs $\bar{\ell}_i$ or Λ_i of the SU(2) framework. As far as variations of m_s around $m_s^{\rm phys}$ are concerned (say for $0 < m_s < 1.5 m_s^{\rm phys}$ at best) the issue can be studied in SU(3) ChPT, and this has been done in a series of papers [56, 231, 232]. However, the effect of sending m_s to infinity, as is the case in $N_f = 2$ lattice studies of SU(2) LECs, cannot be addressed in this way. A unique way to analyze this difference is to compare the numerical values of LECs determined in $N_f = 2$ lattice simulations to those determined in $N_f = 2+1$ lattice simulations (see e.g. [233] for a discussion).
4. Last but not least let us recall that the determination of the LECs is affected by discretization effects, and it is important that these are removed by means of a continuum extrapolation. In this step invoking an extended version of the chiral Lagrangian [234–236] may be useful[20] in case one aims for a global fit of lattice data involving several M_π and a values and several chiral observables.

In the tables and figures we summarize the results of various lattice collaborations for the SU(2) LECs at LO (F or F/F_π, B or Σ) and at NLO ($\bar{\ell}_1 - \bar{\ell}_2$, $\bar{\ell}_3$, $\bar{\ell}_4$, $\bar{\ell}_5$, $\bar{\ell}_6$). Throughout we group the results into those which stem from $N_f = 2+1+1$ calculations, those which come from $N_f = 2+1$ calculations and those which stem from $N_f = 2$ calculations (since, as mentioned above, the LECs are logically distinct even if the current precision of the data is not sufficient to resolve the differences). Furthermore, we make a distinction whether the results are obtained from simulations in the p-regime or whether alternative methods (ϵ-regime, spectral quantities, topological susceptibility, etc.) have been used (this should not affect the result). For comparison we add, in each case, a few phenomenological determinations with high standing.

A generic comment applies to the issue of the scale setting. In the past none of the lattice studies with $N_f \geq 2$ involved simulations in the p-regime at the physical value of m_{ud}. Accordingly, the setting of the scale a^{-1} via an experimentally measurable quantity did necessarily involve a chiral extrapolation, and as a result of this dimensionful quantities used to be particularly sensitive to this extrapolation uncertainty, while in dimensionless ratios such as F_π/F, F/F_0, B/B_0, Σ/Σ_0 this particular problem is much reduced (and often finite lattice-to-continuum renormalization factors drop out). Now, there is a new generation of lattice studies [20, 22, 23, 133, 238, 239] which does involve simulations at physical pion masses.

[20] This means that for any given lattice formulation one needs to determine additional low-energy constants, often denoted W_i. For certain formulations, e.g. the twisted-mass approach, first steps in this direction have already been taken [237].

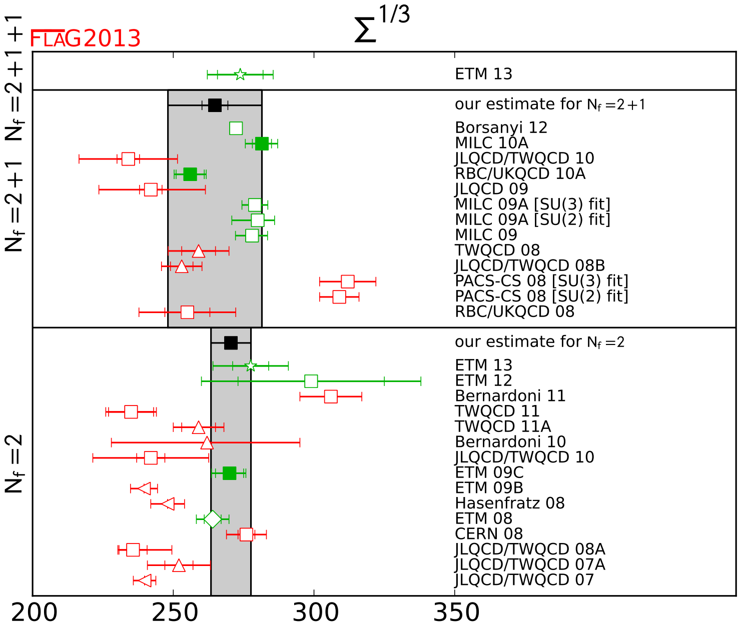

Figure 8: Quark condensate $\Sigma \equiv |\langle \bar{u}u\rangle|_{m_u,m_d\to 0}$ ($\overline{\rm MS}$-scheme, scale $\mu = 2$ GeV). Squares and left triangles indicate determinations from correlators in the p- and ϵ-regimes, respectively. Up triangles refer to extractions from the topological susceptibility, diamonds to determinations from the pion form factor, and star symbols refer to the spectral density method. The black squares and grey bands indicate our estimates. The significance of the colours is explained in section 2.

In such studies even the uncertainty that the scale setting has on dimensionful quantities is much mitigated.

It is worth repeating here that the standard colour-coding scheme of our tables is necessarily schematic and cannot do justice to every calculation. In particular there is some difficulty in coming up with a fair adjustment of the rating criteria to finite-volume regimes of QCD. For instance, in the ϵ-regime[21] we re-express the "chiral extrapolation" criterion in terms of $\sqrt{2m_{\rm min}\Sigma}/F$, with the same threshold values (in MeV) between the three categories as in the p-regime. Also the "infinite volume" assessment is adapted to the ϵ-regime, since the $M_\pi L$ criterion does not make sense here; we assign a green star if at least 2 volumes with $L > 2.5$fm are included, an open symbol if at least 1 volume with $L > 2$fm is invoked and a red square if all boxes are smaller than 2fm. Similarly, in the calculation of form factors and charge radii the tables do not reflect whether an interpolation to the desired q^2 has been performed or whether the relevant q^2 has been engineered by means of "partially-twisted boundary conditions" [242]. In spite of these limitations we feel that these tables give an adequate overview of the qualities of the various calculations.

We begin with a discussion of the lattice results for the SU(2) LEC Σ. We present the results in Table 13 and Figure 8. Regarding the $N_f = 2$ computations there are four entries without a red tag (ETM 08, ETM 09C, ETM 12, ETM 13). Only ETM 09C and ETM 12 are published and thus averaged (here we deviate from our "superseded" rule, since the

[21] Also in case of [240] and [241] the colour-coding criteria for the ϵ-regime have been applied.

Collaboration	Ref.	N_f	publication status	chiral extrapolation	continuum extrapolation	finite volume	renormalization	$\Sigma^{1/3}$
ETM 13	[206]	2+1+1	P	○	★	○	★	274(08)(08)
Borsanyi 12	[238]	2+1	P	★	★	○	★	272.3(1.2)(1.4)
MILC 10A	[75]	2+1	C	○	★	★	○	$281.5(3.4)\left(^{+2.0}_{-5.9}\right)(4.0)$
JLQCD/TWQCD 10	[241]	2+1	A	★	■	○	★	234(4)(17)
RBC/UKQCD 10A	[78]	2+1	A	○	○	★	★	256(5)(2)(2)
JLQCD 09	[240]	2+1	A	★	■	○	★	$242(4)\left(^{+19}_{-18}\right)$
MILC 09A	[37]	2+1	C	○	★	★	○	279(1)(2)(4)
MILC 09A	[37]	2+1	C	○	★	★	○	$280(2)\left(^{+4}_{-8}\right)(4)$
MILC 09	[15]	2+1	A	○	★	★	○	$278(1)\left(^{+2}_{-3}\right)(5)$
TWQCD 08	[243]	2+1	A	○	■	■	★	259(6)(9)
JLQCD/TWQCD 08B	[244]	2+1	C	○	■	■	★	253(4)(6)
PACS-CS 08	[19]	2+1	A	★	■	■	■	312(10)
PACS-CS 08	[19]	2+1	A	★	■	■	■	309(7)
RBC/UKQCD 08	[79]	2+1	A	○	■	★	★	255(8)(8)(13)
ETM 13	[206]	2	P	○	★	○	★	277(06)(12)
ETM 12	[245]	2	A	○	★	○	★	299(26)(29)
Bernardoni 11	[246]	2	C	○	■	■	○	306(11)
TWQCD 11	[174]	2	A	○	■	■	★	235(8)(4)
TWQCD 11A	[247]	2	A	○	■	■	★	259(6)(7)
Bernardoni 10	[248]	2	A	○	■	■	★	$262\left(^{+33}_{-34}\right)\left(^{+4}_{-5}\right)$
JLQCD/TWQCD 10	[241]	2	A	★	■	■	★	242(5)(20)
ETM 09C	[230]	2	A	○	★	○	★	$270(5)\left(^{+3}_{-4}\right)$
ETM 08	[227]	2	A	○	○	○	★	264(3)(5)
CERN 08	[204]	2	A	○	■	○	★	276(3)(4)(5)
JLQCD/TWQCD 08A	[67]	2	A	○	■	■	★	$235.7(5.0)(2.0)\left(^{+12.7}_{-0.0}\right)$
JLQCD/TWQCD 07A	[249]	2	A	○	■	■	★	252(5)(10)
ETM 09B	[250]	2	C	★	○	■	★	239.6(4.8)
Hasenfratz 08	[251]	2	A	○	■	○	★	248(6)
JLQCD/TWQCD 07	[252]	2	A	★	■	■	★	239.8(4.0)

Table 13: Quark condensate $\Sigma \equiv |\langle \bar{u}u \rangle|_{m_u,m_d\to 0}$: colour code and numerical values in MeV (compare Fig. 8).

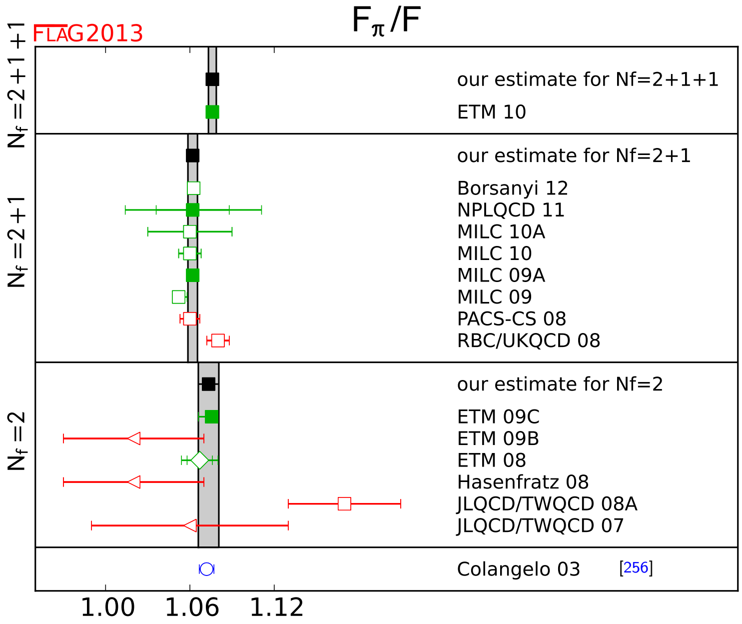

Figure 9: Comparison of the results for the ratio of the physical pion decay constant F_π and the leading-order SU(2) low-energy constant F. The meaning of the symbols is the same as in Figure 8.

latter work has a much bigger error). Regarding the $N_f = 2+1$ computations there are two published papers (RBC/UKQCD 10A and MILC 10A) which make it into the $N_f = 2+1$ average and a preprint (Borsanyi 12) which will be included in a future update.

Regarding the $N_f = 2+1$ average for Σ we remark that the two works included (RBC/UKQCD 10A and MILC 10A) are inconsistent (the new value Borsanyi 12 is in much better agreement with the latter one). For the time being we inflate the error of our $N_f = 2+1$ average such that it includes either central value it is based on. This yields

$$\Sigma\big|_{N_f=2} = 270(7)\,\mathrm{MeV}\ , \qquad \Sigma\big|_{N_f=2+1} = 265(17)\,\mathrm{MeV} \tag{64}$$

where the errors include both statistical and systematic uncertainties. Another look at Figure 8 confirms that these values are well consistent with each other, as well as with the yet unaveraged $N_f = 2+1+1$ result of ETM 13.

The next quantity considered is F, i.e. the pion decay constant in the SU(2) chiral limit ($m_{ud} \to 0$ at fixed physical m_s) in the Bernese normalization. As argued on previous occasions we tend to give preference to F_π/F (here the numerator is meant to refer to the physical-pion-mass point) wherever it is available, since often some of the systematic uncertainties are mitigated. We collect the results in Table 14 and Figure 9. In those cases where the collaboration provides only F, the ratio is computed on the basis of the phenomenological value of F_π, and the corresponding entries in Table 14 are in slanted fonts. Among the $N_f = 2$ determinations only two (ETM 08 and ETM 09C) are without red tags. Since they are by the same collaboration only the latter one enters the average. Among the $N_f = 2+1$ determinations two values (MILC 09A as an obvious update of MILC 09, NPLQCD 11) make

Collaboration	Ref.	N_f	publication status	chiral extrapolation	continuum extrapolation	finite volume	renormalization	F	F_π/F
ETM 11	[253]	2+1+1	C	○	★	○	★	85.60(4)	*1.077(2)*
ETM 10 †	[96]	2+1+1	A	○	○	○	★	85.66(6)(13)	1.076(2)(2)
Borsanyi 12	[238]	2+1	P	★	★	○	★	86.78(05)(25)	1.0627(06)(27)
NPLQCD 11	[254]	2+1	A	○	○	★			$1.062(26)\binom{+42}{-40}$
MILC 10A	[75]	2+1	C	○	★	★	○	$87.5(1.0)\binom{+0.7}{-2.6}$	*1.06(3)*
MILC 10	[151]	2+1	C	○	★	★	○	87.0(4)(5)	*1.060(8)*
MILC 09A	[37]	2+1	C	○	★	★	○	86.8(2)(4)	1.062(1)(3)
MILC 09	[15]	2+1	A	○	★	★			$1.052(2)\binom{+6}{-3}$
PACS-CS 08	[19]	2+1	A	★	■	■	■	89.4(3.3)	1.060(7)
RBC/UKQCD 08	[79]	2+1	A	○	■	★	★	81.2(2.9)(5.7)	1.080(8)
QCDSF 13	[255]	2	P	★	★	■	★	86(1)	*1.07(1)*
Bernardoni 11	[246]	2	C	○	■	■	○	79(4)	*1.17(5)*
TWQCD 11	[174]	2	A	★	■	■	★	83.39(35)(38)	*1.106(6)*
ETM 09C	[230]	2	A	○	★	○			$1.0755(6)\binom{+08}{-94}$
ETM 08	[227]	2	A	○	○	○	★	86.6(7)(7)	1.067(9)(9)
JLQCD/TWQCD 08A	[67]	2	A	○	■	■	★	$79.0(2.5)(0.7)\binom{+4.2}{-0.0}$	*1.17(4)*
ETM 09B §	[250]	2	C	★	○	■	★	90.2(4.8)	*1.02(5)*
Hasenfratz 08	[251]	2	A	○	■	○	★	90(4)	*1.02(4)*
JLQCD/TWQCD 07	[252]	2	A	★	■	■	★	87.3(5.6)	*1.06(6)*
Colangelo 03	[256]							86.2(5)	1.0719(52)

† The values of $M_{\pi^+}L$ correspond to a green tag in the FV-column, while those of $M_{\pi^0}L$ imply a red one; since both masses play a role in finite-volume effects, we opt for open green.

§ Result for $r_0 F$ converted into a value for F via $r_0 = 0.49\,\text{fm}$ (despite ETM quoting smaller values of r_0).

Table 14: Results for the leading-order SU(2) low-energy constant F (in MeV) and for the ratio F_π/F. Numbers in slanted fonts have been calculated by us (see text for details). Horizontal lines establish the same grouping as in Table 13.

it into the average, while Borsanyi 12 is not published prior to our deadline. Finally, there is an $N_f = 2+1+1$ determination which qualifies for an average (ETM 10).

Given this input our averaging procedure yields

$$\frac{F_\pi}{F}\Big|_{N_f=2} = 1.0733(73)\ , \quad \frac{F_\pi}{F}\Big|_{N_f=2+1} = 1.0620(34)\ , \quad \frac{F_\pi}{F}\Big|_{N_f=2+1+1} = 1.0760(28) \qquad (65)$$

where the errors include both statistical and systematic uncertainties. From these numbers (or from a look at Figure 9) it is obvious that the $N_f = 2+1$ and $N_f = 2+1+1$ results are not quite consistent with each other. From a theoretical viewpoint this is rather surprising, since the only difference (the presence of absence of a dynamical charm quark) is expected to have a rather insignificant effect on this ratio (which, in addition, would be monotonic in N_f, contrary to what is seen in Figure 9). In our view this indicates that – in spite of the conservative attitude taken in this report – the theoretical uncertainties in at least one of the three numbers reported in (65) is likely underestimated. We hope that a future release of the FLAG report can clarify the issue.

We move on to a discussion of the lattice results for the NLO LECs $\bar{\ell}_3$ and $\bar{\ell}_4$. We remind the reader that on the lattice the former LEC is obtained as a result of the tiny deviation from linearity seen in M_π^2 versus Bm_{ud}, whereas the latter LEC is extracted from the curvature in F_π versus Bm_{ud}. The available determinations are presented in Table 15 and Figure 10. Among the $N_f = 2$ determinations only ETM 08 and ETM 09C are published and without red tags, and our rules imply that these determinations enter our average. The colour coding of the $N_f = 2+1$ results looks very promising; there is a significant number of lattice determinations without any red tag. According to our rules RBC/UKQCD 10A, MILC 10A, NPLQCD 11 make it into the average, while Borsanyi 12 and RBC/UKQCD 12 were not published prior to our deadline. We annotate that $\bar{\ell}_3$, $\bar{\ell}_4$ of RBC/UKQCD 10A have no systematic error; therefore we included a 10% systematic error estimate for these observables (and only for these) by hand. Among the $N_f = 2+1+1$ determinations ETM 10 is the one which qualifies for an average.

Given this input our averaging procedure yields

$$\bar{\ell}_3\big|_{N_f=2} = 3.45(26)\ , \quad \bar{\ell}_3\big|_{N_f=2+1} = 2.77(1.27)\ , \quad \bar{\ell}_3\big|_{N_f=2+1+1} = 3.70(27)\ , \qquad (66)$$

$$\bar{\ell}_4\big|_{N_f=2} = 4.59(26)\ , \quad \bar{\ell}_4\big|_{N_f=2+1} = 3.95(35)\ , \quad \bar{\ell}_4\big|_{N_f=2+1+1} = 4.67(10) \qquad (67)$$

where the errors include both statistical and systematic uncertainties.

Let us add two remarks. On the input side our procedure[22] symmetrizes the asymmetric error of ETM 09C with a slight adjustment of the central value. On the output side the error of the $\bar{\ell}_4$ average for $N_f = 2+1$, according to the FLAG procedure, got inflated by hand to cover all central values. From these numbers (or from a look at Figure 10) it is clear that the lattice results for $\bar{\ell}_3$ do not show any obvious N_f-dependence – thanks, chiefly, to our conservative error treatment strategy. On the other hand, in the case of $\bar{\ell}_4$ even our practice of inflating the error of the $N_f = 2+1$ average did not manage to avoid some mild inconsistency between the $N_f = 2+1$ average on one side and either the $N_f = 2$ or the

[22] There are two naive procedures to symmetrize an asymmetric systematic error: (i) keep the central value untouched and enlarge the smaller error, (ii) shift the central value by half of the difference between the two original errors and enlarge/shrink both errors by the same amount. Our procedure (iii) is to average the results of (i) and (ii). In other words a result $c(s)\binom{u}{\ell}$ with $\ell > u$ is changed into $c + (u - \ell)/4$ with statistical error s and a symmetric systematic error $(u + 3\ell)/4$. The case $\ell < u$ is handled accordingly.

Collaboration	Ref.	N_f	publication status	chiral extrapolation	continuum extrapolation	finite volume	$\bar{\ell}_3$	$\bar{\ell}_4$
ETM 11	[253]	2+1+1	C	○	★	○	3.53(5)	4.73(2)
ETM 10	[96]	2+1+1	A	○	○	○	3.70(7)(26)	4.67(3)(10)
RBC/UKQCD 12	[25]	2+1	P	★	○	★	2.91(23)(07)	3.99(16)(09)
Borsanyi 12	[238]	2+1	P	★	★	○	3.16(10)(29)	4.03(03)(16)
NPLQCD 11	[254]	2+1	A	○	○	★	$4.04(40)\left(^{+73}_{-55}\right)$	$4.30(51)\left(^{+84}_{-60}\right)$
MILC 10A	[75]	2+1	C	○	★	★	$2.85(81)\left(^{+37}_{-92}\right)$	$3.98(32)\left(^{+51}_{-28}\right)$
MILC 10	[151]	2+1	C	○	★	★	3.18(50)(89)	4.29(21)(82)
RBC/UKQCD 10A	[78]	2+1	A	○	○	★	2.57(18)	3.83(9)
MILC 09A	[37]	2+1	C	○	★	★	3.32(64)(45)	4.03(16)(17)
MILC 09A	[37]	2+1	C	○	★	★	$3.0(6)\left(^{+9}_{-6}\right)$	3.9(2)(3)
PACS-CS 08	[19]	2+1	A	★	■	■	3.47(11)	4.21(11)
PACS-CS 08	[19]	2+1	A	★	■	■	3.14(23)	4.04(19)
RBC/UKQCD 08	[79]	2+1	A	○	■	★	3.13(33)(24)	4.43(14)(77)
QCDSF 13	[255]	2	P	★	★	■		4.2(1)
Bernardoni 11	[246]	2	C	○	■	■	4.46(30)(14)	4.56(10)(4)
TWQCD 11	[174]	2	A	★	■	■	4.149(35)(14)	4.582(17)(20)
ETM 09C	[230]	2	A	○	★	○	$3.50(9)\left(^{+09}_{-30}\right)$	$4.66(4)\left(^{+04}_{-33}\right)$
JLQCD/TWQCD 09	[257]	2	A	○	■	■		4.09(50)(52)
ETM 08	[227]	2	A	○	○	○	3.2(8)(2)	4.4(2)(1)
JLQCD/TWQCD 08A	[67]	2	A	○	■	■	$3.38(40)(24)\left(^{+31}_{-00}\right)$	$4.12(35)(30)\left(^{+31}_{-00}\right)$
CERN-TOV 06	[258]	2	A	○	★	■	3.0(5)(1)	
Colangelo 01	[182]							4.4(2)
Gasser 84	[58]						2.9(2.4)	4.3(9)

Table 15: Results for the SU(2) NLO couplings $\bar{\ell}_3$ and $\bar{\ell}_4$. The MILC 10 results are obtained by converting the SU(3) LECs, while the MILC 10A results are obtained with a direct SU(2) fit. For comparison, the last two lines show results from phenomenological analyses.

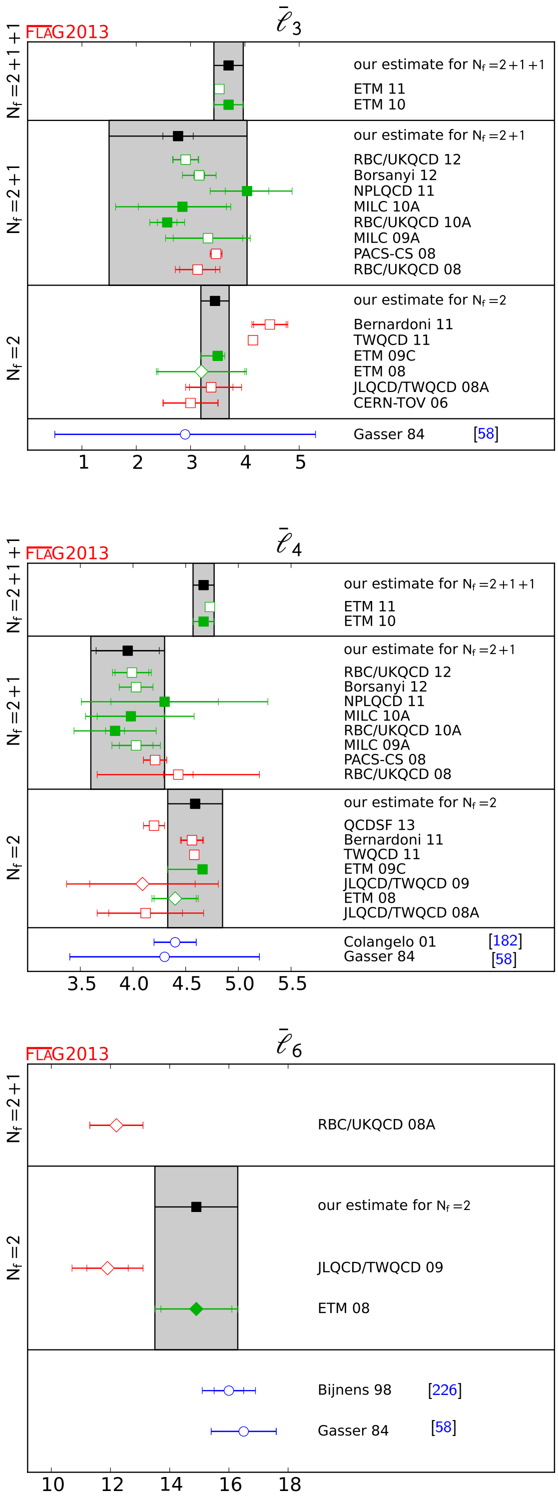

Figure 10: Effective coupling constants $\bar{\ell}_3$, $\bar{\ell}_4$ and $\bar{\ell}_6$. Squares indicate determinations from correlators in the p-regime, diamonds refer to determinations from the pion form factor.

$N_f = 2+1+1$ average on the other side. Again, the dependence of the average on the number of active flavours is not monotonic, and this raises a decent amount of suspicion that some of the systematic errors might still be underestimated.

More specifically, it seems that again the $N_f = 2+1+1$ value by ETMC shows some tension relative to the average $N_f = 2+1$ value quoted above, in close analogy to what happened for F or F_π/F; see the discussion around (65). Since both F and $\bar{\ell}_4$ are determined from the quark-mass dependence of the pseudoscalar decay constant, perhaps the formulas in Refs. [259, 260] for dealing with cut-off and finite-volume effects with twisted-mass data might prove useful in future analysis.

From a more phenomenological viewpoint there is a notable difference between $\bar{\ell}_3$ and $\bar{\ell}_4$ in Figure 10. For $\bar{\ell}_4$ the precision of the phenomenological determination achieved in Colangelo 01 [182] represents a significant improvement compared to Gasser 84 [58]. Picking any N_f, the lattice average of $\bar{\ell}_4$ is consistent with both of the phenomenological values and comes with an error which is roughly comparable to the uncertainty of the result in Colangelo 01 [182]. By contrast, for $\bar{\ell}_3$ the error of the lattice determination is significantly smaller than the error of the estimate given in Gasser 84 [58]. In other words, here the lattice really provides some added value.

We finish with a discussion of the lattice results for $\bar{\ell}_6$ and $\bar{\ell}_1 - \bar{\ell}_2$. The LEC $\bar{\ell}_6$ determines the leading contribution in the chiral expansion of the pion charge radius – see (62). Hence from a lattice study of the vector form factor of the pion with several M_π one may extract the radius $\langle r^2\rangle_V^\pi$, the curvature c_V (both at the physical pion-mass point) and the LEC $\bar{\ell}_6$ in one go. Similarly, the leading contribution in the chiral expansion of the scalar radius of the pion determines $\bar{\ell}_4$ – see (62) – but this LEC is also present in the pion-mass dependence of F_π, as we have seen. The difference $\bar{\ell}_1 - \bar{\ell}_2$, finally, may be obtained from the momentum dependence of the vector and scalar pion form factors, based on the two-loop formulae of [226].

The top part of Table 16 collects the results obtained for the vector form factor of the pion – charge radius, curvature and $\bar{\ell}_6$. The experimental information concerning the charge radius is excellent and the curvature is also known very accurately, based on e^+e^- data and dispersion theory. The vector form factor calculations thus present an excellent testing ground for the lattice methodology. The table shows that most of the available lattice results pass the test. There is, however, one worrisome point. For $\bar{\ell}_6$ the agreement seems less convincing than for the charge radius, even though the two quantities are closely related. So far we have no explanation, but we urge the groups to pay special attention to this point. Similarly, the bottom part of Table 16 collects the results obtained for the scalar form factor of the pion and the combination $\bar{\ell}_1 - \bar{\ell}_2$ that is extracted from it.

Perhaps the most important physics result of this section is that the lattice simulations confirm the approximate validity of the Gell-Mann-Oakes-Renner formula and show that the square of the pion mass indeed grows in proportion to m_{ud}. The formula represents the leading term of the chiral perturbation series and necessarily receives corrections from higher orders. At first nonleading order, the correction is determined by the effective coupling constant $\bar{\ell}_3$. The results collected in Table 15 and in the top panel of Figure 10 show that $\bar{\ell}_3$ is now known quite well. They corroborate the conclusion drawn already in Ref. [264]: the lattice confirms the estimate of $\bar{\ell}_3$ derived in [58]. In the graph of M_π^2 versus m_{ud}, the values found on the lattice for $\bar{\ell}_3$ correspond to remarkably little curvature: the Gell-Mann-Oakes-Renner formula represents a reasonable first approximation out to values of m_{ud} that exceed the physical value by an order of magnitude.

Collaboration	Ref.	N_f	publication status	chiral extrapolation	continuum extrapolation	finite volume	$\langle r^2\rangle_V^\pi$	c_V	$\bar{\ell}_6$
RBC/UKQCD 08A	[242]	2+1	A	○	■	★	0.418(31)		12.2(9)
LHP 04	[261]	2+1	A	○	■	○	0.310(46)		
JLQCD/TWQCD 09	[257]	2	A	○	■	■	0.409(23)(37)	3.22(17)(36)	11.9(0.7)(1.0)
ETM 08	[227]	2	A	○	○	○	0.456(30)(24)	3.37(31)(27)	14.9(1.2)(0.7)
QCDSF/UKQCD 06A	[262]	2	A	○	★	○	0.441(19)(56)(29)		
Bijnens 98	[226]						0.437(16)	3.85(60)	16.0(0.5)(0.7)
NA7 86	[263]						0.439(8)		
Gasser 84	[58]								16.5(1.1)

Collaboration	Ref.	N_f	publication status	chiral extrapolation	continuum extrapolation	finite volume	$\langle r^2\rangle_S^\pi$	$\bar{\ell}_1 - \bar{\ell}_2$
JLQCD/TWQCD 09	[257]	2	A	○	■	■	0.617(79)(66)	-2.9(0.9)(1.3)
Colangelo 01	[182]						0.61(4)	-4.7(6)

Table 16: *Top panel: vector form factor of the pion.* Lattice results for the charge radius $\langle r^2\rangle_V^\pi$ (in fm^2), the curvature c_V (in GeV^{-4}) and the effective coupling constant $\bar{\ell}_6$ are compared with the experimental value obtained by NA7 and some phenomenological estimates. *Bottom panel: scalar form factor of the pion.* Lattice results for the scalar radius $\langle r^2\rangle_S^\pi$ (in fm^2) and the combination $\bar{\ell}_1 - \bar{\ell}_2$ are compared with a dispersive calculation of these quantities [182].

As emphasized by Stern and collaborators [265–267], the analysis in the framework of χPT is coherent only if (*i*) the leading term in the chiral expansion of M_π^2 dominates over the remainder and (*ii*) the ratio m_s/m_{ud} is close to the value 25.6 that follows from Weinberg's leading-order formulae. In order to investigate the possibility that one or both of these conditions might fail, the authors proposed a more general framework, referred to as "Generalized χPT", which includes χPT as a special case. The results found on the lattice demonstrate that QCD does satisfy both of the above conditions – in the context of QCD, the proposed generalization of the effective theory does not appear to be needed. There is a modified version, however, referred to as "Resummed χPT" [268], which is motivated by the possibility that the Zweig rule violating couplings L_4 and L_6 might be larger than expected. The available lattice data do not support this possibility, but they do not rule it out either (see section 5.2.4 for details).

5.2 SU(3) Low-Energy Constants

5.2.1 Quark-mass dependence of pseudoscalar masses and decay constants

In the isospin limit, the relevant SU(3) formulae take the form [56]

$$\begin{aligned}
M_\pi^2 &\overset{\text{NLO}}{=} 2B_0 m_{ud}\Big\{1+\mu_\pi-\frac{1}{3}\mu_\eta+\frac{B_0}{F_0^2}\Big[16m_{ud}(2L_8-L_5)+16(m_s+2m_{ud})(2L_6-L_4)\Big]\Big\}\,,\\
M_K^2 &\overset{\text{NLO}}{=} B_0(m_s+m_{ud})\Big\{1+\frac{2}{3}\mu_\eta+\frac{B_0}{F_0^2}\Big[8(m_s+m_{ud})(2L_8-L_5)+16(m_s+2m_{ud})(2L_6-L_4)\Big]\Big\}\,,\\
F_\pi &\overset{\text{NLO}}{=} F_0\Big\{1-2\mu_\pi-\mu_K+\frac{B_0}{F_0^2}\Big[8m_{ud}L_5+8(m_s+2m_{ud})L_4\Big]\Big\}\,,\\
F_K &\overset{\text{NLO}}{=} F_0\Big\{1-\frac{3}{4}\mu_\pi-\frac{3}{2}\mu_K-\frac{3}{4}\mu_\eta+\frac{B_0}{F_0^2}\Big[4(m_s+m_{ud})L_5+8(m_s+2m_{ud})L_4\Big]\Big\}\,,
\end{aligned}\tag{68}$$

where m_{ud} is the common up and down quark mass (which may be different from the one in the real world), and $B_0=\Sigma_0/F_0^2$, F_0 denote the condensate parameter and the pseudoscalar decay constant in the SU(3) chiral limit, respectively. In addition, we use the notation

$$\mu_P=\frac{M_P^2}{32\pi^2F_0^2}\ln\Big(\frac{M_P^2}{\mu^2}\Big)\,. \tag{69}$$

At the order of the chiral expansion used in these formulae, the quantities μ_π, μ_K, μ_η can equally well be evaluated with the leading-order expressions for the masses,

$$M_\pi^2\overset{\text{LO}}{=}2B_0\,m_{ud}\,,\quad M_K^2\overset{\text{LO}}{=}B_0(m_s+m_{ud})\,,\quad M_\eta^2\overset{\text{LO}}{=}\tfrac{2}{3}B_0(2m_s+m_{ud})\,. \tag{70}$$

Throughout, L_i denotes the renormalized low-energy constant/coupling (LEC) at scale μ, and we adopt the convention which is standard in phenomenology, $\mu=770\,\text{MeV}$. The normalization used for the decay constants is specified in footnote 14.

5.2.2 Charge radius

The SU(3) formula for the slope of the pion vector form factor reads [145]

$$\langle r^2\rangle_V^\pi \;\overset{\text{LO}}{=}\; -\frac{1}{32\pi^2F_0^2}\Big\{3+2\ln\big(\frac{M_\pi^2}{\mu^2}\big)+\ln\big(\frac{M_K^2}{\mu^2}\big)\Big\}+\frac{12L_9}{F_0^2}\,, \tag{71}$$

while the expression $\langle r^2\rangle_S^{\rm oct}$ for the octet part of the scalar radius does not contain any NLO low-energy constant at the one-loop order [145] (cf. 5.1.5 for the situation in SU(2)).

5.2.3 Partially quenched formulae

The term "partially quenched QCD" is used in two ways. For heavy quarks (c, b and sometimes s) it usually means that these flavours are included in the valence sector, but not into the functional determinant. For the light quarks (u, d and sometimes s) it means that they are present in both the valence and the sea sector of the theory, but with different masses (e.g. a series of valence quark masses is evaluated on an ensemble with a fixed sea quark mass).

The program of extending the standard (unitary) SU(3) theory to the (second version of) "partially quenched QCD" has been completed at the two-loop (NNLO) level for masses and decay constants [269]. These formulae tend to be complicated, with the consequence that a state-of-the-art analysis with $O(2000)$ bootstrap samples on $O(20)$ ensembles with $O(5)$ masses each [and hence $O(200'000)$ different fits] will require significant computational resources for the global fits. For an up-to-date summary of recent developments in Chiral Perturbation Theory relevant to lattice QCD we refer to [270].

The theoretical underpinning of how "partial quenching" is to be treated in the (properly extended) chiral framework is given in [271]. Specifically for partially quenched QCD with staggered quarks it is shown that a transfer matrix can be constructed which is not Hermitian but bounded, and can thus be used to construct correlation functions in the usual way.

5.2.4 Lattice determinations

To date, there are three comprehensive SU(3) papers with results based on lattice QCD with $N_f = 2+1$ dynamical flavours [15, 19, 79], and one more with results based on $N_f = 2+1+1$ dynamical flavours [148]. It is an open issue whether the data collected at $m_s \simeq m_s^{\rm phys}$ allow for an unambiguous determination of SU(3) low-energy constants (cf. the discussion in [79]). To make definite statements one needs data at considerably smaller m_s, and so far only MILC has some [15]. We are aware of a few papers with a result on one SU(3) low-energy constant each [78, 158, 242, 272] which we list for completeness. Some particulars of the computations are listed in Table 17.

Results for the SU(3) low-energy constants of leading order are found in Table 17 and analogous results for some of the effective coupling constants that enter the chiral SU(3) Lagrangian at NLO are collected in Table 18. From PACS-CS [19] only those results are quoted which have been *corrected* for finite-size effects (misleadingly labeled "w/FSE" in their tables). For staggered data our colour-coding rule states that M_π is to be understood as $M_\pi^{\rm RMS}$. The rating of [15, 151] is based on the information regarding the RMS masses given in [37].

A graphical summary of the lattice results for the coupling constants L_4, L_5, L_6 and L_8, which determine the masses and the decay constants of the pions and kaons at NLO of the chiral SU(3) expansion, is displayed in Figure 11, along with the two phenomenological determinations quoted in the above tables. The overall consistency seems fairly convincing. To date only the computations MILC 09A [37] (as an obvious update of MILC 09) and HPQCD 13A [148] are free of red tags. Since the latter are not yet published the grey bands in Figure 11 merely represent the former set of results.

Collaboration	Ref.	N_f	publication status	chiral extrapolation	continuum extrapolation	finite volume	renormalization	F_0	F/F_0	B/B_0
JLQCD/TWQCD 10	[241]	3	A	■	■	■	★	71(3)(8)		
MILC 10	[151]	2+1	C	○	★	★	○	80.3(2.5)(5.4)		
MILC 09A	[37]	2+1	C	○	★	★	○	78.3(1.4)(2.9)	*1.104(3)(41)*	*1.21(4)*$\binom{+5}{-6}$
MILC 09	[15]	2+1	A	○	★	★	○		1.15(5)$\binom{+13}{-03}$	*1.15(16)*$\binom{+39}{-13}$
PACS-CS 08	[19]	2+1	A	★	■	■	■	83.8(6.4)	1.078(44)	1.089(15)
RBC/UKQCD 08	[79]	2+1	A	○	■	★	★	66.1(5.2)	1.229(59)	1.03(05)

Collaboration	Ref.	N_f	publication status	chiral extrapolation	continuum extrapolation	finite volume	renormalization	$\Sigma_0^{1/3}$	Σ/Σ_0
JLQCD/TWQCD 10	[241]	3	A	■	■	■	★	214(6)(24)	*1.31(13)(52)*
MILC 09A	[37]	2+1	C	○	★	★	○	245(5)(4)(4)	*1.48(9)(8)(10)*
MILC 09	[15]	2+1	A	○	★	★	○	242(9)$\binom{+05}{-17}$(4)	1.52(17)$\binom{+38}{-15}$
PACS-CS 08	[19]	2+1	A	★	■	■	■	290(15)	1.245(10)
RBC/UKQCD 08	[79]	2+1	A	○	■	★	★		1.55(21)

Table 17: Lattice results for the low-energy constants F_0, B_0 and $\Sigma_0 \equiv F_0^2 B_0$, which specify the effective SU(3) Lagrangian at leading order (MeV units). The ratios F/F_0, B/B_0, Σ/Σ_0, which compare these with their SU(2) counterparts, indicate the strength of the Zweig-rule violations in these quantities (in the large-N_c limit, they tend to unity). Numbers in slanted fonts are calculated by us, from the information given in the quoted references.

In spite of this apparent consistency, there is a point which needs to be clarified as soon as possible. Some collaborations (RBC/UKQCD and PACS-CS) find that they are having difficulties in fitting their partially quenched data to the respective formulas for pion masses above $\simeq$ 400 MeV. Evidently, this indicates that the data are stretching the regime of validity of these formulas. To date it is, however, not clear which subset of the data causes the troubles, whether it is the unitary part extending to too large values of the quark masses or whether it is due to $m^{\rm val}/m^{\rm sea}$ differing too much from one. In fact, little is known, in the framework of partially quenched χPT, about the *shape* of the region of applicability in the $m^{\rm val}$ versus $m^{\rm sea}$ plane for fixed N_f. This point has also been emphasized in [233].

In the large-N_c limit, the Zweig-rule becomes exact, but the quarks have $N_c = 3$. The

	Ref.	N_f	publication status	chiral extrapolation	continuum extrapolation	finite volume	$10^3 L_4$	$10^3 L_6$	$10^3(2L_6-L_4)$
HPQCD 13A	[148]	2+1+1	P	★	★	★	0.09(34)	0.16(20)	0.22(17)
JLQCD/TWQCD 10A	[241]	3	A	■	■	■		0.03(7)(17)	
MILC 10	[151]	2+1	C	○	★	★	-0.08(22)$\binom{+57}{-33}$	*-0.02(16)*$\binom{+33}{-21}$	0.03(24)$\binom{+32}{-27}$
MILC 09A	[37]	2+1	C	○	★	★	0.04(13)(4)	0.07(10)(3)	0.10(12)(2)
MILC 09	[15]	2+1	A	○	★	★	0.1(3)$\binom{+3}{-1}$	0.2(2)$\binom{+2}{-1}$	0.3(1)$\binom{+2}{-3}$
PACS-CS 08	[19]	2+1	A	★	■	■	-0.06(10)(-)	*0.02(5)(-)*	0.10(2)(-)
RBC/UKQCD 08	[79]	2+1	A	○	■	★	0.14(8)(-)	0.07(6)(-)	0.00(4)(-)
Bijnens 11	[270]						0.75(75)	0.29(85)	*-0.17(1.86)*
Gasser 85	[56]						-0.3(5)	-0.2(3)	*-0.1(8)*

	Ref.	N_f					$10^3 L_5$	$10^3 L_8$	$10^3(2L_8-L_5)$
HPQCD 13A	[148]	2+1+1	P	★	★	★	1.19(25)	0.55(15)	-0.10(20)
MILC 10	[151]	2+1	C	○	★	★	0.98(16)$\binom{+28}{-41}$	*0.42(10)*$\binom{+27}{-23}$	-0.15(11)$\binom{+45}{-19}$
MILC 09A	[37]	2+1	C	○	★	★	0.84(12)(36)	0.36(5)(7)	-0.12(8)(21)
MILC 09	[15]	2+1	A	○	★	★	1.4(2)$\binom{+2}{-1}$	0.8(1)(1)	0.3(1)(1)
PACS-CS 08	[19]	2+1	A	★	■	■	1.45(7)(-)	*0.62(4)(-)*	-0.21(3)(-)
RBC/UKQCD 08	[79]	2+1	A	○	■	★	0.87(10)(-)	0.56(4)(-)	0.24(4)(-)
Bijnens 11	[270]						0.58(13)	0.18(18)	*-0.22(38)*
Gasser 85	[56]						1.4(5)	0.9(3)	*0.4(8)*

	Ref.	N_f					$10^3 L_5$	$10^3 L_9$	$10^3 L_{10}$
RBC/UKQCD 09?	[273]	2+1	A	○	■	○			-5.7(11)(07)
RBC/UKQCD 08A	[242]	2+1	A	○	■	★		3.08(23)(51)	
NPLQCD 06	[158]	2+1	A	○	■	■	1.42(2)$\binom{+18}{-54}$		
JLQCD 08A	[272]	2	A	○	■	■			-5.2(2)$\binom{+5}{-3}$
Bijnens 11	[270]						0.58(13)		
Bijnens 02	[274]							5.93(43)	
Davier 98	[275]								-5.13(19)
Gasser 85	[56]						1.4(5)	6.9(7)	-5.5(7)

Table 18: Low-energy constants that enter the effective SU(3) Lagrangian at NLO (running scale $\mu = 770\,\mathrm{MeV}$ – the values in [15, 37, 56, 151] are evolved accordingly). The MILC 10 entry for L_6 is obtained from their results for $2L_6-L_4$ and L_4 (and similarly for other entries in slanted fonts). The JLQCD 08A result [which is for $\ell_5(770\,\mathrm{MeV})$ despite the paper saying $L_{10}(770\,\mathrm{MeV})$] has been converted to L_{10} with the standard one-loop formula, assuming that the difference between $\bar{\ell}_5(m_s = m_s^{\mathrm{phys}})$ [needed in the formula] and $\bar{\ell}_5(m_s=\infty)$ [computed by JLQCD] can be ignored.

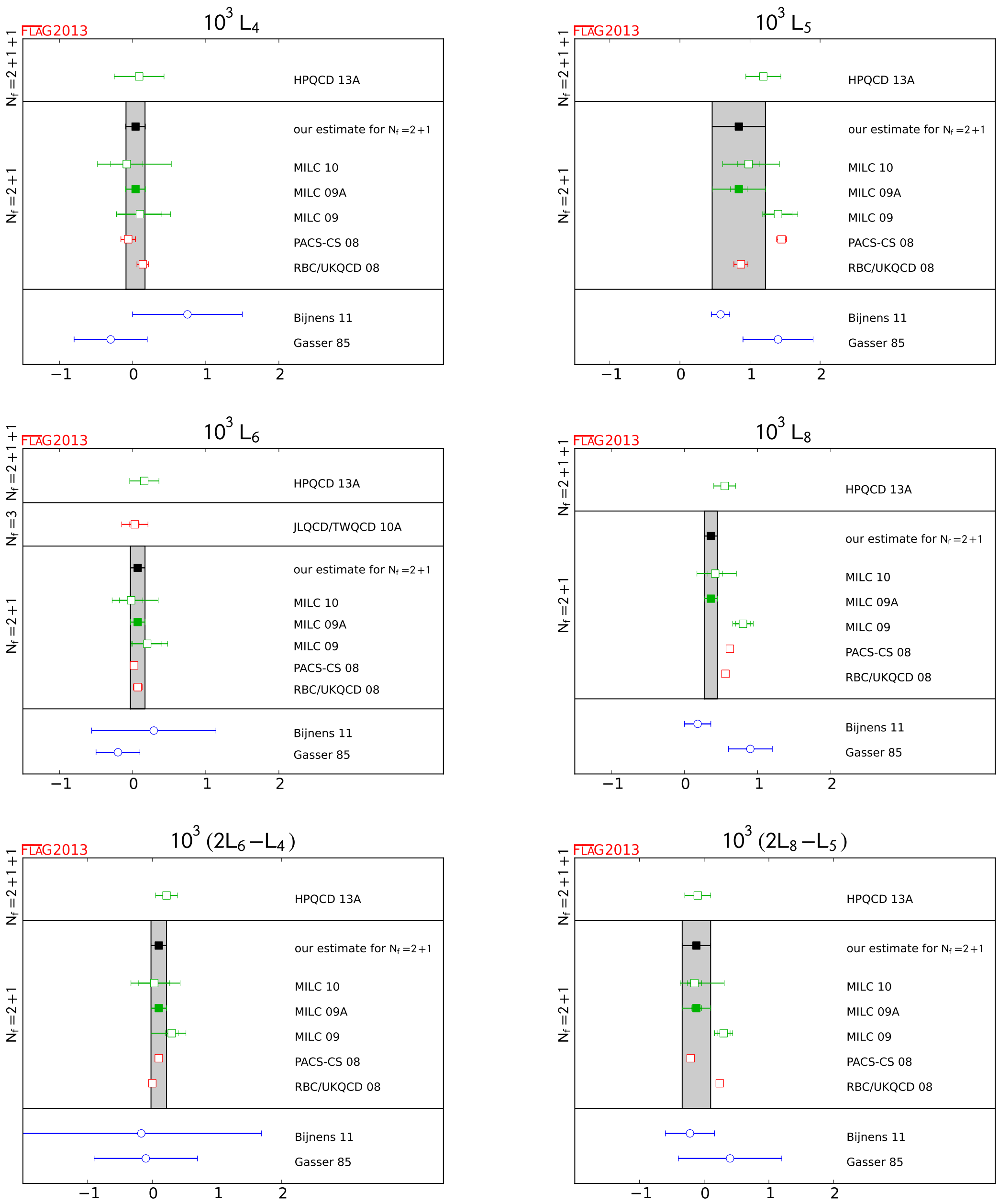

Figure 11: Low-energy constants that enter the effective SU(3) Lagrangian at NLO.

work done on the lattice is ideally suited to disprove or confirm the approximate validity of this rule for QCD. Two of the coupling constants entering the effective SU(3) Lagrangian at NLO disappear when N_c is sent to infinity: L_4 and L_6. The upper part of Table 18 and the left panels of Figure 11 show that the lattice results for these are quite coherent. At the scale $\mu = M_\rho$, L_4 and L_6 are consistent with zero, indicating that these constants do approximately obey the Zweig-rule. As mentioned above, the ratios F/F_0, B/B_0 and Σ/Σ_0 also test the validity of this rule. Their expansion in powers of m_s starts with unity and the contributions of first order in m_s are determined by the constants L_4 and L_6, but they also contain terms of higher order. Apart from measuring the Zweig-rule violations, an accurate determination of these ratios will thus also allow us to determine the range of m_s where the first few terms of the expansion represent an adequate approximation. Unfortunately, at present, the uncertainties in the lattice data on these ratios are too large to draw conclusions, both concerning the relative size of the subsequent terms in the chiral perturbation series and concerning the magnitude of the Zweig-rule violations. The data seem to confirm the *paramagnetic inequalities* [267], which require $F/F_0 > 1$, $\Sigma/\Sigma_0 > 1$, and it appears that the ratio B/B_0 is also larger than unity, but the numerical results need to be improved before further conclusions can be drawn.

In principle, the matching formulae in [56] can be used to calculate[23] the SU(2) couplings $\bar{l}_i$ from the SU(3) couplings L_j. This procedure, however, yields less accurate results than a direct determination within SU(2), as it relies on the expansion in powers of m_s, where the omitted higher-order contributions generate comparatively large uncertainties. We plead with every collaboration performing $N_f = 2 + 1$ simulations to *directly* analyze their data in the SU(2) framework. In practice, lattice simulations are performed at values of m_s close to the physical value and the results are then corrected for the difference of m_s from its physical value. If simulations with more than one value of m_s have been performed, this can be done by interpolation. Alternatively one can use the technique of *reweighting* (for a review see e.g. [276]) to shift m_s to its physical value.

[23] For instance, for the MILC data this yields $\bar{l}_3 = 3.32(64)(45)$ and $\bar{l}_4 = 4.03(16)(17)$ [37].

6 Kaon B-parameter B_K

6.1 Indirect CP-violation and ϵ_K

The mixing of neutral pseudoscalar mesons plays an important role in the understanding of the physics of CP-violation. In this section we will only focus on $K^0 - \bar{K}^0$ oscillations, which probe the physics of indirect CP-violation. We collect here the basic formulae; for extended reviews on the subject see, among others, Refs. [277–279]. Indirect CP-violation arises in $K_L \to \pi\pi$ transitions through the decay of the CP $= +1$ component of K_L into two pions (which are also in a CP $= +1$ state). Its measure is defined as

$$\epsilon_K \;=\; \frac{\mathcal{A}[K_L \to (\pi\pi)_{I=0}]}{\mathcal{A}[K_S \to (\pi\pi)_{I=0}]}\;, \tag{72}$$

with the final state having total isospin zero. The parameter ϵ_K may also be expressed in terms of $K^0 - \bar{K}^0$ oscillations. In particular, to lowest order in the electroweak theory, the contribution to these oscillations arises from so-called box diagrams, in which two W-bosons and two "up-type" quarks (i.e. up, charm, top) are exchanged between the constituent down and strange quarks of the K-mesons. The loop integration of the box diagrams can be performed exactly. In the limit of vanishing external momenta and external quark masses, the result can be identified with an effective four-fermion interaction, expressed in terms of the "effective Hamiltonian"

$$\mathcal{H}_{\rm eff}^{\Delta S=2} \;=\; \frac{G_{\rm F}^2 M_W^2}{16\pi^2}\mathcal{F}^0 Q^{\Delta S=2} \;+\; {\rm h.c.}\;. \tag{73}$$

In this expression, $G_{\rm F}$ is the Fermi coupling, M_W the W-boson mass, and

$$Q^{\Delta S=2} = [\bar{s}\gamma_\mu(1-\gamma_5)d]\,[\bar{s}\gamma_\mu(1-\gamma_5)d] \equiv O_{\rm VV+AA} - O_{\rm VA+AV} \tag{74}$$

is a dimension-six, four-fermion operator. The function $\mathcal{F}^0$ is given by

$$\mathcal{F}^0 \;=\; \lambda_c^2 S_0(x_c) \;+\; \lambda_t^2 S_0(x_t) \;+\; 2\lambda_c\lambda_t S_0(x_c, x_t)\;, \tag{75}$$

where $\lambda_a = V_{as}^* V_{ad}$, and $a = c\,,t$ denotes a flavour index. The quantities $S_0(x_c)$, $S_0(x_t)$ and $S_0(x_c, x_t)$ with $x_c = m_c^2/M_W^2$, $x_t = m_t^2/M_W^2$ are the Inami-Lim functions [280], which express the basic electroweak loop contributions without QCD corrections. The contribution of the up quark, which is taken to be massless in this approach, has been taken into account by imposing the unitarity constraint $\lambda_u + \lambda_c + \lambda_t = 0$. For future reference we note that the dominant contribution comes from the term $\lambda_t^2 S_0(x_t)$. This factor is proportional to $|V_{cb}|^4$ if one enforces the unitarity of the CKM matrix. The dependence on a high power of V_{cb} is important from a phenomenological point of view because it implies that uncertainties in V_{cb} are magnified when considering ϵ_K.

When strong interactions are included, $\Delta S = 2$ transitions can no longer be discussed at the quark level. Instead, the effective Hamiltonian must be considered between mesonic initial and final states. Since the strong coupling constant is large at typical hadronic scales, the resulting weak matrix element cannot be calculated in perturbation theory. The operator product expansion (OPE) does, however, factorize long- and short-distance effects. For energy scales below the charm threshold, the $K^0 - \bar{K}^0$ transition amplitude of the effective

Hamiltonian can be expressed as

$$\langle\bar{K}^0|\mathcal{H}_{\rm eff}^{\Delta S=2}|K^0\rangle \;=\; \frac{G_{\rm F}^2 M_W^2}{16\pi^2}\Big[\lambda_c^2 S_0(x_c)\eta_1 \,+\, \lambda_t^2 S_0(x_t)\eta_2 \,+\, 2\lambda_c\lambda_t S_0(x_c,x_t)\eta_3\Big]$$
$$\times\left(\frac{\bar{g}(\mu)^2}{4\pi}\right)^{-\gamma_0/(2\beta_0)} \exp\left\{\int_0^{\bar{g}(\mu)} dg\left(\frac{\gamma(g)}{\beta(g)}+\frac{\gamma_0}{\beta_0 g}\right)\right\}\langle\bar{K}^0|Q_{\rm R}^{\Delta S=2}(\mu)|K^0\rangle \;+\; {\rm h.c.}\,, \qquad (76)$$

where $\bar{g}(\mu)$ and $Q_{\rm R}^{\Delta S=2}(\mu)$ are the renormalized gauge coupling and four-fermion operator in some renormalization scheme. The factors η_1,η_2 and η_3 depend on the renormalized coupling $\bar{g}$, evaluated at the various flavour thresholds m_t, m_b, m_c and M_W, as required by the OPE and RG-running procedure that separates high- and low-energy contributions. Explicit expressions can be found in [278] and references therein, except that η_1 and η_3 have been recently calculated to NNLO in Refs. [281] and [282], respectively. We follow the same conventions for the RG-equations as in Ref. [278]. Thus the Callan-Symanzik function and the anomalous dimension $\gamma(\bar{g})$ of $Q^{\Delta S=2}$ are defined by

$$\frac{d\bar{g}}{d\ln\mu} = \beta(\bar{g})\,, \qquad \frac{dQ_{\rm R}^{\Delta S=2}}{d\ln\mu} = -\gamma(\bar{g})\,Q_{\rm R}^{\Delta S=2}\,, \qquad (77)$$

with perturbative expansions

$$\begin{aligned}\beta(g) &= -\beta_0\frac{g^3}{(4\pi)^2} \,-\, \beta_1\frac{g^5}{(4\pi)^4} \,-\, \cdots \\ \gamma(g) &= \gamma_0\frac{g^2}{(4\pi)^2} \,+\, \gamma_1\frac{g^4}{(4\pi)^4} \,+\, \cdots\,.\end{aligned} \qquad (78)$$

We stress that β_0, β_1 and γ_0 are universal, i.e. scheme-independent. $K^0-\bar{K}^0$ mixing is usually considered in the naive dimensional regularization (NDR) scheme of $\overline{\rm MS}$, and below we specify the perturbative coefficient γ_1 in that scheme:

$$\begin{aligned}&\beta_0 = \left\{\frac{11}{3}N_c - \frac{2}{3}N_f\right\}, \qquad \beta_1 = \left\{\frac{34}{3}N_c^2 - N_f\left(\frac{13}{3}N_c - \frac{1}{N_c}\right)\right\}, \\ &\gamma_0 = \frac{6(N_c-1)}{N_c}, \qquad \gamma_1 = \frac{N_c-1}{2N_c}\left\{-21 + \frac{57}{N_c} - \frac{19}{3}N_c + \frac{4}{3}N_f\right\}.\end{aligned} \qquad (79)$$

Note that for QCD the above expressions must be evaluated for $N_c = 3$ colours, while N_f denotes the number of active quark flavours. As already stated, Eq. (76) is valid at scales below the charm threshold, after all heavier flavours have been integrated out, i.e. $N_f = 3$.

In Eq. (76), the terms proportional to η_1, η_2 and η_3, multiplied by the contributions containing $\bar{g}(\mu)^2$, correspond to the Wilson coefficient of the OPE, computed in perturbation theory. Its dependence on the renormalization scheme and scale μ is canceled by that of the weak matrix element $\langle\bar{K}^0|Q_{\rm R}^{\Delta S=2}(\mu)|K^0\rangle$. The latter corresponds to the long-distance effects of the effective Hamiltonian and must be computed nonperturbatively. For historical, as well as technical reasons, it is convenient to express it in terms of the B-parameter B_K, defined as

$$B_K(\mu) = \frac{\left\langle\bar{K}^0\left|Q_{\rm R}^{\Delta S=2}(\mu)\right|K^0\right\rangle}{\frac{8}{3}f_{\rm K}^2 m_{\rm K}^2}\,. \qquad (80)$$

The four-quark operator $Q^{\Delta S=2}(\mu)$ is renormalized at scale μ in some regularization scheme, for instance, NDR-$\overline{\rm MS}$. Assuming that $B_K(\mu)$ and the anomalous dimension $\gamma(g)$ are both known in that scheme, the renormalization group invariant (RGI) B-parameter $\hat{B}_K$ is related to $B_K(\mu)$ by the exact formula

$$\hat{B}_K = \left(\frac{\bar{g}(\mu)^2}{4\pi}\right)^{-\gamma_0/(2\beta_0)} \exp\left\{ \int_0^{\bar{g}(\mu)} dg \left(\frac{\gamma(g)}{\beta(g)} + \frac{\gamma_0}{\beta_0 g}\right)\right\} B_K(\mu) \ . \tag{81}$$

At NLO in perturbation theory the above reduces to

$$\hat{B}_K = \left(\frac{\bar{g}(\mu)^2}{4\pi}\right)^{-\gamma_0/(2\beta_0)} \left\{1 + \frac{\bar{g}(\mu)^2}{(4\pi)^2}\left[\frac{\beta_1\gamma_0 - \beta_0\gamma_1}{2\beta_0^2}\right]\right\} B_K(\mu) \ . \tag{82}$$

To this order, this is the scale-independent product of all μ-dependent quantities in Eq. (76).

Lattice QCD calculations provide results for $B_K(\mu)$. These results, however, are usually obtained in intermediate schemes other than the continuum $\overline{\mathrm{MS}}$ scheme used to calculate the Wilson coefficients appearing in Eq. (76). Examples of intermediate schemes are the RI/MOM scheme [283] (also dubbed the "Rome-Southampton method") and the Schrödinger functional (SF) scheme [87], which both allow for a nonperturbative renormalization of the four-fermion operator, using an auxiliary lattice simulation. In this way $B_K(\mu)$ can be calculated with percent-level accuracy, as described below.

In order to make contact with phenomenology, however, and in particular to use the results presented above, one must convert from the intermediate scheme to the $\overline{\mathrm{MS}}$ scheme or to the RGI quantity $\hat{B}_K$. This conversion relies on one or two-loop perturbative matching calculations, the truncation errors in which are, for many recent calculations, the dominant source of error in $\hat{B}_K$ [25, 77, 284–286]. While this scheme-conversion error is not, strictly speaking, an error of the lattice calculation itself, it must be included in results for the quantities of phenomenological interest, namely $B_K(\overline{\mathrm{MS}}, 2\,\mathrm{GeV})$ and $\hat{B}_K$. We note that this error can be minimized by matching between the intermediate scheme and $\overline{\mathrm{MS}}$ at as large a scale μ as possible (so that the coupling constant which determines the rate of convergence is minimized). Recent calculations have pushed the matching μ up to the range $3-3.5\,\mathrm{GeV}$. This is possible because of the use of nonperturbative RG running determined on the lattice [25, 287]. The Schrödinger functional offers the possibility to run nonperturbatively to scales $\mu \sim M_W$ where the truncation error can be safely neglected. However, so far this has been applied only for two flavours of Wilson quarks [288].

Perturbative truncation errors in Eq. (76) also affect the Wilson coefficients η_1, η_2 and η_3. It turns out that the largest uncertainty comes from that in η_1 [281]. Although it is now calculated at NNLO, the series shows poor convergence. The net effect is that the uncertainty in η_1 is larger than that in present lattice calculations of B_K.

The "master formula" for ϵ_K, which connects the experimentally observable quantity ϵ_K to the matrix element of $\mathcal{H}_{\rm eff}^{\Delta S=2}$, is [279, 289–291]

$$\epsilon_K \ = \ \exp(i\phi_\epsilon)\ \sin(\phi_\epsilon) \left[\frac{\mathrm{Im}[\langle \bar{K}^0|\mathcal{H}_{\rm eff}^{\Delta S=2}|K^0\rangle]}{\Delta m_K} \ + \ \rho\frac{\mathrm{Im}(A_0)}{\mathrm{Re}(A_0)}\right] , \tag{83}$$

for λ_u real and positive; the phase of ϵ_K is given by

$$\phi_\epsilon \ = \ \arctan\frac{\Delta m_K}{\Delta\Gamma_K/2} \ . \tag{84}$$

The quantities $\Delta m_K \equiv m_{K_L} - m_{K_S}$ and $\Delta\Gamma_K \equiv \Gamma_{K_S} - \Gamma_{K_L}$ are the mass- and decay width-differences between long- and short-lived neutral Kaons, while A_0 is the amplitude of the

Kaon decay into a two-pion state with isospin zero. The experimentally measured values of the above quantities are [74]:

$$\begin{aligned}|\epsilon_K| &= 2.228(11)\times 10^{-3}\ ,\\ \phi_\epsilon &= 43.52(5)^\circ\ ,\\ \Delta m_K &= 3.4839(59)\times 10^{-12}\,\mathrm{MeV}\ ,\\ \Delta\Gamma_K &= 7.3382(33)\times 10^{-12}\,\mathrm{MeV}\ .\end{aligned} \tag{85}$$

The second term in the square brackets of Eq. (83), has been discussed and estimated, e.g., in Refs. [291, 292]. It can best be thought of as $\xi + (\rho-1)\xi$, with $\xi = \mathrm{Im}(A_0)/\mathrm{Re}(A_0)$. The ξ term is the contribution of direct CP violation to ϵ_K. Using the estimate of ξ from Ref. [292] (obtained from the experimental value of ϵ'/ϵ) this gives a $\sim -6.0(1.5)\%$ correction.[24] The $(\rho-1)\xi$ term arises from long-distance contributions to the imaginary part of $K^0 - \bar{K}^0$ mixing [291] [contributions which are neglected in Eq. (76)]. Using the estimate $\rho = 0.6 \pm 0.3$ [291], this gives a contribution of about $+2\%$ with large errors. Overall these corrections combine to give a $(4\pm 2)\%$ reduction in the prediction for ϵ_K. Although this is a small correction, we note that its contribution to the error of ϵ_K is larger than that arising from the value of B_K reported below.

6.2 Lattice computation of B_K

Lattice calculations of B_K are affected by the same systematic effects discussed in previous sections. However, the issue of renormalization merits special attention. The reason is that the multiplicative renormalizability of the relevant operator $Q^{\Delta S=2}$ is lost once the regularized QCD action ceases to be invariant under chiral transformations. For Wilson fermions, $Q^{\Delta S=2}$ mixes with four additional dimension-six operators, which belong to different representations of the chiral group, with mixing coefficients that are finite functions of the gauge coupling. This complicated renormalization pattern was identified as the main source of systematic error in earlier, mostly quenched calculations of B_K with Wilson quarks. It can be bypassed via the implementation of specifically designed methods, which are either based on Ward identities [295] or on a modification of the Wilson quark action, known as twisted-mass QCD [296, 297].

An advantage of staggered fermions is the presence of a remnant $U(1)$ chiral symmetry. However, at nonvanishing lattice spacing, the symmetry among the extra unphysical degrees of freedom (tastes) is broken. As a result, mixing with other dimension-six operators cannot be avoided in the staggered formulation, which complicates the determination of the B-parameter. The effects of the broken taste symmetry are usually treated via an effective field theory, such as staggered Chiral Perturbation Theory (SχPT).

Fermionic lattice actions based on the Ginsparg-Wilson relation [298] are invariant under the chiral group, and hence four-quark operators such as $Q^{\Delta S=2}$ renormalize multiplicatively. However, depending on the particular formulation of Ginsparg-Wilson fermions, residual chiral symmetry breaking effects may be present in actual calculations. For instance, in the case of domain wall fermions, the finiteness of the extra 5th dimension implies that the decoupling

[24] A very recent lattice calculation of $\mathrm{Im}(A_2)$ by the RBC/UKQCD collaboration opens up the possibility of a more accurate determination of ξ using the measured value of ϵ' [293, 294]. This lattice calculation uses only a single lattice spacing, so we do not quote the resulting value here, but note that it is consistent with that obtained in Ref. [292], with errors estimated to be significantly smaller.

of modes with different chirality is not exact, which produces a residual nonzero quark mass in the chiral limit. Whether or not a significant mixing with dimension-six operators is induced as well must be investigated on a case-by-case basis.

In this section we focus on recent results for B_K, obtained for $N_f = 2$ and $2+1$ flavours of dynamical quarks. A compilation of results is shown in Table 19 and Fig. 12. An overview of the quality of systematic error studies is represented by the colour coded entries in Table 19. In Appendix B.4 we gather the simulation details and results from different collaborations, the values of the most relevant lattice parameters, and comparative tables on the various estimates of systematic errors.

Some of the groups whose results are listed in Table 19 do not quote results for both $B_K(\overline{\rm MS}, 2\,{\rm GeV})$ – which we denote by the shorthand B_K from now on – and $\hat{B}_K$. This concerns Refs. [299, 300] for $N_f = 2$ and [25, 77] for 2+1 flavours. In these cases we perform the conversion ourselves by evaluating the proportionality factor in Eq. (82) at $\mu = 2\,{\rm GeV}$, using the following procedure: For $N_f = 2+1$ we use the value $\alpha_s(M_Z) = 0.1184$ from the PDG [74] and run it across the quark thresholds at $m_b = 4.19\,{\rm GeV}$ and $m_c = 1.27\,{\rm GeV}$, and then run up in the three-flavour theory to $\mu = 2\,{\rm GeV}$. All running is done using the four-loop RG β-function. The resulting value of $\alpha_s(2\,{\rm GeV})$ is then used to evaluate $\hat{B}_K/B_K$ in one-loop perturbation theory, which gives $\hat{B}_K/B_K = 1.369$ in the three-flavour theory.

In two-flavour QCD one can insert the updated nonperturbative estimate for the Λ-parameter by the ALPHA Collaboration [59], i.e. $\Lambda^{(2)} = 310(20)\,{\rm MeV}$, into the NLO expressions for α_s. The resulting value of the perturbative conversion factor $\hat{B}_K/B_K$ for $N_f = 2$ is then equal to 1.386. However, since the running coupling in the $\overline{\rm MS}$ scheme enters at several stages in the entire matching and running procedure, it is difficult to use this estimate of α_s consistently without a partial reanalysis of the data in Refs. [299, 300]. We have therefore chosen to apply the conversion factor of 1.369 not only to results obtained for $N_f = 2+1$ flavours but also to the two-flavour theory (in cases where only one of $\hat{B_K}$ and B_K are quoted). This is a change from the convention used in the previous edition of the FLAG review [1]. We note that the difference between 1.386 and 1.369 will produce an ambiguity of the order of 1%, which is well below the overall uncertainties in Refs. [299, 300]. We have indicated explicitly in Table 19 in which way the conversion factor 1.369 has been applied to the results of Refs. [25, 77, 299, 300].

Note that in this section the colour code for chiral extrapolations is interpreted differently. We recall that the criteria are:

Chiral extrapolation:

- ★ $M_{\pi,\rm min} < 200$ MeV
- ○ 200 MeV $\le M_{\pi,\rm min} \le$ 400 MeV
- ■ $M_{\pi,\rm min} > 400$ MeV

Many calculations of B_K employ partially quenched χPT, and in this case it is the mass of the valence pion which enters in chiral logarithms and leads to the most significant dependence on quark masses. Therefore, whenever a specific calculation employs partially quenched pions, the above colour code is applied with respect to the minimum valence pion mass.[25] As before, it is assumed that the chiral extrapolation is done with at least a three-point analysis

[25] This approach is supported by the results of the calculations using partial quenching (see in particular Refs. [77] and [301]), which find that the dependence on sea-quark masses is weaker than that on the valence-quark masses (which itself is very mild).

– otherwise this will be explicitly mentioned in a footnote. In case of nondegeneracies among the different pion states $M_{\pi,\min}$ stands for a root-mean-squared (RMS) pion mass.

Since the first publication of the FLAG review [1] several new or updated results for the Kaon B-parameter have been reported for $N_f = 2+1$, i.e. BMW 11 [287], SWME 11A [286], Laiho 11 [77], and RBC/UKQCD 12 [25]. No new results for two-flavour QCD have appeared recently. There is a first, preliminary calculation with $N_f = 2+1+1$ [307] from the ETM collaboration. We do not include this result in the following discussion, however, because the interpretation of B_K with active charm involves several subtleties that have yet to be addressed.[26] We briefly discuss the main features of the most recent calculations below.

The BMW Collaboration has produced a new result for B_K [287], using their ensembles of HEX-smeared, tree-level $\mathrm{O}(a)$ improved Wilson fermions [23]. To this end the four finest lattice spacings, with a ranging from $0.054-0.099$ fm, are employed. Simulations are performed close to the physical pion mass, or even below that value (for the two largest lattice spacings). The smearing of the link variables results in a significant suppression of the effects of chiral symmetry breaking, since the coefficients multiplying the dimension-six operators of different chirality are found to be very small, in some cases even compatible with zero. The quoted value for $\hat{B}_K$ is obtained from a combined chiral and continuum extrapolation. In order to investigate the systematics associated with the chiral behaviour, several different cuts on the maximum pion mass are performed. Another important ingredient in BMW 11 [287] is the nonperturbative determination of the continuum step scaling function for scales varying between 1.8 and 3.5 GeV. In this way, the perturbative matching to the RGI B-parameter can be performed at $\mu = 3.5$ GeV, a value where perturbation theory at NLO is found to yield a good description of the scale dependence.

The SWME 11, 11A result [285, 286], is obtained using a mixed action: HYP-smeared valence staggered quarks on the Asqtad improved, rooted staggered MILC ensembles. Compared to the previous edition of the FLAG review[1], the major update is the addition of a fourth, finer, lattice spacing. This allows for a more extensive analysis of the continuum extrapolation, leading to more reliable estimates of the associated error (which is the second-largest error at 1.9%). Other updates include the use of correlated fits in the chiral extrapolation, the inclusion of finite-volume corrections in the chiral fits, and a significant reduction in statistical errors due to the use of an order of magnitude more sources on each lattice. The dominant error remains that from the use of one-loop perturbative matching between lattice and $\overline{\mathrm{MS}}$ schemes. This error is estimated conservatively assuming a missing two-loop matching term of size $1 \times \alpha(1/a)^2$, i.e. with no factors of $1/(4\pi)$ included. The other methods for estimating this error described earlier in this review lead to smaller estimates [308]. This procedure is, in this review, deemed conservative enough to merit inclusion in the global average described below. The resulting matching error is 4.4%.

The Laiho 11 result [77] uses a mixed action, with HYP-smeared domain wall valence quarks on the Asqtad MILC ensembles. Compared to the earlier result obtained by this collaboration (Aubin 09 [284]), the main improvement consists in the implementation of an RI/MOM scheme based on nonexceptional momenta in the nonperturbative renormalization of B_K, as well as the addition of a third lattice spacing. The largest error is still the matching factor between the lattice and $\overline{\mathrm{MS}}$ schemes. This error is 2.4% out of a total quoted error of

[26] For example, the master formula Eq. (83) no longer holds as written because contributions containing two insertions of $\Delta S = 1$ weak Hamiltonians connected by dynamical charm quarks no longer lead to a short-distance $\Delta S = 2$ matrix element.

2.8%. The present calculation uses five additional ensembles over that of the previous edition of the FLAG review [1], leading to a reduction of the chiral/continuum extrapolation error and to the statistical error.

The RBC/UKQCD Collaboration employ domain wall fermions to determine B_K. The main feature of their latest update, Ref. [25], is the addition of two ensembles with unitary pion masses as low as 171 MeV and a minimum partially quenched pion mass of 143 MeV. In order to keep the numerical effort of simulating near-physical pion masses at a manageable level, the new ensembles are generated at a larger lattice spacing. Moreover, in order to control the larger residual chiral symmetry breaking effects which are incurred on coarser lattices, a modified fermion action, the Dislocation Suppressing Determinant Ratio (DSDR) [309–312], is used in the simulations. As in their earlier publication [301], RBC/UKQCD employ nonperturbative renormalization factors computed for a variety of RI/MOM schemes with nonexceptional momenta. Owing to the addition of ensembles with larger lattice spacing, the matching between lattice regularization and the intermediate RI/MOM schemes is performed at the lower scale of 1.4 GeV. When combined with the nonperturbative determinations of the continuum step scaling functions, the perturbative conversion to the $\overline{\text{MS}}$ or RGI schemes can be done at $\mu = 3\,\text{GeV}$. The use of near-physical valence pion masses at a spatial volume of $L \approx 4.6\,\text{fm}$ implies a rather small value of $M_{\pi,\text{min}}L \approx 3.3$. However, the entire set of results collected in Refs. [25, 301] comprises several volumes with $L > 2.7\,\text{fm}$. The combined analysis of all data should allow for a reliable determination of B_K with controlled finite-volume effects. It is noted in Ref. [25] that the inclusion of the lighter pion masses essentially halves the uncertainty in B_K due to the chiral/continuum extrapolation. The largest systematic uncertainty remains the perturbative truncation error of 2.1%. As regards the effects of residual chiral symmetry breaking induced by the finite extent of the 5th dimension in the domain wall fermion formulation, it is noted in Ref. [313] that the mixing of $Q^{\Delta S=2}$ with operators of opposite chirality is negligibly small.

Summarizing the new developments, one must note that the biggest improvements since the previous edition of the FLAG review [1] concern the chiral extrapolation and the issue of renormalization. Ensembles at near-physical pion masses have significantly reduced the uncertainty associated with chiral fits, while nonperturbative running is about to become routine. One must realize that, despite this improvement, perturbative matching is still applied only at moderately large scales. Most collaborations therefore identify the largest uncertainty to arise from neglecting higher orders in the perturbative relation to the RGI or $\overline{\text{MS}}$ schemes.

We now describe our procedure for obtaining global averages. The rules of section 2.1 stipulate that results which are free of red tags and are published in a refereed journal may enter an average. Papers which at the time of writing are still unpublished but are obvious updates of earlier published results can also be taken into account.

In the previous edition of the FLAG review [1] the results by SWME were excluded from the average, since the renormalization factors were estimated in one-loop perturbation theory only. However, in this review such calculations are included as long as the estimate of the matching error is sufficiently conservative. Thus the result of Ref. [286] now qualifies for inclusion, despite the fact that nonperturbative information on the renormalization factors is not available. Ref. [77], Laiho 11 has appeared only as conference proceedings, but since it extends the study of Ref. [284] it will be included in our average.

Thus, for $N_f = 2 + 1$ our global average is based on the results of BMW 11 [287], SWME 11A [285, 286], Laiho 11 [77] and RBC/UKQCD 12 [25]. Our procedure is as follows: in a first step statistical and systematic errors of each individual result for the RGI B-parameter, $\hat{B}_K$, are combined in quadrature. Next, a weighted average is computed from the set of results. For the final error estimate we take correlations between different collaborations into account. To this end we note that we consider the statistical and finite-volume errors of SWME 11A and Laiho 11 to be correlated, since both groups use the Asqtad ensembles generated by the MILC Collaboration. Laiho 11 and RBC/UKQCD 12A both use domain wall quarks in the valence sector and also employ similar procedures for the nonperturbative determination of matching factors. Hence, we treat the quoted renormalization and matching uncertainties by the two groups as correlated. After constructing the global covariance matrix according to Schmelling [16], we arrive at

$$N_f = 2+1: \qquad \hat{B}_K = 0.766(10)\,, \tag{86}$$

with a reduced χ^2-value of 0.512. The error is dominated by systematic uncertainties.[27] By applying the NLO conversion factor $\hat{B}_K/B_K^{\overline{\rm MS}}(2\,{\rm GeV}) = 1.369$, this translates into

$$N_f = 2+1: \qquad B_K^{\overline{\rm MS}}(2\,{\rm GeV}) = 0.560(7)\,. \tag{87}$$

Thus, the accuracy of the current global estimate stands at an impressive 1.3%, which represents a significant improvement over the 2.7% uncertainty quoted in the previous edition of the FLAG review ($\hat{B}_K = 0.738(20)$). The two results are, however, completely consistent.

Passing over to describing the results computed for $N_f = 2$ flavours, we note that the situation is unchanged since the publication of the previous edition of the FLAG review [1]. In particular, the result of ETM 10A [300] is the only one which allows for an extensive investigation of systematic uncertainties. In fact, it is the only published $N_f = 2$ calculation involving data computed at three values of the lattice spacing. Being the only result without red tags, it can therefore be identified with the currently best global estimate for two-flavour QCD, i.e.

$$N_f = 2: \qquad \hat{B}_K = 0.729(25)(17)\,, \qquad B_K^{\overline{\rm MS}}(2\,{\rm GeV}) = 0.533(18)(12)\,. \tag{88}$$

The result in the $\overline{\rm MS}$ scheme has been obtained by applying the same conversion factor of 1.369 as in the three-flavour theory.

The grey bands in Fig. 12 represent the global estimates for $N_f = 2$ and $N_f = 2+1$. It appears that B_K may be slightly smaller in two-flavour QCD, but in view of the relatively large uncertainty of the $N_f = 2$ result, the difference is hardly significant.

[27] We can approximately quantify this as follows. A weighted average of BMW 11, Laiho 11 and RBC/UKQCD 12A using only statistical errors gives $\hat{B}_K = 0.7640(33)$. Taking 0.0033 as the total statistical error, a total systematic error of 0.0094 is needed to obtain the combined total error of 0.0100 quoted in the text. (We exclude the SWME 11A result from this calculation as it is only consistent with the other results when its relatively large systematic error is included.) We note that this estimate of the total systematic error is larger than the smallest individual systematic error (0.0084 from BMW 11).

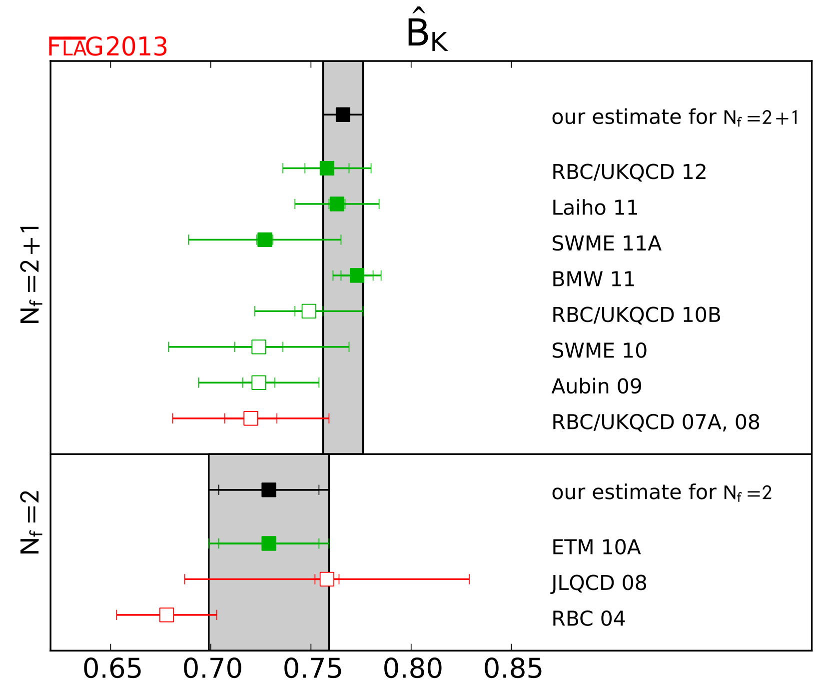

Figure 12: Lattice results for the renormalization group invariant B-parameter (compare Table 19). The black squares and grey bands indicate our global averages (86) and (88). Our $N_f = 2$ estimate coincides with the ETM 10A result. The significance of the colours is explained in section 2.

Collaboration	Ref.	N_f	publication status	continuum extrapolation	chiral extrapolation	finite volume	renormalization	running	B_K	$\hat{B}_K$
RBC/UKQCD 12	[25]	2+1	A	○	★	○	★	*a*	0.554(8)(14)^1	0.758(11)(19)
Laiho 11	[77]	2+1	C	★	○	○	★	–	0.5572(28)(150)	0.7628(38)(205)^2
SWME 11A	[286]	2+1	A	★	○	○	○‡	–	0.531(3)(27)	0.727(4)(38)
BMW 11	[287]	2+1	A	★	★	★	★	*b*	0.5644(59)(58)	0.7727(81)(84)
RBC/UKQCD 10B	[301]	2+1	A	○	○	★	★	*c*	0.549(5)(26)	0.749(7)(26)
SWME 10	[302]	2+1	A	★	○	○	○	–	0.529(9)(32)	0.724(12)(43)
Aubin 09	[284]	2+1	A	○	○	○	★	–	0.527(6)(21)	0.724(8)(29)
RBC/UKQCD 07A, 08	[79, 303]	2+1	A	■	○	★	★	–	0.524(10)(28)	0.720(13)(37)
HPQCD/UKQCD 06	[304]	2+1	A	■	○*	★	■	–	0.618(18)(135)	0.83(18)
ETM 10A	[300]	2	A	★	○	○	★	*d*	0.533(18)(12)^1	0.729(25)(17)
JLQCD 08	[305]	2	A	■	○	■	★	–	0.537(4)(40)	0.758(6)(71)
RBC 04	[299]	2	A	■	■	■†	★	–	0.495(18)	0.678(25)^2
UKQCD 04	[306]	2	A	■	■	■†	■	–	0.49(13)	0.68(18)

‡ The renormalization is performed using perturbation theory at one loop, with a conservative estimate of the uncertainty.

* This result has been obtained with only two "light" sea quark masses.

† These results have been obtained at $(M_\pi L)_{\rm min} > 4$ in a lattice box with a spatial extension $L < 2$ fm.

a B_K is renormalized nonperturbatively at a scale of 1.4 GeV in two RI/SMOM schemes for $N_f = 3$, and then run to 3 GeV using a nonperturbatively determined step-scaling function. Conversion to $\overline{\rm MS}$ is at one-loop order at 3 GeV.

b B_K is renormalized and run nonperturbatively to a scale of 3.4 GeV in the RI/MOM scheme. Nonperturbative and NLO perturbative running agrees down to scales of 1.8 GeV within statistical uncertainties of about 2%.

c B_K is renormalized nonperturbatively at a scale of 2 GeV in two RI/SMOM schemes for $N_f = 3$, and then run to 3 GeV using a nonperturbatively determined step-scaling function. Conversion to $\overline{\rm MS}$ is at one-loop order at 3 GeV.

d B_K is renormalized nonperturbatively at scales $1/a \sim 2 \div 3$ GeV in the $N_f = 2$ RI/MOM scheme. In this scheme, nonperturbative and NLO perturbative running are shown to agree from 4 GeV down 2 GeV to better than 3% [71, 300].

1 $B_K(\overline{\rm MS}, 2\,{\rm GeV})$ is obtained from the estimate for $\hat{B}_K$ using the conversion factor 1.369.

2 $\hat{B}_K$ is obtained from the estimate for $B_K(\overline{\rm MS}, 2\,{\rm GeV})$ using the conversion factor 1.369.

Table 19: Results for the Kaon B-parameter, together with a summary of systematic errors (B_K is the value in the $\overline{\rm MS}$ scheme at scale 2 GeV, $\hat{B}_K$ the corresponding renormalization group invariant result). If information about nonperturbative running is available, this is indicated in the column "running", with details given at the bottom of the table.

7 D-meson decay constants and form factors

Leptonic and semileptonic decays of charmed D and D_s mesons occur via charged W-boson exchange, and are sensitive probes of $c \to d$ and $c \to s$ quark flavour-changing transitions. Given experimental measurements of the branching fractions combined with sufficiently precise theoretical calculations of the hadronic matrix elements, they enable the determination of the CKM matrix elements $|V_{cd}|$ and $|V_{cs}|$ (within the Standard Model) and a precise test of the unitarity of the second row of the CKM matrix. Here we summarize the status of lattice-QCD calculations of the charmed leptonic decay constants and semileptonic form factors. Significant progress has been made in computing $f_{D_{(s)}}$ and the $D \to \pi(K)\ell\nu$ form factors in the last few years, largely due to the introduction of highly-improved lattice-fermion actions that enable the simulation of c-quarks with the same action as for the u, d, and s-quarks.

The charm-quark methods discussed in this review have been validated in a number of ways. Because several groups use the same action for charm and bottom quarks, tests of charm-quark methods are also relevant for the B-physics results discussed in Sec. 8, and are therefore summarized in the introduction of that section. Finally, we note that we limit our review to results based on modern simulations with reasonably light pion masses (below approximately 500 MeV). This excludes results obtained from the earliest unquenched simulations, which typically had two flavours in the sea, and which were limited to heavier pion masses because of the constraints imposed by the computational resources and methods available at that time.

Following our review of lattice-QCD calculations of $D_{(s)}$-meson leptonic decay constants and semileptonic form factors, we then interpret our results within the context of the Standard Model. We combine our best-determined values of the hadronic matrix elements with the most recent experimentally-measured branching fractions to obtain $|V_{cd(s)}|$ and test the unitarity of the second row of the CKM matrix.

7.1 Leptonic decay constants f_D and f_{D_s}

In the Standard Model the decay constant $f_{D_{(s)}}$ of a pseudoscalar D or D_s meson is related to the branching ratio for leptonic decays mediated by a W boson through the formula

$$\mathcal{B}(D_{(s)} \to \ell\nu_\ell) = \frac{G_F^2 |V_{cq}|^2 \tau_{D_{(s)}}}{8\pi} f_{D_{(s)}}^2 m_\ell^2 m_{D_{(s)}} \left(1 - \frac{m_\ell^2}{m_{D_{(s)}}^2}\right)^2 , \qquad (89)$$

where V_{cd} (V_{cs}) is the appropriate CKM matrix element for a D (D_s) meson. The branching fractions have been experimentally measured by CLEO, Belle and Babar with a precision around 5-6% for the D_s-meson; the uncertainties are twice as large for the Cabibbo suppressed D-meson decay modes [74]. When combined with lattice results for the decay constants, they allow for determinations of $|V_{cs}|$ and $|V_{cd}|$.

In lattice-QCD calculations the decay constants $f_{D_{(s)}}$ are extracted from Euclidean matrix elements of the axial current

$$\langle 0|A^\mu_{cq}|D_q(p)\rangle = f_{D_q}\, p^\mu_{D_q} , \qquad (90)$$

with $q = d, s$ and $A^\mu_{cq} = \bar{c}\gamma_\mu\gamma_5 q$. Results for $N_f = 2,\ 2+1$ and $2+1+1$ dynamical flavours are summarized in Table 20 and Figure 13.

The ETM collaboration has published results for D and D_s meson decay constants with two dynamical flavours, using the twisted-mass fermionic action at maximal twist with the

Collaboration	Ref.	N_f	publication status	continuum extrapolation	chiral extrapolation	finite volume	renormalization/matching	heavy quark treatment	f_D	f_{D_s}	f_{D_s}/f_D
FNAL/MILC 12B	[314]	2+1+1	C	★	★	★	★	✓	209.2(3.0)(3.6)	246.4(0.5)(3.6)	1.175(16)(11)
HPQCD 12A	[315]	2+1	A	○	○	★	★	✓	208.3(1.0)(3.3)	246.0(0.7)(3.5)	1.187(4)(12)
FNAL/MILC 11	[316]	2+1	A	○	○	★	○	✓	218.9(11.3)	260.1(10.8)	1.188(25)
PACS-CS 11	[317]	2+1	A	■	★	■	○	✓	226(6)(1)(5)	257(2)(1)(5)	1.14(3)
HPQCD 10A	[318]	2+1	A	★	○	★	★	✓	213(4)*	248.0(2.5)	
HPQCD/UKQCD 07	[157]	2+1	A	★	○	★	★	✓	207(4)	241 (3)	1.164(11)
FNAL/MILC 05	[319]	2+1	A	○	○	★	○	✓	201(3)(17)	249(3)(16)	1.24(1)(7)
ETM 11A	[320]	2	A	★	○	★	★	✓	212(8)	248(6)	1.17(5)
ETM 09	[160]	2	A	○	○	★	★	✓	197(9)	244(8)	1.24(3)

* This result is obtained by using the central value for f_{D_s}/f_D from HPQCD/UKQCD 07 and increasing the error to account for the effects from the change in the physical value of r_1.

Table 20: Decay constants of the D and D_s mesons (in MeV) and their ratio.

tree-level improved Symanzik gauge action. In this setup the decay constants can be extracted from an absolutely normalized current and they are automatically $\mathcal{O}(a)$ improved. In ETM 09 three lattice spacings between 0.1 and 0.07 fm are considered with pion masses down to 270 MeV. Heavy meson χPT formulae plus terms linear in a^2 have been used for the continuum/chiral extrapolations, which have been performed in two different ways in order to estimate sytematic effects. In the first approach $f_{D_s}\sqrt{m_{D_s}}$ and $\frac{f_{D_s}\sqrt{m_{D_s}}}{f_D\sqrt{m_D}}$ are fitted, whereas in the second case the ratios $\frac{f_{D_s}\sqrt{m_{D_s}}}{f_K}$ and $\frac{f_{D_s}\sqrt{m_{D_s}}}{f_K} \times \frac{f_\pi}{f_D\sqrt{m_D}}$ are analyzed. As expected, the pion-mass dependence of $f_{D_s}\sqrt{m_{D_s}}$ turns out to be very mild. In addition the double ratio $\frac{f_{D_s}\sqrt{m_{D_s}}}{f_K} \times \frac{f_\pi}{f_D\sqrt{m_D}}$ shows little dependence on the pion mass as well as on the lattice spacing. Cutoff effects on the contrary are rather large on the decay constants, with the difference between the physical-mass result at the finest lattice spacing and in the continuum being approximately 5%. ETM 11A contains an update of the results in ETM 09 obtained by enlarging the statistics on some of the ensembles and by including a finer lattice resolution with $a \approx 0.054$ fm, which implies a reduction of cutoff effects by a factor two. Moreover in ETM 11A the continuum extrapolations are performed after interpolating the results at different lattice spacings to fixed values of the heavy-quark mass. In the case of the SU(3) breaking ratio f_{D_s}/f_D, the uncertainty associated with the chiral extrapolation is estimated by comparing fits either following heavy meson χPT or assuming a simple linear dependence on the light-quark mass.

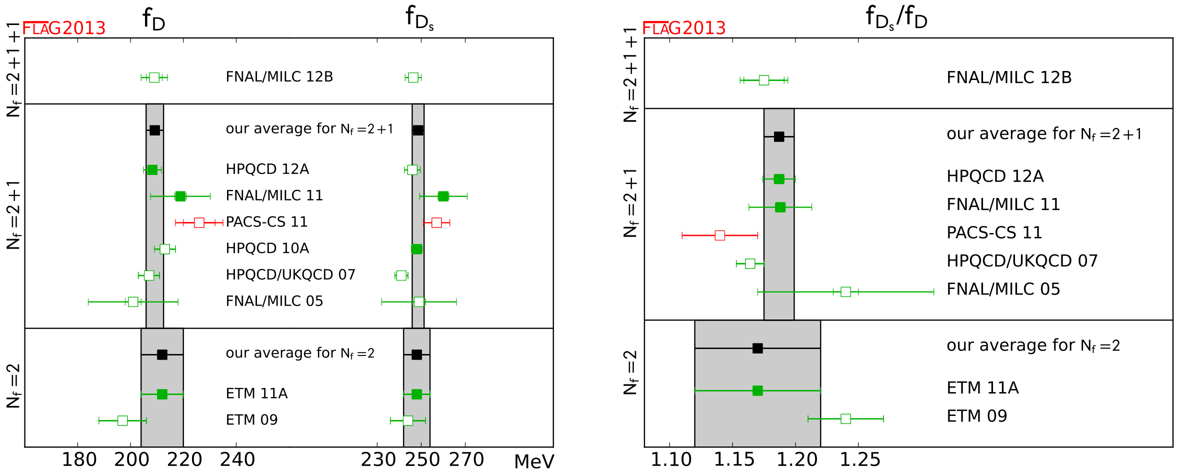

Figure 13: Decay constants of the D and D_s mesons [values in Table 20 and Eqs. (91), (92)]. The significance of the colours is explained in section 2. The black squares and grey bands indicate our averages.

As results from just one collaboration exist in the literature, the $N_f = 2$ averages are simply given by the values in ETM 11A, which read

$$N_f = 2: \quad f_D = (212 \pm 8)\ \text{MeV}, \quad f_{D_s} = (248 \pm 6)\ \text{MeV}, \quad \frac{f_{D_s}}{f_D} = 1.17 \pm 0.05\,. \tag{91}$$

Several collaborations have produced results with $N_f = 2+1$ dynamical flavours. The most precise determinations come from a sequence of publications by HPQCD/UKQCD [157, 315, 318]. In all cases configurations generated by MILC with Asqtad rooted staggered quarks in the sea and a one-loop tadpole improved Symanzik gauge action have been analyzed (see [15] and references therein). The main differences are in the ensembles utilized and in the absolute scale setting. The relative scale is always set through r_1 derived from the static quark-antiquark potential.

In HPQCD/UKQCD 07 [157] three lattice spacings, $a \approx 0.15$, 0.12 and 0.09 fm, with RMS pion masses between 542 and 329 MeV, have been considered. This gives rather large values for the charm-quark mass in lattice units, $0.43 < am_c < 0.85$, and indeed lattice artifacts are estimated to be the second largest systematic uncertainty in the computation. The main systematic error is resulting from the absolute scale setting, which had previously been performed through the Υ spectrum, using NRQCD for the b quark. The estimate reads $r_1 = 0.321(5)$ fm.

In 2010, HPQCD obtained a more precise determination of $r_1 = 0.3133(23)$, based on several different physical inputs (including f_π, f_K and the Υ spectrum) and improved continuum limit extrapolations. It is worth noting that the new r_1 is about 1.5σ lower than the older value. The publications HPQCD 10A [318] and HPCQD 12A [315] update the computations of f_{D_s} and f_D, respectively, using the new scale determination. These results enter our final averages. The change in the scale requires a retuning of the bare quark masses and a change in the conversion of dimensionless quantitities, measured in units of r_1, to physical ones, measured in MeV.

In HPQCD 10A, f_{D_s} is calculated on ensembles with $a \approx 0.06$ and $0,045$ fm and with RMS pion masses ranging between 542 and 258 MeV. The chiral and continuum extrapolations have been performed simultaneously by employing polynomials quadratic in the sea-quark mass $\delta_q = \frac{m_{q,sea}-m_{q,phys}}{m_{q,phys}}$, with $q = s, l$, and through the eighth power of the charm-quark mass, including cross terms of the form $\delta_q(am_c)^n$. The valence strange- and charm-quark masses are fixed to their physical values obtained from matching to the η_s and η_c masses. The fits are robust against variations, such as the exclusion of ensembles with the coarsest and finest lattice spacings, or a change in the functional form such that terms up to $(am_c)^4$ only are kept. The largest source of uncertainty in HPQCD 10A still comes from the value of r_1 and it amounts to 0.6%. The published error includes a 0.1% contribution coming from an estimate of electromagnetic effects obtained using a potential model.

The process of switching to the improved determination of r_1 is finally completed in HPQCD 12A [315], where new values of f_D and the ratio f_{D_s}/f_D are reported. The statistics is enlarged at the $a \approx 0.12$ fm and $a \approx 0.09$ fm lattices and for the latter a more chiral point, with light-quark masses halved with respect to HPQCD/UKQCD 07, is added. The three-point function for $D \to \pi$ at zero recoil momentum (calculated for a different project) is used to perform simultaneous fits to two- and three-point functions. This turns out to be beneficial in reducing the statistical errors on the hadron masses and decay constant matrix elements. Chiral and continuum extrapolations are carried out at the same time adopting partially quenched heavy meson χPT augmented by $(am_c)^2$ and $(am_c)^4$ terms. Given the rather large values of am_c between 0.4 and 0.6, the continuum extrapolation gives the largest systematical uncertainty, amounting to roughly 1% out of the total 1.7% and 1.1% total errors on f_D and on f_{D_s}/f_D respectively. Finally, the HPQCD collaboration also calculates the ratio $f_+^{D\to\pi}(0)/f_D$ using the result for the semileptonic form factor from [321] and find good agreement with the experimental ratio which is independent of $|V_{cd}|$. Summarizing the computations by HPQCD: concerning f_D, HPQCD 12A supersedes HPQCD/UKQCD 07 and HPQCD 10A because of the more chiral points considered but does not supersede HPQCD 10A for f_{D_s} as finer resolutions are included in the latter, which contains the collaboration's most precise result for the D_s meson decay constant.

The PACS-CS Collaboration published in 2011 a computation of the D and D_s decay constants with 2+1 flavours of nonperturbatively $\mathcal{O}(a)$ improved Wilson fermions and the Iwasaki gauge action [317]. For the charm quark the Tsukuba heavy quark action is used. The parameters in the action and the renormalization constants of the charm-light and charm-strange axial currents are computed in a mixed setup, partly nonperturbatively (typically the massless contribution) and partly relying on one-loop perturbation theory, see Appendix A for details. This leaves residual cutoff and matching effects of $\mathcal{O}(\alpha_s^2 a\Lambda_{QCD}, (a\Lambda)^2, \alpha_s^2)$ in the computation, which, in addition is carried out at one value of the lattice spacing only ($a \approx 0.09$ fm). Quark masses are quite low, yielding $m_\pi = 152(6)$ MeV and the ensemble is reweighted to the physical point using the technique in [20]. However, measurements are performed on only one set of configurations with $L/a = 32$, such that $m_\pi L$ is around 2.2. For this reason, and for the limitation to a single lattice spacing, the PACS-CS 11 results do not enter our averages.

The Fermilab Lattice and MILC collaborations have presented several computations of $D_{(s)}$ meson decay constants with $2+1$ flavours of dynamical quarks [316, 319]. Their first published results are in Ref. [319] (FNAL/MILC 05), which were later updated and superseded in Ref. [316] (FNAL/MILC 11). The MILC Asqtad ensembles, as for the HPQCD results, have been used in both cases. For the charm quark the Fermilab action is adopted, with mostly nonperturbative (mNPR) renormalization of the axial currents (see Appendix A for details). In FNAL/MILC 05 three lattice spacings with $a \approx 0.18,\ 0.12$ and 0.09 fm, according to the original estimate $r_1 = 0.321(5)$ fm, have been considered. RMS pion masses are slightly larger than 400 MeV. Chiral and continuum extrapolations are performed at the same time by using the χPT expressions at NLO for staggered quarks. Discretization effects and the chiral fits are the largest sources of systematic errors in f_D and in f_{D_s}, each effect being responsible for a systematic between 4% and 6%. Cutoff effects are significantly smaller in the ratio f_{D_s}/f_D, whose systematic uncertainty (around 5%) is dominated by the chiral extrapolation.

These uncertainties are reduced in FNAL/MILC 11. The same setup concerning lattice actions and renormalization is used as in FNAL/MILC 05 but lighter pion masses (down to 320 MeV for the RMS values) are included in the analysis and the extremely coarse 0.18 fm ensembles are replaced by finer 0.15 fm ones. The scale is set through $r_1 = 0.3120(22)$ fm, as obtained from an average of previous MILC and HPQCD determinations. One-loop rooted staggered partially quenched χPT plus leading order in the heavy-quark expansion formulae are used for the chiral and continuum extrapolations. The expressions parameterize also the effects of hyperfine and flavour splittings. Discretization effects are estimated using a combination of heavy-quark and Symanzik effective theories to be around 3% for $f_{D_{(s)}}$ and negligible for the ratio. At this level of accuracy the truncation errors in the small correction factor inherent in the mNPR method are not negligible anymore; the authors conservatively estimate the two-loop and higher-order perturbative truncation errors to the full size of the known one-loop term, i.e. roughly 1% for the decay constants.

As shown in Table 20 the $N_f = 2+1$ computations which fulfill our quality criteria and can enter the averages are HPCQD 12A and FNAL/MILC 11 for f_D and the SU(3) breaking ratio f_{D_s}/f_D, and HPQCD 10A and FNAL/MILC 11 for f_{D_s}. Because FNAL/MILC and HPQCD use a largely overlapping set of configurations, we treat the statistical errors as 100% correlated and finally quote

$$N_f = 2+1: \quad f_D = (209.2 \pm 3.3)\ \text{MeV}, \quad f_{D_s} = (248.6 \pm 2.7)\ \text{MeV}, \quad \frac{f_{D_s}}{f_D} = 1.187 \pm 0.012\ . \quad (92)$$

The only computation of f_D and f_{D_s} with $N_f = 2+1+1$ sea quarks is presented in Ref. [314] (FNAL/MILC 12B), recently published as a proceeding contribution to the Lattice 2012 Conference. The calculation is performed on configurations generated by the MILC Collaboration using HISQ sea quarks and a one-loop tadpole improved Symanzik gauge action [239]. Light, strange and charm valence quarks are also in the HISQ regularization. Four lattice resolutions in the range $a \approx 0.15 - 0.06$ fm are considered. RMS pion masses vary between 306 and 144 MeV and include ensembles at each lattice spacing with Goldstone pions at the physical point. The dominant systematic uncertainties are due to the scale setting (through f_π) and the continuum extrapolation, and they are both estimated to be at the percent level.

As a final remark, since the accuracy of the lattice determinations of the D meson decay constant is rapidly improving, it will become important in the future, especially when comparing to experimental numbers, to distinguish between f_{D^+} and the average of f_{D^+} and f_{D^0}. The current status is summarized as follows: FNAL/MILC results concern f_{D^+}, whereas HPQCD, PACS-CS and ETMC numbers correspond to the average of the decay constants for D^+ and D^0.

7.2 Semileptonic form factors for $D \to \pi\ell\nu$ and $D \to K\ell\nu$

The form factors for semileptonic $D \to \pi\ell\nu$ and $D \to K\ell\nu$ decay, when combined with experimental measurements of the decay widths, enable determinations of the CKM matrix elements $|V_{cd}|$ and $|V_{cs}|$ via:

$$\frac{d\Gamma(D\to P\ell\nu)}{dq^2} = \frac{G_F^2|V_{cx}|^2}{24\pi^3}\frac{(q^2-m_\ell^2)^2\sqrt{E_P^2-m_P^2}}{q^4m_D^2}\left[\left(1+\frac{m_\ell^2}{2q^2}\right)m_D^2(E_P^2-m_P^2)|f_+(q^2)|^2 \right.$$
$$\left. +\frac{3m_\ell^2}{8q^2}(m_D^2-m_P^2)^2|f_0(q^2)|^2\right], \tag{93}$$

where $x = d, s$ is the daughter light quark, $P = \pi, K$ is the daughter light pseudoscalar meson, and $q = (p_D - p_P)$ is the momentum of the outgoing lepton pair. The vector and scalar form factors $f_+(q^2)$ and $f_0(q^2)$ parameterize the hadronic matrix element of the heavy-to-light quark flavour-changing vector current $V_\mu = i\overline{x}\gamma_\mu c$:

$$\langle P|V_\mu|D\rangle = f_+(q^2)\left(p_{D\mu} + p_{P\mu} - \frac{m_D^2-m_P^2}{q^2}\,q_\mu\right) + f_0(q^2)\frac{m_D^2-m_P^2}{q^2}\,q_\mu\,, \tag{94}$$

and satisfy the kinematic constraint $f_+(0) = f_0(0)$ at zero momentum-transfer. Because the contribution to the decay width from the scalar form factor is proportional to m_ℓ^2, it can be neglected for $\ell = e, \nu$, and Eq. (93) simplifies to

$$\frac{d\Gamma(D\to P\ell\nu)}{dq^2} = \frac{G_F^2}{24\pi^3}|\vec{p}_P|^3|V_{cx}|^2|f_+^{DP}(q^2)|^2\,. \tag{95}$$

In practice, most lattice-QCD calculations of $D \to \pi\ell\nu$ and $D \to K\ell\nu$ focus on providing the value of the vector form factor at a single value of the momentum transfer, $f_+(q^2 = 0)$, which is sufficient to obtain $|V_{cd}|$ and $|V_{cs}|$. Because the decay rate cannot be measured directly at zero momentum transfer, comparison of these lattice-QCD results with experiment requires a slight extrapolation of the experimental measurement. Some lattice-QCD calculations also provide determinations of the $D \to \pi\ell\nu$ and $D \to K\ell\nu$ form factors over the full kinematic range $0 < q^2 < q^2_{\rm max} = (m_D - m_P)^2$, thereby allowing a comparison of the shapes of the lattice simulation and experimental data. This nontrivial test in the D system provides a strong check of lattice-QCD methods that are also used in the B-meson system.

Lattice-QCD calculations of the $D \to \pi\ell\nu$ and $D \to K\ell\nu$ form factors typically use the same light-quark and charm-quark actions as those of the leptonic decay constants f_D and f_{D_s}. Therefore many of the same issues arise, *e.g.* chiral extrapolation of the light-quark mass(es) to the physical point and discretization errors from the charm quark, and matching the lattice weak operator to the continuum, as discussed in the previous section. Two strategies have been adopted to eliminate the need to renormalize the heavy-light vector current in recent calculations of $D \to \pi\ell\nu$ and $D \to K\ell\nu$, both of which can be applied to simulations in which the same relativistic action is used for the light (u, d, s) and charm quarks. The first method was proposed by Bećirević and Haas in Ref. [322], and introduces double-ratios of lattice three-point correlation functions in which the vector current renormalization cancels. Discretization errors in the double ratio are of $\mathcal{O}((am_h)^2)$ provided that the vector-current matrix elements are $\mathcal{O}(a)$ improved. The vector and scalar form factors $f_+(q^2)$ and $f_0(q^2)$ are obtained by taking suitable linear combinations of these double ratios. The second method was introduced by the HPQCD Collaboration in Ref. [323]. In this case, the quantity $(m_c - m_x)\langle P|S|D\rangle$, where m_x and m_c are the bare lattice quark masses and $S = \bar{x}c$ is the lattice scalar current, does not get renormalized. The desired form factor at zero momentum transfer can be obtained by (i) using a Ward identity to relate the matrix element of the vector current to that of the scalar current, and (ii) taking advantage of the kinematic identity at zero momentum transfer $f_+(0) = f_0(0)$, such that $f_+(q^2 = 0) = (m_c - m_x)\langle P|S|D\rangle/(m_D^2 - m_P^2)$.

Additional complications enter for semileptonic decay matrix elements due to the nonzero momentum of the outgoing pion or kaon. Both statistical errors and discretization errors increase at larger momenta, so results for the lattice form factors are most precise at $q^2_{\rm max}$. However, because lattice calculations are performed in a finite spatial volume, the pion or kaon three-momentum can only take discrete values in units of $2\pi/L$ when periodic boundary conditions are used. For typical box sizes in recent lattice D- and B-meson form-factor calculations, $L \sim 2.5$–3 fm; thus the smallest nonzero momentum in most of these analyses ranges from $\vec{p}_P \sim 400$–500 MeV. The largest momentum in lattice heavy-light form-factor calculations is typically restricted to $\vec{p}_P \leq 2\pi/L(2,0,0)$. For $D \to \pi\ell\nu$ and $D \to K\ell\nu$, $q^2 = 0$ corresponds to $p_\pi \sim 940$ MeV and $p_K \sim 1$ GeV, respectively, and the full recoil-momentum region is within the range of accessible lattice momenta.[28] Therefore the interpolation to $q^2 = 0$ is relatively insensitive to the fit function used to parameterize the momentum dependence, and the associated systematic uncertainty in $f_+(0)$ is small. The parameterization of the momentum dependence can be a significant source of uncertainty, however, for other semileptonic decays for which the momentum range needed to connect to experiment is far from q^2_{max}, such as $B \to \pi\ell\nu$; approaches to address this issue are discussed in Sec. 8.3.

The most advanced $N_f = 2$ lattice-QCD calculation of the $D \to \pi\ell\nu$ and $D \to K\ell\nu$ form factors is by the ETM Collaboration [326]. This still preliminary work uses the twisted-mass Wilson action for both the light and charm quarks, with three lattice spacings down to $a \approx 0.068$ fm and (charged) pion masses down to $m_\pi \approx 270$ MeV. The calculation employs the ratio method of Ref. [322] to avoid the need to renormalize the vector current, and extrapolates to the physical light-quark masses using $SU(2)$ heavy-light meson χPT formulated for twisted-mass fermions. ETM simulate with nonperiodic boundary conditions for the valence quarks to access arbitrary momentum values over the full physical q^2 range, and interpolate to $q^2 = 0$ using the Bećirević-Kaidalov ansatz [329]. The statistical errors in $f_+^{D\pi}(0)$ and $f_+^{DK}(0)$ are 9% and 7%, respectively, and lead to rather large systematic uncertainties in the fits to the light-quark mass and energy dependence (7% and 5%, respectively). Another significant source of uncertainty is from discretization errors (5% and 3%, respectively). On the finest lattice spacing used in this analysis $am_c \sim 0.17$, so $\mathcal{O}((am_c)^2)$ cutoff errors are expected to be about 5%. This can be reduced by including the existing $N_f = 2$ twisted-mass ensembles with $a \approx 0.051$ fm discussed in Ref. [230]. Work is in progress by the ETM Collaboration to compute $f_+^{D\pi}(0)$ and $f_+^{DK}(0)$ using the same methods on the $N_f = 2 + 1 + 1$ twisted-mass Wilson lattices [96]. This calculation will include dynamical charm-quark effects and use three lattice spacings down to $a \approx 0.06$ fm.

The first published $N_f = 2{+}1$ lattice-QCD calculation of the $D \to \pi\ell\nu$ and $D \to K\ell\nu$ form factors is by the Fermilab Lattice, MILC, and HPQCD Collaborations [330]. (Because only two of the authors of this work are in HPQCD, and to distinguish it from other more recent works on the same topic by HPQCD, we hereafter refer to this work as "FNAL/MILC.") This work uses Asqtad-improved staggered sea quarks and light (u, d, s) valence quarks and

[28] This situation differs from that of calculations of the $K \to \pi\ell\nu$ form factor, where the physical pion recoil momenta are smaller than $2\pi/L$. For $K \to \pi\ell\nu$ it is now standard to use nonperiodic ("twisted") boundary conditions [324, 325] to simulate directly at $q^2 = 0$; see Sec. 4.3. Some collaborations have also begun to use twisted boundary conditions for D decays [326–328].

the Fermilab action for the charm quarks, with a single lattice spacing of $a \approx 0.12$ fm. At this lattice spacing, the staggered taste splittings are still fairly large, and the minimum RMS pion mass is $\approx$ 510 MeV. This calculation renormalizes the vector current using a mostly nonperturbative approach, such that the perturbative truncation error is expected to be negligible compared to other systematics. The Fermilab Lattice and MILC Collaborations present results for the $D \to \pi\ell\nu$ and $D \to K\ell\nu$ semileptonic form factors over the full kinematic range, rather than just at zero momentum transfer. In fact, the publication of this result predated the precise measurements of the $D \to K\ell\nu$ decay width by the FOCUS [331] and Belle experiments [332], and predicted the shape of $f_+^{DK}(q^2)$ quite accurately. This bolsters confidence in calculations of the B-meson semileptonic decay form factors using the same methodology. Work is in progress [333] to reduce both the statistical and systematic errors in $f_+^{D\pi}(q^2)$ and $f_+^{DK}(q^2)$ through increasing the number of configurations analyzed, simulating with lighter pions, and adding lattice spacings as fine as $a \approx 0.045$ fm. In parallel, the Fermilab Lattice and MILC collaborations are initiating a new calculation of $D \to \pi\ell\nu$ and $D \to K\ell\nu$ using the HISQ action for all valence and sea quarks [169]; this calculation will focus on obtaining the form factors at zero momentum transfer using the scalar form-factor method [323] to avoid the need for current renormalization and (partially) twisted boundary conditions [325, 334] to simulate directly at $q^2 = 0$.

Collaboration	Ref.	N_f	publication status	continuum extrapolation	chiral extrapolation	finite volume	renormalization	heavy-quark treatment	$f_+^{D\pi}(0)$	$f_+^{DK}(0)$
HPQCD 11	[321]	2+1	A	○	○	★	★	✓	0.666(29)	
HPQCD 10B	[323]	2+1	A	○	○	★	★	✓		0.747(19)
FNAL/MILC 04	[330]	2+1	A	■	■	★	○	✓	0.64(3)(6)	0.73(3)(7)
ETM 11B	[326]	2	C	○	○	★	★	✓	0.65(6)(6)	0.76(5)(5)

Table 21: $D \to \pi\ell\nu$ and $D \to K\ell\nu$ semileptonic form factors at zero momentum transfer.

The most precise calculations of the $D \to \pi\ell\nu$ [321] and $D \to K\ell\nu$ [323] form factors are by the HPQCD Collaboration. These analyses also use the $N_f = 2+1$ Asqtad-improved staggered MILC configurations at two lattice spacings $a \approx 0.09$ and 0.12 fm, but use the HISQ action for the valence u, d, s, and c quarks. In these mixed-action calculations, the HISQ valence light-quark masses are tuned so that the ratio m_l/m_s is approximately the same as for the sea quarks; the minimum RMS sea-pion mass is $\approx$ 390 MeV. They calculate the form factors at zero momentum transfer by relating them to the matrix element of the scalar current, which is not renormalized. They also introduce a "modified z-expansion" to simultaneously extrapolate to the physical light-quark masses and continuum and interpolate to $q^2 = 0$. In this approach they parameterize the momentum dependence as a series in the variable $z(q^2)$ (see Sec. 8.3 for the explicit relation between z and q^2), but allow the coefficients of the series expansion to vary with the light-quark mass, charm-quark mass, and lattice spacing. The form of the light-quark dependence is inspired by χPT, and includes logarithms of the form $m_\pi^2 \log(m_\pi^2)$ as well as polynomials in the valence-, sea-, and charm-quark masses. Polynomials in $E_{\pi(K)}$ are also included to parameterize momentum-dependent discretization errors. The coefficients of each term are constrained using Gaussian priors with widths guided by power-counting estimates, and the number of terms is increased until the result for $f_+(0)$ stabilizes. With this approach, the fit error for $f_+(0)$ includes both statistical uncertainties and those due to most systematics. The largest uncertainties in these calculations are from statistics and charm-quark discretization errors. Work is in progress by the HPQCD collaboration to determine the D-meson semileptonic form factors over the full kinematic range [327, 328]. In this case, the spatial vector current renormalization factor is obtained by requiring that $f_+(0)^{H\to H} = 1$ for $H = D, D_s, \eta_s$, and η_c. The renormalization factors for the flavour-diagonal currents agree for different momenta as well as for charm-charm and charm-strange external mesons, and are then used to renormalize the flavour-changing charm-strange and charm-light currents.

Table 21 summarizes the existing $N_f = 2$ and $N_f = 2+1$ calculations of the $D \to \pi\ell\nu$ and $D \to K\ell\nu$ semileptonic form factors. The quality of the systematic error studies is indicated by the symbols. Additional tables in appendix B.5.2 provide further details on the simulation parameters and comparisons of the error estimates. Recall that only calculations without red tags that are published in a referred journal are included in the FLAG average. Of the calculations described above, only those of HPQCD 10B,11 satisfy all of the quality criteria. Therefore our average of the $D \to \pi\ell\nu$ and $D \to K\ell\nu$ semileptonic form factors from $N_f = 2+1$ lattice QCD is

$$N_f = 2+1: \qquad f_+^{D\pi}(0) = 0.666(29)\,, \qquad f_+^{DK}(0) = 0.747(19)\,. \tag{96}$$

Figure 14 plots the existing $N_f = 2$ and $N_f = 2+1$ results for $f_+^{D\pi}(0)$ and $f_+^{DK}(0)$; the grey bands show our average of these quantities. Section 7.3 discusses the implications of these results for determinations of the CKM matrix elements $|V_{cd}|$ and $|V_{cs}|$ and tests of unitarity of the second row of the CKM matrix.

7.3 Determinations of $|V_{cd}|$ and $|V_{cs}|$ and test of second-row CKM unitarity

We now interpret the lattice-QCD results for the $D_{(s)}$ meson decay constants and semileptonic form factors as determinations of the CKM matrix elements $|V_{cd}|$ and $|V_{cs}|$ in the Standard Model.

For the leptonic decays, we use the latest experimental averages from Rosner and Stone for the Particle Data Group [111] (where electromagnetic corrections of $\sim 1\%$ have been removed):

$$f_D|V_{cd}| = 46.40(1.98)\ \text{MeV}\,, \qquad f_{D_s}|V_{cs}| = 253.1(5.3)\ \text{MeV}\,. \tag{97}$$

We combine these with the average values of f_D and f_{D_s} from the individual $N_f = 2$ and $N_f = 2+1$ lattice-QCD calculations that satisfy the FLAG criteria, and summarize the results for the CKM matrix elements $|V_{cd}|$ and $|V_{cs}|$ in Table 22. For our preferred values we use the

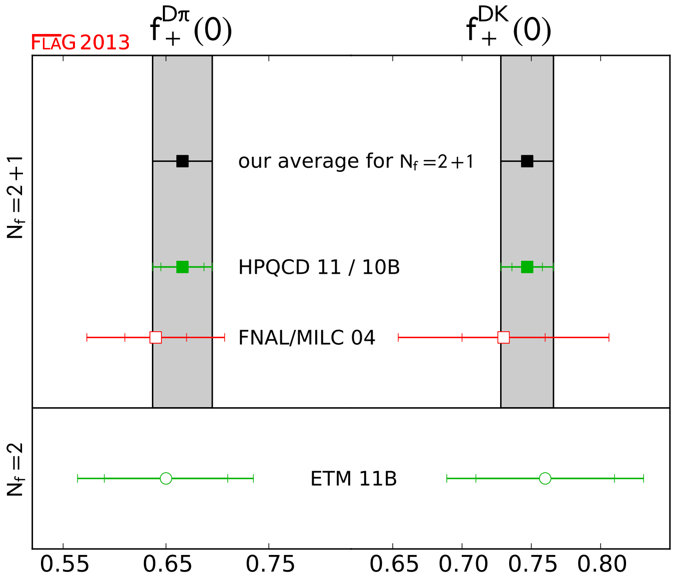

Figure 14: $D \to \pi\ell\nu$ and $D \to K\ell\nu$ semileptonic form factors at zero momentum transfer. The HPQCD result for $f_+^{D\pi}(0)$ is from HPQCD 11, the one for $f_+^{DK}(0)$ represents HPQCD 10B (see Table 21).

averaged $N_f = 2$ and $N_f = 2+1$ results for f_D and f_{D_s} in Eqs. (91) and (92). We obtain

$$|V_{cd}| = 0.2218(35)(95)\,, \quad |V_{cs}| = 1.018(11)(21)\,, \quad \text{(leptonic decays, } N_f = 2+1) \quad (98)$$

$$|V_{cd}| = 0.2189(83)(94)\,, \quad |V_{cs}| = 1.021(25)(21)\,, \quad \text{(leptonic decays, } N_f = 2) \quad (99)$$

where the errors shown are from the lattice calculation and experiment (plus non-lattice theory), respectively. For the $N_f = 2+1$ determinations, the uncertainties from the lattice-QCD calculations of the decay constants are two to three times smaller than the experimental uncertainties in the branching fractions; the lattice central values and errors are dominated by those of the HPQCD calculations. Although the $N_f = 2$ and $N_f = 2+1$ results for $|V_{cs}|$ are slightly larger than one, they are both consistent with unity within errors.

For the semileptonic decays, we use the latest experimental averages from the Heavy Flavor Averaging Group [123]:[29]

$$f_+^{D\pi}(0)|V_{cd}| = 0.146(3)\,, \qquad f_+^{DK}(0)|V_{cs}| = 0.728(5)\,. \quad (100)$$

For each of $f_+^{D\pi}(0)$ and $f_+^{DK}(0)$, there is only a single $N_f = 2+1$ lattice-QCD calculation that satisfies the FLAG criteria. Using these results, which are given in Eq. (96), we obtain our preferred values for $|V_{cd}|$ and $|V_{cs}|$:

$$|V_{cd}| = 0.2192(95)(45)\,, \quad |V_{cs}| = 0.9746(248)(67)\,, \quad \text{(semileptonic decays, } N_f = 2+1) \quad (101)$$

[29] We note that HFAG currently averages results for neutral and charged D meson decays without first removing the correction due to the Coulomb attraction between the charged final-state particles for the neutral D meson decays.

Collaboration	Ref.	N_f	from	$\lvert V_{cd}\rvert$ or $\lvert V_{cs}\rvert$
HPQCD 12A	[315]	2+1	f_D	0.2228(36)(95)
FNAL/MILC 11	[316]	2+1	f_D	0.2120(109)(91)
HPQCD 11	[321]	2+1	$D \to \pi\ell\nu$	0.2192(95)(45)
ETM 11A	[320]	2	f_D	0.2189(83)(94)
HPQCD 10A	[318]	2+1	f_{D_s}	1.021(10)(21)
FNAL/MILC 11	[316]	2+1	f_{D_s}	0.9731(404)(202)
HPQCD 10B	[323]	2+1	$D \to K\ell\nu$	0.9746(248)(67)
ETM 11A	[320]	2	f_{D_s}	1.021(25)(21)

Table 22: Determinations of $|V_{cd}|$ (upper panel) and $|V_{cs}|$ (lower panel) obtained from lattice calculations of D-meson leptonic decay constants and semileptonic form factors. The errors shown are from the lattice calculation and experiment (plus non-lattice theory), respectively.

where the errors shown are from the lattice calculation and experiment (plus non-lattice theory), respectively.

Table 23 summarizes the results for $|V_{cd}|$ and $|V_{cs}|$ from leptonic and semileptonic decays, and compares them to determinations from neutrino scattering (for $|V_{cd}|$ only) and CKM unitarity. These results are also plotted in Fig. 15. The determinations of $|V_{cd}|$ all agree within uncertainties, but the errors in the direct determinations from leptonic and semileptonic decays are approximately ten times larger than the indirect determination from CKM unitarity. The determination of $|V_{cs}|$ from $N_f = 2+1$ lattice-QCD calculations of leptonic decays is noticeably larger than that from both semileptonic decays and CKM unitarity. The disagreement between $|V_{cs}|$ from leptonic and semileptonic decays is slight (only 1.2σ assuming no correlations), but the disagreement between $|V_{cs}|$ from leptonic decays and CKM unitarity is larger at 1.9σ. This tension with CKM unitarity is driven primarily by the HPQCD calculation of f_{D_s} in Ref. [318], but we note that the ETM $N_f = 2$ calculation of f_{D_s} in Ref. [320] leads to the same high central value of $|V_{cs}|$, just with larger uncertainties. Further, a recent preliminary lattice-QCD calculation of f_{D_s} using $N_f = 2+1+1$ configurations with dynamical HISQ quarks Fermilab/MILC [314] agrees with the HPQCD result with similar uncertainties, so it will be interesting to see how this tension evolves with improved experimental measurements and more independent lattice-QCD results with competitive errors.

The $N_f = 2+1$ averages for $|V_{cd}|$ and $|V_{cs}|$ in Fig. 15 are obtained by averaging the results in Table 22 including correlations. We assume that the statistical errors are 100% correlated between all of the calculations because they use the MILC Asqtad gauge configurations. We also assume that the heavy-quark discretization errors are 100% correlated between the HPQCD calculations of leptonic and semileptonic decays because they use the same charm-quark action, and that the scale-setting uncertainties are 100% correlated between the HPQCD results as well. Finally, we include the 100% correlation between the experimental inputs for the two extractions of $|V_{cd(s)}|$ from leptonic decays. We obtain

$$|V_{cd}| = 0.2191(83)\,, \quad |V_{cs}| = 0.996(21)\,, \quad (\text{our average}, N_f = 2+1) \tag{102}$$

where the errors include both theoretical and experimental uncertainties, and the error on

	from	Ref.	$\lvert V_{cd}\rvert$	$\lvert V_{cs}\rvert$
$N_f = 2+1$	f_D & f_{D_s}		0.2218(101)	1.018(24)
$N_f = 2$	f_D & f_{D_s}		0.2189(125)	1.021(33)
$N_f = 2+1$	$D \to \pi\ell\nu$ and $D \to K\ell\nu$		0.2192(105)	0.9746(257)
PDG	neutrino scattering	[74]	0.230(11)	
Rosner 12 (*for the* PDG)	CKM unitarity	[111]	0.2245(12)	0.97345(22)

Table 23: Comparison of determinations of $|V_{cd}|$ and $|V_{cs}|$ obtained from lattice methods with non-lattice determinations and the Standard-Model prediction assuming CKM unitarity.

$|V_{cs}|$ has been increased by $\sqrt{\chi^2/\mathrm{dof}} = 1.03$.

Using the determinations of $|V_{cd}|$ and $|V_{cs}|$ in Eq. (102), we can test the unitarity of the second row of the CKM matrix. We obtain

$$|V_{cd}|^2 + |V_{cs}|^2 + |V_{cb}|^2 - 1 = 0.04(6) \tag{103}$$

which agrees with the Standard Model at the percent level. Given the current level of precision, this result does not depend on the value used for $|V_{cb}|$, which is of $\mathcal{O}(10^{-2})$ [see Eq. (153)].

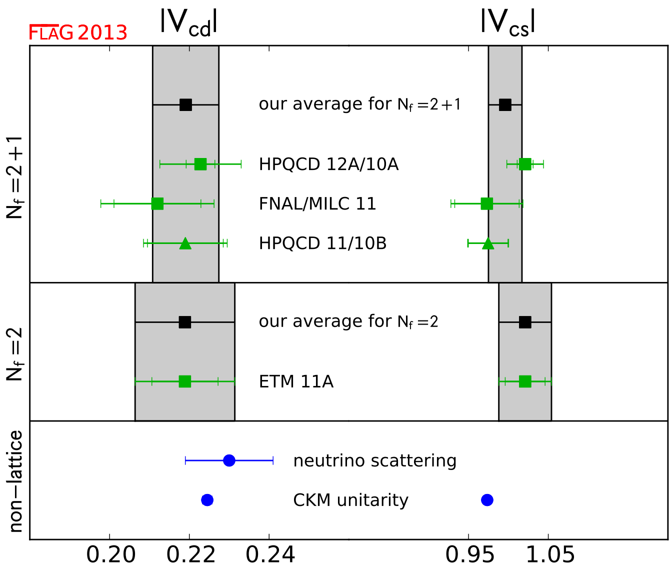

Figure 15: Comparison of determinations of $|V_{cd}|$ and $|V_{cs}|$ obtained from lattice methods with non-lattice determinations and the Standard-Model prediction based on CKM unitarity. When two references are listed on a single row, the first corresponds to the lattice input for $|V_{cd}|$ and the second to that for $|V_{cs}|$. The results denoted by squares are from leptonic decays, while those denoted by triangles are from semileptonic decays.

8 B-meson decay constants, mixing parameters and form factors

Leptonic and semileptonic decays of bottom B and B_s mesons probe the quark-flavour changing transitions $b \to u$ and $b \to c$. Tree-level semileptonic B decays with light charged leptons ($\ell = e, \mu$) in the final state, such as $B \to \pi \ell \nu$ and $B \to D^{(*)} \ell \nu$, enable determinations of the CKM matrix elements $|V_{ub}|$ and $|V_{cb}|$ within the Standard Model. Semileptonic B decays that occur via loops in the Standard Model, such as $B \to K^{(*)} \ell^+ \ell^-$, provide sensitive probes of physics beyond-the-Standard Model because contributions from new heavy particles in the loops may be comparable to the Standard-Model "background." Further, because B mesons are sufficiently massive, they can decay to final states involving τ-leptons. Tree-level decays such as $B \to \tau \nu$ and $B \to D^{(*)} \tau \nu$ are promising new-physics search channels because they can receive significant contributions from charged-Higgs bosons.

Mixing of neutral B^0_d and B^0_s mesons occurs in the Standard Model via one-loop box diagrams containing up-type quarks (u, c, t) and charged W bosons. Because the Standard-Model contributions are proportional to the CKM factors $|V_{u(c,t)q} V^*_{u(c,t)b}|^2$ (where $q = d, s$) and the quark masses $m^2_{u(c,t)}$, neutral B-meson mixing is dominated by intermediate top quarks. Thus experimental measurements of the neutral $B^0_{d(s)}$-meson oscillation frequencies, $\Delta M_{d(s)}$ combined with sufficiently precise theoretical calculations of the hadronic mixing matrix elements (often presented as dimensionless "bag" parameters), enable the determination of the CKM matrix elements $|V_{td}|$ and $|V_{ts}|$ within the Standard Model. Conversely, neutral B-meson mixing places stringent constraints on the scale of generic new heavy particles that can enter the loops in beyond-the-Standard Model scenarios. Finally, neutral meson mixing is also sensitive to the phase of the CKM matrix (ρ, η). Thus the ratio of oscillation frequencies $\Delta M_d / \Delta M_s$ places a tight constraint on the apex of the CKM unitarity triangle that is complementary to those from other observables.

Lattice-QCD calculations of b quarks have an added complication not present for charm and light quarks: at the lattice spacings that are currently used in numerical simulations, the b quark mass is of order one in lattice units. Therefore a direct treatment of b quarks with the fermion actions commonly used for light quarks will result in large cutoff effects, and all current lattice-QCD calculations of b quark quantities make use of effective field theory at some stage. The two most widely used general approaches for lattice b quarks are (i) direct application of effective field theory treatments such as HQET or NRQCD, which allow for a systematic expansion in $1/m_b$; or (ii) the interpretation of a relativistic quark action in a manner suitable for heavy quarks using an extended Symanzik improvement program to suppress cutoff errors. This introduces new systematic uncertainties that are not present in light-quark calculations, either from truncation of the effective theory, or from more complicated lattice-spacing dependence. Further, because with these approaches the light and bottom quarks are simulated with different fermion actions, it is in general not possible to construct absolutely normalized bottom-light currents; this leads to systematic uncertainties due to matching the lattice operators to the continuum that can be significant. A third approach is to use an improved light-quark action to calculate the quantity of interest over a range of heavy-quark masses with $am_h < 1$, and then use heavy-quark effective theory and/or knowledge of the static limit to extrapolate or interpolate to the physical b-quark mass. Such methods can avoid some of the aforementioned complications, but require simulations at very small lattice spacings in order to keep discretization errors under control. Appendix A.1.3

reviews the methods used to treat b quarks on the lattice in more detail.

Here we summarize the status of lattice-QCD calculations of the bottom leptonic decay constants, neutral meson mixing parameters, and semileptonic form factors. We limit our review to results based on modern simulations with reasonably light pion masses (below approximately 500 MeV). This excludes results obtained from the earliest unquenched simulations, which typically had two flavours in the sea, and which were limited to heavier pion masses because of the constraints imposed by the computational resources and methods available at that time. Fewer collaborations have presented results for these quantities than for the light-quark sector (u, d, s), and the calculations tend to be on coarser lattice spacings with heavier pions. Therefore, for some quantities, there is only a single lattice calculation that satisfies the criteria to be included in our average. Several collaborations, however, are currently pursuing the needed matrix-element calculations with different lattice b-quark actions, finer lattice spacings, and lighter pions, so we expect the appearance of many new results with controlled errors in the next year or two.

We also note that the heavy-quark methods discussed in this review have been validated in a number of ways. Because several groups use the same action for charm and bottom quarks, tests of such methods with charm quarks are relevant for B physics results, and are therefore included in the following discussion. Calculations of hadron masses with one or more heavy (charm or bottom) valence quark provide phenomenological tests of the heavy-quark action. Such calculations have been performed with NRQCD, HQET, Fermilab, RHQ, Tsukuba, HISQ, Overlap, twisted-mass Wilson, and other $\mathcal{O}(a)$ improved Wilson heavy quarks for the hyperfine splittings in the $D_{(s)}$ and $B_{(s)}$ meson systems [317, 318, 335–346], and for the low-lying charmonium [317, 339, 340, 343, 347–351], bottomonium [352–358], and B_c [336, 341, 359–361] systems. All of them are in good agreement with experimental measurements. Hyperfine splittings are sensitive to higher-order terms in the heavy-quark action and therefore provide particularly good tests of such terms. The comparison of lattice-QCD calculations of hadronic matrix elements for leptonic and radiative decays in charmonium [349, 361] with experimental measurements provides CKM-free tests of heavy-HISQ currents. The comparison of lattice-QCD calculations of the shape of the semileptonic form factors for $D \to \pi(K)\ell\nu$ [330] with experimental measurements provides CKM independent tests of charm-quark currents with the Fermilab action. In two of the above mentioned tests, the lattice-QCD calculations were predictions, in one case predating the experimental discovery of the B_c mass, and in the other predating experimental measurements of the shape of the semilleptonic D-meson form factors with comparable precision. Truncation errors in HQET have been studied by comparing simulations of the effective field theory with corresponding quenched simulations using a nonperturbatively improved Wilson action with heavy quark masses in the charm-mass region in large volumes [362] and up to the b-quark mass in small volumes [363]. Moreover, the consistency between independent determinations of the bottom [72, 320, 337, 342, 364–366] and charm [60, 72, 73, 85, 317, 367, 368] quark masses using NRQCD, HQET, Tsukuba, HISQ, twisted-mass Wilson, and other $\mathcal{O}(a)$ improved Wilson heavy quarks, as well as their agreement with non-lattice determinations [74] further validate lattice heavy-quark methods.

Following our review of lattice-QCD calculations of $B_{(s)}$-meson leptonic decay constants, neutral meson mixing parameters, and semileptonic form factors, we then interpret our results within the context of the Standard Model. We combine our best-determined values of the hadronic matrix elements with the most recent experimentally-measured branching fractions to obtain $|V_{(u)cb}|$ and compare these results to those obtained from inclusive semileptonic B

decays.

8.1 Leptonic decay constants f_B and f_{B_s}

The B and B_s meson decay constants are relevant for decays of charged B-mesons to a lepton-neutrino pair via the charged current interaction, as well as for rare leptonic decays of neutral $B_{d(s)}$ mesons to a charged-lepton pair via a flavour-changing neutral current (FCNC) interaction.

In the Standard Model the decay rate for $B^+ \to \ell^+\nu_\ell$ is given by a formula identical to the one for D decays in Eq. (7.1) but with $D_{(s)}$ replaced by B and the relevant CKM matrix element V_{cq} replaced by V_{ub}:

$$\Gamma(B \to \ell\nu_\ell) = \frac{m_B}{8\pi} G_F^2 f_B^2 |V_{ub}|^2 m_\ell^2 \left(1 - \frac{m_\ell^2}{m_B^2}\right)^2 \ . \tag{104}$$

The only charged-current B meson decay that has been observed so far is $B \to \tau\nu_\tau$, which has been measured by the Belle and Babar collaborations with a combined precision of 20% [74]. This measurement can therefore be used to determine $|V_{ub}|$ when combined with lattice-QCD predictions of the corresponding decay constant.

The decay of a neutral $B_{d(s)}$ meson to a charged lepton pair is loop-suppressed in the Standard Model. The corresponding expression for the branching fraction has the form

$$B(B_q \to \ell^+\ell^-) = \tau_{B_q} \frac{G_F^2}{\pi}\, Y \left(\frac{\alpha}{4\pi \sin^2\Theta_W}\right)^2 m_{B_q} f_{B_q}^2 |V_{tb}^* V_{tq}|^2 m_\ell^2 \sqrt{1 - 4\frac{m_\ell^2}{m_B^2}} \ , \tag{105}$$

where the light quark $q = s$ or d, and the loop function Y includes NLO QCD and electroweak corrections [369]. Evidence for $B_s \to \mu^+\mu^-$ decay was recently seen at LHCb at the 3.5σ level, with a branching fraction of $BR(B_s \to \mu^+\mu^-) = (3.2^{+1.5}_{-1.2})\, 10^{-9}$ [370].

The decay constants f_{B_q} (with $q = u, d, s$) parameterize the matrix elements of the corresponding axial-vector currents, $A^\mu_{bq} = \bar{b}\gamma^\mu\gamma^5 q$, analogously to the definition of f_{D_q} in section 7.1:

$$\langle 0|A^\mu|B_q(p)\rangle = p_B^\mu f_{B_q} \ . \tag{106}$$

For heavy-light mesons, it is convenient to define and analyze the quantity

$$\Phi_{B_q} \equiv f_{B_q}\sqrt{m_{B_q}} \ , \tag{107}$$

which approaches a constant (up to logarithmic corrections) in the $m_B \to \infty$ limit. In the following discussion we denote lattice data for $\Phi(f)$ obtained at a heavy quark mass m_h and light valence-quark mass m_ℓ as $\Phi_{h\ell}(f_{hl})$, to differentiate them from the corresponding quantities at the physical b and light-quark masses.

The SU(3) breaking ratio f_{B_s}/f_B is an interesting quantity to study with lattice QCD, since most systematic errors partially cancel in this ratio, including discretization errors, heavy-quark mass tuning effects, and renormalization errors, among others. The SU(3) breaking ratio is however sensitive to the chiral extrapolation. So one can, in principle, combine a lattice-QCD calculation of the SU(3) breaking ratio that includes a careful study of the chiral extrapolation, with a different lattice-QCD calculation of f_{B_s} (which is relatively insensitive to chiral extrapolation errors) that includes a careful study of all other systematic errors to obtain a more precise result for f_B than would be possible from either lattice-QCD calculation alone. Indeed, this strategy is used by both the ETM and HPQCD collaborations, as described below.

A number of different heavy-quark formulations are being used to obtain results for B_q meson decay constants from numerical simulations with $N_f = 2$, $N_f = 2{+}1$, and $N_f = 2{+}1{+}1$ sea quarks. They are summarized in Tables 24 and 25 and in Figure 16. Additional details about the underlying simulations and systematic error estimates are given in Appendix B.6.1.

Collaboration	Ref.	N_f	publication status	continuum extrapolation	chiral extrapolation	finite volume	renormalization/matching	heavy quark treatment	f_{B^+}	f_{B^0}	f_B	f_{B_s}
HPQCD 13	[371]	2+1+1	P	★	★	★	○	✓	184(4)	188(4)	186(4)	224(5)
HPQCD 12	[372]	2+1	A	○	○	★	○	✓	–	–	191(9)	228(10)
HPQCD 12	[372]	2+1	A	○	○	★	○	✓	–	–	189(4)$^\diamond$	–
HPQCD 11A	[338]	2+1	A	★	○	★	★	✓	–	–	–	225(4)$^\nabla$
FNAL/MILC 11	[316]	2+1	A	○	○	★	○	✓	197(9)	–	–	242(10)
HPQCD 09	[373]	2+1	A	○	○	★	○	✓	–	–	190(13)$^\bullet$	231(15)$^\bullet$
ALPHA 12A	[342]	2	C	★	★	★	★	✓	–	–	193(9)(4)	219(12)
ETM 12B†	[365]	2	C	★	○	★	○	✓	–	–	197(10)	234(6)
ALPHA 11	[337]	2	C	★	○	★	★	✓	–	–	174(11)(2)	–
ETM 11A	[320]	2	A	○	○	★	○	✓	–	–	195(12)	232(10)
ETM 09D	[364]	2	A	○	○	○	○	✓	–	–	194(16)	235(12)

$^\diamond$Obtained by combining f_{B_s} from HPQCD 11A with f_{B_s}/f_B calculated in this work.
$^\nabla$This result uses one ensemble per lattice spacing with light to strange sea-quark mass ratio $m_\ell/m_s \approx 0.2$.
$^\bullet$This result uses an old determination of $r_1 = 0.321(5)$ fm from Ref. [352] that has since been superseded.
†Update of ETM 11A.

Table 24: Decay constants of the B, B^+, B^0 and B_s mesons (in MeV). Here f_B stands for the mean value of f_{B^+} and f_{B^0}, extrapolated (or interpolated) in the mass of the light valence-quark to the physical value of m_{ud}.

The ETM collaboration has presented a series of calculations of the B meson decay constants based on simulations with $N_f = 2$ sea quarks [320, 364, 365]. Three lattice spacings in the range $a \approx 0.067 - 0.098\,\text{fm}$ are used in ETM 09D [364]. In ETM 11A and 12B [320, 365] additional ensembles at $a \approx 0.054$ fm are included. The valence and sea quarks are simulated with two different versions of the twisted-mass Wilson fermion action. The heavy-quark masses are in the charm region and above while keeping $am_h \lesssim 0.5$. ETM 12B includes slightly heavier masses than ETM 11A. The ETM collaboration uses two methods to obtain $f_{B_{(s)}}$ from their heavy Wilson data: the ratio and the interpolation methods. In the interpolation method they supplement their heavy Wilson data with a static limit calculation. In the ratio method (see Appendix A.1.3) they construct ratios (called $z_{(s)}$) from a combination

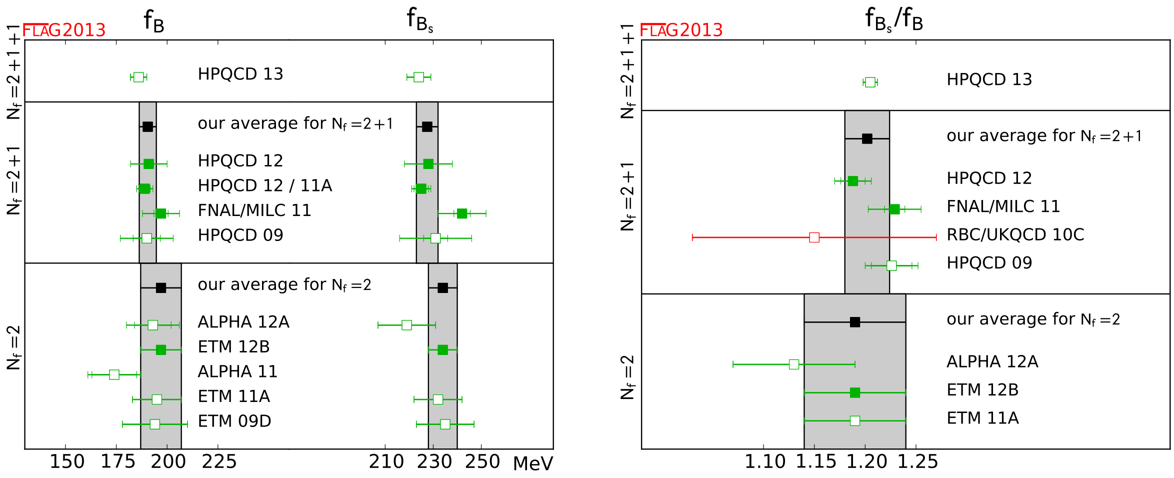

Figure 16: Decay constants of the B and B_s mesons. The values are taken from Table 24 (the f_B entry for FNAL/MILC 11 represents f_{B^+}). The significance of the colours is explained in section 2. The black squares and grey bands indicate our averages in (108) and (109).

of the decay constants $f_{h\ell(s)}$ and the heavy-quark pole masses that are equal to unity in the static limit. Ratios of pole-to-$\overline{\rm MS}$ mass conversion factors are included at NLO in continuum perturbation theory. Both, the interpolation and ratio methods are employed in ETM 11A to calculate f_B, f_{B_s}, and f_{B_s}/f_B, while ETM 09D and ETM 12B use only the ratio method. Finally, ETM analyzes the SU(3) breaking ratio $\Phi_{hs}/\Phi_{h\ell}$ (or the ratio of ratios, z_s/z) and combines it with Φ_{hs} or (z_s) to obtain f_B, instead of directly extracting it from their $\Phi_{h\ell}$ (or z) data. In ETM 11A and 12B for both the interpolation and ratio methods, the data are interpolated to a fixed set of reference masses on all ensembles, and subsequently extrapolated to the continuum and to the physical light-quark masses in a combined fit. The static limit calculation for the interpolation method in ETM 11A is done at two intermediate lattice spacings, $a \approx 0.085, 0.067$ fm. In ETM 11A the results from both methods are averaged for their final results. In ETM 12B, the final result for the decay constants is from the ratio method only. The results from the interpolation method have larger (statistical and systematic) errors than those from the ratio method, since statistical and systematic errors tend to cancel in the ratios. The observed discretization effects (as measured by the percentage difference between the lattice data at the smallest lattice spacing and the continuum extrapolated results) are smaller than what would be expected from power-counting estimates. Over the range of heavy quark masses used in their simulations ETM finds discretization errors $\lesssim 3\%$ for Φ_{hs} and $\lesssim 1.5\%$ for the ratio z_s. As a result, the dominant error on f_{B_s} is the statistical (combined with the chiral and continuum extrapolation and heavy quark interpolation) uncertainty, whereas the dominant error on the SU(3) breaking ratio is due to the chiral extrapolation.

The ALPHA collaboration calculates the B and B_s meson decay constants at the physical b-quark mass using nonperturbative lattice HQET through $\mathcal{O}(1/m_h)$ on ensembles with $N_f = 2$ nonperturbatively $\mathcal{O}(a)$ improved Wilson quarks at three lattice spacings in the range $a \approx 0.048 - 0.075$ fm. The parameters of the HQET action and the static current renormalization are determined nonperturbatively in a separate matching calculation using small physical

Collaboration	Ref.	N_f	publication status	continuum extrapolation	chiral extrapolation	finite volume	renormalization/matching	heavy quark treatment	f_{B_s}/f_{B^+}	f_{B_s}/f_{B^0}	f_{B_s}/f_B
HPQCD 13	[371]	2+1+1	P	★	★	★	○	✓	1.217(8)	1.194(7)	1.205(7)
HPQCD 12	[372]	2+1	A	○	○	★	○	✓	–	–	1.188(18)
FNAL/MILC 11	[316]	2+1	A	○	○	★	○	✓	1.229(26)	–	–
RBC/UKQCD 10C	[374]	2+1	A	■	■	★	○	✓	–	–	1.15(12)
HPQCD 09	[373]	2+1	A	○	○	★	○	✓	–	–	1.226(26)
ALPHA 12A	[342]	2	C	★	★	★	★	✓	–	–	1.13(6)
ETM 12B†	[365]	2	C	★	○	★	○	✓	–	–	1.19(5)
ETM 11A	[320]	2	A	○	○	★	○	✓	–	–	1.19(5)

†Update of ETM 11A.

Table 25: Ratios of decay constants of the B and B_s mesons (for details see Table 24).

volumes ($L \simeq 0.4$ fm) with Schrödinger functional boundary conditions together with a recursive finite-size scaling procedure to obtain the nonperturbative parameters at the large physical volumes used in the simulations. In ALPHA 11 [337] ensembles with pion masses in the range $m_\pi \approx 440 - 267$ MeV are used. ALPHA 12A [342] includes an ensemble at a lighter sea quark mass corresponding to $m_\pi \approx 190$ MeV. ALPHA 11 presents results for f_B only, while ALPHA 12A also presents a preliminary result for f_{B_s}. The combined statistical and extrapolation errors are of order 5% in this calculation, and are larger than the chiral fit uncertainty. Truncation errors which are $\mathcal{O}(\Lambda_{\rm QCD}/m_h)^2$ are not included in this error budget. Simple power-counting would suggest that they are $\approx 1 - 4\%$. However, the results from both the ETM collaboration discussed above and the HPQCD collaboration (from their heavy HISQ analysis) discussed below, as well as results obtained by ALPHA in the quenched approximation [362] indicate that $\mathcal{O}(\Lambda_{\rm QCD}/m_h)^2$ effects are probably quite small for heavy-light decay constants at the physical b-quark mass.

For the $N_f = 2+1$ case there are currently four published papers describing lattice-QCD calculations of $f_{B_{(s)}}$ performed by two different groups: FNAL/MILC and HPQCD. The HPQCD collaboration has published several calculations of the B meson decay constants with NRQCD b quarks [372, 373]. In Ref. [373] (HPQCD 09) they use Asqtad light valence quarks, and include ensembles at two lattice spacings $a \approx 0.12, 0.09$ fm and sea quarks with minimum RMS sea-pion masses $m_{\pi,\rm RMS} \approx 400$ MeV equal to the light sea-quark masses. In Ref. [372] HISQ light valence quarks are employed instead. This analysis uses the same Asqtad ensembles as in HPQCD 09 but includes an additional ensemble at $a \approx 0.09$ fm at a lighter sea-quark mass, so that the minimum RMS sea pion mass is approximately 320 MeV. The HISQ light valence masses are matched to the Asqtad sea-quark masses via the ratio m_ℓ/m_s. The dominant systematic error in both calculations is due to using one-loop mean-field improved lattice perturbation theory for the current renormalization. In both calculations, HPQCD performs a combined chiral and continuum extrapolation of the data, in the first case using NLO (full QCD) heavy meson rooted staggered χPT (HMrSχPT) and in the latter case using NLO continuum partially quenched HMχPT, supplemented in both cases by NNLO analytic and generic discretization terms. HPQCD finds a significant reduction in discretization errors in their calculation with HISQ light valence quarks, as compared to their calculation with Asqtad valence quarks. Indeed, in HPQCD 12 the continuum extrapolated results overlap within errors with the data at finite lattice spacing.

Another calculation of the B_s meson decay constant is presented by the HPQCD collaboration in Ref. [338] , this time using the HISQ action for the strange and heavy valence quarks, i.e. the heavy HISQ method. This analysis includes Asqtad ensembles over a large range of lattice spacings, $a \approx 0.15 - 0.045$ fm and heavy-quark masses in the range $am_h \approx 0.2 - 0.85$. Only one sea-quark ensemble per lattice spacing is included in this analysis, all with a sea-quark to strange-quark mass ratio of $m_\ell/m_s \approx 0.2$, yielding a minimum RMS sea pion mass of approximately 330 MeV. The sea-quark mass dependence is assumed to be negligible, which is based on the analysis of f_{D_s} in Ref. [318]. HPQCD uses an HQET-type expansion in $1/m_H$ (where m_H is the mass of an h-flavoured meson) with coefficients that are polynomials in am_h, $a\Lambda$, and am_s to perform a combined fit to all their data, including terms up to $1/m_H^3$, $(am_h)^6$, $(a\Lambda)^6$, and $(am_s)^6$. The continuum extrapolated fit curve is then used to obtain the decay constant at the physical B_s meson mass, which requires another small extrapolation. As can be seen in Figure 1 of Ref. [338], discretization errors (as measured by the percentage difference between the lattice data and the continuum fit curve) are smaller for a given value of am_h when m_H is larger. This somewhat counterintuitive result for an action that formally contains discretization errors of $\mathcal{O}(am_h)^2$ is likely due to coefficients in the form of powers of v/c that suppress these errors. After statistical (and extrapolation) errors, the largest sources of uncertainty in this analysis are discretization and heavy-quark extrapolation errors. They are estimated by varying the fit Ansatz and by excluding data at the largest and smallest lattice spacings as well as data at the largest values of am_h.

The Fermilab Lattice and MILC collaborations present a lattice-QCD calculation of the D and B meson decay constants in Ref. [316], which uses the Fermilab method for the heavy (b and c) valence quarks together with Asqtad light and strange valence quarks on a subset of the MILC Asqtad $N_f = 2+1$ ensembles. The current renormalizations are calculated using a mostly nonperturbative renormalization (mNPR) method. Their estimate of the perturbative errors for the small perturbative correction factors calculated at one-loop in mean field improved lattice perturbation theory are comparable to the size of actual one-loop corrections. The simulations include lattice spacings in the range $a \approx 0.15 - 0.09$ fm and a minimum RMS pion mass of approximately 320 MeV. In this calculation lattice data at $9 - 12$ valence light-quark masses are generated for each sea-quark ensemble. The chiral and continuum extrapolated results are obtained from combined chiral and continuum fits. The chiral fit function uses NLO partially quenched HMrSχPT including $1/m_h$ terms and supplemented by NNLO analytic terms. Also included are light-quark as well as heavy-quark discretization terms. The dominant uncertainties after statistical errors are due to heavy-quark discretization effects, heavy-quark mass tuning, and correlator fit errors. A calculation of the B and D meson decay constants using Fermilab heavy quarks on the full set of Asqtad ensembles is still in progress [375].

The RBC/UKQCD collaboration has presented a result for the SU(3) breaking ratio in Ref. [374] using a static-limit action on $N_f = 2+1$ domain wall ensembles at a single lattice spacing $a \approx 0.11$ fm with a minimum pion mass of approximately 430 MeV. They use both HYP and APE smearing for the static action and one-loop mean field improved lattice perturbation theory to renormalize and improve the static-limit current. Their static-limit action and current do not, however, include $1/m_h$ effects. Ref. [374] includes an estimate of this effect via power counting as $\mathcal{O}((m_s - m_d)/m_b)$ in the error budget. The statistical errors in this work are significantly larger ($\sim 5-8\%$), as are the chiral extrapolation errors ($\sim 7\%$), due to the rather large pion masses used in this work. With data at only one lattice spacing, discretization errors cannot be estimated from the data. A power counting estimate of this error of 3% is included in the systematic error budget. The RBC/UKQCD collaboration has also presented a preliminary calculation of the B meson decay constants using the RHQ action (another relativistic heavy-quark action) on $N_f = 2+1$ domain wall ensembles at two lattice spacings [376], but without quotable results.

Finally, the first results for B meson decay constants with $N_f = 2+1+1$ sea quarks are presented by the HPQCD collaboration [371] (HPQCD 13) using the MILC HISQ ensembles at three lattice spacings, $a \approx 0.15, 0.12, 0.09$ fm, where at each lattice spacing one ensemble with Goldstone pions at the physical value is included. HPQCD 13 uses NRQCD b quarks and HISQ light valence quarks. The combined chiral interpolation and continuum extrapolation is performed using NLO (full QCD) HMχPT, supplemented by generic discretization terms of $O(a^2, a^4)$. HPQCD also performs a continuum extrapolation of the data at the physical point only, with results that are in good agreement with the extrapolated results obtained from the full data set. The dominant systematic error in this calculation is due to using one-loop mean-field improved lattice perturbation theory for the current renormalization. In HPQCD 13 it is estimated at 1.4%, almost a factor of 3 smaller than in HPQCD 12, after reorganizing the perturbative series similar to the mNPR method, and using the fact that the heavy-heavy NRQCD temporal vector current is absolutely normalized and that the light-light HISQ vector current has a small one-loop correction. The next largest uncertainties are due to heavy-quark truncation effects and statistics and scale setting. In this work the scale is set using the $\Upsilon(2S-1S)$ splitting calculated in Ref. [355] without using r_1 to set the relative scale between ensembles at different lattice spacings, as was done in previous HPQCD work. Since HPQCD 13 is not yet published, it is not included in our averages.

As shown in Tables 24 and 25, for the $N_f = 2+1$ case there currently are four different results for the B and B_s meson decay constants and three different results for the SU(3) breaking ratio that satisfy the quality criteria. However, they all use overlapping subsets of MILC Asqtad ensembles. We therefore treat the statistical errors between the results as 100% correlated. Furthermore, one of the results for f_B in HPQCD 12 [372] is obtained by combining HPQCD 12's result for the ratio f_{B_s}/f_B using NRQCD b quarks with HPQCD 11A's result for f_{B_s}. However, no itemized error budget is given for the so-combined f_B result. In order to include sensible correlations between the two HPQCD results for f_B, we construct an itemized error budget for the combined f_B from the individual itemized error budgets, by adding the itemized errors in quadrature. This is conservative, because the resulting total uncertainty on the combined f_B is slightly larger than the quoted uncertainty in Ref. [372], 4.3 MeV compared to 4 MeV. We then treat the chiral extrapolation errors, the light-quark discretization errors, the scale setting errors, and renormalization errors as 100% correlated between the two f_B results in HPQCD 12. Finally, the HPQCD 09 result was obtained using a value for the scale r_1 that has since been superseded. We drop this result from the average, since it is effectively updated by HPQCD 12. We obtain:

$$N_f = 2{+}1: \; f_B = (190.5{\pm}4.2)\,\mathrm{MeV}, \; f_{B_s} = (227.7{\pm}4.5)\,\mathrm{MeV}, \; f_{B_s}/f_B = 1.202{\pm}0.022\,. \quad (108)$$

The uncertainties on the averages for f_{B_s} and for the SU(3) ratio include PDG rescaling factors of 1.1 and 1.3, respectively.

For the $N_f = 2$ case, only ETM's results qualify for averaging, since ALPHA's results have appeared in conference proceedings only so far. Since ETM 12B updates the published ETM 11A result, we use it for our average:

$$N_f = 2: \; f_B = (197 \pm 10)\,\mathrm{MeV}, \; f_{B_s} = (234 \pm 6)\,\mathrm{MeV}, \; f_{B_s}/f_B = 1.19 \pm 0.05\,. \quad (109)$$

A comparison of all $N_f = 2$ and $N_f = 2+1$ lattice-QCD results for f_B, f_{B_s}, and their ratio is shown in Figure 16. The averages presented in Eqs. (108) and (109) are represented by the grey bands in the figures.

A final comment concerns which light valence-quark mass is used for the chiral extrapolations (or interpolations) to the physical point. First, we note that all the results discussed in this review use simulations with degenerate up and down sea-quark masses. However, since the observed sea-quark mass dependence is much smaller than the valence-quark mass dependence, the dominant contribution to differences between B^+ and B^0 meson quantities is due to the light valence quarks. Almost all the results quoted in this review are obtained from chiral extrapolations to the average of the up- and down-quark masses, and therefore correspond to the average of the B^0 and B^+ meson decay constants. The exceptions are FNAL/MILC 11 and HPQCD 13 which both quote results for the B^+ meson decay constant from chiral extrapolations (interpolations) of the light valence-quark to the physical up-quark mass. HPQCD 13 also quotes results for the B^0 meson decay constant from chiral interpolations to the physical down-quark mass as well as results for the average of the B^+ and B^0 mesons. The $N_f = 2+1$ and $N_f = 2$ averages presented in Eqs. (108) and (109) are for the average of the B^+ and B^0 meson decay constant, f_B, and the corresponding ratio, f_{B_s}/f_B. Given the errors quoted in the results that enter our averages, we currently include the FNAL/MILC 11 results for the B^+ meson in Eq. (108). As the precision with which B meson decay constants are obtained continues to improve, especially given the availability of physical mass ensembles, future reviews will need to distinguish between these cases. Indeed HPQCD 13 finds a 2% difference between the B^+ and B^0 decay constants, which is the same size as the total uncertainty in this calculation. We strongly recommend that future lattice-QCD calculations of B meson decay constants quote results for the B^+ and B^0 mesons separately.

8.2 Neutral B-meson mixing matrix elements

Neutral B-meson mixing is induced in the Standard Model through one-loop box diagrams to lowest order in the electroweak theory, similar to those for neutral kaon mixing. The effective Hamiltonian is given by

$$\mathcal{H}_{\rm eff}^{\Delta B=2,{\rm SM}} \;=\; \frac{G_F^2 M_{\rm W}^2}{16\pi^2}(\mathcal{F}_d^0 \mathcal{Q}_1^d + \mathcal{F}_s^0 \mathcal{Q}_1^s) \;+\; {\rm h.c.}\,, \quad (110)$$

with

$$\mathcal{Q}_1^q = \left[\bar{b}\gamma_\mu(1-\gamma_5)q\right]\left[\bar{b}\gamma_\mu(1-\gamma_5)q\right], \quad (111)$$

where $q = d$ or s. The short-distance function $\mathcal{F}_q^0$ in Eq. (110) is much simpler compared to the kaon mixing case due to the hierarchy in the CKM matrix elements. Here, only one term is relevant,

$$\mathcal{F}_q^0 = \lambda_{tq}^2 S_0(x_t) \tag{112}$$

where

$$\lambda_{tq} = V_{tq}^* V_{tb}, \tag{113}$$

and where $S_0(x_t)$ is an Inami-Lim function with $x_t = m_t^2/M_W^2$, which describes the basic electroweak loop contributions without QCD [280]. The transition amplitude for B_q^0 with $q = d$ or s can be written as

$$\begin{aligned}\langle \bar{B}_q^0 | \mathcal{H}_{\rm eff}^{\Delta B=2} | B_q^0 \rangle \;&=\; \frac{G_F^2 M_{\rm W}^2}{16\pi^2} \Big[\lambda_{tq}^2 S_0(x_t) \eta_{2B} \Big] \\ \times \left(\frac{\bar{g}(\mu)^2}{4\pi} \right)^{-\gamma_0/(2\beta_0)} &\exp\left\{ \int_0^{\bar{g}(\mu)} dg \left(\frac{\gamma(g)}{\beta(g)} + \frac{\gamma_0}{\beta_0 g} \right) \right\} \langle \bar{B}_q^0 | Q_{\rm R}^q(\mu) | B_q^0 \rangle \;+\; {\rm h.c.}\;, \end{aligned} \tag{114}$$

where $Q_{\rm R}^q(\mu)$ is the renormalized four-fermion operator (usually in the NDR scheme of $\overline{\rm MS}$). The running coupling ($\bar{g}$), the β-function ($\beta(g)$), and the anomalous dimension of the four quark operator ($\gamma(g)$) are defined in Eqs. (77) and (78). The product of μ dependent terms on the second line of Eq. (114) is, of course, μ independent (up to truncation errors if perturbation theory is used). The explicit expression for the short-distance QCD correction factor η_{2B}(calculated to NLO) can be found in Ref. [278].

For historical reasons the B-meson mixing matrix elements are often parameterized in terms of bag parameters defined as

$$B_{B_q}(\mu) = \frac{\langle \bar{B}_q^0 | Q_{\rm R}^q(\mu) | B_q^0 \rangle}{\frac{8}{3} f_{B_q}^2 m_{\rm B}^2} \;. \tag{115}$$

The RGI B parameter $\hat{B}$ is defined, as in the case of the kaon, and expressed to two-loop order as

$$\hat{B}_{B_q} = \left(\frac{\bar{g}(\mu)^2}{4\pi} \right)^{-\gamma_0/(2\beta_0)} \left\{ 1 + \frac{\bar{g}(\mu)^2}{(4\pi)^2} \left[\frac{\beta_1\gamma_0 - \beta_0\gamma_1}{2\beta_0^2} \right] \right\} B_{B_q}(\mu) \;, \tag{116}$$

with β_0, β_1, γ_0, and γ_1 defined in Eq. (79).

Nonzero transition amplitudes result in a mass difference between the CP eigenstates of the neutral B meson system. Writing the mass difference for a B_q^0 meson as Δm_q, its Standard Model prediction is

$$\Delta m_q = \frac{G_F^2 m_W^2 m_{B_q}}{16\pi^2} |\lambda_{tq}|^2 S_0(x_t) \eta_{2B} f_{B_q}^2 \hat{B}_{B_q}. \tag{117}$$

Experimentally the mass difference is measured as oscillation frequency of the CP eigenstates. The frequencies are measured precisely with an error of less than a percent. Many different experiments have measured Δm_d, but the current average [74] is dominated by measurements from the B-factory experiments Belle and Babar, and from the LHC experiment LHCb. For Δm_s the experimental average is based on results from the Tevatron experiment CDF and from the LHC experiment LHCb [74]. With these experimental results and lattice-QCD calculations of $f_{B_q}^2 \hat{B}_{B_q}$ at hand, λ_{tq} can be determined. In lattice-QCD calculations the flavour $SU(3)$ breaking ratio

$$\xi^2 = \frac{f_{B_s}^2 B_{B_s}}{f_{B_d}^2 B_{B_d}} \tag{118}$$

can be obtained more precisely than the individual B_q-mixing matrix elements because statistical and systematic errors cancel in part. With this ratio $|V_{td}/V_{ts}|$ can be determined, which can be used to constrain the apex of the CKM triangle.

Neutral B-meson mixing, being loop-induced in the Standard Model is also a sensitive probe of new physics. The most general $\Delta B = 2$ effective Hamiltonian that describes contributions to B-meson mixing in the Standard Model and beyond is given in terms of five local four-fermion operators:

$$\mathcal{H}_{\rm eff}^{\Delta B=2} = \sum_{i=1}^{5} \mathcal{C}_i \mathcal{Q}_i \,, \tag{119}$$

where $\mathcal{Q}_1$ is defined in Eq. (111) and where

$$\mathcal{Q}_2^q = \left[\bar{b}(1-\gamma_5)q\right]\left[\bar{b}(1-\gamma_5)q\right], \qquad \mathcal{Q}_3^q = \left[\bar{b}^\alpha(1-\gamma_5)q^\beta\right]\left[\bar{b}^\beta(1-\gamma_5)q^\alpha\right],$$

$$\mathcal{Q}_4^q = \left[\bar{b}(1-\gamma_5)q\right]\left[\bar{b}(1+\gamma_5)q\right], \qquad \mathcal{Q}_5^q = \left[\bar{b}^\alpha(1-\gamma_5)q^\beta\right]\left[\bar{b}^\beta(1+\gamma_5)q^\alpha\right], \tag{120}$$

with the superscripts α, β denoting colour indices, which are shown only when they are contracted across the two bilinears. The short-distance Wilson coefficients $\mathcal{C}_i$ depend on the underlying theory and can be calculated perturbatively. In the Standard Model only matrix elements of $\mathcal{Q}_1^q$ contribute to Δm_q, and combinations of matrix elements of $\mathcal{Q}_1^q$, $\mathcal{Q}_2^q$, and $\mathcal{Q}_3^q$ contribute to the width difference $\Delta\Gamma_q$ [377, 378]. Matrix elements of $\mathcal{Q}_4^q$ and $\mathcal{Q}_5^q$ are needed for calculating the contributions to B_q-meson mixing from beyond the Standard Model theories.

In this section we report on results from lattice-QCD calculations for the neutral B-meson mixing parameters $\hat{B}_{B_d}$, $\hat{B}_{B_s}$, $f_{B_d}\sqrt{\hat{B}_{B_d}}$, $f_{B_s}\sqrt{\hat{B}_{B_s}}$ and the $SU(3)$ breaking ratios B_{B_s}/B_{B_d} and ξ defined in Eqs. (115), (116), and (118). The results are summarized in Tables 26 and 27 and in Figures 17 and 18. Additional details about the underlying simulations and systematic error estimates are given in Appendix B.6.2. Some collaborations do not provide the RGI quantities $\hat{B}_{B_q}$ but quote instead $B_B(\mu)^{\overline{MS},NDR}$. In such cases we convert the results to the RGI quantities quoted in Table 26 using Eq. (116). More details on the conversion factors are provided below in the descriptions of the individual results. One group also reports results for B-meson matrix elements of the other operators $\mathcal{Q}_{2-5}$ in Ref. [379], which is a conference proceedings.

The ETM collaboration has presented their first results for B-mixing quantities with $N_f = 2$ sea quarks in Refs. [365, 381] (ETM 12A, 12B) using ensembles at three lattice spacings in the range $a \approx 0.065-0.098$ fm with a minimum pion mass of 270 MeV. The valence and sea quarks are simulated with two different versions of the twisted-mass Wilson fermion action. The heavy-quark masses are in the charm region and above while keeping $am_h \lesssim 0.6$. In ETM 12A and 12B the ratio method first developed for B-meson decay constants (see Appendix A.1.3 and Section 8.1) is extended to B-meson mixing quantities. ETM again constructs ratios of B-mixing matrix elements (now called $\omega_{d(s)}$) that are equal to unity in the static limit, including also an analogous ratio for ξ. The renormalization of the four-quark operator is calculated nonperturbatively in the RI'/MOM scheme. As an intermediate step for the interpolation to the physical b-quark mass, these ratios include perturbative matching factors to match the four-quark operator from QCD to HQET, included here at tree-level and leading log order. Similar to their decay constant analysis, ETM analyzes the $SU(3)$ breaking ratio of ratios, ω_s/ω_ℓ, and combines it with ω_s to obtain B_{B_d}. The data are interpolated to a

Collaboration	Ref.	N_f	publication status	continuum extrapolation	chiral extrapolation	finite volume	renormalization/matching	heavy quark treatment	$f_{\rm B_d}\sqrt{\hat{B}_{\rm B_d}}$	$f_{\rm B_d}\sqrt{\hat{B}_{\rm B_s}}$	$\hat{B}_{\rm B_d}$	$\hat{B}_{\rm B_s}$
FNAL/MILC 11A	[379]	2+1	C	★	○	★	○	✓	250(23)†	291(18)†	–	–
HPQCD 09	[373]	2+1	A	○	○$^\nabla$	★	○	✓	216(15)*	266(18)*	1.27(10)*	1.33(6)*
HPQCD 06A	[380]	2+1	A	■	■	★	○	✓	–	281(21)	–	1.17(17)
ETM 12A, 12B	[365, 381]	2	C	★	○	★	★	✓	–	–	1.32(8)$^\diamond$	1.36(8)$^\diamond$

† Reported $f_B^2 B$ at $\mu = m_b$ is converted to RGI by multiplying the two-loop factor 1.517.
$^\nabla$ Wrong-spin contributions are not included in the rSχPT fits.
* This result uses an old determination of $r_1 = 0.321(5)$ fm from Ref. [352] that has since been superseded.
$^\diamond$ Reported B at $\mu = m_b = 4.35$ GeV is converted to RGI by multiplying the two-loop factor 1.521.

Table 26: Neutral B and $B_{\rm s}$ meson mixing matrix elements (in MeV) and bag parameters.

fixed set of heavy-quark reference masses on all ensembles, and subsequently extrapolated to the continuum and to the physical light-quark masses in a combined fit. The interpolation to the physical b-quark mass is linear or quadratic in the inverse of the heavy-quark mass. This work reports $B_B(m_b)^{\overline{MS},NDR}$ at $m_b = 4.35$ GeV. Taking $\alpha_s(M_Z) = 0.1184$ [95], we apply an RGI conversion factor of $\hat{B}_B/B_B(m_b)^{\overline{MS},NDR} = 1.521$ to obtain the $\hat{B}_B$ values quoted in Table 26. The observed discretization effects (as measured by the percentage difference between the lattice data at the smallest lattice spacing and the continuum extrapolated results) are $\lesssim 1\%$ over the range of heavy-quark masses used in their simulations. As a result, the dominant error on the bag parameters and on the ratio of bag parameters is the combined statistical uncertainty, whereas the dominant error on the $SU(3)$ breaking ratio ξ is due to the chiral extrapolation. Since this study is published in conference proceedings only, these results do not enter our averages.

For the $N_f = 2+1$ case there are three collaborations that have presented results for $B - \bar{B}$ mixing matrix elements: HPQCD, RBC/UKQCD, and FNAL/MILC. The first published results are by the HPQCD collaboration [373, 380] and use NRQCD b quarks and Asqtad light valence quarks on $N_f = 2+1$ MILC Asqtad ensembles. In HPQCD 06A [380] results are presented for B_s-mixing quantities only, using one lattice spacing and two light sea-quark masses with a minimum RMS pion mass of 510 MeV. The observed sea-quark mass dependence is much smaller than the rather large statistical errors. This calculation uses one-loop mean-field improved lattice perturbation theory for the operator renormalization. Discretization errors cannot be estimated from the data with only one lattice spacing, but are estimated using power counting arguments to be smaller than the dominant statistical and renormalization errors. With only one lattice spacing and given the rather large minimum RMS pion mass, this result does not enter our averages. These shortcomings are removed

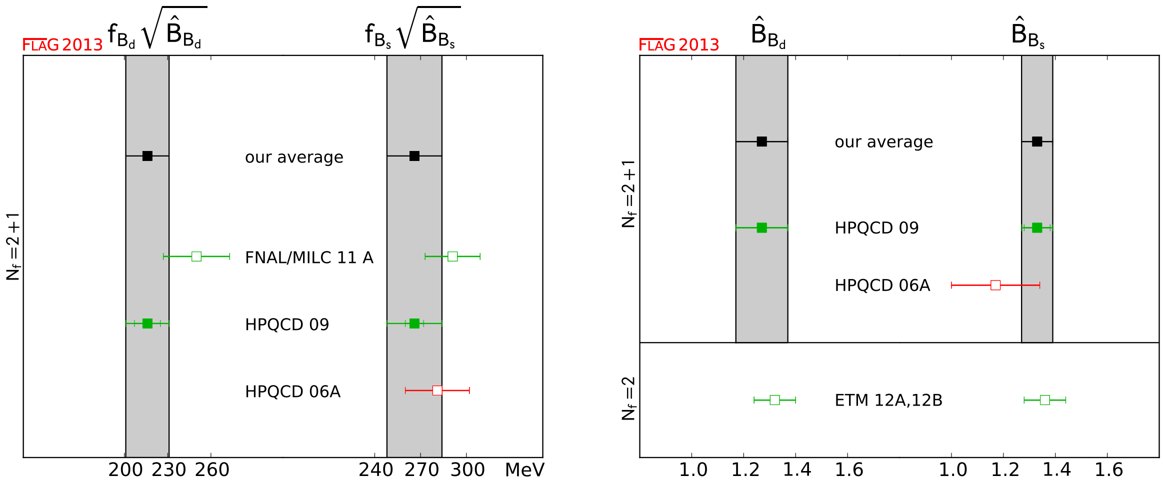

Figure 17: Neutral B and B_s meson mixing matrix elements and bag parameters [values in Table 26 and Eqs. (121), (122)]. All results shown in the left plot are obtained on $N_f = 2+1$ ensembles.

in HPQCD 09 [373] with two lattice spacings, ($a \approx 0.09, 0.12$ fm) and four or two sea-quark masses per lattice spacing with a minimum RMS pion mass of about 400 MeV. The calculation is also extended to include both B_d and B_s mixing quantities and thus also the $SU(3)$ breaking ratios. A combined chiral and continuum extrapolation of the data is performed, using NLO HMrSχPT, supplemented by NNLO analytic and generic discretization terms of $\mathcal{O}(\alpha_s a^2, a^4)$. The dominant systematic error is due to using one-loop mean-field improved lattice perturbation theory for the operator renormalization and matching, the same as in HPQCD 06. It is estimated as 4% and 2.5%, respectively, consistent with power counting. The statistical, chiral, and continuum extrapolation uncertainties are also prominent sources of uncertainty, followed by heavy-quark truncation and scale setting errors. The dominant error on ξ is due to statistics and chiral extrapolation. Finally, we note that this work uses an old determination of $r_1 = 0.321(5)$ fm from Ref. [352] to set the scale, that has since been superseded, and that differs from the new value by about two standard deviations. Dimensionless quantities are, of course, affected by a change in r_1 only through the inputs, which are a subdominant source of uncertainty. The scale uncertainty itself is also subdominant in the error budget, and this change therefore does not affect HPQCD 09's results for $f_{B_q}\sqrt{B_{B_q}}$ outside of the total error.

The RBC/UKQCD collaboration has presented a result for the $SU(3)$ breaking ratio ξ in Ref. [374] using a static-limit action on $N_f = 2+1$ domain wall ensembles at a single lattice spacing $a \approx 0.11$ fm with a minimum pion mass of approximately 430 MeV. They use both HYP and APE smearing for the static-limit action and one-loop mean field improved lattice perturbation theory to renormalize the static-limit four-quark operators. Effects of $\mathcal{O}(1/m_h)$ are not included in the static-limit action and operators, but Ref. [374] includes an estimate of this effect via power counting as $\mathcal{O}\left((m_s - m_d)/m_b\right)$ in the error budget. The statistical errors in this work are significant ($\sim 5-6\%$), as are the chiral extrapolation errors ($\sim 7\%$, estimated from the difference between fits using NLO $SU(2)$ HMχPT and a linear fit function), due to the rather large pion masses used in this in this work. With data at only one lattice spacing, discretization errors cannot be estimated from the data, but a power counting estimate of

Collaboration	Ref.	N_f	publication status	continuum extrapolation	chiral extrapolation	finite volume	renormalization/matching	heavy quark treatment	ξ	B_{B_s}/B_{B_d}
FNAL/MILC 12	[382]	2+1	A	○	○	★	○	✓	1.268(63)	1.06(11)
RBC/UKQCD 10C	[374]	2+1	A	■	■	★	○	✓	1.13(12)	–
HPQCD 09	[373]	2+1	A	○	○$^\triangledown$	★	○	✓	1.258(33)	1.05(7)
ETM 12A, 12B	[365, 381]	2	C	★	○	★	★	✓	1.21(6)	1.03(2)

$^\triangledown$Wrong-spin contributions are not included in the rSχPT fits.

Table 27: Results for $SU(3)$ breaking ratios of neutral B_d and B_s meson mixing matrix elements and bag parameters.

this error of 4% is included in the systematic error budget. With only one lattice spacing this result does not enter our averages.

Another calculation of the $SU(3)$ breaking ratio ξ is presented by the Fermilab Lattice and MILC collaborations in Ref. [382] (FNAL/MILC 12). The calculation uses the Fermilab method for the b quarks together with Asqtad light and strange valence quarks on a subset of the MILC Asqtad $N_f = 2+1$ ensembles, including lattice spacings in the range $a \approx 0.09 - 0.12$ fm and a minimum RMS pion mass of approximately 320 MeV. This analysis includes partially-quenched lattice data at six valence light-quark masses for each sea-quark ensemble. The operator renormalizations are calculated using one-loop mean-field improved lattice perturbation theory, which does not result in a significant source of uncertainty for the $SU(3)$ breaking ratios. The combined chiral and continuum extrapolations use a chiral fit function based on NLO partially quenched HMrSχPT supplemented by NNLO analytic terms. Also included are light-quark discretization terms of $\mathcal{O}(\alpha_s^2 a^2, a^4)$. The combined statistical, light-quark discretization, and chiral extrapolation error dominates the error budget together with an uncertainty that is described as the error due to the omission of "wrong-spin contributions" (see below). First results for the B mixing matrix elements from an ongoing FNAL/MILC calculation of all B meson mixing quantities on the full set of Asqtad ensembles are presented in [379], including the matrix elements of all five operators that contribute to B meson mixing in the Standard Model and beyond . The dominant uncertainties on the matrix elements are due to the combined statistical, chiral extrapolation, and light-quark discretization error and due to the one-loop matching. FNAL/MILC 11A reports results for $f_{B_q}\sqrt{B_{B_q}}$ evaluated at $\mu = m_b$ in the $\overline{\rm MS}$ NDR scheme. Taking $\alpha_s(M_Z) = 0.1184$ [95] and $m_b = 4.19$ GeV [74], we apply an RGI conversion factor of $\hat{B}_B/B_B(m_b)^{\overline{MS},NDR} = 1.517$ to obtain the values for the RGI quantities listed in Table 26. Ref. [379] presents a complete error budget, but since the paper is a conference proceedings, its results are not included in

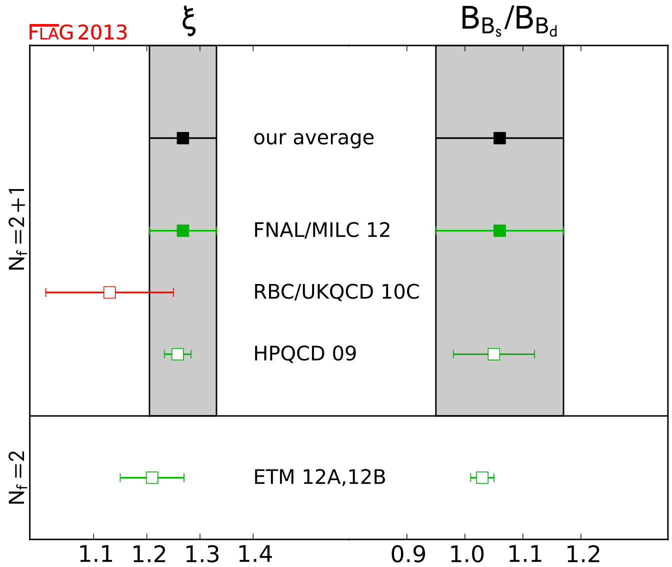

Figure 18: The $SU(3)$ breaking quantities ξ and B_{B_s}/B_{B_d} [values in Table 27 and Eq. (123)].

our averages.

For the $N_f = 2$ case there are no published results, so we do not quote an average for this case. For $N_f = 2+1$ only the results of HPQCD 09 and FNAL/MILC 12 enter our averages. First, we must consider the issue of the so-called "wrong-spin contributions," described in Ref. [382] and explained in detail in Ref. [383]. With staggered light quarks, interactions between different unphysical species ("tastes") of quarks induce mixing between the operator $\mathcal{Q}_1^q$ in Eq. (111) and the operators $\mathcal{Q}_2^q$ and $\mathcal{Q}_3^q$ in Eq. (120) at $\mathcal{O}(a^2)$. These additional contributions to the matrix element $f_{B_q}\sqrt{B_{B_q}}$ are discretization errors that vanish in the continuum limit. The contributions of $\mathcal{Q}_1^q$–$\mathcal{Q}_5^q$ have been derived at next-to-leading order in HMrSχPT [383]. The result is that, in the chiral expansion of the matrix elements of $\mathcal{Q}_1^q$, the matrix elements of $\mathcal{Q}_{2,3}^q$ appear with $\mathcal{O}(a^2)$ coefficients that depend upon the light-quark masses. These contributions can be accounted for in the chiral-continuum extrapolation by fitting the numerical results for the matrix elements of the three operators simultaneously. Further, if the matrix elements of all five basis operators in Eqs. (111) and (120) are computed on the lattice, then no additional low-energy constants are required to describe the wrong-spin contributions effects in the chiral-continuum extrapolation. In principle, instead of using HMrSχPT as described above, it is possible to account for the wrong-spin terms via the inclusion of generic mass-dependent terms such as $O(a^2 m_\pi^2)$ in the combined chiral-continuum extrapolation, provided that the lattice spacing and light-quark masses are small enough.

Both HPQCD 09 and FNAL/MILC 11A use chiral fit functions based on NLO HMrSχPT. Since, however, these works predate Refs. [382, 383], the wrong-spin terms are not included in their chiral extrapolations. The calculation in FNAL/MILC 12 also does not include the matrix elements of all three operators, so here the effect of the wrong-spin contributions is treated as a systematic error, which is estimated using the lattice data described in Ref. [379]. As discussed above, the estimated uncertainty of 3% for ξ is a dominant contribution to the error budget in Ref. [382]. Because, however, HPQCD 09 does not include the wrong-spin contributions in its chiral extrapolations, we must consider how they affect the results. First, the chiral fit functions used in HPQCD 09 and in FNAL/MILC 12 are very similar with similar (though not identical) choices for prior widths. The main difference is that the generic light-quark discretization term of $\mathcal{O}(\alpha_s a^2)$ included in HPQCD 09 is a little less constrained than the $\mathcal{O}(\alpha_s^2 a^2)$ term included in FNAL/MILC 12. It is therefore possible that the chiral extrapolation in HPQCD 09 accounts for the wrong-spin contributions via the generic discretization terms. Furthermore, for $f_{B_q}\sqrt{B_{B_q}}$ the chiral extrapolation error, while not insignificant, is not a dominant source of error in the HPQCD calculation. For ξ, however, the chiral extrapolation error is a dominant source of uncertainty, and the FNAL/MILC 12 analysis indicates that the omission of the wrong-spin contributions from HMrSχPT fits may also be a significant source of error. We therefore make the conservative choice of excluding HPQCD 09's result for ξ from our average, but keeping HPQCD 09's results for $f_{B_q}\sqrt{B_{B_q}}$ and B_{B_q} in our averages. As a result, we now have only one calculation that enters our averages for each quantity. Our averages are ($N_f = 2+1$):

$$f_{B_d}\sqrt{\hat{B}_{B_d}} = 216(15)\ \text{ MeV}\,, \qquad f_{B_s}\sqrt{\hat{B}_{B_s}} = 266(18)\ \text{ MeV}\,, \tag{121}$$

$$\hat{B}_{B_d} = 1.27(10)\,, \qquad \hat{B}_{B_s} = 1.33(6)\,, \tag{122}$$

$$\xi = 1.268(63)\,, \qquad B_{B_s}/B_{B_d} = 1.06(11). \tag{123}$$

Finally, we note that the above results are all correlated with each other: the numbers in (121) and (122) are from HPQCD 09 [373], while those in (123) are from FNAL/MILC 12 [382] – the same Asqtad MILC ensembles are used in these simulations. The results are also correlated with the averages obtained in Section 8.1 and shown in Eq. (108), because the calculations of B-meson decay constants and mixing quantities are performed on the same (or on similar) sets of ensembles, and results obtained by a given collaboration use the same actions and setups. These correlations must be considered when using our averages as inputs to UT fits. In the future, as more independent calculations enter the averages, correlations between the lattice-QCD inputs to the UT fit will become less significant.

8.3 Semileptonic form factors for B decays to light flavours

The Standard-Model differential rate for the decay $B_{(s)} \to P\ell\nu$ involving a quark-level $b \to u$ transition is given, at leading order in the weak interaction, by a formula identical to the one for D decays in Eq. (93) but with $D \to B_{(s)}$ and the relevant CKM matrix element $|V_{cq}| \to |V_{ub}|$:

$$\frac{d\Gamma(B_{(s)}\to P\ell\nu)}{dq^2} = \frac{G_F^2|V_{ub}|^2}{24\pi^3}\,\frac{(q^2-m_\ell^2)^2\sqrt{E_P^2-m_P^2}}{q^4 m_{B_{(s)}}^2}\left[\left(1+\frac{m_\ell^2}{2q^2}\right) m_{B_{(s)}}^2 (E_P^2 - m_P^2)|f_+(q^2)|^2 \right.$$
$$\left. + \frac{3m_\ell^2}{8q^2}(m_{B_{(s)}}^2 - m_P^2)^2 |f_0(q^2)|^2\right]. \tag{124}$$

Again, for $\ell = e, \mu$ the contribution from the scalar form factor f_0 can be neglected, and one has a similar expression to Eq. (95), which in principle allows for a direct extraction of $|V_{ub}|$ by matching theoretical predictions to experimental data. However, while for D (or K) decays the entire physical range $0 \le q^2 \le q^2_{\rm max}$ can be covered with moderate momenta accessible to lattice simulations, in $B \to \pi\ell\nu$ decays one has $q^2_{\rm max} \sim 26\ \text{GeV}^2$ and only part of the full kinematic range is reachable. As a consequence, obtaining $|V_{ub}|$ from $B \to \pi\ell\nu$ is more complicated then obtaining $|V_{cd(s)}|$ from semileptonic D-meson decays. The standard procedure involves the matching of theoretical predictions and experimental data for the integrated decay rate over a limited q^2 range,

$$\Delta\zeta = \frac{1}{|V_{ub}|^2} \int_{q_1^2}^{q_2^2} \left(\frac{d\Gamma}{dq^2}\right) dq^2 \,. \tag{125}$$

This requires knowledge of the relevant form factor(s) within the integration interval. In practice, lattice computations are restricted to small values of the momentum transfer (see Sec. 7.2) where statistical and momentum-dependent discretization errors can be controlled,[30] which in existing calculations roughly cover the upper third of the kinematically allowed q^2 range. Experimental results normally cover the whole interval, but are more precise in the low-q^2 region. Therefore, both experimental and lattice data for the q^2 dependence have to be parameterized by fitting data to a specific ansatz, either separately or jointly (with the relative normalization $|V_{ub}|^2$ as a free parameter). A good control of the systematic uncertainty induced by the choice of parameterization is hence crucial to obtain a precise determination of $|V_{ub}|$.

8.3.1 Parameterizations of heavy-to-light semileptonic form factors

All form factors are analytic functions of q^2 outside physical poles and inelastic threshold branch points; in the case of $B \to \pi\ell\nu$, the only pole expected below the $B\pi$ production region, starting at $q^2 = t_+ = (m_B + m_\pi)^2$, is the B^*. A simple ansatz for the q^2 dependence of the $B \to \pi\ell\nu$ semileptonic form factors that incorporates vector-meson dominance is the Bećirević-Kaidalov (BK) parameterization [329]:

$$f_+(q^2) = \frac{f(0)}{(1-q^2/m_{B^*}^2)(1-\alpha q^2/m_{B^*}^2)}\,, \qquad\qquad f_0(q^2) = \frac{f(0)}{1-\frac{1}{\beta}\, q^2/m_{B^*}^2}\,. \tag{126}$$

Because the BK ansatz has few free parameters, it has been used extensively to parameterize the shape of experimental branching-fraction measurements and theoretical form-factor calculations. A variant of this parameterization proposed by Ball and Zwicky (BZ) adds extra pole factors to the expressions in Eq. (126) in order to mimic the effect of multiparticle states [385]. Another variant (RH) has been proposed by Hill in [386]. Although all of these parameterizations capture some known properties of form factors, they do not manifestly satisfy others. For example, perturbative QCD scaling constrains the high-q^2 behaviour to be $f_+(q^2) \sim 1/q^2$ up to logarithmic corrections [387–389], and angular momentum conservation constrains the asymptotic behaviour near thresholds — e.g. $\mathrm{Im}\, f_+(q^2) \sim (q^2 - t_+)^{3/2}$ (see e.g. [390]). Further, they do not allow for an easy quantification of systematic uncertainties.

A more systematic approach that improves upon the use of simple models for the q^2 behavior exploits the positivity and analyticity properties of two-point functions of vector currents to obtain optimal parameterizations of form factors [389, 391–395]. Any form factor f can be shown to admit a series expansion of the form

$$f(q^2) = \frac{1}{B(q^2)\phi(q^2,t_0)} \sum_{n=0}^{\infty} a_n(t_0)\, z(q^2,t_0)^n \,, \tag{127}$$

[30] The variance of hadron correlation functions at nonzero momentum is dominated at large Euclidean times by zero-momentum multiparticle states [384]; therefore the noise-to-signal grows more rapidly than for the vanishing momentum case.

where the squared momentum transfer is replaced by the variable

$$z(q^2, t_0) = \frac{\sqrt{t_+ - q^2} - \sqrt{t_+ - t_0}}{\sqrt{t_+ - q^2} + \sqrt{t_+ - t_0}} \,. \tag{128}$$

This is a conformal transformation, depending on an arbitrary real parameter $t_0 < t_+$, that maps the q^2 plane cut for $q^2 \geq t_+$ onto the disk $|z(q^2, t_0)| < 1$ in the z complex plane. The function $B(q^2)$ is called the *Blaschke factor*, and contains poles and cuts below t_+ — for instance, in the case of $B \to \pi$ decays

$$B(q^2) = \frac{z(q^2,t_0) - z(m_{B^*}^2,t_0)}{1 - z(q^2,t_0) z(m_{B^*}^2,t_0)} = z(q^2, m_{B^*}^2) \,. \tag{129}$$

Finally, the quantity $\phi(q^2, t_0)$, called the *outer function*, is an analytic function that does not introduce further poles or branch cuts. The crucial property of this series expansion is that the sum of the squares of the coefficients

$$\sum_{n=0}^{\infty} a_n^2 = \frac{1}{2\pi i} \oint \frac{dz}{z} \, |B(z)\phi(z)f(z)|^2 \,, \tag{130}$$

is a finite quantity. Therefore, by using this parameterization an absolute bound to the uncertainty induced by truncating the series can be obtained. The criteria involved in the optimal choice of ϕ then aim at obtaining a bound that is useful in practice, while (ideally) preserving the correct behaviour of the form factor at high q^2 and around thresholds.

The simplest form of the bound would correspond to $\sum_{n=0}^{\infty} a_n^2 = 1$. *Imposing* this bound yields the following "standard" choice for the outer function

$$\begin{aligned} \phi(q^2, t_0) = & \sqrt{\frac{1}{32\pi\chi_{1^-}(0)}} \left(\sqrt{t_+ - q^2} + \sqrt{t_+ - t_0}\right) \\ & \times \left(\sqrt{t_+ - q^2} + \sqrt{t_+ - t_-}\right)^{3/2} \left(\sqrt{t_+ - q^2} + \sqrt{t_+}\right)^{-5} \frac{t_+ - q^2}{(t_+ - t_0)^{1/4}} \,, \end{aligned} \tag{131}$$

where $\chi_{1^-}(0)$ is the derivative of the transverse component of the polarisation function (i.e. the Fourier transform of the vector two-point function) $\Pi_{\mu\nu}(q)$ at Euclidian momentum $Q^2 = -q^2 = 0$. It is computed perturbatively, using operator product expansion techniques, by relating the $B \to \pi\ell\nu$ decay amplitude to $\ell\nu \to B\pi$ inelastic scattering via crossing symmetry and reproducing the correct value of the inclusive rate $\ell\nu \to X_b$. We will refer to the series parameterization with the outer function in Eq. (131) as Boyd, Grinstein, and Lebed (BGL). The perturbative and OPE truncations imply that the bound is not strict, and one should take it as

$$\sum_{n=0}^{N} a_n^2 \lesssim 1 \,, \tag{132}$$

where this holds for any choice of N. Since the values of $|z|$ in the kinematical region of interest are well below 1 for judicious choices of t_0, this provides a very stringent bound on systematic uncertainties related to truncation for $N \geq 2$. On the other hand, the outer function in Eq. (131) is somewhat unwieldy and, more relevantly, spoils the correct large q^2 behavior and induces an unphysical singularity at the $B\pi$ threshold.

A simpler choice of outer function has been proposed by Bourrely, Caprini and Lellouch (BCL) in [390], which leads to a parameterization of the form

$$f_+(q^2) = \frac{1}{1-q^2/m_{B^*}^2} \sum_{n=0}^{N} a_n(t_0) z(q^2,t_0)^n \,. \tag{133}$$

This satisfies all the basic properties of the form factor, at the price of changing the expression for the bound to

$$\sum_{j,k=0}^{N} B_{jk}(t_0) a_j(t_0) a_k(t_0) \leq 1 \,. \tag{134}$$

The constants B_{jk} can be computed and shown to be $|B_{jk}| \lesssim \mathcal{O}(10^{-2})$ for judicious choices of t_0; therefore, one again finds that truncating at $N \geq 2$ provides sufficiently stringent bounds for the current level of experimental and theoretical precision. It is actually possible to optimise the properties of the expansion by taking

$$t_0 = t_{\rm opt} = (m_B - m_\pi)(\sqrt{m_B} - \sqrt{m_\pi})^2 \,, \tag{135}$$

which for physical values of the masses results in the semileptonic domain being mapped onto the symmetric interval $|z| \lesssim 0.279$ (where this range differs slightly for the $B^\pm$ and B^0 decay channels), minimizing the maximum truncation error. If one also imposes that the asymptotic behaviour $\mathrm{Im}\, f_+(q^2) \sim (q^2 - t_+)^{3/2}$ near threshold is satisfied, then the highest-order coefficient is further constrained as

$$a_N = -\frac{(-1)^N}{N} \sum_{n=0}^{N-1} (-1)^n \, n \, a_n \,. \tag{136}$$

Substituting the above constraint on a_N into Eq. (133) leads to the constrained BCL parameterization

$$f_+(q^2) = \frac{1}{1-q^2/m_{B^*}^2} \sum_{n=0}^{N-1} a_n \left[z^n - (-1)^{n-N} \, \frac{n}{N} \, z^N \right] \,, \tag{137}$$

which is the standard implementation of the BCL parameterization used in the literature.

Parameterizations of the BGL and BCL kind (to which we will refer collectively as "z-parameterizations") have already been adopted by the Babar and Belle collaborations to report their results, and also by the Heavy Flavor Averaging Group (HFAG). Some lattice collaborations, such as FNAL/MILC and ALPHA, have already started to report their results for form factors in this way. The emerging trend is to use the BCL parameterization as a standard way of presenting results for the q^2 dependence of semileptonic form factors. Our policy will be to quote results for z-parameterizations when the latter are provided in the paper (including the covariance matrix of the fits); when this is not the case, but the published form factors include the full correlation matrix for values at different q^2, we will perform our own fit to the constrained BCL ansatz in Eq.(137); otherwise no fit will be quoted.

8.3.2 Form factors for $B \to \pi\ell\nu$ and $B_s \to K\ell\nu$

Results for the $B \to \pi\ell\nu$ form factors have been published by the HPQCD [396] and FNAL/MILC [397] Collaborations, in both cases for $N_f = 2+1$ dynamical quark flavours. Work is also underway by ALPHA [398, 399] (on $N_f = 2$ nonperturbatively $\mathcal{O}(a)$ improved Wilson configurations), FNAL/MILC [400] (updating the published analysis), HPQCD [401] ($N_f = 2+1$ HISQ), and the RBC/UKQCD Collaborations [402] ($N_f = 2+1$ DWF). These calculations, however, are so far described only in conference proceedings which do not provide quotable results, so they will not be discussed in this report.

Both the HPQCD and the FNAL/MILC computations of the $B \to \pi\ell\nu$ amplitudes use ensembles of gauge configurations with $N_f = 2+1$ flavours of rooted staggered quarks produced by the MILC Collaboration at two different values of the lattice spacing ($a \sim 0.12,\ 0.09$ fm). The relative scale is fixed in both cases through r_1/a, while the absolute scale is set through the Υ $2S$–$1S$ splitting for HPQCD and f_π (with uncertainty estimated from the same Υ splitting) for FNAL/MILC. The spatial extent of the lattices is $L \simeq 2.4$ fm, save for the lightest mass point ($a \sim 0.09$ fm) for which $L \simeq 2.9$ fm. The lightest RMS pion mass is around 400 MeV. Lattice-discretization effects are estimated within HMrSχPT in the FNAL/MILC computation, while HPQCD quotes the results at $a \sim 0.12$ fm as central values and uses the $a \sim 0.09$ fm results to quote an uncertainty.

The main difference between the computations lies in the treatment of heavy quarks. HPQCD uses the NRQCD formalism, with a one-loop matching of the relevant currents to the ones in the relativistic theory. FNAL/MILC employs the clover action with the Fermilab interpretation, with a mostly nonperturbative renormalization of the relevant currents, within which light-light and heavy-heavy currents are renormalized nonperturbatively and one-loop perturbation theory is used for the relative normalization. (See Table 28; full details about the computations are provided in tables in Appendix B.6.3.)

Chiral extrapolations are an important source of systematic uncertainty, since the pion masses at which the computations are carried out are relatively heavy. In order to control deviations from the expected χPT behavior, FNAL/MILC supplements $SU(3)$ HMrSχPT formulae with higher-order powers in E_π to extend the form factor parameterization up to $E_\pi \sim 1$ GeV. Chiral extrapolation effects do indeed make the largest contribution to their systematic error budget. HPQCD performs chiral extrapolations using HMrSχPT formulae, and estimates systematic uncertainties by comparing the result with the ones from fits to a linear behavior in the light-quark mass, continuum HMχPT, and partially quenched HMrSχPT formulae (including also data with different sea and valence light quark masses). This is again the dominant contribution to the error budget of the computation, along with the matching of the heavy-light current.

HPQCD provides results for both $f_+(q^2)$ and $f_0(q^2)$. In this case, the parameterization of the q^2 dependence of form factors is somewhat intertwined with chiral extrapolations: a set of fiducial values $\{E_\pi^{(n)}\}$ is fixed for each value of the light-quark mass, and $f_{+,0}$ are interpolated to each of the $E_\pi^{(n)}$; chiral extrapolations are then performed at fixed E_π. The interpolation is performed using a BZ ansatz. The q^2 dependence of the resulting form factors in the chiral limit is then described by means of a BZ ansatz, which is cross-checked against BK, RH, and BGL parameterizations. FNAL/MILC presents results for $f_+(q^2)$ only, and provides as its preferred description a three-parameter fit to the BGL form in a companion paper [403]; this result is quoted in Table 28. HPQCD, on the other hand, does not provide the correlation matrix for the values of $f_+(q^2)$ in the chiral limit, and therefore no independent fit to a

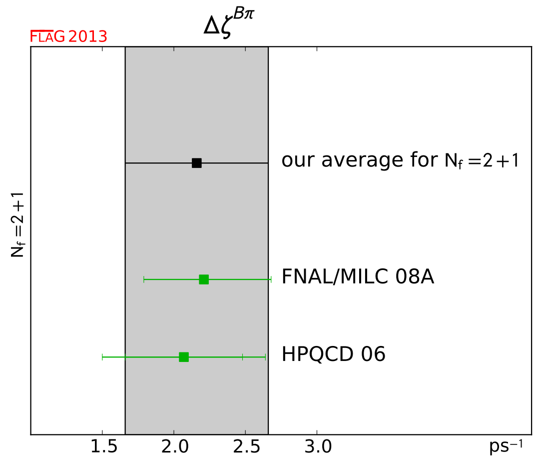

Figure 19: Integrated width of the decay $B \to \pi \ell \nu$ divided by $|V_{ub}|^2$ [values in Table 28 and Eq. (138)].

z-parameterization is possible.

Results for the integrated decay rate $\Delta\zeta^{B\pi}$, which is defined in equation (125) and depends on the chosen interval of integration, are available in both cases (see Table 28 and Fig. 19). We quote the average ($q_1 = 4\,\mathrm{GeV}$, $q_2 = q_{max}$):

$$N_f = 2+1: \qquad \Delta\zeta^{B\pi} = 2.16(50)\ \mathrm{ps}^{-1}\,, \tag{138}$$

where we have conservatively assumed that the calculations are 100% correlated because neither FNAL/MILC nor HPQCD provide itemized error budgets for $\Delta\zeta^{B\pi}$.[31]

The results for $f_+(q^2)$ in HPQCD 06 and FNAL/MILC 08A can also be combined into a single fit to our preferred BCL z-parameterization, Eq. (137). While FNAL/MILC 08A provides the full correlation matrix between $f_+(q^2)$ values, this information is not available for HPQCD data; we thus perform a simultaneous fit including all the $f_+(q^2)$ values from FNAL/MILC 08A and only one point from HPQCD 06. The value of f_+ from HPQCD 06 that we choose to include in the fit is the one at the lowest quoted momentum transfer for which no extrapolation in the energy of the final state pion is involved in the computation, $q^2_{\rm min} = 17.35\ \mathrm{GeV}^2$. Since in FNAL/MILC 08A $q^2_{\rm min} = 18.4\ \mathrm{GeV}^2$, this extends the covered kinematical range, and, together with the smaller relative error of the HPQCD datum, results in the latter having a significant weight in the fit. The HPQCD and FNAL/MILC computations are correlated by the use of an overlapping set of gauge-field ensembles for the evaluation of observables. We therefore treat the combined statistical plus chiral-extrapolation errors as 100% correlated between the two calculations in the fit. We treat the other systematic uncertainties as uncorrelated because they are mostly associated with the choice of b-quark action, which is different in the two calculations.

We fit the two sets of lattice data for $f_+(q^2)$ together to the BCL parameterization in Eq. (137) and assess the systematic uncertainty due to truncating the series expansion by

[31] These calculations are based on an overlapping set of gauge-field ensembles, so their statistical errors are highly correlated. They use different heavy-quark actions, renormalization methods, and chiral extrapolation fit functions, however, so we expect their systematic errors to be largely uncorrelated. Therefore we expect that assuming 100% correlation will lead to a conservative (over)estimate for the errors in $\Delta\zeta^{B\pi}$.

Collaboration	Ref.	N_f	publication status	continuum extrapolation	chiral extrapolation	finite volume	renormalization	heavy-quark treatment	$\Delta\zeta^{B\pi}$	z-parameterization type	$\{a_0, a_1, a_2\}$	cov. matrix
FNAL/MILC 08A	[397]	2+1	A	○	○	★	○	✓	$2.21^{+0.47\dagger}_{-0.42}$	BGL‡	$\{0.0216(27), -0.038(19), -0.113(27)\}$	yes§
HPQCD 06	[396]	2+1	A	○	○	★	○	✓	2.07(41)(39)	–	–	no

† Value based on the calculation of Ref. [397] (private communication with the FNAL/MILC collaboration).
‡ Result of BGL fit to FNAL/MILC data in Ref. [397] using $\chi_{1^-}(0) = 6.88919 \times 10^{-4}$ and given in [403].
§ Covariance matrix $C_{ij} = \text{cov}(a_i, a_j)$ given in Table IV of Ref. [403].

Table 28: Results for the $B \to \pi\ell\nu$ semileptonic form factor. The quantity $\Delta\zeta$ is defined in Eq. (125); the quoted values correspond to $q_1 = 4$ GeV, $q_2 = q_{max}$, and are given in ps^{-1}. The "cov. matrix" entry indicates whether or not the correlations, either between the lattice form-factor data at different values of q^2, or between the coefficients of a z-parameterization, are provided. This information is needed to use the lattice results in a combined fit to obtain $|V_{ub}|$.

considering fits to different orders in z. Figure 20 plots the FNAL/MILC and HPQCD data points for $(1 - q^2/m_{B^*}^2)f_+(q^2)$ versus z; the data is highly linear, and only a simple two-parameter fit is needed for a good χ^2/d.o.f.. (Note that a fit to the constrained BCL form in Eq. (137) with two free parameters corresponds to a polynomial through $\mathcal{O}(z^2)$, etc.) Further, we cannot constrain the coefficients of the z-expansion beyond this order, as evidenced by the error on the coefficient a_2 being significantly greater than 100% for a three-parameter fit. Because the FNAL/MILC synthetic data points are all from the output of the same chiral-continuum extrapolation, they are strongly correlated, so inverting the full 12×12 correlation matrix is problematic. We address these correlations in the FNAL/MILC data in several ways and make sure that the outcome of the fit is stable: we thin the data set to either six (every other) or four (every third) points, and imposing singular value decomposition (SVD) cuts of various severities in the construction of the pseudoinverse. The results (central values and errors) for the fit parameters are all very consistent irrespective of the treatment of correlations.

We quote as our preferred result the outcome of the three-parameter $\mathcal{O}(z^3)$ BCL fit using a thinned FNAL/MILC dataset that includes every second data point starting at

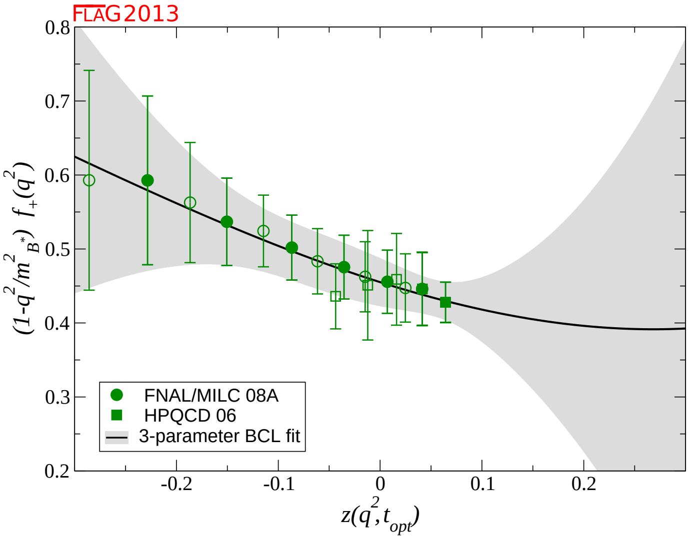

Figure 20: The form factors $(1 - q^2/m^2_{B^*})f_+(q^2)$ versus z. The filled symbols denote data points included in the fit, while the open symbols show points that are not included in the fit (either because of unknown correlations or strong correlations). The grey band displays our preferred three-parameter BCL fit to the plotted data with errors.

$q^2 = 18.4$ GeV^2 in addition to the HPQCD point at $q^2 = 17.35$ GeV^2:

$$N_f = 2+1: \qquad a_0 = 0.453(33)\,, \qquad a_1 = -0.43(33)\,, \qquad a_2 = 0.9(3.9)\,; \tag{139}$$

$$\mathrm{cov}(a_i, a_j) = \begin{pmatrix} 1.00 & -0.55 & -0.63 \\ -0.55 & 1.00 & 0.59 \\ -0.63 & 0.59 & 1.00 \end{pmatrix},$$

where the above uncertainties encompass both the lattice errors and the systematic error due to truncating the series in z. This can be used as the averaged FLAG result for the lattice-computed form factor $f_+(q^2)$. The coefficient a_3 can be obtained from the values for a_0–a_2 using Eq. (136). We emphasize that future lattice-QCD calculations of semileptonic form factors should publish their full statistical and systematic correlation matrices to enable others to use the data fully.

No unquenched computation of $B_s \to K\ell\nu$ form factors is currently available. Preliminary results by the HPQCD Collaboration are reported in [401], while work in progress by the FNAL/MILC Collaboration is mentioned in [400].

8.3.3 Form factors for radiative B semileptonic decays to light flavours

Lattice-QCD input is also available for some exclusive semileptonic decay channels involving neutral-current $b \to s$ transitions at the quark level. Being forbidden at tree level in the SM, these processes allow for stringent tests of potential new physics; simple examples are

$B \to K^*\gamma$ and $B \to K^{(*)}\ell^+\ell^-$, where the B meson (and therefore the kaon) can be either neutral or charged.

Due to their radiative nature, however, the corresponding SM effective weak Hamiltonian is considerably more complicated than the one for the tree-level processes discussed above: after neglecting top quark effects, as many as ten dimension-six operators formed by the product of two hadronic currents or one hadronic and one leptonic current appear.[32] Three of the latter, coming from penguin and box diagrams, dominate at short distances, and within a reasonable approximation one can keep these contributions only. Long-distance hadronic physics is then again encoded in matrix elements of current operators (vector, tensor, and axial-vector) between one-hadron states, which in turn can be parameterized in terms of a number of form factors (see [405] for a complete description). In addition, the lattice computation of the relevant form factors in channels with a vector meson in the final state faces extra challenges on top of those already present when the decay product is a Goldstone boson: the state is unstable and the extraction of the relevant matrix element from correlation functions is significantly more complicated; and χPT cannot be used as a guide to extrapolate results at unphysically heavy pion masses to the chiral limit. As a result, the current lattice methods and simulations that allow for control over systematic errors for kaon and pion final states leave uncontrolled systematic errors in calculations of weak decay form factors into unstable vector meson final states, such as the K^* or ρ mesons.

Various collaborations are currently working on the determination of $B \to K^{(*)}$ form factors, and have reported preliminary results in conference proceedings. All of them are based on the MILC $N_f = 2+1$ rooted Aqstad staggered gauge configurations. Liu et al. [406] have provided preliminary results with statistical errors only for the six form factors governing $B \to K\ell^+\ell^-$ and $B \to K^*\gamma$ transitions, using NRQCD bottom quarks. The FNAL/MILC Collaboration has reported in [400] preliminary results for the three form factors appearing in $B \to K\ell^+\ell^-$ transitions, with Fermilab bottom quarks. Finally, HPQCD has reported in [401] on their determination of the three form factors for $B \to K\ell^+\ell^-$ with NRQCD b quarks and HISQ valence light quarks, as well as on a computation of form factors for the unphysical transition $B_s \to \eta_s$.

8.4 Semileptonic form factors for $B \to D\ell\nu$, $B \to D^*\ell\nu$, and $B \to D\tau\nu$

The semileptonic processes $B \to D\ell\nu$ and $B \to D^*\ell\nu$ ($\ell = e, \mu$) have been studied extensively by experimentalists and theorists over the years. They allow for the determination of the CKM matrix element $|V_{cb}|$, an extremely important parameter of the Standard Model. $|V_{cb}|$ appears in many quantities that serve as inputs into CKM Unitarity Triangle analyses and reducing its uncertainties is of paramount importance. For example, when ϵ_K, the measure of indirect CP-violation in the neutral kaon system, is written in terms of the parameters ρ and η that specify the apex of the unitarity triangle, a factor of $|V_{cb}|^4$ multiplies the dominant term. As a result, the errors coming from $|V_{cb}|$ (and not those from B_K) are now the dominant uncertainty in the Standard Model (SM) prediction for this quantity. Decay rates for $B \to D^{(*)}\ell\nu$ processes can be parameterized as

$$\frac{d\Gamma_{B^-\to D^0\ell^-\bar{\nu}}}{dw} = \frac{G_\mu^2 m_D^3}{48\pi^3}(m_B + m_D)^2(w^2-1)^{3/2}|\eta_{\rm EW}|^2|V_{cb}|^2|\mathcal{G}(w)|^2, \tag{140}$$

$$\frac{d\Gamma_{B^-\to D^{0*}\ell^-\bar{\nu}}}{dw} = \frac{G_\mu^2 m_{D^*}^3}{4\pi^3}(m_B - m_{D^*})^2(w^2-1)^{1/2}|\eta_{\rm EW}|^2|V_{cb}|^2\chi(w)|\mathcal{F}(w)|^2, \tag{141}$$

[32] See e.g. [404] and references therein.

where $w \equiv v_B \cdot v_{D^{(*)}}$ and $\eta_{\rm EW} = 1.0066$ is the one-loop electroweak correction [407]. The function $\chi(w)$ in Eq. (141) depends upon the recoil w and the meson masses, and reduces to unity at zero recoil [404]. These formulas do not include terms that are proportional to the lepton mass squared which can be neglected for $\ell = e, \mu$.

Unquenched lattice calculations for $B \to D^* l\nu$ and $B \to Dl\nu$ decays to date focus mainly on the form factors at zero recoil [408, 409] $\mathcal{F}^{B\to D^*}(1)$ and $\mathcal{G}^{B\to D}(1)$. These can then be combined with experimental input to extract $|V_{cb}|$. The main reasons for concentrating on the zero recoil point are that (i) the decay rate then depends on a single form factor, and (ii) for $B \to D^* \ell\nu$, there are no $\mathcal{O}(\Lambda_{QCD}/m_Q)$ contributions due to Luke's theorem. Further, the zero recoil form factor can be computed via a double ratio in which most of the current renormalization cancels and heavy-quark discretization errors are suppressed by an additional power of Λ_{QCD}/m_Q.

8.4.1 $B \to D^*$ decays

The most precise determination of $|V_{cb}|$ from exclusive B semileptonic decays comes from the $B \to D^* \ell\nu$ form factor at zero recoil, $\mathcal{F}^{B\to D^*}(1)$, calculated by the Fermilab Lattice and MILC Collaborations [408, 409]. This work uses the MILC $N_f = 2{+}1$ ensembles. The bottom and charm quarks are simulated using the clover action with the Fermilab interpretation and light quarks are treated via the Asqtad staggered fermion action. At zero recoil $\mathcal{F}^{B\to D^*}(1)$ reduces to a single form factor, $h_{A_1}(1)$, coming from the axial-vector current

$$\langle D^*(v, \epsilon')|\mathcal{A}_\mu|\overline{B}(v)\rangle = i\sqrt{2m_B 2m_{D^*}}\ {\epsilon'_\mu}^* h_{A_1}(1), \tag{142}$$

where ϵ' is the polarization of the D^*. Reference [409] introduces a new ratio of three-point correlators which directly gives $|h_{A_1}(1)|$:

$$\mathcal{R}_{A_1} = \frac{\langle D^*|\bar{c}\gamma_j\gamma_5 b|\overline{B}\rangle\ \langle\overline{B}|\bar{b}\gamma_j\gamma_5 c|D^*\rangle}{\langle D^*|\bar{c}\gamma_4 c|D^*\rangle\ \langle\overline{B}|\bar{b}\gamma_4 b|\overline{B}\rangle} = |h_{A_1}(1)|^2. \tag{143}$$

In reference [409] simulation data are obtained on MILC ensembles with three lattice spacings, $a \approx 0.15$, 0.12, and 0.09 fm, for 2, 4 or 3 different light-quark masses respectively. Results are then extrapolated to the physical, continuum/chiral, limit employing staggered χPT.

The D^* meson is not a stable particle in QCD and decays predominantly into a D plus a pion. Nevertheless, heavy-light meson χPT can be applied to extrapolate lattice simulation results for the $B \to D^* \ell\nu$ form factor to the physical light-quark mass. The D^* width is quite narrow, 0.096 MeV for the $D^{*\pm}(2010)$ and less than 2.1MeV for the $D^{*0}(2007)$, making this system much more stable and long lived than the ρ or the K^* systems. By coincidence the $D^* - D$ mass difference is close to the pion mass and this leads to the well known "cusp" in $\mathcal{R}_{A_1}$ just above the physical pion mass [410–412]. This cusp makes the chiral extrapolation sensitive to values used in the χPT formulas for the $D^*D\pi$ coupling $g_{D^*D\pi}$. The error budget in reference [409] includes a separate error of 0.9% coming from the uncertainty in $g_{D^*D\pi}$ in addition to general chiral extrapolation errors in order to take this sensitivity into account.

The final value presented in [409], $\mathcal{F}^{B\to D^*}(1) = h_{A_1}(1) = 0.921(13)(20)$, where the first error is statistical, and the second the sum of systematic errors added in quadrature, has a total error of 2.6%. This result is updated in reference [408] after increasing statistics and adding data from $a \approx 0.06$ fm lattices. The new value is

$$\mathcal{F}^{B\to D^*}(1) = 0.9017(51)(156), \tag{144}$$

with total errors reduced to 1.8%. The largest systematic uncertainty comes from discretization errors followed by effects of higher-order corrections in the chiral perturbation theory ansatz.

8.4.2 $B \to D$ decays

The only unquenched lattice result for the $B \to D\ell\nu$ form factor $\mathcal{G}^{B\to D}(1)$ at zero recoil appears in a conference proceeding by FNAL/MILC [413]. This calculation employs MILC $N_f = 2+1$ configurations at a single lattice spacing, again with Fermilab bottom and charm quarks and Asqtad light quarks. Three values of the light-quark mass are used and results extrapolated linearly to the chiral limit. The preliminary result is $\mathcal{G}^{B\to D}(1) = 1.074(18)(16)$. Work is underway by FNAL/MILC to investigate $B \to D^{(*)}\ell\nu$ at and away from the zero recoil point employing a large number of MILC ensembles at several lattice spacings and light-quark masses [414]. Going to finer lattice spacings will help reduce heavy-quark discretization errors, which are the largest uncertainty for $B \to D^*\ell\nu$.

Collaboration	Ref.	N_f	publication status	continuum extrapolation	chiral extrapolation	finite volume	renormalization	heavy-quark treatment	form factor	
FNAL/MILC 10	[408]	2+1	C†	★	○	★	○	✓	$\mathcal{F}^{B\to D^*}(1)$	0.9017(51)(87)(83)(89)(30)(33) ‡
FNAL/MILC 08	[409]	2+1	A	★	○	★	○	✓	$\mathcal{F}^{B\to D^*}(1)$	0.921(13)(8)(8)(14)(6)(3)(4)
FNAL/MILC 04A	[413]	2+1	C	■	■	○*	○†	✓	$\mathcal{G}^{B\to D}(1)$	1.074(18)(16)
FNAL/MILC 12A	[415]	2+1	A	○	○	★	○	✓	$R(D)$	0.316(12)(7)

† Update of FNAL/MILC 08 for CKM 2010.
‡ Value of $\mathcal{F}(1)$ presented in Ref. [408] includes 0.7% correction η_{EW}. This correction is unrelated to the lattice calculation and has been removed here.
* No explicit estimate of FV error, but expected to be small.
† No explicit estimate of perturbative truncation error in vector current renormalization factor, but expected to be small because of mostly-nonperturbative approach.

Table 29: Lattice results for the $B \to D^*\ell\nu$ and $B \to D\ell\nu$ semileptonic form factors.

8.4.3 $B \to D^{(*)}\tau\nu$ decays

Another interesting semileptonic process is $B \to D^{(*)}\tau\nu$. Here the mass of the outgoing charged lepton cannot be neglected in the decay rate formula, so that both vector and scalar form factors come into play. Recently Babar announced their first observations of the semileptonic decays of B mesons into third generation leptons at a rate in slight excess over SM expectations. Since the lepton mass is now large enough for the branching fraction $\mathcal{B}(B \to D\tau\nu)$ to be sensitive to the scalar form factor $f_0(q^2)$, this could be a hint for some New Physics scalar exchange contribution. Accurate SM predictions for the ratio

$$R(D^{(*)}) = \mathcal{B}(B \to D^{(*)}\tau\nu)/\mathcal{B}(B \to D^{(*)}\ell\nu) \qquad \text{with } \ell = e, \mu \tag{145}$$

have therefore become important and timely. FNAL/MILC has published the first unquenched lattice determination of $R(D)$ [415]. They use a subset of the MILC ensembles from the ongoing $B \to D\ell\nu$ semileptonic project [414], namely two light-quark masses each on $a \approx 0.12$ and 0.09 fm lattices, and find,

$$R(D) = 0.316(12)(7). \tag{146}$$

This SM prediction is about $\sim 1.7\sigma$ lower than the Babar measurement.

8.4.4 Ratios of B and B_s semileptonic decay form factors

In addition to $B \to D\ell\nu$ semileptonic decays there is also interest in $B_s \to D_s\ell\nu$ semileptonic decays. In particular, $[B_s \to D_s\ell\nu]/[B \to D\ell\nu]$ semileptonic form factor ratios can be used to obtain ratios of B_q meson $(q = d, s)$ fragmentation fractions, f_s/f_d. This latter ratio enters into LHCb's analysis of $B_s \to \mu^+\mu^-$ decays. There is now one unquenched calculation by FNAL/MILC of ratios of the scalar form factors $f_0^{(q)}(q^2)$ [416]:

$$f_0^{(s)}(M_\pi^2)/f_0^{(d)}(M_K^2) = 1.046(44)(15), \qquad f_0^{(s)}(M_\pi^2)/f_0^{(d)}(M_\pi^2) = 1.054(47)(17), \tag{147}$$

where the first error is statistical and the second systematic. These results lead to fragmentation fraction ratios f_s/f_d that are consistent with LHCb's measurements via other methods.

8.4.5 Summary

In Table 29 we summarize the existing results for the $B \to D^*\ell\nu$ and $B \to D\ell\nu$ form factors at zero recoil, $\mathcal{F}^{B\to D^*}(1)$ and $\mathcal{G}^{B\to D}(1)$, and for the ratio $R(D) = \mathcal{B}(B \to D\tau\nu)/\mathcal{B}(B \to Dl\nu)$. Further details of the lattice calculations are provided in Appendix B.6.4. Selecting those results that are published in refereed journals (or are straightforward updates thereof) and have no red tags, our averages for $\mathcal{F}^{B\to D^*}(1)$ and $R(D)$ are

$$N_f = 2+1: \quad \mathcal{F}^{B\to D^*} = 0.9017(51)(156), \quad R(D) = 0.316(12)(7). \tag{148}$$

8.5 Determination of $|V_{ub}|$

We now use the lattice-determined Standard-Model transition amplitudes for leptonic (Sec. 8.1) and semileptonic (Sec. 8.3) B-meson decays to obtain exclusive determinations of the CKM matrix element $|V_{ub}|$. The relevant formulae are Eqs. (104) and (124). Among leptonic channels the only input comes from $B \to \tau\nu_\tau$, since the rates for decays to e and μ have not yet been measured. In the semileptonic case we only consider $B \to \pi\ell\nu_\ell$ transitions (experimentally measured for $\ell = e, \mu$), since no theoretical prediction for hadronic effects in other $b \to u$ transitions is currently available that satisfies FLAG requirements for controlled systematics.

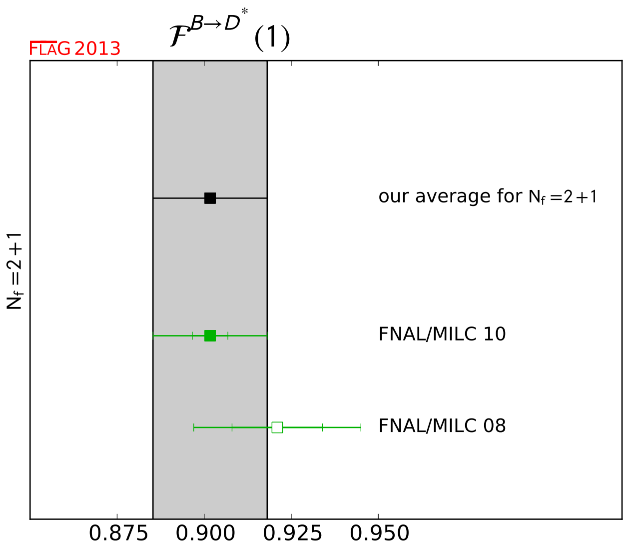

Figure 21: $B \to D^* \ell\nu$ semileptonic form factor at zero recoil [values in Table 29 and Eq. (148)].

The branching fraction for the decay $B \to \tau\nu_\tau$ has been measured by the Belle and Babar collaborations with both semileptonic [417, 418] and hadronic tagging [419, 420] methods. The uncertainties in these measurements are still dominated by statistical errors, and none of them individually are of 5σ significance. When combined, however, they cross the threshold needed to establish discovery of this mode. Until recently, the various largely-independent measurements have agreed well within errors. Earlier this year, however, the Belle collaboration published the single-most precise measurement of $B \to \tau\nu$ using the hadronic tagging method with an improved efficiency and the full dataset [420], and obtained a result which is more than 2σ below the previous average [74, 123]. The errors on the analogous measurement from Babar [419] are not competitive due to the smaller available data set, and the Babar result has not yet been published.

Both Belle and Babar quote averages of the hadronic and the semileptonic tagging modes that we can use to obtain $|V_{ub}|$. In the case of Belle, the average $BR(B^+ \to \tau^+\nu_\tau) = (0.96 \pm 0.26) \times 10^{-4}$ [420] includes slight correlations between systematics with the two tagging methods, but does not include a rescaling factor due to the fact that the hadronic and semileptonic measurements are inconsistent at the $\sim 1.5\sigma$ level. The Babar average $BR(B^+ \to \tau^+\nu_\tau) = (1.79 \pm 0.48) \times 10^{-4}$ [419] neglects correlations. By combining these values with the mean B^+-meson lifetime $\tau_{B^+} = 1.641(8)$ ps quoted by the PDG, and our averages $f_B = 197 \pm 10$ MeV ($N_f = 2$) and $f_B = 190.5 \pm 4.2$ MeV ($N_f = 2+1$) for the B-meson decay constants, we obtain

$$\begin{aligned}
\text{Belle } B \to \tau\nu_\tau : \quad & |V_{ub}| = 3.74(51)(19) \times 10^{-3}\,, \quad && N_f = 2\,, \\
\text{Belle } B \to \tau\nu_\tau : \quad & |V_{ub}| = 3.87(52)(9) \times 10^{-3}\,, \quad && N_f = 2+1\,; \\
\text{Babar } B \to \tau\nu_\tau : \quad & |V_{ub}| = 5.11(68)(26) \times 10^{-3}\,, \quad && N_f = 2\,, \\
\text{Babar } B \to \tau\nu_\tau : \quad & |V_{ub}| = 5.28(71)(12) \times 10^{-3}\,, \quad && N_f = 2+1\,.
\end{aligned} \tag{149}$$

where the first error comes from experiment and the second comes from the uncertainty in f_B. We can also average all four results for $BR(B^+ \to \tau^+\nu_\tau)$ from Belle and Babar. The measurements using hadronic and semileptonic tagging are statistically independent; further, because the measurements are dominated by statistical errors, the correlations between systematic errors in the two approaches can be reasonably neglected. We obtain $BR(B^+ \to \tau^+\nu_\tau) = (1.12 \pm 0.28) \times 10^{-4}$, where we have applied a $\sqrt{(\chi^2/\mathrm{d.o.f.})} \sim 1.3$ rescaling factor because the Belle hadronic tagging measurement differs significantly from the other three. Using this value for the branching fraction, and again combining with the $N_f = 2$ and $N_f = 2+1$ lattice-QCD averages for f_B from Eqs. (108) and (109), our preferred determinations of $|V_{ub}|$ from leptonic $B \to \tau\nu$ decay are

$$\begin{aligned} &\text{Belle + Babar } B \to \tau\nu_\tau : \quad && |V_{ub}| = 4.04(51)(21) \times 10^{-3}\,, \quad && N_f = 2\,, \\ &\text{Belle + Babar } B \to \tau\nu_\tau : \quad && |V_{ub}| = 4.18(52)(9) \times 10^{-3}\,, \quad && N_f = 2+1\,, \end{aligned} \tag{150}$$

where the errors are from experiment and from f_B, respectively.

In semileptonic decays, the experimental value of $|V_{ub}|f_+(q^2)$ can be extracted from the measured branching fractions of $B^0 \to \pi^-\ell^+\nu$ decays by applying Eq. (124); $|V_{ub}|$ can then be determined by performing fits to the constrained BCL z-parameterization of the form factor $f_+(q^2)$ given in Eq. (137). This can be done in two ways: one option is to perform separate fits to lattice (cf. Sec. 8.3) and experimental results, and extract the value of $|V_{ub}|$ from the ratio of the respective a_0 coefficients; a second option is to perform a simultaneous fit to lattice and experimental data, leaving their relative normalization $|V_{ub}|$ as a free parameter. We adopt the second strategy because it more optimally combines the lattice and experimental information and minimizes the uncertainty in $|V_{ub}|$. As experimental input we take the latest untagged 12-bin Babar data [421] and 13-bin Belle data [422], and we assume no correlation between experimental and lattice data. As in the fit to lattice data only in Sec. 8.3, we assume that the statistics plus chiral-extrapolation errors are 100% correlated between the FNAL/MILC 08A and HPQCD 06 data, and we reduce the correlations in the FNAL/MILC data by keeping only every second data point.

Figure 22 shows both the lattice and experimental data for $(1 - q^2/m^2_{B^*})f_+(q^2)$ versus z. For illustration, the experimental data are divided by the value of $|V_{ub}|$ obtained from the preferred fit. Both the lattice-QCD and experimental data are linear and display no visible signs of curvature; further, the slopes of the lattice and experimental data sets appear consistent. A simple three-parameter constrained BCL fit (*i.e.* through $\mathcal{O}(z^2)$ plus $|V_{ub}|$) is sufficient to describe the combined data sets with a good $\chi^2/\mathrm{d.o.f.}$, however, the addition of the experimental points enables a better determination of higher-order terms in the z-expansion than from the lattice-only fit. In order to address the potential systematic uncertainty due to truncating the series in z, we continue to add terms to the fit until the result for $|V_{ub}|$ stabilizes, *i.e.* the central value settles and the errors stop increasing. We find that this happens at $\mathcal{O}(z^3)$, and take the value of $|V_{ub}|$ from this combined fit of the lattice-QCD and experimental data as our preferred result:

$$\begin{aligned} &\text{global lattice + Babar:} \quad && |V_{ub}| = 3.37(21) \times 10^{-3}\,, \quad && N_f = 2+1\,, \\ &\text{global lattice + Belle:} \quad && |V_{ub}| = 3.47(22) \times 10^{-3}\,, \quad && N_f = 2+1\,. \end{aligned} \tag{151}$$

We do not quote a result for a combined lattice + Babar + Belle fit, since we are unable to properly take into account possible correlations between experimental results. Again, we emphasize the importance of publishing statistical and systematic correlation matrices in future lattice-QCD work on semileptonic form factors, so that the lattice results can be fully used to obtain CKM matrix elements and for other phenomenological applications.

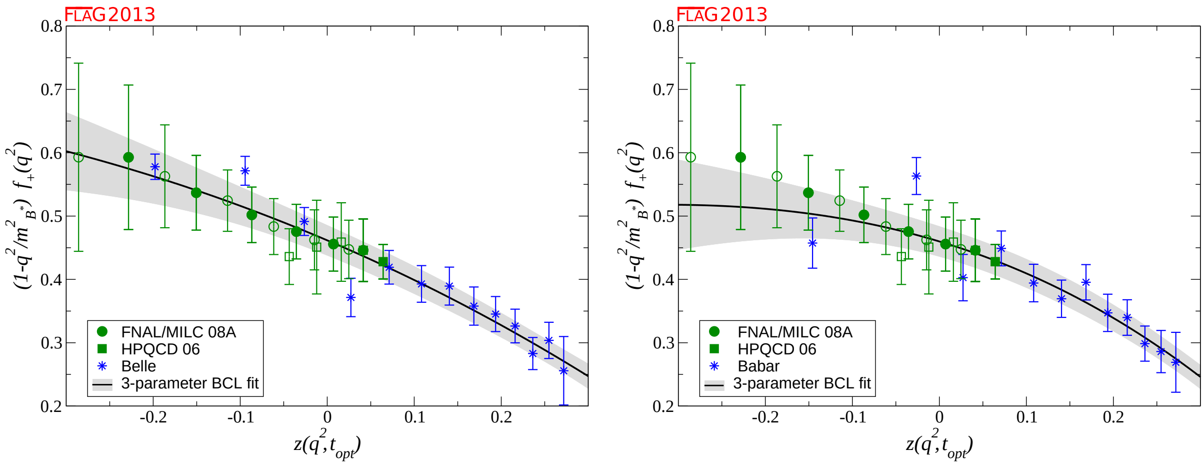

Figure 22: Lattice and experimental data for $(1 - q^2/m_{B^*}^2)f_+(q^2)$ versus z. The filled green symbols denote lattice-QCD points included in the fit, while the open green symbols show those that are not included in the fit (either because of unknown correlations or strong correlations). The blue stars show the experimental data divided by the value of $|V_{ub}|$ obtained from the fit. The grey band in the left (right) plots shows the preferred three-parameter BCL fit to the lattice-QCD and Belle (Babar) data with errors.

Our results for $|V_{ub}|$ are summarized in Table 30 and Figure 23, where we also show the inclusive determinations from HFAG for comparison. The spread of values for $|V_{ub}|$ does not yield a clear picture. We observe the well-known $\sim 3\sigma$ tension between determinations of $|V_{ub}|$ from exclusive and inclusive semileptonic decays. The determination of $|V_{ub}|$ from leptonic $B \to \tau\nu$ decay lies in between the inclusive and exclusive determinations, but the experimental errors in $\text{BR}(B \to \tau\nu)$ are so large that it agrees with both within $\sim 1.5\sigma$. If, however, we consider separately the different experimental measurements of $\text{BR}(B \to \tau\nu)$, the Belle measurement from hadronic tagging leads to a value of $|V_{ub}|$ that agrees well with the one from exclusive $B \to \pi\ell\nu$ decay, while the remaining Belle and Babar measurements lead to values of $|V_{ub}|$ that are larger than both the latter and inclusive determinations. The exclusive determination of $|V_{ub}|$ will improve in the next few years with better lattice-QCD calculations of the $B \to \pi\ell\nu$ form factor, while the improvement in $|V_{ub}|$ from $B \to \tau\nu$ decays will have to wait longer for the Belle II experiment, which aims to begin running in 2016, to collect a larger data set than is currently available.

8.6 Determination of $|V_{cb}|$

We now interpret the lattice-QCD results for the $B \to D^{(*)}\ell\nu$ form factors as determinations of the CKM matrix element $|V_{cb}|$ in the Standard Model.

For the experimental branching fractions at zero recoil, we use the latest experimental

	from	$\lvert V_{ub}\rvert \times 10^3$
our result for $N_f = 2$	$B \to \tau\nu$	4.04(51)(21)
our result for $N_f = 2+1$	$B \to \tau\nu$	4.18(52)(9)
our result for $N_f = 2+1$	$B \to \pi\ell\nu$ (Babar)	3.37(21)
our result for $N_f = 2+1$	$B \to \pi\ell\nu$ (Belle)	3.47(22)
Bauer 01 [423]	$B \to X_u\ell\nu$	4.62(20)(29)
Lange 05 [424]	$B \to X_u\ell\nu$	$4.40(15)(^{+19}_{-21})$
Andersen 05 [425], Gardi 08 [426]	$B \to X_u\ell\nu$	$4.45(15)(^{+15}_{-16})$
Gambino 07 [427]	$B \to X_u\ell\nu$	$4.39(15)(^{+12}_{-14})$
Aglietti 07 [428]	$B \to X_u\ell\nu$	$4.03(13)(^{+18}_{-12})$
HFAG inclusive average [123]	$B \to X_u\ell\nu$	4.40(15)(20)

Table 30: Comparison of exclusive determinations of $|V_{ub}|$ (upper panel) and inclusive determinations (lower panel). For $B \to \tau\nu$, the two uncertainties shown come from experiment (plus non-lattice theory) and from the lattice calculation, respectively. Each inclusive determination corresponds to a different theoretical treatment of the same experimental partial branching fractions compiled by the Heavy Flavor Averaging Group [429]; the errors shown are experimental and theoretical, respectively.

averages from the Heavy Flavor Averaging Group [123]:[33]

$$\mathcal{F}^{B\to D^*}(1)\eta_{\rm EW}|V_{cb}| = 35.90(45)\,, \qquad \mathcal{G}^{B\to D}(1)\eta_{EW}|V_{cb}| = 42.64(1.53)\,. \tag{152}$$

For $\mathcal{F}^{B\to D^*}(1)$, there is only a single $N_f = 2+1$ lattice-QCD calculation that satisfies the FLAG criteria, while there is no such calculation of $\mathcal{G}^{B\to D}(1)$. Using the result given in Eq. (148), we obtain our preferred value for $|V_{cb}|$:

$$B \to D^*\ell\nu: \quad |V_{cb}| = 39.55(72)(50)\times 10^{-3}\,, \qquad N_f = 2+1 \tag{153}$$

where the errors shown are from the lattice calculation and experiment (plus non-lattice theory), respectively. Table 31 compares the determination of $|V_{cb}|$ from exclusive $B \to D^*\ell\nu$ decays to that from inclusive $B \to X_c\ell\nu$ decays, where X_c denotes all possible charmed hadronic final states. The results, also shown in Fig. 23, differ by approximately 2.3σ. The exclusive determination of $|V_{cb}|$ will improve significantly over the next year or two with new lattice-QCD calculations of the $B \to D^{(*)}\ell\nu$ form factors at nonzero recoil.

[33] We note that HFAG currently averages results for neutral and charged B meson decays without first removing the correction due to the Coulomb attraction between the charged final-state particles for the neutral B meson decays.

	Ref.	from	$\|V_{cb}\| \times 10^3$
our average for $N_f = 2+1$	[408]	$B \to D^* \ell \nu$	39.55(72)(50)
Inclusive (Gambino 13)	[430]	$B \to X_c \ell \nu$	42.42(86)

Table 31: Determinations of $|V_{cb}|$ obtained from semileptonic B decay. The errors shown in the first row indicate those from lattice and experimental (plus non-lattice theory) uncertainties, respectively, while the error shown in the second row is the total (experimental plus theoretical) uncertainty.

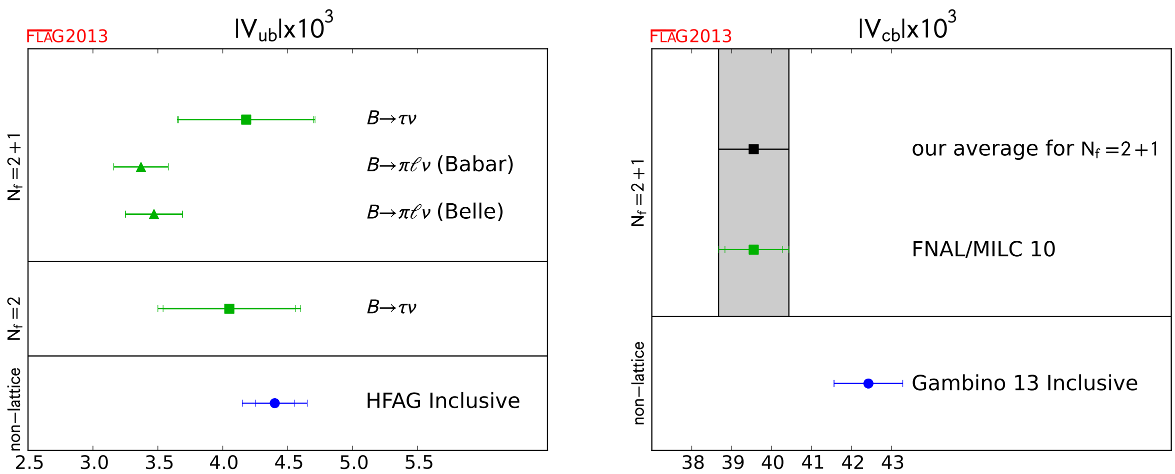

Figure 23: Comparison of the results for $|V_{ub}|$ and $|V_{cb}|$ obtained from lattice methods with non-lattice determinations based on inclusive semileptonic B decays. In the left plot, the results denoted by squares are from leptonic decays, while those denoted by triangles are from semileptonic decays. The grey band indicates our $N_f = 2+1$ average.

Acknowledgments

We wish to thank Nuria Carrasco, Christine Davies, Rachel Dowdall, Petros Dimopoulos, Jochen Dingfelder, Elvira Gamiz, Andreas Kronfeld, Peter Lepage, Heechang Na, Jim Simone, Doug Toussaint for correspondence and useful comments. C.P. acknowledges the support of the Spanish MICINN under grant FPA2009-08785, the Spanish MINECO under grant FPA2012-31686 and the "Centro de excelencia Severo Ochoa Program" SEV-2012-0249, the Community of Madrid under grant HEPHACOS S2009/ESP-1473, and the European Union under the Marie Curie-ITN Program STRONGnet, grant PITN-GA-2009-238353. A.X.K. thanks the Fermilab theory group for hospitality while this review was finalized. The Albert Einstein Center for Fundamental Physics at the University of Bern is supported by the "Innovations- und Kooperationsprojekt C-13" of the "Schweizerische Universitätskonferenz SUK/CRUS". Fermilab is operated by Fermi Research Alliance, LLC, under Contract No. DE-AC02-07CH11359 with the U.S. Department of Energy. This work was partially supported by Grant-in-Aid for Scientific Research (25287046) and SPIRE (Strategic Program for Innovative Research) of MEXT, Japan, by the JSPS Kakenhi Grant, No. 22224003, by MIUR (Italy) under the contract PRIN 2010-2011, by the US Department of Energy under grant numbers DE-FG02-91ER40628, DE-FG02-92ER40716, DOE DE-FG02-13ER42001, DE-FG02-96ER40956, by the OCEVU Labex (ANR-11-LABX-0060) and the A*MIDEX project (ANR-11-IDEX-0001-02) funded by the "Investissements d'Avenir" French government program managed by the ANR, by UK STFC grant ST/G000557/1, by the Helmholtz Association through the virtual institute "Spin and strong QCD" (VH-VI-231), by the Swiss National Science Foundation, by the Spanish Minister of Education and Science, project RyC-2011-08557 and by a URA Visiting Scholarship. The research leading to these results has also received funding from the European Research Council under the European Community's Seventh Framework Programme (FP7/2007-2013) ERC grant agreement No 279757.

A Glossary

A.1 Lattice actions

In this appendix we give brief descriptions of the lattice actions used in the simulations and summarize their main features.

A.1.1 Gauge actions

The simplest and most widely used discretization of the Yang-Mills part of the QCD action is the Wilson plaquette action [431]:

$$S_{\rm G} = \beta \sum_x \sum_{\mu<\nu} \Big(1 - \tfrac{1}{3}{\rm Re\ Tr}\, W_{\mu\nu}^{1\times 1}(x)\Big), \tag{154}$$

where $\beta \equiv 6/g_0^2$ (with g_0 the bare gauge coupling) and the plaquette $W_{\mu\nu}^{1\times1}(x)$ is the product of link variables around an elementary square of the lattice, i.e.

$$W_{\mu\nu}^{1\times1}(x) \equiv U_\mu(x)U_\nu(x+a\hat{\mu})U_\mu(x+a\hat{\nu})^{-1}U_\nu(x)^{-1}. \tag{155}$$

This expression reproduces the Euclidean Yang-Mills action in the continuum up to corrections of order a^2. There is a general formalism, known as the "Symanzik improvement programme" [9, 10], which is designed to cancel the leading lattice artifacts, such that observables have an accelerated rate of convergence to the continuum limit. The improvement programme is implemented by adding higher-dimensional operators, whose coefficients must be tuned appropriately in order to cancel the leading lattice artifacts. The effectiveness of this procedure depends largely on the method with which the coefficients are determined. The most widely applied methods (in ascending order of effectiveness) include perturbation theory, tadpole-improved (partially resummed) perturbation theory, renormalization group methods, and the nonperturbative evaluation of improvement conditions.

In the case of Yang-Mills theory, the simplest version of an improved lattice action is obtained by adding rectangular 1×2 loops to the plaquette action, i.e.

$$S_{\rm G}^{\rm imp} = \beta \sum_x \left\{ c_0 \sum_{\mu<\nu} \Big(1 - \tfrac{1}{3}{\rm Re\ Tr}\, W_{\mu\nu}^{1\times1}(x)\Big) + c_1 \sum_{\mu,\nu} \Big(1 - \tfrac{1}{3}{\rm Re\ Tr}\, W_{\mu\nu}^{1\times2}(x)\Big) \right\}, \tag{156}$$

where the coefficients c_0, c_1 satisfy the normalization condition $c_0 + 8c_1 = 1$. The *Symanzik-improved* [432], *Iwasaki* [433], and *DBW2* [434, 435] actions are all defined through eq. (156) via particular choices for c_0, c_1. Details are listed in Table 32 together with the abbreviations used in the summary tables.

Abbrev.	c_1	Description
Wilson	0	Wilson plaquette action
tlSym	$-1/12$	tree-level Symanzik-improved gauge action
tadSym	variable	tadpole Symanzik-improved gauge action
Iwasaki	-0.331	Renormalization group improved (“Iwasaki”) action
DBW2	-1.4088	Renormalization group improved (“DBW2”) action

Table 32: Summary of lattice gauge actions. The leading lattice artifacts are $O(a^2)$ or better for all discretizations.

A.1.2 Light-quark actions

If one attempts to discretize the quark action, one is faced with the fermion doubling problem: the naive lattice transcription produces a 16-fold degeneracy of the fermion spectrum.

Wilson fermions

Wilson's solution to the fermion doubling problem is based on adding a dimension-5 (irrelevant) operator to the lattice action. The Wilson-Dirac operator for the massless case reads [431, 436]

$$D_{\mathrm{w}} = \frac{1}{2}\gamma_\mu(\nabla_\mu + \nabla^*_\mu) + a\nabla^*_\mu\nabla_\mu, \tag{157}$$

where ∇_μ, ∇^*_μ denote the covariant forward and backward lattice derivatives, respectively. The addition of the Wilson term $a\nabla^*_\mu\nabla_\mu$, results in fermion doublers acquiring a mass proportional to the inverse lattice spacing; close to the continuum limit these extra degrees of freedom are removed from the low-energy spectrum. However, the Wilson term also results in an explicit breaking of chiral symmetry even at zero bare quark mass. Consequently, it also generates divergences proportional to the UV cutoff (inverse lattice spacing), besides the usual logarithmic ones. Therefore the chiral limit of the regularized theory is not defined simply by the vanishing of the bare quark mass but must be appropriately tuned. As a consequence quark mass renormalization requires a power subtraction on top of the standard multiplicative logarithmic renormalization. The breaking of chiral symmetry also implies that the nonrenormalization theorem has to be applied with care [437, 438], resulting in a normalization factor for the axial current which is a regular function of the bare coupling. On the other hand, vector symmetry is unaffected by the Wilson term and thus a lattice (point split) vector current is conserved and obeys the usual nonrenormalization theorem with a trivial (unity) normalization factor. Thus, compared to lattice fermion actions which preserve chiral symmetry, or a subgroup of it, the Wilson regularization typically results in more complicated renormalization patterns.

Furthermore, the leading order lattice artifacts are of order a. With the help of the Symanzik improvement programme, the leading artifacts can be cancelled in the action by adding the so-called "Clover" or Sheikholeslami-Wohlert (SW) term [439]. The resulting expression in the massless case reads

$$D_{\mathrm{sw}} = D_{\mathrm{w}} + \tfrac{ia}{4}\, c_{\mathrm{sw}}\sigma_{\mu\nu}\widehat{F}_{\mu\nu}, \tag{158}$$

where $\sigma_{\mu\nu} = \frac{i}{2}[\gamma_\mu, \gamma_\nu]$, and $\widehat{F}_{\mu\nu}$ is a lattice transcription of the gluon field strength tensor $F_{\mu\nu}$. The coefficient c_{sw} can be determined perturbatively at tree-level ($c_{\mathrm{sw}} = 1$; tree-level improvement or tlSW for short), via a mean field approach [440] (mean-field improvement or mfSW) or via a nonperturbative approach [441] (nonperturbatively improved or npSW). Hadron masses, computed using D_{sw}, with the coefficient c_{sw} determined nonperturbatively, will approach the continuum limit with a rate proportional to a^2; with tlSW for c_{sw} the rate is proportional to $g_0^2 a$.

Other observables require additional improvement coefficients [439]. A common example consists in the computation of the matrix element $\langle\alpha|Q|\beta\rangle$ of a composite field Q of dimension-d with external states $|\alpha\rangle$ and $|\beta\rangle$. In the simplest cases, the above bare matrix element diverges logarithmically and a single renormalization parameter Z_Q is adequate to render it finite. It then approaches the continuum limit with a rate proportional to the lattice spacing a, even when the lattice action contains the Clover term. In order to reduce discretization errors to $\mathcal{O}(a^2)$, the lattice definition of the composite operator Q must be modified (or "improved"), by the addition of all dimension-$(d+1)$ operators with the same lattice symmetries as Q. Each of these terms is accompanied by a coefficient which must be tuned in a way analogous to that of $c_{\rm sw}$. Once these coefficients are determined nonperturbatively, the renormalized matrix element of the improved operator, computed with a npSW action, converges to the continuum limit with a rate proportional to a^2. A tlSW improvement of these coefficients and $c_{\rm sw}$ will result in a rate proportional to $g_0^2 a$.

It is important to stress that the improvement procedure does not affect the chiral properties of Wilson fermions; chiral symmetry remains broken.

Finally, we mention "twisted-mass QCD" as a method which was originally designed to address another problem of Wilson's discretization: the Wilson-Dirac operator is not protected against the occurrence of unphysical zero modes, which manifest themselves as "exceptional" configurations. They occur with a certain frequency in numerical simulations with Wilson quarks and can lead to strong statistical fluctuations. The problem can be cured by introducing a so-called "chirally twisted" mass term. The most common formulation applies to a flavour doublet $\bar{\psi} = (u \quad d)$ of mass degenerate quarks, with the fermionic part of the QCD action in the continuum assuming the form [296]

$$S_{\rm F}^{\rm tm;cont} = \int d^4x\, \overline{\psi}(x)(\gamma_\mu D_\mu + m + i\mu_{\rm q}\gamma_5\tau^3)\psi(x). \tag{159}$$

Here, $\mu_{\rm q}$ is the twisted mass parameter, and τ^3 is a Pauli matrix in flavour space. The standard action in the continuum can be recovered via a global chiral field rotation. The physical quark mass is obtained as a function of the two mass parameters m and $\mu_{\rm q}$. The corresponding lattice regularization of twisted-mass QCD (tmWil) for $N_f = 2$ flavours is defined through the fermion matrix

$$D_{\rm w} + m_0 + i\mu_{\rm q}\gamma_5\tau^3 \ . \tag{160}$$

Although this formulation breaks physical parity and flavour symmetries, resulting in non-degenerate neutral and charged pions, is has a number of advantages over standard Wilson fermions. Firstly, the presence of the twisted mass parameter $\mu_{\rm q}$ protects the discretized theory against unphysical zero modes. A second attractive feature of twisted-mass lattice QCD is the fact that, once the bare mass parameter m_0 is tuned to its "critical value" (corresponding to massless pions in the standard Wilson formulation), the leading lattice artifacts are of order a^2 without the need to add the Sheikholeslami-Wohlert term in the action, or other improving coefficients [442]. A third important advantage is that, although the problem of explicit chiral symmetry breaking remains, quantities computed with twisted fermions with a suitable tuning of the mass parameter $\mu_{\rm q}$, are subject to renormalization patterns which are simpler than the ones with standard Wilson fermions. Well known examples are the pseudoscalar decay constant and $B_{\rm K}$.

Staggered Fermions

An alternative procedure to deal with the doubling problem is based on so-called "staggered" or Kogut-Susskind fermions [443–446]. Here the degeneracy is only lifted partially, from 16 down to 4. It has become customary to refer to these residual doublers as "tastes" in order to distinguish them from physical flavours. Taste changing interactions can occur via the exchange of gluons with one or more components of momentum near the cutoff π/a. This leads to the breaking of the SU(4) vector symmetry among tastes, thereby generating order a^2 lattice artifacts.

The residual doubling of staggered quarks (four tastes per flavour) is removed by taking a fractional power of the fermion determinant [447] — the "fourth-root procedure," or, sometimes, the "fourth root trick." This procedure would be unproblematic if the action had full SU(4) taste symmetry, which would give a Dirac operator that was block-diagonal in taste space. However, the breaking of taste symmetry at nonzero lattice spacing leads to a variety of problems. In fact, the fourth root of the determinant is not equivalent to the determinant of any local lattice Dirac operator [448]. This in turn leads to violations of unitarity on the lattice [449–452].

According to standard renormalization group lore, the taste violations, which are associated with lattice operators of dimension greater than four, might be expected go away in the continuum limit, resulting in the restoration of locality and unitarity. However, there is a problem with applying the standard lore to this nonstandard situation: the usual renormalization group reasoning assumes that the lattice action is local. Nevertheless, Shamir [453, 454] shows that one may apply the renormalization group to a "nearby" local theory, and thereby gives a strong argument that that the desired local, unitary theory of QCD is reproduced by the rooted staggered lattice theory in the continuum limit.

A version of chiral perturbation that includes the lattice artifacts due to taste violations and rooting ("rooted staggered chiral perturbation theory") can also be worked out [455–457] and shown to correctly describe the unitarity-violating lattice artifacts in the pion sector [450, 458]. This provides additional evidence that the desired continuum limit can be obtained. Further, it gives a practical method for removing the lattice artifacts from simulation results. Versions of rooted staggered chiral perturbation theory exist for heavy-light mesons with staggered light quarks but nonstaggered heavy quarks [459], heavy-light mesons with staggered light and heavy quarks [460, 461], staggered baryons [462], and mixed actions with a staggered sea [302, 463], as well as the pion-only version referenced above.

There is also considerable numerical evidence that the rooting procedure works as desired. This includes investigations in the Schwinger model [464–466], studies of the eigenvalues of the Dirac operator in QCD [467–470], and evidence for taste restoration in the pion spectrum as $a \to 0$ [15, 36].

Issues with the rooting procedure have led Creutz [471–477] to argue that the continuum limit of the rooted staggered theory cannot be QCD. These objections have however been answered in Refs. [12–14, 470, 478–481]. In particular, a claim that the continuum 't Hooft vertex [482, 483] could not be properly reproduced by the rooted theory has been refuted [470, 479].

Overall, despite the lack of rigorous proof of the correctness of the rooting procedure, we think the evidence is strong enough to consider staggered QCD simulations on a par with simulations using other actions. See the following reviews for further evidence and discussion: [11–15].

Improved Staggered Fermions

An improvement program can be used to suppress taste-changing interactions, leading to "improved staggered fermions," with the so-called "Asqtad" [484], "HISQ" [485], "Stout-smeared" [486], and "HYP" [487] actions as the most common versions. All these actions smear the gauge links in order to reduce the coupling of high-momentum gluons to the quarks, with the main goal of decreasing taste-violating interactions. In the Asqtad case, this is accomplished by replacing the gluon links in the derivatives by averages over 1-, 3-, 5-, and 7-link paths. The other actions reduce taste changing even further by smearing more. In addition to the smearing, the Asqtad and HISQ actions include a three-hop term in the action (the "Naik term" [488]) to remove order a^2 errors in the dispersion relation, as well as a "Lepage term" [489] to cancel other order a^2 artifacts introduced by the smearing. In both the Asqtad and HISQ actions, the leading taste violations are of order $\alpha_S^2 a^2$, and "generic" lattices artifacts (those associated with discretization errors other than taste violations) are of order $\alpha_S a^2$. The overall coefficients of these errors are, however, significantly smaller with HISQ than with Asqtad. With the Stout-smeared and HYP actions, the errors are formally larger (order $\alpha_S a^2$ for taste violations and order a^2 for generic lattices artifacts). Nevertheless, the smearing seems to be very efficient, and the actual size of errors at accessible lattice spacings appears to be at least as small as with HISQ.

Although logically distinct from the light-quark improvement program for these actions, it is customary with the HISQ action to include an additional correction designed to reduce discretization errors for heavy quarks (in practice, usually charm quarks) [485]. The Naik term is adjusted to remove leading $(am_c)^4$ and $\alpha_S(am_c)^2$ errors, where m_c is the charm quark mass and "leading" in this context means leading in powers of the heavy-quark velocity v ($v/c \sim 1/3$ for D_s). With these improvements, the claim is that one can use the staggered action for charm quarks, although it must be emphasized that it is not obvious *a priori* how large a value of am_c may be tolerated for a given desired accuracy, and this must be studied in the simulations.

Ginsparg-Wilson fermions

Fermionic lattice actions, which do not suffer from the doubling problem whilst preserving chiral symmetry go under the name of "Ginsparg-Wilson fermions". In the continuum the massless Dirac operator (D) anti-commutes with γ_5. At nonzero lattice spacing a chiral symmetry can be realized if this condition is relaxed to [490–492]

$$\{D, \gamma_5\} = aD\gamma_5 D, \tag{161}$$

which is now known as the Ginsparg-Wilson relation [298]. The Nielsen-Ninomiya theorem [493], which states that any lattice formulation for which D anticommutes with γ_5 necessarily has doubler fermions, is circumvented since $\{D, \gamma_5\} \neq 0$.

A lattice Dirac operator which satisfies eq. (161) can be constructed in several ways. The so-called "overlap" or Neuberger-Dirac operator [494] acts in four space-time dimensions and is, in its simplest form, defined by

$$D_{\rm N} = \frac{1}{\overline{a}}\left(1 - \epsilon(A)\right), \quad \text{where} \quad \epsilon(A) \equiv A(A^\dagger A)^{-1/2}, \quad A = 1 + s - aD_{\rm w}, \quad \overline{a} = \frac{a}{1+s}, \tag{162}$$

$D_{\rm w}$ is the massless Wilson-Dirac operator and $|s| < 1$ is a tunable parameter. The overlap operator $D_{\rm N}$ removes all doublers from the spectrum, and can readily be shown to satisfy the Ginsparg-Wilson relation. The occurrence of the sign function $\epsilon(A)$ in $D_{\rm N}$ renders the application of $D_{\rm N}$ in a computer program potentially very costly, since it must be implemented using, for instance, a polynomial approximation.

The most widely used approach to satisfying the Ginsparg-Wilson relation eq. (161) in large-scale numerical simulations is provided by *Domain Wall Fermions* (DWF) [495–497] and we therefore describe this in some more detail. Following early exploratory studies [498]. this approach has been developed into a practical formulation of lattice QCD with good chiral and flavour symmetries leading to results which contribute significantly to this review. In this formulation, the fermion fields $\psi(x,s)$ depend on a discrete fifth coordinate $s=1,N$ as well as the physical 4-dimensional space-time coordinates x_μ, $\mu=1\cdots 4$ (the gluon fields do not depend on s). The lattice on which the simulations are performed, is therefore a five-dimensional one of size $L^3\times T\times N$, where L, T and N represent the number of points in the spatial, temporal and fifth dimensions respectively. The remarkable feature of DWF is that for each flavour there exists a physical light mode corresponding to the field $q(x)$:

$$q(x) \;=\; \tfrac{1+\gamma^5}{2}\psi(x,1)+\tfrac{1-\gamma^5}{2}\psi(x,N) \tag{163}$$

$$\bar{q}(x) \;=\; \overline{\psi}(x,N)\tfrac{1+\gamma^5}{2}+\overline{\psi}(x,1)\tfrac{1-\gamma^5}{2}\,. \tag{164}$$

The left and right-handed modes of the physical field are located on opposite boundaries in the 5th dimensional space which, for $N\to\infty$, allows for independent transformations of the left and right components of the quark fields, that is for chiral transformations. Unlike Wilson fermions, where for each flavour the quark mass parameter in the action is fine-tuned requiring a subtraction of contributions of $O(1/a)$ where a is the lattice spacing, with DWF no such subtraction is necessary for the physical modes, whereas the unphysical modes have masses of $O(1/a)$ and decouple.

In actual simulations N is finite and there are small violations of chiral symmetry which must be accounted for. The theoretical framework for the study of the residual breaking of chiral symmetry has been a subject of intensive investigation (for a review and references to the original literature see e.g. [499]). The breaking requires one or more *crossings* of the fifth dimension to couple the left and right-handed modes; the more crossings that are required the smaller the effect. For many physical quantities the leading effects of chiral symmetry breaking due to finite N are parameterized by a *residual* mass, $m_{\rm res}$. For example, the PCAC relation (for degenerate quarks of mass m) $\partial_\mu A_\mu(x)=2mP(x)$, where A_μ and P represent the axial current and pseudoscalar density respectively, is satisfied with $m=m^{\rm DWF}+m_{\rm res}$, where $m^{\rm DWF}$ is the bare mass in the DWF action. The mixing of operators which transform under different representations of chiral symmetry is found to be negligibly small in current simulations. The important thing to note is that the chiral symmetry breaking effects are small and that there are techniques to mitigate their consequences.

The main price which has to be paid for the good chiral symmetry is that the simulations are performed in 5 dimensions, requiring approximately a factor of N in computing resources and resulting in practice in ensembles at fewer values of the lattice spacing and quark masses than is possible with other formulations. The current generation of DWF simulations is being performed at physical quark masses so that ensembles with good chiral and flavour symmetries are being generated and analysed [25]. For a discussion of the equivalence of DWF and overlap fermions see [500, 501].

A third example of an operator which satisfies the Ginsparg-Wilson relation is the so-called fixed-point action [502–504]. This construction proceeds via a renormalization group approach. A related formalism are the so-called “chirally improved” fermions [505].

Abbrev.	Discretization	Leading lattice artifacts	Chiral symmetry	Remarks
Wilson	Wilson	$O(a)$	broken	
tmWil	twisted-mass Wilson	$O(a^2)$ at maximal twist	broken	flavour symmetry breaking: $(M_{\rm PS}^0)^2 - (M_{\rm PS}^{\pm})^2 \sim O(a^2)$
tlSW	Sheikholeslami-Wohlert	$O(g^2 a)$	broken	tree-level impr., $c_{\rm sw} = 1$
n-HYP tlSW	Sheikholeslami-Wohlert	$O(g^2 a)$	broken	tree-level impr., $c_{\rm sw} = 1$, n-HYP smeared gauge links
stout tlSW	Sheikholeslami-Wohlert	$O(g^2 a)$	broken	tree-level impr., $c_{\rm sw} = 1$, stout smeared gauge links
HEX tlSW	Sheikholeslami-Wohlert	$O(g^2 a)$	broken	tree-level impr., $c_{\rm sw} = 1$, HEX smeared gauge links
mfSW	Sheikholeslami-Wohlert	$O(g^2 a)$	broken	mean-field impr.
npSW	Sheikholeslami-Wohlert	$O(a^2)$	broken	nonperturbatively impr.
KS	Staggered	$O(a^2)$	$\mathrm{U}(1) \otimes \mathrm{U}(1)$ subgr. unbroken	rooting for $N_f < 4$
Asqtad	Staggered	$O(a^2)$	$\mathrm{U}(1) \otimes \mathrm{U}(1)$ subgr. unbroken	Asqtad smeared gauge links, rooting for $N_f < 4$
HISQ	Staggered	$O(a^2)$	$\mathrm{U}(1) \otimes \mathrm{U}(1)$ subgr. unbroken	HISQ smeared gauge links, rooting for $N_f < 4$
DW	Domain Wall	asymptotically $O(a^2)$	remnant breaking exponentially suppr.	exact chiral symmetry and $O(a)$ impr. only in the limit $L_s \to \infty$
overlap	Neuberger	$O(a^2)$	exact	

Table 33: The most widely used discretizations of the quark action and some of their properties. Note that in order to maintain the leading lattice artifacts of the action in nonspectral observables (like operator matrix elements) the corresponding nonspectral operators need to be improved as well.

Smearing

A simple modification which can help improve the action as well as the computational performance is the use of smeared gauge fields in the covariant derivatives of the fermionic action. Any smearing procedure is acceptable as long as it consists of only adding irrelevant (local) operators. Moreover, it can be combined with any discretization of the quark action. The "Asqtad" staggered quark action mentioned above [484] is an example which makes use of so-called "Asqtad" smeared (or "fat") links. Another example is the use of n-HYP smeared [487, 506], stout smeared [507, 508] or HEX (hypercubic stout) smeared [509] gauge links in the tree-level clover improved discretization of the quark action, denoted by "n-HYP tlSW", "stout tlSW" and "HEX tlSW" in the following.

In Table 33 we summarize the most widely used discretizations of the quark action and their main properties together with the abbreviations used in the summary tables. Note that in order to maintain the leading lattice artifacts of the actions as given in the table in nonspectral observables (like operator matrix elements) the corresponding nonspectral operators need to be improved as well.

A.1.3 Heavy-quark actions

Charm and bottom quarks are often simulated with different lattice-quark actions than up, down, and strange quarks because their masses are large relative to typical lattice spacings in current simulations; for example, $am_c \sim 0.4$ and $am_b \sim 1.3$ at $a = 0.06$ fm. Therefore, for the actions described in the previous section, using a sufficiently small lattice spacing to control generic $(am_h)^n$ discretization errors is computationally costly, and in fact prohibitive at the physical b-quark mass.

One approach for lattice heavy quarks is direct application of effective theory. In this case the lattice heavy-quark action only correctly describes phenomena in a specific kinematic regime, such as Heavy-Quark Effective Theory (HQET) [510–512] or Nonrelativistic QCD (NRQCD) [513, 514]. One can discretize the effective Lagrangian to obtain, for example, Lattice HQET [515] or Lattice NRQCD [516, 517], and then simulate the effective theory numerically. The coefficients of the operators in the lattice-HQET and lattice-NRQCD actions are free parameters that must be determined by matching to the underlying theory (QCD) through the chosen order in $1/m_h$ or v_h^2, where m_h is the heavy-quark mass and v_h is the heavy-quark velocity in the the heavy-light meson rest frame.

Another approach is to interpret a relativistic quark action such as those described in the previous section in a manner suitable for heavy quarks. One can extend the standard Symanzik improvement program, which allows one to systematically remove lattice cutoff effects by adding higher-dimension operators to the action, by allowing the coefficients of the dimension 4 and higher operators to depend explicitly upon the heavy-quark mass. Different prescriptions for tuning the parameters correspond to different implementations: those in common use are often called the Fermilab action [518], the relativistic heavy-quark action (RHQ) [519], and the Tsukuba formulation [520]. In the Fermilab approach, HQET is used to match the lattice theory to continuum QCD at the desired order in $1/m_h$.

More generally, effective theory can be used to estimate the size of cutoff errors from the various lattice heavy-quark actions. The power counting for the sizes of operators with heavy quarks depends on the typical momenta of the heavy quarks in the system. Bound-state dynamics differ considerably between heavy-heavy and heavy-light systems. In heavy-light systems, the heavy quark provides an approximately static source for the attractive binding force, like the proton in a hydrogen atom. The typical heavy-quark momentum in the bound-state rest frame is $|\vec{p}_h| \sim \Lambda_{\rm QCD}$, and heavy-light operators scale as powers of $(\Lambda_{\rm QCD}/m_h)^n$. This is often called "HQET power-counting", although it applies to heavy-light operators in HQET, NRQCD, and even relativistic heavy-quark actions described below. Heavy-heavy systems are similar to positronium or the deuteron, with the typical heavy-quark momentum $|\vec{p}_h| \sim \alpha_S m_h$. Therefore motion of the heavy quarks in the bound state rest frame cannot be neglected. Heavy-heavy operators have complicated power counting rules in terms of v_h^2 [517]; this is often called "NRQCD power counting."

Alternatively, one can simulate bottom or charm quarks with the same action as up, down, and strange quarks provided that (1) the action is sufficiently improved, and (2) the lattice spacing is sufficiently fine. These qualitative criteria do not specify precisely how large a numerical value of am_h can be allowed while obtaining a given precision for physical quantities; this must be established empirically in numerical simulations. At present, both the HISQ and twisted-mass Wilson actions discussed previously are being used to simulate charm quarks. Simulations with HISQ quarks have employed heavier quark masses than those with twisted-mass Wilson quarks because the action is more highly improved, but neither action can be used to simulate at the physical am_b for current lattice spacings. Therefore calculations of heavy-light decay constants with these actions still rely on effective theory to reach the b-quark mass: the ETM Collaboration interpolates between twisted-mass Wilson data generated near am_c and the static point [320], while the HPQCD Collaboration extrapolates HISQ data generated below am_b up to the physical point using an HQET-inspired series expansion in $(1/m_h)^n$ [338].

Heavy-quark effective theory

HQET was introduced by Eichten and Hill in Ref. [511]. It provides the correct asymptotic description of QCD correlation functions in the static limit $m_h/|\vec{p}_h| \to \infty$. Subleading effects are described by higher dimensional operators whose coupling constants are formally of $\mathcal{O}((1/m_h)^n)$. The HQET expansion works well for heavy-light systems in which the heavy-quark momentum is small compared to the mass.

The HQET Lagrangian density at the leading (static) order in the rest frame of the heavy quark is given by

$$\mathcal{L}^{\rm stat}(x) = \overline{\psi}_h(x)\, D_0\, \psi_h(x)\ , \tag{165}$$

with

$$P_+\psi_h = \psi_h\ , \qquad \overline{\psi}_h P_+ = \overline{\psi}_h\ , \qquad P_+ = \frac{1+\gamma_0}{2}\ . \tag{166}$$

A bare quark mass $m_{\rm bare}^{\rm stat}$ has to be added to the energy levels $E^{\rm stat}$ computed with this Lagrangian to obtain the physical ones. For example, the mass of the B meson in the static approximation is given by

$$m_B = E^{\rm stat} + m_{\rm bare}^{\rm stat}\ . \tag{167}$$

At tree-level $m_{\rm bare}^{\rm stat}$ is simply the (static approximation of the) b-quark mass, but in the quantized lattice formulation it has to further compensate a divergence linear in the inverse lattice spacing. Weak composite fields are also rewritten in terms of the static fields, e.g.

$$A_0(x)^{\rm stat} = Z_{\rm A}^{\rm stat}\left(\overline{\psi}(x)\gamma_0\gamma_5\psi_h(x)\right)\ , \tag{168}$$

where the renormalization factor of the axial current in the static theory $Z_{\rm A}^{\rm stat}$ is scale-dependent. Recent lattice-QCD calculations using static b quarks and dynamical light quarks [320, 374] perform the operator matching at one-loop in mean-field improved lattice perturbation theory [521, 522]. Therefore the heavy-quark discretization, truncation, and matching errors in these results are of $\mathcal{O}(a^2\Lambda_{\rm QCD}^2)$, $\mathcal{O}(\Lambda_{\rm QCD}/m_h)$, and $\mathcal{O}(\alpha_s^2, \alpha_s^2 a\Lambda_{\rm QCD})$.

In order to reduce heavy-quark truncation errors in B-meson masses and matrix elements to the few-percent level, state-of-the-art lattice-HQET computations now include corrections of $\mathcal{O}(1/m_h)$. Adding the $1/m_h$ terms, the HQET Lagrangian reads

$$\mathcal{L}^{\rm HQET}(x) \;=\; \mathcal{L}^{\rm stat}(x) - \omega_{\rm kin}\mathcal{O}_{\rm kin}(x) - \omega_{\rm spin}\mathcal{O}_{\rm spin}(x)\,, \tag{169}$$

$$\mathcal{O}_{\rm kin}(x) \;=\; \overline{\psi}_h(x)\mathbf{D}^2\psi_h(x)\,, \quad \mathcal{O}_{\rm spin}(x) = \overline{\psi}_h(x)\boldsymbol{\sigma}\cdot\mathbf{B}\psi_h(x)\,. \tag{170}$$

At this order, two other parameters appear in the Lagrangian, $\omega_{\rm kin}$ and $\omega_{\rm spin}$. The normalization is such that the tree-level values of the coefficients are $\omega_{\rm kin} = \omega_{\rm spin} = 1/(2m_h)$. Similarly the operators are formally expanded in inverse powers of the heavy-quark mass. The time component of the axial current, relevant for the computation of mesonic decay constants is given by

$$A_0^{\rm HQET}(x) = Z_{\rm A}^{\rm HQET}\left(A_0^{\rm stat}(x) + \sum_{i=1}^{2} c_{\rm A}^{(i)} A_0^{(i)}(x)\right) , \qquad (171)$$

$$A_0^{(1)}(x) = \overline{\psi}\tfrac{1}{2}\gamma_5\gamma_k(\nabla_k - \overleftarrow{\nabla}_k)\psi_h(x), \qquad k = 1,2,3 \qquad (172)$$

$$A_0^{(2)} = -\partial_k A_k^{\rm stat}(x) , \quad A_k^{\rm stat} = \overline{\psi}(x)\gamma_k\gamma_5\psi_h(x) , \qquad (173)$$

and depends on two additional parameters $c_{\rm A}^{(1)}$ and $c_{\rm A}^{(2)}$.

A framework for nonperturbative HQET on the lattice has been introduced in [515, 523]. As pointed out in Refs [524, 525], since $\alpha_s(m_h)$ decreases logarithmically with m_h, whereas corrections in the effective theory are power-like in Λ/m_h, it is possible that the leading errors in a calculation will be due to the perturbative matching of the action and the currents at a given order $(\Lambda/m_h)^l$ rather than to the missing $\mathcal{O}((\Lambda/m_h)^{l+1})$ terms. Thus, in order to keep matching errors below the uncertainty due to truncating the HQET expansion, the matching is performed nonperturbatively beyond leading order in $1/m_h$. The asymptotic convergence of HQET in the limit $m_h \to \infty$ indeed holds only in that case.

The higher dimensional interaction terms in the effective Lagrangian are treated as space-time volume insertions into static correlation functions. For correlators of some multi-local fields $\mathcal{O}$ and up to the $1/m_h$ corrections to the operator, this means

$$\langle\mathcal{O}\rangle = \langle\mathcal{O}\rangle_{\rm stat} + \omega_{\rm kin} a^4 \sum_x \langle\mathcal{O}\mathcal{O}_{\rm kin}(x)\rangle_{\rm stat} + \omega_{\rm spin} a^4 \sum_x \langle\mathcal{O}\mathcal{O}_{\rm spin}(x)\rangle_{\rm stat} , \qquad (174)$$

where $\langle\mathcal{O}\rangle_{\rm stat}$ denotes the static expectation value with $\mathcal{L}^{\rm stat}(x) + \mathcal{L}^{\rm light}(x)$. Nonperturbative renormalization of these correlators guarantees the existence of a well-defined continuum limit to any order in $1/m_h$. The parameters of the effective action and operators are then determined by matching a suitable number of observables calculated in HQET (to a given order in $1/m_h$) and in QCD in a small volume (typically with $L \simeq 0.5$ fm), where the full relativistic dynamics of the b-quark can be simulated and the parameters can be computed with good accuracy. In [523, 526] the Schrödinger Functional (SF) setup has been adopted to define a set of quantities, given by the small volume equivalent of decay constants, pseudoscalar-vector splittings, effective masses and ratio of correlation functions for different kinematics, that can be used to implement the matching conditions. The kinematical conditions are usually modified by changing the periodicity in space of the fermions, i.e. by directly exploiting a finite-volume effect. The new scale L, which is introduced in this way, is chosen such that higher orders in $1/m_hL$ and in $\Lambda_{\rm QCD}/m_h$ are of about the same size. At the end of the matching step the parameters are known at lattice spacings which are of the order of 0.01 fm, significantly smaller than the resolutions used for large volume, phenomenological, applications. For this reason a set of SF-step scaling functions is introduced in the effective theory to evolve the parameters to larger lattice spacings. The whole procedure yields the nonperturbative parameters with an accuracy which allows to compute phenomenological quantities with a precision of a few percent (see [342, 362] for the case of the $B_{(s)}$ decay constants). Such an accuracy can not be achieved by performing the nonperturbative matching in large volume against experimental measurements, which in addition would reduce the predictivity of the theory. For the lattice-HQET action matched nonperturbatively through $\mathcal{O}(1/m_h)$, discretization and truncation errors are of $\mathcal{O}(a\Lambda_{\rm QCD}^2/m_h, a^2\Lambda_{\rm QCD}^2)$ and $\mathcal{O}((\Lambda_{\rm QCD}/m_h)^2)$.

The noise-to-signal ratio of static-light correlation functions grows exponentially in Euclidean time, $\propto e^{\mu x_0}$. The rate μ is nonuniversal but diverges as $1/a$ as one approaches the continuum limit. By changing the discretization of the covariant derivative in the static action one may achieve an exponential reduction of the noise to signal ratio. Such a strategy led to the introduction of the $S^{\text{stat}}_{\text{HYP1,2}}$ actions [527], where the thin links in D_0 are replaced by HYP-smeared links [487]. These actions are now used in all lattice applications of HQET.

Nonrelativistic QCD

Nonrelativistic QCD (NRQCD) [516, 517] is an effective theory that can be matched to full QCD order by order in the heavy-quark velocity v_h^2 (for heavy-heavy systems) or in Λ_{QCD}/m_h (for heavy-light systems) and in powers of α_s. Relativistic corrections appear as higher-dimensional operators in the Hamiltonian.

As an effective field theory, NRQCD is only useful with an ultraviolet cutoff of order m_h or less. On the lattice this means that it can be used only for $am_h > 1$, which means that $O(a^n)$ errors cannot be removed by taking $a \to 0$ at fixed m_h. Instead heavy-quark discretization errors are systematically removed by adding additional operators to the lattice Hamiltonian. Thus, while strictly speaking no continuum limit exists at fixed m_h, continuum physics can be obtained at finite lattice spacing to arbitrarily high precision provided enough terms are included, and provided that the coefficients of these terms are calculated with sufficient accuracy. Residual discretization errors can be parameterized as corrections to the coefficients in the nonrelativistic expansion, as shown in Eq. (177). Typically they are of the form $(a|\vec{p}_h|)^n$ multiplied by a function of am_h that is smooth over the limited range of heavy-quark masses (with $am_h > 1$) used in simulations, and can therefore can be represented by a low-order polynomial in am_h by Taylor's theorem (see Ref. [336] for further discussion). Power-counting estimates of these effects can be compared to the observed lattice spacing dependence in simulations. Provided that these effects are small, such comparisons can be used to estimate and correct the residual discretization effects.

An important feature of the NRQCD approach is that the same action can be applied to both heavy-heavy and heavy-light systems. This allows, for instance, the bare b-quark mass to be fixed via experimental input from Υ so that simulations carried out in the B or B_s systems have no adjustable parameters left. Precision calculations of the B_s meson mass (or of the mass splitting $M_{B_s} - M_\Upsilon/2$) can then be used to test the reliability of the method before turning to quantities one is trying to predict, such as decay constants f_B and f_{B_s}, semileptonic form factors or neutral B mixing parameters.

Given the same lattice-NRQCD heavy-quark action, simulation results will not be as accurate for charm quarks as for bottom ($1/m_b < 1/m_c$, and $v_b < v_c$ in heavy-heavy systems). For charm, however, a more serious concern is the restriction that am_h must be greater than one. This limits lattice-NRQCD simulations at the physical am_c to relatively coarse lattice spacings for which light-quark and gluon discretization errors could be large. Thus recent lattice-NRQCD simulations have focused on bottom quarks because $am_b > 1$ in the range of typical lattice spacings between ≈ 0.06 and 0.15 fm.

In most simulations with NRQCD b-quarks during the past decade one has worked with an NRQCD action that includes tree-level relativistic corrections through $\mathcal{O}(v_h^4)$ and discretization corrections through $\mathcal{O}(a^2)$,

$$S_{\rm NRQCD} = a^4 \sum_x \left\{ \Psi_t^\dagger \Psi_t - \Psi_t^\dagger \left(1 - \frac{a\delta H}{2}\right)_t \left(1 - \frac{aH_0}{2n}\right)^n_t \right.$$

$$\left. \times \quad U_t^\dagger(t-a) \left(1 - \frac{aH_0}{2n}\right)^n_{t-a} \left(1 - \frac{a\delta H}{2}\right)_{t-a} \Psi_{t-a} \right\}, \tag{175}$$

where the subscripts "t" and "$t-a$" denote that the heavy-quark, gauge, **E**, and **B**-fields are on time slices t or $t-a$, respectively. H_0 is the nonrelativistic kinetic energy operator,

$$H_0 = -\frac{\Delta^{(2)}}{2m_h}, \tag{176}$$

and δH includes relativistic and finite-lattice-spacing corrections,

$$\begin{aligned} \delta H \quad = \quad & -c_1 \frac{(\Delta^{(2)})^2}{8m_h^3} + c_2 \frac{ig}{8m_h^2} \left(\nabla \cdot \tilde{\mathbf{E}} - \tilde{\mathbf{E}} \cdot \nabla \right) \\ & -c_3 \frac{g}{8m_h^2} \boldsymbol{\sigma} \cdot (\tilde{\nabla} \times \tilde{\mathbf{E}} - \tilde{\mathbf{E}} \times \tilde{\nabla}) \\ & -c_4 \frac{g}{2m_h} \boldsymbol{\sigma} \cdot \tilde{\mathbf{B}} + c_5 \frac{a^2 \Delta^{(4)}}{24m_h} - c_6 \frac{a(\Delta^{(2)})^2}{16nm_h^2}. \end{aligned} \tag{177}$$

m_h is the bare heavy-quark mass, $\Delta^{(2)}$ the lattice Laplacian, ∇ the symmetric lattice derivative and $\Delta^{(4)}$ the lattice discretization of the continuum $\sum_i D_i^4$. $\tilde{\nabla}$ is the improved symmetric lattice derivative and the $\tilde{\mathbf{E}}$ and $\tilde{\mathbf{B}}$ fields have been improved beyond the usual clover leaf construction. The stability parameter n is discussed in [517]. In most cases the c_i's have been set equal to their tree-level values $c_i = 1$. With this implementation of the NRQCD action, errors in heavy-light meson masses and splittings are of $\mathcal{O}(\alpha_S \Lambda_{\rm QCD}/m_h)$, $\mathcal{O}(\alpha_S(\Lambda_{\rm QCD}/m_h)^2)$, $\mathcal{O}((\Lambda_{\rm QCD}/m_h)^3)$, and $\mathcal{O}(\alpha_s a^2 \Lambda_{\rm QCD}^2)$, with coefficients that are functions of am_h. One-loop corrections to many of the coefficients in Eq. (177) have now been calculated, and are starting to be included in simulations [355, 528, 529].

Most of the operator matchings involving heavy-light currents or four-fermion operators with NRQCD b-quarks and AsqTad or HISQ light quarks have been carried out at one-loop order in lattice perturbation theory. In calculations published to date of electroweak matrix elements, heavy-light currents with massless light quarks have been matched through $\mathcal{O}(\alpha_s, \Lambda_{\rm QCD}/m_h, \alpha_s/(am_h), \alpha_s \Lambda_{\rm QCD}/m_h)$, and four-fermion operators through $\mathcal{O}(\alpha_s, \Lambda_{\rm QCD}/m_h, \alpha_s/(am_h))$. NRQCD/HISQ currents with massive HISQ quarks are also of interest, e.g. for the bottom-charm currents in $B \to D^{(*)}, l\nu$ semileptonic decays and the relevant matching calculations have been performed at one-loop order in Ref. [530]. Taking all the above into account, the most significant systematic error in electroweak matrix elements published to date with NRQCD b-quarks is the $\mathcal{O}(\alpha_s^2)$ perturbative matching uncertainty. Work is therefore underway to use current-current correlator methods combined with very high order continuum perturbation theory to do current matchings nonperturbatively [531].

Relativistic heavy quarks

An approach for relativistic heavy-quark lattice formulations was first introduced by El Khadra, Kronfeld, and Mackenzie in Ref. [518]. Here they showed that, for a general lattice action with massive quarks and non-Abelian gauge fields, discretization errors can be factorized into the form $f(m_h a)(a|\vec{p}_h|)^n$, and that the function $f(m_h a)$ is bounded to be of $\mathcal{O}(1)$ or less for all values of the quark mass m_h. Therefore cutoff effects are of $\mathcal{O}(a\Lambda_{\rm QCD})^n$ and $\mathcal{O}((a|\vec{p}_h|)^n)$, even for $am_h \gtrsim 1$, and can be controlled using a Symanzik-like procedure. As in the standard Symanzik improvement program, cutoff effects are systematically removed by introducing higher-dimension operators to the lattice action and suitably tuning their coefficients. In the relativistic heavy-quark approach, however, the operator coefficients are allowed to depend explicitly on the quark mass. By including lattice operators through dimension n and adjusting their coefficients $c_{n,i}(m_h a)$ correctly, one enforces that matrix elements in the lattice theory are equal to the analogous matrix elements in continuum QCD through $(a|\vec{p}_h|)^n$, such that residual heavy-quark discretization errors are of $\mathcal{O}(a|\vec{p}_h|)^{n+1}$.

The relativistic heavy-quark approach can be used to compute the matrix elements of states containing heavy quarks for which the heavy-quark spatial momentum $|\vec{p}_h|$ is small compared to the lattice spacing. Thus it is suitable to describe bottom and charm quarks in both heavy-light and heavy-heavy systems. Calculations of bottomonium and charmonium spectra serve as nontrivial tests of the method and its accuracy.

At fixed lattice spacing, relativistic heavy-quark formulations recover the massless limit when $(am_h) \ll 1$, recover the static limit when $(am_h) \gg 1$, and smoothy interpolate between the two; thus they can be used for any value of the quark mass, and, in particular, for both charm and bottom. Discretization errors for relativistic heavy-quark formulations are generically of the form $\alpha_s^k f(am_h)(a|\vec{p}_h|)^n$, where k reflects the order of the perturbative matching for operators of $\mathcal{O}((a|\vec{p}_h|)^n)$. For each n, such errors are removed completely if the operator matching is nonperturbative. When $(am_h) \sim 1$, this gives rise to nontrivial lattice-spacing dependence in physical quantities, and it is prudent to compare estimates based on power-counting with a direct study of scaling behavior using a range of lattice spacings. At fixed quark mass, relativistic heavy-quark actions possess a smooth continuum limit without power-divergences. Of course, as $m_h \to \infty$ at fixed lattice spacing, the power divergences of the static limit are recovered (see, e.g. Ref. [532]).

The relativistic heavy-quark formulations in use all begin with the anisotropic Sheikholeslami-Wohlert ("clover") action [533]:

$$S_{\rm lat} = a^4 \sum_{x,x'} \bar{\psi}(x') \left(m_0 + \gamma_0 D_0 + \zeta \vec{\gamma}\cdot\vec{D} - \tfrac{a}{2}(D^0)^2 - \tfrac{a}{2}\zeta(\vec{D})^2 + \sum_{\mu,\nu} \tfrac{ia}{4} c_{\rm SW}\sigma_{\mu\nu}F_{\mu\nu} \right)_{x'x} \psi(x)\,, \tag{178}$$

where D_μ is the lattice covariant derivative and $F_{\mu\nu}$ is the lattice field-strength tensor. Here we show the form of the action given in Ref. [519]. The introduction of a space-time anisotropy, parameterized by ζ in Eq. (178), is convenient for heavy-quark systems because the characteristic heavy-quark four-momenta do not respect space-time axis exchange ($\vec{p}_h < m_h$ in the bound-state rest frame). Further, the Sheikoleslami-Wohlert action respects the continuum heavy-quark spin and flavour symmetries, so HQET can be used to interpret and estimate lattice discretization effects [532, 534, 535]. We discuss three different prescriptions for tuning the parameters of the action in common use below. In particular, we focus on aspects of the action and operator improvement and matching relevant for evaluating the quality of the calculations discussed in the main text.

The meson energy-momentum dispersion relation plays an important role in relativistic heavy-quark formulations:

$$E(\vec{p}) = M_1 + \frac{\vec{p}^2}{2M_2} + \mathcal{O}(\vec{p}^4)\,, \tag{179}$$

where M_1 and M_2 are known as the rest and kinetic masses, respectively. Because the lattice breaks Lorentz invariance, there are corrections proportional to powers of the momentum. Further, the lattice rest masses and kinetic masses are not equal ($M_1 \neq M_2$), and only become equal in the continuum limit.

The Fermilab interpretation [518] is suitable for calculations of mass splittings and matrix elements of systems with heavy quarks. The Fermilab action is based on the hopping-parameter form of the Wilson action, in which κ_h parameterizes the heavy-quark mass. In practice, κ_h is tuned such that the the kinetic meson mass equals the experimentally-measured heavy-strange meson mass (m_{B_s} for bottom and m_{D_s} for charm). In principle, one could also tune the anisotropy parameter such that $M_1 = M_2$. This is not necessary, however, to obtain mass splittings and matrix elements, which are not affected by M_1 [534]. Therefore in the Fermilab action the anisotropy parameter is set equal to unity. The clover coefficient in the Fermilab action is fixed to the value $c_{\rm SW} = 1/u_0^3$ from mean-field improved lattice perturbation theory [440]. With this prescription, discretization effects are of $\mathcal{O}(\alpha_s a|\vec{p}_h|, (a|\vec{p}_h|)^2)$. Calculations of electroweak matrix elements also require improving the lattice current and four-fermion operators to the same order, and matching them to the continuum. Calculations with the Fermilab action remove tree-level $\mathcal{O}(a)$ errors in electroweak operators by rotating the heavy-quark field used in the matrix element and setting the rotation coefficient to its tadpole-improved tree-level value (see *e.g.* Eqs. (7.8) and (7.10) of Ref. [518]). Finally, electroweak operators are typically renormalized using a mostly nonperturbative approach in which the flavour-conserving light-light and heavy-heavy current renormalization factors Z_V^{ll} and Z_V^{hh} are computed nonperturbatively [536]. The flavour-conserving factors account for most of the heavy-light current renormalization. The remaining correction is expected to be close to unity due to the cancellation of most of the radiative corrections including tadpole graphs [532]; therefore it can be reliably computed at one-loop in mean-field improved lattice perturbation theory with truncation errors at the percent to few-percent level.

The relativistic heavy-quark (RHQ) formulation developed by Li, Lin, and Christ builds upon the Fermilab approach, but tunes all the parameters of the action in Eq. (178) nonperturbatively [519]. In practice, the three parameters $\{m_0 a, c_{\rm SW}, \zeta\}$ are fixed to reproduce the experimentally-measured B_s meson mass and hyperfine splitting ($m_{B_s^*} - m_{B_s}$), and to make the kinetic and rest masses of the lattice B_s meson equal [357]. This is done by computing the heavy-strange meson mass, hyperfine splitting, and ratio M_1/M_2 for several sets of bare parameters $\{m_0 a, c_{\rm SW}, \zeta\}$ and interpolating linearly to the physical B_s point. By fixing the B_s-meson hyperfine splitting, one loses a potential experimental prediction with respect to the Fermilab formulation. However, by requiring that $M_1 = M_2$, one gains the ability to use the meson rest masses, which are generally more precise than the kinetic masses, in the RHQ approach. The nonperturbative parameter-tuning procedure eliminates $\mathcal{O}(a)$ errors from the RHQ action, such that discretization errors are of $\mathcal{O}((a|\vec{p}_h|)^2)$. Calculations of B-meson decay constants and semileptonic form factors with the RHQ action are in progress [376, 402], as is the corresponding one-loop mean-field improved lattice perturbation theory [537]. For these works, cutoff effects in the electroweak vector and axial-vector currents will be removed through $\mathcal{O}(\alpha_s a)$, such that the remaining discretization errors are of $\mathcal{O}(\alpha_s^2 a|\vec{p}_h|, (a|\vec{p}_h|)^2)$. Matching the lattice operators to the continuum will be done following the mostly nonperturbative approach described above.

The Tsukuba heavy-quark action is also based on the Sheikholeslami-Wohlert action in Eq. (178), but allows for further anisotropies and hence has additional parameters: specifically the clover coefficients in the spatial (c_B) and temporal (c_E) directions differ, as do the anisotropy coefficients of the $\vec{D}$ and $\vec{D}^2$ operators [520]. In practice, the contribution to the clover coefficient in the massless limit is computed nonperturbatively [538], while the mass-dependent contributions, which differ for c_B and c_E, are calculated at one-loop in mean-field improved lattice perturbation theory [539]. The hopping parameter is fixed nonperturbatively to reproduce the experimentally-measured spin-averaged $1S$ charmonium mass [317]. One of the anisotropy parameters (r_t in Ref. [317]) is also set to its one-loop perturbative value, while the other (ν in Ref. [317]) is fixed noperturbatively to obtain the continuum dispersion relation for the spin-averaged charmonium $1S$ states (such that $M_1 = M_2$). For the renormalization and improvement coefficients of weak current operators, the contributions in the chiral limit are obtained nonperturbatively [21, 540], while the mass-dependent contributions are estimated using one-loop lattice perturbation theory [541]. With these choices, lattice cutoff effects from the action and operators are of $\mathcal{O}(\alpha_s^2 a|\vec{p}|, (a|\vec{p}_h|)^2)$.

Light-quark actions combined with HQET

The heavy-quark formulations discussed in the previous sections use effective field theory to avoid the occurence of discretization errors of the form $(am_h)^n$. In this section we describe methods that use improved actions that were originally designed for light-quark systems for B physics calculations. Such actions unavoidably contain discretization errors that grow as a power of the heavy-quark mass. In order to use them for heavy-quark physics, they must be improved to at least $\mathcal{O}(am_h)^2$. However, since $am_b > 1$ at the smallest lattice spacings available in current simulations, these methods also require input from HQET to guide the simulation results to the physical b-quark mass.

The ETM collaboration has developed two methods, the "ratio method" [364] and the "interpolation method" [542, 543]. They use these methods together with simulations with twisted-mass Wilson fermions, which have discretization errors of $O(am_h)^2$. In the interpolation method Φ_{hs} and $\Phi_{h\ell}$ (or $\Phi_{hs}/\Phi_{h\ell}$) are calculated for a range of heavy-quark masses in the charm region and above, while roughly keeping $am_h \lesssim 0.5$. The relativistic results are combined with a separate calculation of the decay constants in the static limit, and then interpolated to the physical b quark mass. In ETM's implementation of this method, the heavy Wilson decay constants are matched to HQET using NLO in continuum perturbation theory. The static limit result is renormalized using one-loop mean-field improved lattice perturbation theory, while for the relativistic data PCAC is used to calculate absolutely normalized matrix elements. Both, the relativistic and static limit data are then run to the common reference scale $\mu_b = 4.5\,\text{GeV}$ at NLO in continuum perturbation theory. In the ratio method, one constructs physical quantities $P(m_h)$ from the relativistic data that have a well-defined static limit ($P(m_h) \to$ const. for $m_h \to \infty$) and evaluates them at the heavy-quark masses used in the simulations. Ratios of these quantities are then formed at a fixed ratio of heavy quark masses, $z = P(m_h)/P(m_h/\lambda)$ (where $1 < \lambda \lesssim 1.3$), which ensures that z is equal to unity in the static limit. Hence, a separate static limit calculation is not needed with this method. In ETM's implementation of the ratio method for the B-meson decay constant, $P(m_h)$ is constructed from the decay constants and the heavy-quark pole mass as $P(m_h) = f_{h\ell}(m_h) \cdot (m_h^{\text{pole}})^{1/2}$. The corresponding z-ratio therefore also includes ratios of perturbative matching factors for the pole mass to $\overline{\text{MS}}$ conversion. For the interpolation to the physical b-quark mass, ratios of perturbative matching factors converting the data from QCD to HQET are also included. The QCD-to-HQET matching factors improve the approach to the static limit by removing the leading logarithmic corrections. In ETM's implementation of this method (ETM 11 and 12) both conversion factors are evaluated at NLO in continuum perturbation theory. The ratios are then simply fit to a polynomial in $1/m_h$ and interpolated to the physical b-quark mass. The ratios constructed from $f_{h\ell}$ (f_{hs}) are called z (z_s). In order to obtain the B meson decay constants, the ratios are combined with relativistic decay constant data evaluated at the smallest reference mass.

The HPQCD collaboration has introduced a method in Ref. [338] which we shall refer to as the "heavy HISQ" method. The first key ingredient is the use of the HISQ action for the heavy and light valence quarks, which has leading discretization errors of $\mathcal{O}\left(\alpha_s(v/c)(am_h)^2, (v/c)^2(am_h)^4\right)$. With the same action for the heavy and light valence quarks it is possible to use PCAC to avoid renormalization uncertainties. Another key ingredient is the availability of gauge ensembles over a large range of lattice spacings, in this case in the form of the library of $N_f = 2+1$ asqtad ensembles made public by the MILC collaboration which includes lattice spacings as small as $a \approx 0.045$ fm. Since the HISQ action is so highly improved and with lattice spacings as small as 0.045 fm, HPQCD is able to use a large range of heavy-quark masses, from below the charm region to almost up to the physical b quark mass with $am_h \lesssim 0.85$. They then fit their data in a combined continuum and HQET fit (i.e. using a fit function that is motivated by HQET) to a polynomial in $1/m_H$ (the heavy pseudo scalar meson mass of a meson containing a heavy (h) quark).

In Table 34 we list the discretizations of the quark action most widely used for heavy c and b quarks together with the abbreviations used in the summary tables. We also summarize the main properties of these actions and the leading lattice discretization errors for calculations of heavy-light meson matrix quantities with them. Note that in order to maintain the leading lattice artifacts of the actions as given in the table in nonspectral observables (like operator matrix elements) the corresponding nonspectral operators need to be improved as well.

Abbrev.	Discretization	Leading lattice artifacts and truncation errors for heavy-light mesons	Remarks
tmWil	twisted-mass Wilson	$\mathcal{O}\big((am_h)^2\big)$	PCAC relation for axial-vector current
HISQ	Staggered	$\mathcal{O}\big(\alpha_S(am_h)^2(v/c), (am_h)^4(v/c)^2\big)$	PCAC relation for axial-vector current; Ward identity for vector current
static	static effective action	$\mathcal{O}\big(a^2\Lambda_{\rm QCD}^2, \Lambda_{\rm QCD}/m_h, \alpha_s^2, \alpha_s^2 a\Lambda_{\rm QCD}\big)$	implementations use APE, HYP1, and HYP2 smearing
HQET	Heavy-Quark Effective Theory	$\mathcal{O}\big(a\Lambda_{\rm QCD}^2/m_h, a^2\Lambda_{\rm QCD}^2, (\Lambda_{\rm QCD}/m_h)^2\big)$	Nonperturbative matching through $\mathcal{O}(1/m_h)$
NRQCD	Nonrelativistic QCD	$\mathcal{O}\big(\alpha_S\Lambda_{\rm QCD}/m_h, \alpha_S(\Lambda_{\rm QCD}/m_h)^2, (\Lambda_{\rm QCD}/m_h)^3, \alpha_s a^2\Lambda_{\rm QCD}^2\big)$	Tree-level relativistic corrections through $\mathcal{O}(v_h^4)$ and discretization corrections through $\mathcal{O}(a^2)$
Fermilab	Sheikholeslami-Wohlert	$\mathcal{O}\big(\alpha_s a\Lambda_{\rm QCD}, (a\Lambda_{\rm QCD})^2\big)$	Hopping parameter tuned nonperturbatively; clover coefficient computed at tree-level in mean-field improved lattice perturbation theory
Tsukuba	Sheikholeslami-Wohlert	$\mathcal{O}\big(\alpha_s^2 a\Lambda_{\rm QCD}, (a\Lambda_{\rm QCD})^2\big)$	NP clover coefficient at $ma = 0$ plus mass-dependent corrections calculated at one-loop in lattice perturbation theory; ν calculated NP from dispersion relation; r_s calculated at one-loop in lattice perturbation theory

Table 34: Discretizations of the quark action most widely used for heavy c and b quarks and some of their properties.

A.2 Setting the scale

In simulations of lattice QCD quantities such as hadron masses and decay constants are obtained in "lattice units" i.e. as dimensionless numbers. In order to convert them into physical units they must be expressed in terms of some experimentally known, dimensionful reference quantity Q. This procedure is called "setting the scale". It amounts to computing the nonperturbative relation between the bare gauge coupling g_0 (which is an input parameter in any lattice simulation) and the lattice spacing a expressed in physical units. To this end one chooses a value for g_0 and computes the value of the reference quantity in a simulation: This yields the dimensionless combination, $(aQ)|_{g_0}$, at the chosen value of g_0. The calibration of the lattice spacing is then achieved via

$$a^{-1}\,[\mathrm{MeV}] = \frac{Q|_{\mathrm{exp}}\,[\mathrm{MeV}]}{(aQ)|_{g_0}}, \tag{180}$$

where $Q|_{\mathrm{exp}}$ denotes the experimentally known value of the reference quantity. Common choices for Q are the mass of the nucleon, the Ω baryon or the decay constants of the pion and the kaon. Vector mesons, such as the ρ or K^*-meson, are unstable and therefore their masses are not very well suited for setting the scale, despite the fact that they have been used over many years for that purpose.

Another widely used quantity to set the scale is the hadronic radius r_0, which can be determined from the force between static quarks via the relation [65]

$$F(r_0)r_0^2 = 1.65. \tag{181}$$

If the force is derived from potential models describing heavy quarkonia, the above relation determines the value of r_0 as $r_0 \approx 0.5\,\mathrm{fm}$. A variant of this procedure is obtained [544] by using the definition $F(r_1)r_1^2 = 1.00$, which yields $r_1 \approx 0.32\,\mathrm{fm}$. It is important to realize that both r_0 and r_1 are not directly accessible in experiment, so that their values derived from phenomenological potentials are necessarily model-dependent. Inspite of the inherent ambiguity whenever hadronic radii are used to calibrate the lattice spacing, they are very useful quantities for performing scaling tests and continuum extrapolations of lattice data. Furthermore, they can be easily computed with good statistical accuracy in lattice simulations.

A.3 Matching and running

The lattice formulation of QCD amounts to introducing a particular regularization scheme. Thus, in order to be useful for phenomenology, hadronic matrix elements computed in lattice simulations must be related to some continuum reference scheme, such as the $\overline{\mathrm{MS}}$-scheme of dimensional regularization. The matching to the continuum scheme usually involves running to some reference scale using the renormalization group.

In principle, the matching factors which relate lattice matrix elements to the $\overline{\mathrm{MS}}$-scheme, can be computed in perturbation theory formulated in terms of the bare coupling. It has been known for a long time, though, that the perturbative expansion is not under good control. Several techniques have been developed which allow for a nonperturbative matching between lattice regularization and continuum schemes, and are briefly introduced here.

Regularization-independent Momentum Subtraction

In the *Regularization-independent Momentum Subtraction* ("RI/MOM" or "RI") scheme [283] a nonperturbative renormalization condition is formulated in terms of Green functions involving quark states in a fixed gauge (usually Landau gauge) at nonzero virtuality. In this way one relates operators in lattice regularization nonperturbatively to the RI scheme. In a second step one matches the operator in the RI scheme to its counterpart in the $\overline{\text{MS}}$-scheme. The advantage of this procedure is that the latter relation involves perturbation theory formulated in the continuum theory. The uncontrolled use of lattice perturbation theory can thus be avoided. A technical complication is associated with the accessible momentum scales (i.e. virtualities), which must be large enough (typically several GeV) in order for the perturbative relation to $\overline{\text{MS}}$ to be reliable. The momentum scales in simulations must stay well below the cutoff scale (i.e. 2π over the lattice spacing), since otherwise large lattice artifacts are incurred. Thus, the applicability of the RI scheme traditionally relies on the existence of a "window" of momentum scales, which satisfy

$$\Lambda_{\text{QCD}} \lesssim p \lesssim 2\pi a^{-1}. \tag{182}$$

However, solutions for mitigating this limitation, which involve continuum limit, nonperturbative running to higher scales in the RI/MOM scheme, have recently been proposed and implemented [22, 23, 301, 545].

Schrödinger functional

Another example of a nonperturbative matching procedure is provided by the Schrödinger functional (SF) scheme [87]. It is based on the formulation of QCD in a finite volume. If all quark masses are set to zero the box length remains the only scale in the theory, such that observables like the coupling constant run with the box size L. The great advantage is that the RG running of scale-dependent quantities can be computed nonperturbatively using recursive finite-size scaling techniques. It is thus possible to run nonperturbatively up to scales of, say, 100 GeV, where one is sure that the perturbative relation between the SF and $\overline{\text{MS}}$-schemes is controlled.

Perturbation theory

The third matching procedure is based on perturbation theory in which higher order are effectively resummed [440]. Although this procedure is easier to implement, it is hard to estimate the uncertainty associated with it.

Mostly nonperturbative renormalization

Some calculations of heavy-light and heavy-heavy matrix elements adopt a mostly nonperturbative matching approach. Let us consider a weak decay process mediated by a current with quark flavours h and q, where h is the initial heavy quark (either bottom or charm) and q can be a light ($\ell = u, d$), strange, or charm quark. The matrix elements of lattice current J_{hq} are matched to the corresponding continuum matrix elements with continuum current

$\mathcal{J}_{hq}$ by calculating the renormalization factor $Z_{J_{hq}}$. The mostly nonperturbative renormalization method takes advantage of rewriting the current renormalization factor as the following product:

$$Z_{J_{hq}} = \rho_{J_{hq}} \sqrt{Z_{V^4_{hh}} Z_{V^4_{qq}}} \tag{183}$$

The flavour-conserving renormalization factors $Z_{V^4_{hh}}$ and $Z_{V^4_{qq}}$ can be obtained nonperturbatively from standard heavy-light and light-light meson charge normalization conditions. $Z_{V^4_{hh}}$ and $Z_{V^4_{qq}}$ account for the bulk of the renormalization. The remaining correction $\rho_{J_{hq}}$ is expected to be close to unity because most of the radiative corrections, including self-energy corrections and contributions from tadpole graphs, cancel in the ratio [532, 535]. The one-loop coefficients of $\rho_{J_{hq}}$ have been calculated for heavy-light and heavy-heavy currents for Fermilab heavy and both (improved) Wilson light [532, 535] and asqtad light [546] quarks. In all cases the one-loop coefficients are found to be very small, yielding sub-percent to few percent level corrections.

In Table 35 we list the abbreviations used in the compilation of results together with a short description.

Abbrev.	Description
RI	regularization-independent momentum subtraction scheme
SF	Schrödinger functional scheme
PT1ℓ	matching/running computed in perturbation theory at one loop
PT2ℓ	matching/running computed in perturbation theory at two loops
mNPR	mostly nonperturbative renormalization

Table 35: The most widely used matching and running techniques.

A.4 Chiral extrapolation

As mentioned in the introduction, Symanzik's framework can be combined with Chiral Perturbation Theory. The well-known terms occurring in the chiral effective Lagrangian are then supplemented by contributions proportional to powers of the lattice spacing a. The additional terms are constrained by the symmetries of the lattice action and therefore depend on the specific choice of the discretization. The resulting effective theory can be used to analyze the a-dependence of the various quantities of interest – provided the quark masses and the momenta considered are in the range where the truncated chiral perturbation series yields an adequate approximation. Understanding the dependence on the lattice spacing is of central importance for a controlled extrapolation to the continuum limit.

For staggered fermions, this program has first been carried out for a single staggered flavour (a single staggered field) [455] at $O(a^2)$. In the following, this effective theory is denoted by SχPT. It was later generalized to an arbitrary number of flavours [456, 547], and to next-to-leading order [457]. The corresponding theory is commonly called Rooted Staggered chiral perturbation theory and is denoted by RSχPT.

For Wilson fermions, the effective theory has been developed in [234, 235, 548] and is called WχPT, while the theory for Wilson twisted-mass fermions [259, 549, 550] is termed tmWχPT.

Another important approach is to consider theories in which the valence and sea quark masses are chosen to be different. These theories are called *partially quenched*. The acronym for the corresponding chiral effective theory is PQχPT [551–554].

Finally, one can also consider theories where the fermion discretizations used for the sea and the valence quarks are different. The effective chiral theories for these "mixed action" theories are referred to as MAχPT [236, 463, 555–559].

A.5 Summary of simulated lattice actions

In the following two tables we summarize the gauge and quark actions used in the various calculations. Abbreviations are explained in section A.1.1, A.1.2 and A.1.3, and summarized in tables 32, 33 and 34.

Collab.	Ref.	N_f	gauge action	quark action
ALPHA 12	[59]	2	Wilson	npSW
RM123 11, 13	[45, 102]	2	tlSym	tmWil
Dürr 11	[61]	2	Wilson	npSW
ALPHA 05	[64]	2	Wilson	npSW
CERN-TOV 06	[258]	2	Wilson	Wilson/npSW
CERN 08	[204]	2	Wilson	npSW
Bernardoni 10	[248]	2	Wilson	npSW †
CP-PACS 01	[63]	2	Iwasaki	mfSW
ETM 07, 07A, 08, 09, 09A-D, 10B, D	[60, 62, 138, 139, 160, 227, 230, 250, 364, 560]	2	tlSym	tmWil
Hasenfratz 08	[251]	2	tadSym	n-HYP tlSW
JLQCD 08	[305]	2	Iwasaki	overlap
JLQCD 02, 05	[70, 142]	2	Wilson	npSW
JLQCD/TWQCD 07, 08A, 10	[67, 241, 252]	2	Iwasaki	overlap
QCDSF 07	[140]	2	Wilson	npSW
QCDSF/UKQCD 04, 06, 06A, 07	[66, 68, 161, 262]	2	Wilson	npSW
RBC 07	[34]	2	DBW2	DW
RBC 04, 06	[141, 299]	2	DBW2	DW
SPQcdR 05	[69]	2	Wilson	Wilson
UKQCD 04, 07	[137, 306]	2	Wilson	npSW

† The calculation uses overlap fermions in the valence quark sector.

Table 36: Summary of simulated lattice actions with $N_f = 2$ quark flavours.

Collab.	Ref.	N_f	gauge action	quark action
Aubin 08, 09, Laiho 11	[77, 155, 284]	$2+1$	tadSym	Asqtad †
SWME 10, 11	[285, 302]	$2+1$	tadSym	Asqtad $^{+}$
Blum 10	[32]	$2+1$	Iwasaki	DW
BMW 10A-C	[22, 23, 43]	$2+1$	tlSym	2-level HEX tlSW
BMW 10	[153]	$2+1$	tlSym	6-level stout tlSW
CP-PACS/JLQCD 07	[80]	$2+1$	Iwasaki	npSW
ETM 10, 10E	[96, 150]	$2+1+1$	Iwasaki	tmWil
FNAL/MILC 12B	[314]	$2+1+1$	tadSym	HISQ
HPQCD 05	[81]	$2+1$	tadSym	Asqtad
HPQCD/UKQCD 06	[304]	$2+1$	tadSym	Asqtad
HPQCD/UKQCD 07, 10	[72, 157]	$2+1$	tadSym	Asqtad *
HPQCD/MILC/UKQCD 04	[82]	$2+1$	tadSym	Asqtad
JLQCD 09	[240]	$2+1$	Iwasaki	overlap
JLQCD/TWQCD 08B, 09A	[154, 244]	$2+1$	Iwasaki	overlap
JLQCD/TWQCD 10	[241]	$2+1, 3$	Iwasaki	overlap

† The calculation uses domain wall fermions in the valence quark sector.

* The calculation uses HISQ staggered fermions in the valence quark sector.

$^{+}$ The calculation uses HYP smeared improved staggered fermions in the valence quark sector.

Table 37: Summary of simulated lattice actions with $N_f = 2+1$ or $N_f = 2+1+1$ quark flavours.

Collab.	Ref.	N_f	gauge action	quark action
LHP 04	[261]	$2+1$	tadSym	Asqtad †
MILC 04, 07, 09, 09A, 10, 10A	[15, 36, 75, 82, 151, 561]	$2+1$	tadSym	Asqtad
NPLQCD 06	[158]	$2+1$	tadSym	Asqtad †
PACS-CS 08, 08A, 09, 10, 12	[19–21, 156]	$2+1$	Iwasaki	npSW
RBC/UKQCD 07, 08, 08A, 10, 10A-B, 11, 12	[25, 78, 79, 136, 242, 301, 303, 562]	$2+1$	Iwasaki, Iwasaki+DSDR	DW
TWQCD 08	[243]	$2+1$	Iwasaki	DW

Table 37: (cntd.) Summary of simulated lattice actions with $N_f = 2+1$ or $N_f = 2+1+1$ quark flavours.

Collab.	Ref.	N_f	Gauge action	Quark actions sea	light valence	heavy
ETM 09, 09D, 11B, 12A, 12B	[160, 326, 364, 365, 381]	2	tlSym	tmWil	tmWil	tmWil
ETM 11A	[320]	2	tlSym	tmWil	tmWil	tmWil, static
ALPHA 11, 12A	[337, 342]	2	plaquette	npSW	npSW	HQET
FNAL/MILC 04, 04A, 05, 08, 08A, 10, 11, 11A, 12	[316, 319, 330, 379, 382, 397, 408, 409, 413]	2+1	tadSym	Asqtad	Asqtad	Fermilab
FNAL/MILC 12B	[314]	2+1+1	tadSym	HISQ	HISQ	HISQ
HPQCD 06, 06A, 09	[373, 380, 396]	2+1	tadSym	Asqtad	Asqtad	NRQCD
HPQCD 12	[372]	2+1	tadSym	Asqtad	HISQ	NRQCD
HPQCD/UKQCD 07, HPQCD 10A, 10B, 11, 11A, 12A	[157, 315, 318, 321, 323, 338]	2+1	tadSym	Asqtad	HISQ	HISQ
HPQCD 13	[371]	2+1+1	tadSym	HISQ	HISQ	NRQCD
RBC/UKQCD 10C	[374]	2+1	Iwasaki	DWF	DWF	static
PACS-CS 11	[317]	2+1	Iwasaki	npSW	npSW	Tsukuba

Table 38: Summary of lattice simulations with b and c valence quarks.

B Notes

B.1 Notes to section 3 on quark masses

Collab.	Ref.	N_f	a [fm]	Description
RBC/UKQCD 12	[25]	2+1	0.144, 0.113, 0.085	Scale set through M_Ω. Coarsest lattice uses Iwasaki+DSDR gauge action.
PACS-CS 12	[76]	1+1+1	0.09	Reweighting of PACS-CS 08 $N_f = 2+1$ QCD configurations with e.m. and $m_u \neq m_d$.
Laiho 11	[77]	2+1	0.15,0.09,0.06	MILC staggered ensembles [75], scale set using r_1 determined by HPQCD with Υ splittings, pseudoscalar decay constants, through r_1 [175].
PACS-CS 10	[21]	2+1	0.09	cf. PACS-CS 08
MILC 10A	[75]	2+1		cf. MILC 09, 09A
BMW 10A, 10B	[22, 23]	2+1	0.116,0.093,0.077, 0.065,0.054	Scale setting via M_π, M_K, M_Ω.
RBC/UKQCD 10A	[78]	2+1	0.114, 0.087	Scale set through M_Ω.
Blum 10	[32]	2+1	0.11	Relies on RBC/UKQCD 08 scale setting.
PACS-CS 09	[20]	2+1	0.09	Scale setting via M_Ω.
HPQCD 09A, 10	[72, 73]	2+1		
MILC 09A, 09	[15, 37]	2+1	0.045, 0.06, 0.09	Scale set through r_1 and Υ and continuum extrapolation based on RSχPT.
PACS-CS 08	[19]	2+1	0.09	Scale set through M_Ω. Non-perturbatively $O(a)$-improved.
RBC/UKQCD 08	[79]	2+1	0.11	Scale set through M_Ω. Automatic $O(a)$-improvement due to appoximate chiral symmetry. $(\Lambda_{\rm QCD}a)^2 \approx 4\%$ systematic error due to lattice artifacts added.
CP-PACS/JLQCD 07	[80]	2+1	0.07,0.10,0.12	Scale set through M_K or M_ϕ. Non-perturbatively $O(a)$-improved.
HPQCD 05	[81]	2+1	0.09,0.12	Scale set through the $\Upsilon - \Upsilon'$ mass difference.
HPQCD/MILC/UKQCD 04, MILC 04	[36, 82]	2+1	0.09,0.12	Scale set through r_1 and Υ and continuum extrapolation based on RSχPT.

Table 39: Continuum extrapolations/estimation of lattice artifacts in determinations of m_{ud}, m_s and, in some cases m_u and m_d, with $N_f = 2+1$ quark flavours.

Collab.	Ref.	N_f	a [fm]	Description
RM123 13	[45]	2	0.098, 0.085, 0.067, 0.054	cf. ETM 10B
ALPHA 12	[59]	2	0.076, 0.066, 0.049	Scale set through F_K.
RM123 11	[102]	2	0.098, 0.085, 0.067, 0.054	cf. ETM 10B
Dürr 11	[61]	2	0.076, 0.072, 0.060	Scale for light quark masses set through m_c.
ETM 10B	[60]	2	0.098, 0.085, 0.067, 0.054	Scale set through F_π.
JLQCD/TWQCD 08A	[67]	2	0.12	Scale set through r_0.
RBC 07	[34]	2	0.12	Scale set through M_ρ.
ETM 07	[62]	2	0.09	Scale set through F_π.
QCDSF/UKQCD 06	[68]	2	0.065–0.09	Scale set through r_0.
SPQcdR 05	[69]	2	0.06,0.08	Scale set through M_{K^*}.
ALPHA 05	[64]	2	0.07-0.12	Scale set through r_0.
QCDSF/UKQCD 04	[66]	2	0.07-0.12	Scale set through r_0.
JLQCD 02	[70]	2	0.09	Scale set through M_ρ.
CP-PACS 01	[63]	2	0.11,0.16,0.22	Scale set through M_ρ.

Table 40: Continuum extrapolations/estimation of lattice artifacts in determinations of m_{ud}, m_s and, in some cases m_u and m_d, with $N_f = 2$ quark flavours.

Collab.	Ref.	N_f	$M_{\pi,\text{min}}$ [MeV]	Description
RBC/UKQCD 12	[25]	2+1	170	Combined fit to Iwasaki and Iwasaki+DSDR gauge action ensembles.
PACS-CS 12	[76]	1+1+1		cf. PACS-CS 08
Laiho 11	[77]	2+1	210 (val.) 280 (sea-RMS)	NLO SU(3), mixed-action χPT [463], with $\mathrm{N^2LO}$-$\mathrm{N^4LO}$ analytic terms.
PACS-CS 10	[21]	2+1		cf. PACS-CS 08
MILC 10A	[75]	2+1		NLO SU(2) SχPT. Cf. also MILC 09A,09.
BMW 10A, 10B	[22, 23]	2+1	135	Interpolation to the physical point.
RBC/UKQCD 10A	[78]	2+1	290	
Blum 10	[32, 79]	2+1	242 (valence), 330 (sea)	Extrapolation done on the basis of PQχPT formulae with virtual photons.
PACS-CS 09	[20]	2+1	135	Physical point reached by reweighting technique, no chiral extrapolation needed.
HPQCD 09A, 10	[72, 73]	2+1		
MILC 09A, 09	[15, 37]	2+1	177, 240	NLO SU(3) RSχPT, continuum χPT at NNLO and NNNLO and NNNNLO analytic terms. The lightest Nambu-Goldstone mass is 177 MeV (09A) and 224 MeV (09) (at a =0.09fm) and the lightest RMS mass is 258MeV (at a =0.06fm).
PACS-CS 08	[19]	2+1	156	NLO SU(2) χPT and SU(3) (Wilson)χPT.
RBC/UKQCD 08	[79]	2+1	242 (valence), 330 (sea)	SU(3) PQχPT and heavy kaon NLO SU(2) PQχPT fits.
CP-PACS/JLQCD 07	[80]	2+1	620	NLO Wilson χPT fits to meson masses.
HPQCD 05	[81]	2+1	240	PQ RSχPT fits.
HPQCD/MILC/UKQCD 04, MILC 04	[36, 82]	2+1	240	PQ RSχPT fits.

Table 41: Chiral extrapolation/minimum pion mass in determinations of m_{ud}, m_s and, in some cases m_u and m_d, with $N_f = 2+1$ quark flavours.

Collab.	Ref.	N_f	$M_{\pi,\text{min}}$ [MeV]	Description
RM123 13	[45]	2	270	Fits based on NLO χPT and Symanzik expansion up to $O(a^2)$. $O(\alpha)$ e.m. effects included.
ALPHA 12	[59]	2	270	NLO SU(2) and SU(3) χPT and $O(a^2)$ on LO LEC.
RM123 11	[102]	2	270	Fits based on NLO χPT and Symanzik expansion up to $O(a^2)$.
Dürr 11	[61]	2	285	m_c/m_s determined by quadratic or cubic extrapolation in M_π.
ETM 10B	[60]	2	270	Fits based on NLO χPT and Symanzik expansion up to $O(a^2)$.
JLQCD/TWQCD 08A	[67]	2	290	NLO χPT fits.
RBC 07	[34]	2	440	NLO fit including $O(\alpha)$ effects.
ETM 07	[62]	2	300	Polynomial and PQχPT fits.
QCDSF/UKQCD 06	[68]	2	520 (valence), 620 (sea)	NLO (PQ)χPT fits.
SPQcdR 05	[69]	2	600	Polynomial fit.
ALPHA 05	[64]	2	560	LO χPT fit.
QCDSF/UKQCD 04	[66]	2	520 (valence), 620 (sea)	NLO (PQ)χPT fits.
JLQCD 02	[70]	2	560	Polynomial and χPT fits.
CP-PACS 01	[63]	2	430	Polynomial fits.

Table 42: Chiral extrapolation/minimum pion mass in determinations of m_{ud}, m_s and, in some cases m_u and m_d, with $N_f = 2$ quark flavours.

Collab.	Ref.	N_f	L [fm]	$M_{\pi,\min}L$	Description
RBC/UKQCD 12	[25]	2+1	2.7, 4.6	$\gtrsim 4.0$	Uses FV chiral perturbation theory to estimate the error.
PACS-CS 12	[76]	1+1+1			cf. PACS-CS 08
Laiho 11	[77]	2+1	2.5, 2.9, 3.0, 3.6, 3.8, 4.8	4.1 (val.) 4.1 (sea)	Data corrected using NLO SU(3) χPT finite-V formulae.
PACS-CS 10	[21]	2+1			cf. PACS-CS 08
MILC 10A	[75]	2+1			cf. MILC 09A,09
BMW 10A, 10B	[22, 23]	2+1	$\gtrsim 5.0$	$\gtrsim 4.0$	FS corrections below 5 per mil on the largest lattices.
RBC/UKQCD 10A	[78]	2+1	2.7	$\gtrsim 4.0$	
Blum 10	[32]	2+1	1.8, 2.7	—	Simulations done with quenched photons; large finite volume effects analytically corrected for, but not related to $M_\pi L$.
PACS-CS 09	[20]	2+1	2.9	2.0	Only one volume.
HPQCD 09A, 10	[72, 73]	2+1			
MILC 09A, 09	[15, 37]	2+1	2.5, 2.9, 3.4, 3.6, 3.8, 5.8	4.1, 3.8	
PACS-CS 08	[19]	2+1	2.9	2.3	Correction for FSE from χPT using [563].
RBC/UKQCD 08	[79]	2+1	1.8, 2.7	4.6	Various volumes for comparison and correction for FSE from χPT [178, 179, 563].
CP-PACS/JLQCD 07	[80]	2+1	2.0	6.0	Estimate based on the comparison to a $L = 1.6$ fm volume assuming powerlike dependence on L.
HPQCD 05	[81]	2+1	2.4, 2.9	3.5	
HPQCD/MILC/UKQCD 04, MILC 04	[36, 82]	2+1	2.4, 2.9	3.5	NLO SχPT.

Table 43: Finite volume effects in determinations of m_{ud}, m_s and, in some cases m_u and m_d, with $N_f = 2+1$ quark flavours.

Collab.	Ref.	N_f	L [fm]	$M_{\pi,\min}L$	Description
RM123 13	[45]	2	$\gtrsim 2.0$	3.5	One volume $L = 1.7$ fm at $m_\pi = 495$, $a = 0.054$fm.
ALPHA 12	[59]	2	2.1–3.2	4.2	Roughly 2 distinct volumes; no analysis of FV effects.
RM123 11	[102]	2	$\gtrsim 2.0$	3.5	One volume $L = 1.7$ fm at $m_\pi = 495$, $a = 0.054$fm.
Dürr 11	[61]	2	1.22-2.30	2.8	A number of volumes in determination of m_c/m_s, but all but one have $L < 2$ fm.
ETM 10B	[60]	2	$\gtrsim 2.0$	3.5	One volume $L = 1.7$ fm at $m_\pi = 495$, $a = 0.054$fm.
JLQCD/TWQCD 08A	[67]	2	1.9	2.8	Corrections for FSE based on NLO χPT.
RBC 07	[34]	2	1.9	4.3	Estimate of FSE based on a model.
ETM 07	[62]	2	2.1	3.2	NLO PQχPT
QCDSF/UKQCD 06	[68]	2	1.4–1.9	4.7	
SPQcdR 05	[69]	2	1.0–1.5	4.3	Comparison between 1.0 and 1.5 fm.
ALPHA 05	[64]	2	2.6	7.4	
QCDSF/UKQCD 04	[66]	2	1.7–2.0	4.7	
JLQCD 02	[70]	2	1.8	5.1	Numerical study with three volumes.
CP-PACS 01	[63]	2	2.0–2.6	5.7	

Table 44: Finite volume effects in determinations of m_{ud}, m_s and, in some cases m_u and m_d, with $N_f = 2$ quark flavours.

Collab.	Ref.	N_f	Description
RBC/UKQCD 12	[25]	2+1	Non-perturbative renormalization (RI/SMOM).
PACS-CS 12	[76]	1+1+1	cf. PACS-CS 10
Laiho 11	[77]	2+1	Z_A from AWI and $Z_A/Z_S - 1$ from 1-loop, tadpole-improved, perturbation theory.
PACS-CS 10	[21]	2+1	Non-perturbative renormalization and running; Schrödinger functional method.
MILC 10A	[75]	2+1	cf. MILC 09A,09
BMW 10A, 10B	[22, 23]	2+1	Non-perturbative renormalization (tree-level improved RI-MOM), non-perturbative running.
RBC/UKQCD 10A	[78]	2+1	Non-perturbative renormalization (RI/SMOM).
Blum 10	[32]	2+1	Relies on non-perturbative renormalization factors calculated by RBC/UKQCD 08; no QED renormalization.
PACS-CS 09	[20]	2+1	Non-perturbative renormalization; Schrödinger functional method.
HPQCD 09A, 10	[72, 73]	2+1	Lattice calculation of m_s/m_c: m_s derived from a perturbative determination of m_c.
MILC 09A, 09	[15, 37]	2+1	2-loop perturbative renormalization.
PACS-CS 08	[19]	2+1	1-loop perturbative renormalization.
RBC/UKQCD 08	[79]	2+1	Non-perturbative renormalization, 3-loop perturbative matching.
CP-PACS/JLQCD 07	[80]	2+1	1-loop perturbative renormalization, tadpole improved.
HPQCD 05	[81]	2+1	2-loop perturbative renormalization.
HPQCD/MILC/UKQCD 04, MILC 04	[36, 82]	2+1	1-loop perturbative renormalization.

Table 45: Renormalization in determinations of m_{ud}, m_s and, in some cases m_u and m_d, with $N_f = 2+1$ quark flavours.

Collab.	Ref.	N_f	Description
RM123 13	[45]	2	Non-perturbative renormalization.
ALPHA 12	[59]	2	Non-perturbative renormalization.
RM123 11	[102]	2	Non-perturbative renormalization.
Dürr 11	[61]	2	Lattice calculation of m_s/m_c: m_s derived from a perturbative determination of m_c.
ETM 10B	[60]	2	Non-perturbative renormalization.
JLQCD/TWQCD 08A	[67]	2	Non-perturbative renormalization.
RBC 07	[34]	2	Non-perturbative renormalization.
ETM 07	[62]	2	Non-perturbative renormalization.
QCDSF/UKQCD 06	[68]	2	Non-perturbative renormalization.
SPQcdR 05	[69]	2	Non-perturbative renormalization.
ALPHA 05	[64]	2	Non-perturbative renormalization.
QCDSF/UKQCD 04	[66]	2	Non-perturbative renormalization.
JLQCD 02	[70]	2	1-loop perturbative renormalization.
CP-PACS 01	[63]	2	1-loop perturbative renormalization.

Table 46: Renormalization in determinations of m_{ud}, m_s and, in some cases m_u and m_d, with $N_f = 2$ quark flavours.

B.2 Notes to section 4 on $|V_{ud}|$ and $|V_{us}|$

Collab.	Ref.	N_f	a [fm]	Description
MILC 12	[133]	2+1	0.09, 0.12	Relative scale r_1, physical scale determined from a mixture of f_π, f_K, radial excitation of Υ and $m_{D_s} - \frac{1}{2}m_{\eta_c}$.
JLQCD 12	[134]	2+1	0.112	Scale set through Ω mass.
JLQCD 11	[135]	2+1	0.112	Scale set through Ω mass.
RBC/UKQCD 07,10	[136, 137]	2+1	0.114(2)	Scale fixed through Ω baryon mass. Add $(\Lambda_{\rm QCD}a)^2 \approx 4\%$ systematic error for lattice artifacts. Fifth dimension with extension $L_s = 16$, therefore small residual chiral symmetry breaking and approximate $O(a)$-improvement.
ETM 10D	[138]	2	0.05, 0.07, 0.09, 0.10	Scale set through F_π. Automatic $O(a)$ impr., flavour symmetry breaking: $(M_{PS}^0)^2 - (M_{PS}^\pm)^2 \sim O(a^2)$.
ETM 09A	[139]	2	0.07, 0.09, 0.10	Scale set through F_π. Automatic $O(a)$ impr., flavour symmetry breaking: $(M_{PS}^0)^2 - (M_{PS}^\pm)^2 \sim O(a^2)$. Three lattice spacings only for pion mass 470 MeV.
QCDSF 07	[140]	2	0.075	Scale set with r_0. Non-perturbatively $O(a)$-improved Wilson fermions, not clear whether currents improved.
RBC 06	[141]	2	0.12	Scale set through M_ρ. Automatic $O(a)$-improvement due to approximate chiral symmetry of the action.
JLQCD 05	[142]	2	0.0887	Scale set through M_ρ. Non-perturbatively $O(a)$-improved Wilson fermions.

Table 47: Continuum extrapolations/estimation of lattice artifacts in determinations of $f_+(0)$.

Collab.	Ref.	N_f	$M_{\pi,\text{min}}$ [MeV]	Description
MILC 12	[133]	2+1	$378_{\text{RMS}}(263_{\pi,5})$	NLO SU(3) PQ staggered χPT with either phenomenological NNLO ansatz or NNLO χPT. Lightest Nambu-Goldstone mass is 263 MeV with $a = 0.12$ fm and lightest RMS mass is 378 MeV with $a = 0.09$ fm.
JLQCD 12	[134]	2+1	290	NLO SU(3) χPT with phenomenological ansatz for higher orders.
JLQCD 11	[135]	2+1	290	NLO SU(3) χPT with phenomenological ansatz for higher orders.
RBC/UKQCD 07,10	[136, 137]	2+1	330	NLO SU(3) χPT with phenomenological ansatz for higher orders.
ETM 10D	[138]	2	$210_{\pi^0}(260_{\pi^\pm})$	NLO heavy kaon SU(2) χPT and NLO SU(3) χPT and phenomenological ansatz for higher orders. Average of $f_+(0)$-fit and joint $f_+(0)$-f_K/f_π-fit.
ETM 09A	[139]	2	$210_{\pi^0}(260_{\pi^\pm})$	NLO heavy kaon SU(2) χPT and NLO SU(3) χPT and phenomenological ansatz for higher orders.
QCDSF 07	[140]	2	591	Only one value for the pion mass.
RBC 06	[141]	2	490	NLO SU(3) χPT and phenomenological ansatz for higher orders.
JLQCD 05	[142]	2	550	NLO SU(3) χPT and phenomenological ansatz for higher orders.

Table 48: Chiral extrapolation/minimum pion mass in determinations of $f_+(0)$. The subscripts RMS and $\pi, 5$ in the case of staggered fermions indicate the root-mean-square mass and the Nambu-Goldstone boson mass, respectively. In the case of twisted-mass fermions π^0 and $\pi^\pm$ indicated the neutral and charged pion mass where applicable.

Collab.	Ref.	N_f	L [fm]	$M_{\pi,\mathrm{min}}L$	Description
MILC 12	[133]	2+1	2.4–3.4	$6.2_{\mathrm{RMS}}(3.8_{\pi,5})$	The values correspond to $M_{\pi,\mathrm{RMS}} = 378$ MeV and $M_{\pi,5} = 263$ MeV, respectively.
JLQCD 12	[134]	2+1	1.8, 2.7	4.1	
JLQCD 11	[135]	2+1	1.8, 2.7	4.1	
RBC/UKQCD 07,10	[136, 137]	2+1	1.8,2.7	4.7	Two volumes for all but the lightest pion mass.
ETM 10D	[138]	2	2.1–2.8	$3.0_{\pi^0}(3.7_{\pi^\pm})$	
ETM 09A	[139]	2	2.1, 2.8	$3.0_{\pi^0}(3.7_{\pi^\pm})$	Two volumes at $M_\pi = 300\,\mathrm{MeV}$ and χPT-motivated estimate of the error due to FSE.
QCDSF 07	[140]	2	1.9	5.4	
RBC 06	[141]	2	1.9	4.7	
JLQCD 05	[142]	2	1.8	4.9	

Table 49: Finite volume effects in determinations of $f_+(0)$. The subscripts RMS and $\pi, 5$ in the case of staggered fermions indicate the root-mean-square mass and the Nambu-Goldstone boson mass, respectively. In the case of twisted-mass fermions π^0 and $\pi^\pm$ indicated the neutral and charged pion mass where applicable.

Collab.	Ref.	N_f	a [fm]	Description
HPQCD 13A	[148]	2+1+1	0.09, 0.12, 0.15	Relative scale through Wilson flow and absolute scale though f_π.
MILC 13	[149]	2+1+1	0.06, 0.09, 0.12, 0.15	Absolute scale though f_π.
ETM 10E	[150]	2+1+1	0.061, 0.078	Scale set through f_π/m_π. Two lattice spacings but a-dependence ignored in all fits. Finer lattice spacing from [253].
MILC 11	[24]	2+1+1	0.12, 0.09	Relative scale through $f_{\rm PS}/m_{\rm PS}$ = fixed, absolute scale though f_π.
RBC/UKQCD 12	[25]	2+1	0.09, 0.11, 0.14	scale though m_Ω.
LAIHO 11	[77]	2+1	0.125, 0.09, 0.06	Scale set through r_1 and Υ and continuum extrapolation based on MAχPT.
JLQCD/TWQCD 10	[152]	2+1	0.112	Scale set through M_Ω.
RBC/UKQCD 10A	[78]	2+1	0.114, 0.087	Scale set through M_Ω.
MILC 10	[151]	2+1	0.09, 0.06, 0.045	3 lattice spacings, continuum extrapolation by means of RSχPT.
BMW 10	[153]	2+1	0.07, 0.08, 0.12	Scale set through $M_{\Omega,\Xi}$. Perturbative $O(a)$-improvement.
JLQCD/TWQCD 09A	[67]	2+1	0.1184(3)(21)	Scale set through F_π. Automatic $O(a)$-improvement due to chiral symmetry of action.
PACS-CS 09	[20]	2+1	0.0900(4)	Scale set through M_Ω.
MILC 09A	[37]	2+1	0.045, 0.06, 0.09	Scale set through r_1 and Υ and continuum extrapolation based on RSχPT.
MILC 09	[15]	2+1	0.045, 0.06, 0.09, 0.12	Scale set through r_1 and Υ and continuum extrapolation based on RSχPT.
Aubin 08	[155]	2+1	0.09, 0.12	Scale set through r_1 and Υ and continuum extrapolation based on MAχPT.
PACS-CS 08, 08A	[19, 156]	2+1	0.0907(13)	Scale set through M_Ω. Non-perturbatively $O(a)$-improved.
HPQCD/UKQCD 07	[157]	2+1	0.09, 0.12, 0.15	Scale set through r_1 and Υ and continuum extrapolation on continuum-χPT motivated ansatz. Taste breaking of sea quarks ignored.
RBC/UKQCD 08	[79]	2+1	0.114(2)	Scale set through M_Ω. Automatic $O(a)$-improvement due to appoximate chiral symmetry. $(\Lambda_{\rm QCD}a)^2 \approx 4\%$ systematic error due to lattice artifacts added.
NPLQCD 06	[158]	2+1	0.125	Scale set through r_0 and F_π. Taste breaking of sea quarks ignored.
ETM 10D	[138]	2	0.05, 0.07, 0.09, 0.10	Scale set through F_π. Automatic $O(a)$ impr., flavour symmetry breaking: $(M_{PS}^0)^2-(M_{PS}^\pm)^2 \sim O(a^2)$.
ETM 09	[160]	2	0.07, 0.09, 0.10	Scale set through F_π. Automatic $O(a)$ impr., flavour symmetry breaking: $(M_{PS}^0)^2-(M_{PS}^\pm)^2 \sim O(a^2)$.
QCDSF/UKQCD 07	[161]	2	0.06, 0.07	Scale set through F_π. Non-perturbative $O(a)$-improvement.

Table 50: Continuum extrapolations/estimation of lattice artifacts in determinations of $f_K/f\pi$.

Collab.	Ref.	N_f	$M_{\pi,\rm min}$ [MeV]	Description
HPQCD 13A	[148]	2+1+1	$173_{\rm RMS}(128_{\pi,5})$	NLO χPT supplemented by model for NNLO. Both the lightest RMS and the lightest Nambu-Goldstone mass are from the $a = 0.09$ fm ensemble.
MILC 13	[149]	2+1+1	$143_{\rm RMS}(128_{\pi,5})$	Linear interpolation to physical point. The lightest RMS mass is from the $a = 0.06$ fm ensemble and the lightest Nambu-Goldstone mass is from the $a = 0.09$ fm ensemble.
ETM 10E	[150]	2+1+1	$215_{\pi^0}(265_{\pi^\pm})$	
MILC 11	[24]	2+1+1	$173_{\rm RMS}(128_{\pi,5})$	Quoted result from polynomial interpolation to the physical point. The lightest RMS mass is from the $a = 0.06$ fm ensemble and lightest the Nambu-Goldstone mass is from the $a = 0.09$ fm ensemble.

Table 51: Chiral extrapolation/minimum pion mass in determinations of $f_K/f\pi$ for $N_f = 2+1+1$ simulations. The subscripts RMS and $\pi, 5$ in the case of staggered fermions indicate the root-mean-square mass and the Nambu-Goldstone boson mass. In the case of twisted-mass fermions π^0 and $\pi^\pm$ indicated the neutral and charged pion mass and where applicable, "val" and "sea" indicate valence and sea pion masses.

Collab.	Ref.	N_f	$M_{\pi,\mathrm{min}}$ [MeV]	Description
RBC/UKQCD 12	[25]	2+1	171_{sea}, 143_{val}	NLO PQ SU(2) χPT as well as analytic ansätze.
LAIHO 11	[77]	2+1	$250_{\mathrm{RMS}}(220_{\pi,5})$	NLO MAχPT
JLQCD/TWQCD 10	[152]	2+1	290	NNLO χPT
RBC/UKQCD 10A	[78]	2+1	290	Results are based on heavy kaon NLO SU(2) PQχPT.
MILC 10	[151]	2+1	$258_{\mathrm{RMS}}(177_{\pi,5})$	Lightest Nambu-Goldstone mass is 177 MeV (at 0.09 fm) and lightest RMS mass is 258 MeV (at 0.06 fm). NLO rSχPT and NNLO χPT.
BMW 10	[153]	2+1	190	Comparison of various fit-ansätze: SU(3) χPT, heavy kaon SU(2) χPT, polynomial.
JLQCD/TWQCD 09A	[67]	2+1	290	NNLO SU(3) χPT.
PACS-CS 09	[20]	2+1	156	NNLO χPT
MILC 09A	[37]	2+1	$258_{\mathrm{RMS}}(177_{\pi,5})$	NLO SU(3) RSχPT, continuum χPT at NNLO and up to NNNNLO analytic terms. Heavy kaon SU(2) RSχPT with NNLO continuum chiral logs on a sub-set of the lattices. The lightest Nambu-Goldstone mass is 177 MeV (at $a = 0.09$ fm) and the lightest RMS mass is 258 MeV (at $a = 0.06$ fm).
MILC 09	[15]	2+1	$258_{\mathrm{RMS}}(224_{\pi,5})$	NLO SU(3) RSχPT with continuum χPT NNLO and NNNLO analytic terms added. According to [37] the lightest sea Nambu-Goldstone mass is 224 MeV and the lightest RMS mass is 258 MeV (at $a = 0.06$ fm).
Aubin 08	[155]	2+1	$329_{\mathrm{RMS}}(246_{\pi,5})$	NLO MAχPT. According to [37] the lightest sea Nambu-Goldstone mass is 246 MeV (at $a = 0.09$ fm) and the lightest RMS mass is 329 MeV (at $a = 0.09$ fm).
PACS-CS 08, 08A	[19, 156]	2+1	156	NLO SU(2) χPT and SU(3) (Wilson)χPT.
HPCD/UKQCD 07	[157]	2+1	$375_{\mathrm{RMS}}(263_{\pi,5})$	NLO SU(3) chiral perturbation theory with NNLO and NNNLO analytic terms. The lightest RMS mass is from the $a = 0.09$ fm ensemble and the lightest Nambu-Goldstone mass is from the $a = 0.12$ fm ensemble.
RBC/UKQCD 08	[79]	2+1	330_{sea}, 242_{val}	While SU(3) PQχPT fits were studied, final results are based on heavy kaon NLO SU(2) PQχPT.
NPLQCD 06	[158]	2+1	300	NLO SU(3) χPT and some NNLO terms. The sea RMS mass for the employed lattices is heavier.
ETM 10D	[138]	2	$210_{\pi^0}(260_{\pi^\pm})$	NLO SU(3) χPT and phenomenological ansatz for higher orders. Joint $f_+(0)$-f_K/f_π-fit.
ETM 09	[160]	2	$210_{\pi^0}(260_{pi^\pm})$	NLO heavy meson SU(2) χPT and NLO SU(3) χPT.
QCDSF/UKQCD 07	[161]	2	300	Linear extrapolation of lattice data.

Table 52: Chiral extrapolation/minimum pion mass in determinations of $f_K/f\pi$ for $N_f = 2{+}1$ and $N_f = 2$ simulations. The subscripts RMS and $\pi, 5$ in the case of staggered fermions indicate the root-mean-square mass and the Nambu-Goldstone boson mass. In the case of twisted-mass fermions π^0 and $\pi^\pm$ indicated the neutral and charged pion mass and where applicable, “val” and “sea” indicate valence and sea pion masses.

Collab.	Ref.	N_f	L [fm]	$M_{\pi,\min}L$	Description
HPQCD 13A	[148]	2+1+1	2.5-5.8	$4.9_{\rm RMS}(3.7_{\pi,5})$	
MILC 13	[149]	2+1+1	2.8-5.8	$3.9_{\rm RMS}(3.7_{\pi,5})$	
ETM 10E	[150]	2+1+1	1.9 - 2.9	$3.1_{\pi^0}(3.9_{\pi^\pm})$	Simulation parameters from [253, 564].
MILC 11	[24]	2+1+1	5.6, 5.7	$4.9_{\rm RMS}(3.7_{\pi,5})$	
RBC/UKQCD 12	[25]	2+1	2.7, 4.6	3.3	For partially quenched $M_\pi = 143$MeV, $M_\pi L = 3.3$ and for unitary $M_\pi = 171$MeV, $M_\pi L = 4.0$.
LAIHO 11	[77]	2+1	2.5–4.0	$4.9_{\rm RMS}(4.3_{\pi,5})$	
JLQCD/TWQCD 10	[152]	2+1	1.8, 2.7	4.0	
RBC/UKQCD 10A	[78]	2+1	2.7	4.0	$M_\pi L = 4.0$ for lightest sea quark mass and $M_\pi L = 3.1$ for lightest partially quenched quark mass.
MILC 10	[151]	2+1	2.5-3.8	$7.0_{\rm RMS}(4.0_{\pi,5})$	$L \geq 2.9$ fm for the lighter masses.
BMW 10	[153]	2+1	2.0–5.3	4.0	Various volumes for comparison and correction for FSE from χPT using [563].
JLQCD/TWQCD 09A	[67]	2+1	1.9	2.8	Estimate of FSE using χPT [563, 565]
PACS-CS 09	[20]	2+1	2.9	2.28	after reweighting to the physical point $M_{\pi,\min}L = 1.97$
MILC 09A	[37]	2+1	2.5–5.8	$7.0_{\rm RMS}(4.1_{\pi,5})$	
MILC 09	[15]	2+1	2.4–5.8	$7.0_{\rm RMS}(4.8_{\pi,5})$	Various volumes for comparison and correction for FSEs from (RS)χPT [563].
Aubin 08	[155]	2+1	2.4–3.6	4.0	Correction for FSE from MAχPT.
PACS-CS 08, 08A	[19, 156]	2+1	2.9	2.3	Correction for FSE from χPT using [563].
HPCD/UKQCD 07	[157]	2+1	2.4–2.9	$4.1_{\rm RMS}(3.8_{\pi,5})$	Correction for FSE from χPT using [563].
RBC/UKQCD 08	[79]	2+1	1.8, 2.7	$4.6_{\rm sea}$, 3.4_{rval}	Various volumes for comparison and correction for FSE from χPT [178, 179, 563].
NPLQCD 06	[158]	2+1	2.5	3.8	Correction for FSE from SχPT [456, 547]
ETM 10D	[138]	2	2.1–2.8	$3.0_{\pi^0}(3.7_{\pi^\pm})$	
ETM 09	[160]	2	2.0–2.7	$3.0_{\pi^0}(3.7_{\pi^\pm})$	Correction for FSE from χPT [178, 179, 563].
QCDSF/UKQCD 07	[161]	2	1.4,. . . ,2.6	4.2	Correction for FSE from χPT

Table 53: Finite volume effects in determinations of $f_K/f\pi$. The subscripts RMS and $\pi,5$ in the case of staggered fermions indicate the root-mean-square mass and the Nambu-Goldstone boson mass. In the case of twisted-mass fermions π^0 and $\pi^\pm$ indicated the neutral and charged pion mass and where applicable, "val" and "sea" indicate valence and sea pion masses.

B.3 Notes to section 5 on Low-Energy Constants

Collab.	Ref.	N_f	a [fm]	Description
HPQCD 13A	[148]	2+1+1	0.09–0.15	Configurations are shared with MILC.
ETM 13	[206]	2+1+1	0.0607–0.0863	Configurations are shared with ETM 11.
ETM 11	[253]	2+1+1	0.0607–0.0863	Three lattice spacings fixed through F_π/M_π.
ETM 10	[96]	2+1+1	0.078, 0.086	Two lattice spacings fixed through F_π/M_π.
Borsanyi 12	[238]	2+1	0.097–0.284	Scale fixed through F_π/M_π.
NPLQCD 11	[254]	2+1	0.09, 0.125	Configurations are shared with MILC 09 [15].
MILC 10, 10A	[75, 151]	2+1	0.045 - 0.09	3 lattice spacings, continuum extrapolation by means of RSχPT.
JLQCD/TWQCD 10	[241]	2+1, 3	0.11	One lattice spacing, scale fixed through m_Ω.
RBC/UKQCD 9, 10A	[78, 273]	2+1	0.1106(27), 0.0888(12)	Two lattice spacings. Data combined in global chiral-continuum fits.
JLQCD 09	[240]	2+1	0.1075(7)	Scale fixed through r_0.
MILC 09, 09A	[15, 37]	2+1	0.045 - 0.18	Total of 6 lattice spacings, continuum extrapolation by means of RSχPT.
TWQCD 08	[243]	2+1	0.122(3)	Scale fixed through m_ρ, r_0.
JLQCD/TWQCD 08B	[244]	2+1	0.1075(7)	Scale fixed through r_0.
PACS-CS 08	[19]	2+1	0.0907	One lattice spacing.
RBC/UKQCD 08	[79]	2+1	0.114	One lattice spacing, attempt to estimate cut-off effects via formal argument.
RBC/UKQCD 08A	[242]	2+1	0.114	Only one lattice spacing, attempt to estimate size of cut-off effects via formal argument.
NPLQCD 06	[158]	2+1	0.125	One lattice spacing, continuum χPT used.
LHP 04	[261]	2+1	$\simeq 0.12$	Only one lattice spacing, mixed discretization approach.

Table 54: Continuum extrapolations/estimation of lattice artifacts in $N_f = 2+1+1$ and $2+1$ determinations of the Low-Energy Constants.

Collab.	Ref.	N_f	a [fm]	Description
ETM 13	[206]	2	0.05–0.1	Configurations are shared with ETM 09C.
ETM 12	[245]	2	0.05–0.1	Configurations are shared with ETM 09C.
Bernardoni 11	[246]	2	0.0649(10)	Configurations are shared with CLS.
TWQCD 11	[174]	2	0.1034(1)(2)	Scale fixed through r_0.
TWQCD 11A	[247]	2	0.1032(2)	Scale fixed through r_0.
Bernardoni 10	[248]	2	0.0784(10)	Scale fixed through M_K. Non-perturbative $O(a)$ improvement. No estimate of systematic error.
JLQCD/TWQCD 09, 10	[241]	2	0.11	One lattice spacing fixed through r_0.
ETM 09B	[250]	2	0.063, 0.073	Automatic $O(a)$ impr. $r_0 = 0.49\,\mathrm{fm}$ used.
ETM 09C	[230]	2	0.051 - 0.1	Automatic $O(a)$ impr. Scale fixed through F_π. 4 lattice spacings, continuum extrapolation.
ETM 08	[227]	2	0.07-0.09	Automatic $O(a)$ impr. Two lattice spacings. Scale fixed through F_π.
JLQCD/TWQCD 08A JLQCD 08A	[67] [272]	2	0.1184(3)(21)	Automatic $O(a)$ impr., exact chiral symmetry. Scale fixed through r_0.
CERN 08	[204]	2	0.0784(10)	Scale fixed through M_K. Non-perturbative $O(a)$ improvement.
Hasenfratz 08	[251]	2	0.1153(5)	Tree level $O(a)$ improvement. Scale fixed through r_0. Estimate of lattice artifacts via WχPT [566].
JLQCD/TWQCD 07	[252]	2	0.1111(24)	Automatic $O(a)$ impr., exact chiral symmetry. Scale fixed through r_0.
JLQCD/TWQCD 07A	[249]	2	$\simeq 0.12$	Automatic $O(a)$ impr., exact chiral symmetry. Scale fixed through r_0.
CERN-TOV 06	[258]	2	0.0717(15), 0.0521(7), 0.0784(10)	Scale fixed through M_K. The lattice with $a = 0.0784(10)$ is obtained with non-perturbative $O(a)$ improvement.
QCDSF/UKQCD 06A	[262]	2	0.07-0.115	5 lattice spacings. Non-perturbative $O(a)$ improvement. Scale fixed through r_0.

Table 55: Continuum extrapolations/estimation of lattice artifacts in $N_f = 2$ determinations of the Low-Energy Constants.

Collab.	Ref.	N_f	$M_{\pi,\text{min}}$ [MeV]	Description
HPQCD 13A	[148]	2+1+1	128	NLO chiral fit.
ETM 13	[206]	2+1+1	270	Linear fit in the quark mass.
ETM 11	[253]	2+1+1	270	NLO SU(2) chiral fit.
ETM 10	[96]	2+1+1	270	SU(2) NLO and NNLO fits.
Borsanyi 12	[238]	2+1	135	NNLO SU(2) chiral fit.
NPLQCD 11	[254]	2+1	235	NNLO SU(2) mixed action χPT.
MILC 10, 10A	[75, 151]	2+1		Cf. MILC 09A.
JLQCD/TWQCD 09, 10	[241]	2+1,3	100(ϵ-reg.), 290(p-reg.)	The $N_f = 2+1$ runs both in the ϵ- and p-regimes. The $N_f = 3$ runs only in the p-regime. NLO χPT fit of the spectral density interpolating the two regimes.
RBC/UKQCD 9, 10A	[78, 273]	2+1	290-420	Valence pions mass is 225-420 MeV. NLO SU(2) χPT fit.
MILC 09, 09A	[15]	2+1	258	Lightest Nambu-Goldstone mass is 224 MeV and lightest RMS mass is 258 MeV (at 0.06 fm).
TWQCD 08	[243]	2+1	$m_{ud} = m_s/4$, $m_s \sim$ phys.	Quark condensate extracted from topological susceptibility, LO chiral fit.
JLQCD/TWQCD 08B	[244]	2+1	$m_{ud} = m_s/6 - m_s$, $m_s \sim$ phys.	Quark condensate extracted from topological susceptibility, LO chiral fit.
PACS-CS 08	[19]	2+1	156	To date, lightest published quark mass reached in a direct simulation.
RBC/UKQCD 08	[79]	2+1	330	Lightest velence pion mass is 242 MeV.
RBC/UKQCD 08A	[242]	2+1	330	Pion electromagnetic form factor computed at one pion mass.
NPLQCD 06	[158]	2+1	460	Value refers to lightest RMS mass at $a = 0.125$ fm as quoted in [37].
LHP 04	[261]	2+1	318	Pion form factor extracted from vector meson dominance fit.

Table 56: Chiral extrapolation/minimum pion mass in $N_f = 2{+}1{+}1$ and $2{+}1$ determinations of the Low-Energy Constants.

Collab.	Ref.	N_f	$M_{\pi,\text{min}}$ [MeV]	Description
ETM 13	[206]	2	260	Configurations are shared with ETM 09C.
ETM 12	[245]	2	260	Configurations are shared with ETM 09C.
Bernardoni 11	[246]	2	312	Overlap varence + O(a) improved Wilson sea, mixed regime χPT.
TWQCD 11	[174]	2	230	NLO SU(2) χPT fit.
TWQCD 11A	[247]	2	220	NLO χPT (infinite V) for topological susceptibility χ_{top}.
Bernardoni 10	[248]	2	297, 377, 426	NLO SU(2) fit of χ_{top}.
JLQCD/TWQCD 10	[241]	2	$\sqrt{2m_{\text{min}}\Sigma}/F$=120 ($\epsilon$-reg.), 290 ($p$-reg.)	Data both in the p and ϵ-regime. NLO chiral fit of the spectral density interpolating the two regimes.
JLQCD/TWQCD 09	[257]	2	290	LECs extracted from NNLO chiral fit of vector and scalar radii $\langle r^2\rangle^{\pi}_{V,S}$.
ETM 09B	[250]	2	$\sqrt{2m_{\text{min}}\Sigma}/F$=85	NLO SU(2) ϵ-regime fit.
ETM 09C	[230]	2	280	NNLO SU(2) fit.
ETM 08	[227]	2	260	From pion form factor using NNLO χPT and exp. value of $\langle r^2\rangle^{\pi}_{S}$.
JLQCD/TWQCD 08A JLQCD 08A	[67] [272]	2	290	NNLO SU(2) fit.
CERN 08	[204]	2	$m_{q,\text{min}}$=13 MeV	NLO SU(2) fit for the mode number.
Hasenfratz 08	[251]	2	$\sqrt{2m_{\text{min}}\Sigma}/F$=220	NLO SU(2) ϵ-regime fit.
JLQCD/TWQCD 07	[252]	2	$\sqrt{2m_{\text{min}}\Sigma}/F$=120	NLO SU(2) ϵ-regime fit.
JLQCD/TWQCD 07A	[249]	2	$m_{ud} = m_s/6 - m_s$	Quark condensate from topological susceptibility, LO chiral fit.
CERN-TOV 06	[258]	2	403, 381, 377	NLO SU(2) fit.
QCDSF/UKQCD 06A	[262]	2	400	Several fit functions to extrapolate the pion form factor.

Table 57: Chiral extrapolation/minimum pion mass in $N_f = 2$ determinations of the Low-Energy Constants.

Collab.	Ref.	N_f	L [fm]	$M_{\pi,\min}L$	Description
HPQCD 13A	[148]	2+1+1	4.8–5.5	3.3	3 volumes are compared.
ETM 13	[206]	2+1+1	1.9–2.8	3.0	4 volumes compared.
ETM 11	[253]	2+1+1	1.9–2.8	3.0	See [96].
ETM 10	[96]	2+1+1	1.9-2.8	3.0	FSE estimate using [563]. $M_{\pi^+}L \gtrsim 4$, but $M_{\pi^0}L \sim 2$.
Borsanyi 12	[238]	2+1	3.9	3.3	Expected to be less than 1%.
NPLQCD 11	[254]	2+1	2.5–3.5	3.6	Expected to be less than 1%.
MILC 10, 10A	[75, 151]	2+1	2.52	4.11	$L \geq 2.9$ fm for lighter mass.
JLQCD/TWQCD 09, 10	[241]	2+1, 3	1.9, 2.7		2 volues are compared for a fixed quark mass.
RBC/UKQCD 9, 10A	[78, 273]	2+1	2.7	$\simeq 4$	FSE estimated using χPT. .
MILC 09, 09A	[15, 37]	2+1	2.4/2.9	3.5/4.11	$L \geq 2.9$ fm for lighter masses.
TWQCD 08	[243]	2+1	1.95	-	No estimate of FSE.
JLQCD/TWQCD 08B	[244]	2+1	1.72	-	Fixing topoloical charge (to $\nu = 0$) gives FSE [567].
PACS-CS 08	[19]	2+1	2.9	2.3	FSE is the main concern of the authors.
RBC/UKQCD 08	[79]	2+1	2.74	4.6	FSE by means of χPT.
RBC/UKQCD 08A	[242]	2+1	2.74	4.6	FSE estimated to be $< 1\%$ using χPT.
NPLQCD 06	[158]	2+1	2.5	3.7	Value refers to lightest valence pion mass.
LHP 04	[261]	2+1	$\simeq 2.4$	3.97	Value refers to domain-wall valence pion mass.

Table 58: Finite volume effects in $N_f = 2+1+1$ and $2+1$ determinations of the Low-Energy Constants.

Collab.	Ref.	N_f	L [fm]	$M_{\pi,\mathrm{min}}L$	Description
ETM 13	[206]	2	2.0–2.5	3–4	Configs. shared with ETM 09C.
ETM 12	[245]	2	2.0–2.5	3–4	Configs. shared with ETM 09C.
Bernardoni 11	[246]	2	1.56	2.5	Mixed regime χPT for FSE used.
TWQCD 11	[174]	2	1.65	1.92	SU(2) χPT is used for FSE.
TWQCD 11A	[247]	2	1.65	1.8	No estimate of FSE.
Bernardoni 10	[248]	2	1.88	2.8	FSE included in the NLO chiral fit.
JLQCD/TWQCD 10	[241]	2	1.8-1.9		FSE estimated from different topological sectors.
JLQCD/TWQCD 09	[257]	2	1.89	2.9	FSE by NLO χPT, Additional FSE for fixing topology [567].
ETM 09B	[250]	2	1.3, 1.5	ϵ-regime	Topology: not fixed. 2 volumes.
ETM 09C	[230]	2	2.0-2.5	3.2–4.4	Several volumes. Finite-volume effects estimated through [563].
ETM 08	[227]	2	2.1, 2.8	3.4, 3.7	Only data with $M_\pi L \gtrsim 4$ are considered. .
JLQCD/TWQCD 08A JLQCD 08A	[67] [272]	2	1.89	2.9	FSE estimates through [563]. Additional FSE for fixing topology [567].
CERN 08	[204]	2	1.88, 2.51	-	Two volumes compared.
Hasenfratz 08	[251]	2	1.84, 2.77	ϵ-regime	Topology: not fixed, 2 volumes.
JLQCD/TWQCD 07	[252]	2	1.78	ϵ-regime	Topology: fixed to $\nu = 0$.
JLQCD/TWQCD 07A	[249]	2	1.92	-	Topology fixed to $\nu = 0$ [567].
CERN-TOV 06	[258]	2	1.72, 1.67, 1.88	3.5, 3.2, 3.6	No estimate for FSE.
QCDSF/UKQCD 06A	[262]	2	1.4-2.0	3.8	NLO χPT estimate for FSE [568].

Table 59: Finite volume effects in $N_f = 2$ determinations of the Low-Energy Constants.

Collab.	Ref.	N_f	Description
HPQCD 13A	[148]	2+1+1	—
ETM 13	[206]	2+1+1	Non-perturbative
ETM 11	[253]	2+1+1	Non-perturbative
ETM 10	[96]	2+1+1	Non-perturbative
Borsanyi 12	[238]	2+1	(Indirectly) non-perturbative through [22]
NPLQCD 11	[254]	2+1	Not needed (no result for Σ).
JLQCD/TWQCD 10	[241]	2+1, 3	Non-perturbative
MILC 10, 10A	[75, 151]	2+1	2 loop
RBC/UKQCD 10A	[78]	2+1	Non-perturbative
JLQCD 09	[240]	2+1	Non-perturbative
MILC 09, 09A	[15, 37]	2+1	2 loop
TWQCD 08	[243]	2+1	Non-perturbative
JLQCD/TWQCD 08B	[244]	2+1	Non-perturbative
PACS-CS 08	[19]	2+1	1 loop
RBC/UKQCD 08, 08A	[79, 242]	2+1	Non-perturbative
NPLQCD 06	[158]	2+1	—
LHP 04	[261]	2+1	—
All collaborations		2	Non-perturbative

Table 60: Renormalization in determinations of the Low-Energy Constants.

B.4 Notes to section 6 on Kaon B-parameter B_K

In the following, we summarize the characteristics (lattice actions, pion masses, lattice spacings, etc.) of the recent $N_f = 2+1$ and $N_f = 2$ runs. We also provide brief descriptions of how systematic errors are estimated by the various authors.

Collab.	Ref.	N_f	a [fm]	Description
RBC/UKQCD 12	[25]	2+1	0.146, 0.114, 0.087	Coarsest lattice spacing uses different action. Combined continuum and chiral fits.
Laiho 11	[77]	2+1	0.12, 0.09, 0.06	Combined continuum and chiral extrapolation based on SU(3) mixed-action partially quenched χPT.
SWME 11, 11A	[285, 286]	2+1	0.12, 0.09, 0.06, 0.045	Continuum extrapolation with the coarsest lattice spacing omitted; residual discretization error of 1.9% from difference between fit to a constant and a constrained five-parameter extrapolation.
BMW 11	[287]	2+1	0.09, 0.08, 0.07, 0.05	Combined continuum and chiral extrapolation; discretization error of 0.1% from comparison of $O(\alpha_s a)$ and $O(a^2)$ extrapolations.
RBC/UKQCD 10B	[301]	2+1	0.114, 0.087	Two lattice spacings. Combined chiral and continuum fits.
SWME 10	[302]	2+1	0.12, 0.09, 0.06	Continuum extrapolation of results obtained at four lattice spacings; residual discretization error of 0.21% from difference to result at smallest lattice spacing.
Aubin 09	[284]	2+1	0.12, 0.09	Two lattice spacings; quote 0.3% discretization error, estimated from various a^2-terms in fit function
RBC/UKQCD 07A, 08	[79, 303]	2+1	0.114(2)	Single lattice spacing; quote 4% discretization error, estimated from the difference between computed and experimental values of f_π.
HPQCD/UKQCD 06	[304]	2+1	0.12	Single lattice spacing; 3% discretization error quoted without providing details.
ETM 10A	[300]	2	0.1, 0.09, 0.07	Three lattice spacings; 1.2% error quoted.
JLQCD 08	[305]	2	0.118(1)	Single lattice spacing; no error quoted.
RBC 04	[299]	2	0.117(4)	Single lattice spacing; no error quoted.
UKQCD 04	[306]	2	0.10	Single lattice spacing; no error quoted.

Table 61: Continuum extrapolations/estimation of lattice artifacts in determinations of B_K.

Collab.	Ref.	N_f	$M_{\pi,\text{min}}$ [MeV]	Description
RBC/UKQCD 12	[25]	2+1	140/170, 240/330, 220/290	Valence/sea $M_{\pi,\text{min}}$ entries correspond to the three lattice spacings. Combined chiral & continuum extrapolation, using $M_\pi < 350$ MeV.
Laiho 11	[77]	2+1	210/280	$M_{\pi,\text{min}}$ entries correspond to the smallest valence/sea quark masses. Chiral & continuum fits based on NLO mixed action χPT, including a subset of NNLO terms. Systematic error estimated from spread arising from variations in the fit function.
SWME 11, 11A	[285, 286]	2+1	442/445, 299/325, 237/340, 222/334	Valence/sea RMS $M_{\pi,\text{min}}$ entries correspond to the four lattice spacings. Chiral extrapolations based on SU(2) staggered χPT at NNLO (with some coefficients fixed by Bayesian priors), and also including one analytic NNNLO term. Residual error of 0.33% error from doubling the widths of Bayesian priors.
BMW 11	[287]	2+1	219, 182, 120, 131	$M_{\pi,\text{min}}$ entries correspond to the four lattice spacings used in the final result. Combined fit to the chiral and continuum behaviour. Systematics investigated by applying cuts to the maximum pion mass used in fits. Uncertainty of 0.1% assigned to chiral fit.
RBC/UKQCD 10B	[301]	2+1	240/330, 220/290	Valence/sea $M_{\pi,\text{min}}$ entries correspond to the two lattice spacings. Combined chiral and continuum extrapolations.
SWME 10	[302]	2+1	442/445, 299/325, 237/340	Valence/sea $M_{\pi,\text{min}}$ entries correspond to the three lattice spacings. Chiral extrapolations based on SU(2) staggered χPT at NLO, including some analytic NNLO terms. SU(3) staggered χPT as cross-check. Combined 1.1% error from various different variations in the fit procedure.
Aubin 09	[284]	2+1	240/370	$M_{\pi,\text{min}}$ entries correspond to the smallest valence/sea quark masses. Chiral & continuum fits based on NLO mixed action χPT at NLO, including a subset of NNLO terms. Systematic error estimated from spread arising from variations in the fit function.
RBC/UKQCD 07A, 08	[79, 303]	2+1	330	Fits based on SU(2) PQχPT at NLO. Effect of neglecting higher orders estimated at 6% via difference between fits based on LO and NLO expressions.
HPQCD/UKQCD 06	[304]	2+1	360	3% uncertainty from chiral extrapolation quoted, without giving further details.

Table 62: Chiral extrapolation/minimum pion mass in determinations of B_K.

Collab.	Ref.	N_f	$M_{\pi,\mathrm{min}}$ [MeV]	Description
ETM 10A	[300]	2	400, 270, 300	Each $M_{\pi,\mathrm{min}}$ entry corresponds to a different lattice spacing. Simultaneous chiral & continuum extrapolations, based on χPT at NLO, are carried out. Systematic error from several sources, including lattice calibration, quark mass calibration, chiral and continuum extrapolation etc., estimated at 3.1%.
JLQCD 08	[305]	2	290	Fits based on NLO PQχPT. Range of validity investigated. Fit error included in statistical uncertainty.
RBC 04	[299]	2	490	Fits based on NLO PQχPT. Fit error included in statistical uncertainty.
UKQCD 04	[306]	2	780	Fits to continuum chiral behaviour at fixed sea quark mass. Separate extrapolation in sea quark mass. Fit error included in overall uncertainty.

Table 62: (cntd.) Chiral extrapolation/minimum pion mass in determinations of B_K in two-flavour QCD.

Collab.	Ref.	N_f	L [fm]	$M_{\pi,\rm min}L$	Description
RBC/UKQCD 12	[25]	2+1	4.6, 2.7, 2.8	$\gtrsim 3.2$	L entries correspond to the three lattice spacings. Finite volume effects estimated using NLO χPT.
Laiho 11	[77]	2+1	2.4, 3.4, 3.8	$\gtrsim 3.5$	L entries correspond to the three lattice spacings. Finite volume effects estimated using NLO χPT.
SWME 11, 11A	[285, 286]	2+1	2.4/3.3, 2.4, 2.8, 2.8	$\gtrsim 3.2$	L entries correspond to the four lattice spacings, with two volumes at the coarsest lattice. Finite-volume effects estimated using NLO χPT.
BMW 11	[287]	2+1	6.0, 4.9, 4.2, 3.5	$\gtrsim 3.8, 3.0$	L entries correspond to the four lattice spacings, and are the largest of several volumes at each a. $M_{\pi,\rm min}L \approx 3.0$ for the ensemble at $a \approx 0.08$ fm. Finite volume effects estimated in χPT and by combined fit to multiple volumes.
RBC/UKQCD 10B	[301]	2+1	2.7, 2.8	$\gtrsim 3.1$	L entries correspond to the three lattice spacings. Finite volume effects estimated using NLO χPT.
SWME 10	[302]	2+1	2.4/3.3, 2.4,2.8	$\gtrsim 3.4$	L entries correspond to the three lattice spacings, with two volumes for the coarsest spacing. Finite-volume error of 0.9% estimated from difference obtained these two volumes.
Aubin 09	[284]	2+1	2.4, 3.4	3.5	L entries correspond to the two lattice spacings. Keep $m_\pi L \gtrsim 3.5$; no comparison of results from different volumes; 0.6% error estimated from mixed action χPT correction.
RBC/UKQCD 07A, 08	[79, 303]	2+1	1.83/2.74	4.60	Each L entry corresponds to a different volume at the same lattice spacing; 1% error from difference in results on two volumes.
HPQCD/UKQCD 06	[304]	2+1	2.46	4.49	Single volume; no error quoted.

Table 63: Finite volume effects in determinations of B_K. If partially-quenched fits are used, the quoted $M_{\pi,\rm min}L$ is for lightest valence (RMS) pion.

Collab.	Ref.	N_f	L [fm]	$M_{\pi,\min}L$	Description
ETM 10A	[300]	2	2.1, 2.2/2.9, 2.2	5, 3.3/4.3, 3.3	Each L entry corresponds to a different lattice spacing, with two volumes at the intermediate lattice spacing. Results from these two volumes at $M_\pi \sim 300$ MeV are compatible.
JLQCD 08	[305]	2	1.89	2.75	Single volume; data points with $m_{\rm val} < m_{\rm sea}$ excluded; 5% error quoted as upper bound of PQχPT estimate of the effect.
RBC 04	[299]	2	1.87	4.64	Single volume; no error quoted.
UKQCD 04	[306]	2	1.6	6.51	Single volume; no error quoted.

Table 63: (cntd.) Finite volume effects in determinations of B_K in two-flavour QCD.

Collab.	Ref.	N_f	Ren.	running match.	Description
RBC/UKQCD 12	[25]	2+1	RI	PT1ℓ	Two different RI-SMOM schemes used to estimate 2% systematic error in conversion to $\overline{\mathrm{MS}}$.
Laiho 11	[77]	2+1	RI	PT1ℓ	Total uncertainty in matching & running of 3%. Perturbative truncation error in the conversion to $\overline{\mathrm{MS}}$, RGI schemes is dominant uncertainty.
SWME 11, 11A	[285, 286]	2+1	PT1ℓ	PT1ℓ	Uncertainty from neglecting higher orders estimated at 4.4% by identifying the unknown 2-loop coefficient with result at the smallest lattice spacing.
BMW 11	[287]	2+1	RI	PT1ℓ	Uncertainty of 0.05% in the determination of the renormalisation factor included. 1% error estimated due to truncation of perturbative matching to $\overline{\mathrm{MS}}$ and RGI schemes at NLO.
RBC/UKQCD 10B	[301]	2+1	RI	PT1ℓ	Variety of different RI-MOM schemes including non-exceptional momenta. Residual uncertainty of 2% uncertainty in running & matching.
SWME 10	[302]	2+1	PT1ℓ	PT1ℓ	Uncertainty from neglecting higher orders estimated at 5.5% by identifying the unknown 2-loop coefficient with result at the smallest lattice spacing.
Aubin 09	[284]	2+1	RI	PT1ℓ	Total uncertainty in matching & running of 3.3%, estimated from a number of sources, including chiral extrapolation fit ansatz for n.p. determination, strange sea quark mass dependence, residual chiral symmetry breaking, perturbative matching & running.
RBC/UKQCD 07A, 08	[79, 303]	2+1	RI	PT1ℓ	Uncertainty from n.p. determination of ren. factor included in statistical error; 2% systematic error from perturbative matching to $\overline{\mathrm{MS}}$ estimated via size of correction itself.
HPQCD/UKQCD 06	[304]	2+1	PT1ℓ	PT1ℓ	Uncertainty due to neglecting 2-loop order in perturbative matching and running estimated by multiplying result by α^2.

Table 64: Running and matching in determinations of B_K.

Collab.	Ref.	N_f	Ren.	running match.	Description
ETM 10A	[300]	2	RI	PT1ℓ	Uncertainty from RI renormalization estimated at 2.5%.
JLQCD 08	[305]	2	RI	PT1ℓ	Uncertainty from n.p. determination of ren. factor included in statistical error; 2.3% systematic error from perturbative matching to $\overline{\mathrm{MS}}$ estimated via size of correction itself.
RBC 04	[299]	2	RI	PT1ℓ	Uncertainty from n.p. determination of ren. factor included.
UKQCD 04	[306]	2	PT1ℓ	PT1ℓ	No error quoted.

Table 64: (cntd.) Running and matching in determinations of B_K in two-flavour QCD.

B.5 Notes to section 7 on D-meson decay constants and form factors

In the following, we summarize the characteristics (lattice actions, pion masses, lattice spacings, etc.) of the recent $N_f = 2 + 1$ and $N_f = 2$ runs. We also provide brief descriptions of how systematic errors are estimated by the various authors. We focus on calculations with either preliminary or published quantitative results.

B.5.1 $D_{(s)}$-meson decay constants

Collab.	Ref.	N_f	$M_{\pi,\text{min}}$ [MeV]	Description
FNAL/MILC 12B	[314]	2+1+1	306, 244, 174, 144	Chiral and continuum extrapolations are peformed simultaneously. Central values are produced using a fit function quadratic in a^2 and linear in the sea-quark mass.
HPQCD 12A	[315]	2+1	460, 329	Chiral and continuum extrapolations are peformed simultaneously using PQHMχPT augmented by a dependent terms: $c_0(am_c)^2 + c_1(am_c)^4$.
FNAL/MILC 11	[316]	2+1	570, 440, 320	Chiral and continuum extrapolations are peformed simultaneously using HMχPT for rooted staggered quarks. Effects of hyperfine and flavor splittings are also included.
PACS-CS 11	[317]	2+1	152	Simulations are reweighted in the light- and strange-quark masses to the physical point.
HPQCD 10A	[318]	2+1	542, 460, 329, 258, 334	Chiral and continuum extrapolations are performed simultaneously. Polynomials up to $\left(\frac{m_{q,sea}-m_{q,phys}}{m_{q,phys}}\right)^2$ for $q = s, l$ and up to $(am_c)^8$ are kept.
HPQCD/UKQCD 07	[157]	2+1	542, 460, 329	Combined chiral and continuum extrapolations using HMχPT at NLO augmented by second and third-order polynomial terms in m_q and terms up to a^4.
FNAL/MILC 05	[319]	2+1	$>$ 440 , 440 , 400	Chiral extrapolations are first performed at each lattice spacing uisng NLO HMχPT for rooted staggered quarks. Lattice artefacts are then extrapolated linearly in a^2.
ETM 09, (ETM 11A)	[160, 320]	2	410, 270, 310, (270)	$M_{\pi,\text{min}}$ refers to the charged pions. NLO SU(2) HMχPT supplemented by terms linear in a^2 and in $m_D a^2$ is used in the combined chiral/continuum extrapolation. To estimate the systematic due to chiral extrapolation, once $f_{D_s}\sqrt{m_{D_s}}$ and $f_{D_s}\sqrt{m_{D_s}}/(f_D\sqrt{m_D})$ and once $f_{D_s}\sqrt{m_{D_s}}/f_K$ and $f_{D_s}\sqrt{m_{D_s}}/f_K \times f_\pi/(f_D\sqrt{m_D})$ are fitted.

Table 65: Chiral extrapolation/minimum pion mass in determinations of the D and D_s meson decay constants. For actions with multiple species of pions, masses quoted are the RMS pion masses. The different $M_{\pi,\text{min}}$ entries correspond to the different lattice spacings.

Collab.	Ref.	N_f	L [fm]	$M_{\pi,\min}L$	Description
FNAL/MILC 12B	[314]	2+1+1	2.4/4.8, 2.88/5.76, 2.88/5.76, 2.88/5.76	3.3, 3.9, 3.7, 4	FV errors estimated in χPT and by analyzing otherwise identical ensembles with three different spatial sizes at $a = 0.12$ fm and $m_l/m_s = 0.1$.
HPQCD 12A	[315]	2+1	2.4/2.8, 2.4/3.4	3.8, 4.2	FV errors estimated by comparing finite and infinite volume χPT.
FNAL/MILC 11	[316]	2+1	2.4, 2.4/2.88, 2.52/3.6	3.9, 3.8, 4,2	FV errors estimated using finite-volume χPT.
PACS-CS 11	[317]	2+1	2.88	2.2 (before reweighting)	No discussion of FSE.
HPQCD 10A	[318]	2+1	2.4, 2.4/2.88/3.36, 2.52, 2.88, 2.82	3.9, 3.8, 4.1, 4.5, 4.6	FV errors estimated using finite- vs infinite-volume χPT.
HPQCD/UKQCD 07	[157]	2+1	2.4, 2.4/2.88, 2.52	3.9, 3.8, 4.1	FV errors estimated using finite- vs infinite-volume χPT.
FNAL/MILC 05	[319]	2+1	2.8, 2.9, 2.5	3.8, 3.8, 4.1	FV errors estimated to be 1.5% or less from χPT.
ETM 09, (ETM 11A)	[160, 320]	2	2.4, 2.0/2.7, 2.1, (2.6)	5, 3.3, 3.3, (3.5)	FV errors are found to be negligible by comparing results at $m_\pi L = 3.3$ and $m_\pi L = 4.3$ for $m_\pi \simeq 310$ MeV.

Table 66: Finite volume effects in determinations of the D and D_s meson decay constants. Each L-entry corresponds to a different lattice spacing, with multiple spatial volumes at some lattice spacings. For actions with multiple species of pions, the lightest masses are quoted.

Collab.	Ref.	N_f	a [fm]	Continuum extrapolation	Scale Setting
FNAL/MILC 12B	[314]	2+1+1	0.15, 0.12, 0.09, 0.06	Chiral and continuum extrapolations performed simultaneously. Central values produced using a fit function quadratic in a^2 and linear in the sea quark mass.	Scale set through f_π; the uncertainty is propagated in the statistical error.
HPQCD 12A	[315]	2+1	0.12, 0.09	Chiral and continuum extrapolations peformed simultaneously using PQHMχPT augmentd by a dependent terms: $c_0(am_c)^2 + c_1(am_c)^4$.	Relative scale set through r_1; absolute scale from f_π, f_K and the Υ splitting. Uncertainties from both r_1 and r_1/a propagated.
FNAL/MILC 11	[316]	2+1	0.15, 0.12, 0.09	Chiral and continuum extrapolations peformed simultaneously using one-loop HMχPT for rooted staggered quarks. Effects of hyperfine and flavor splittings are also included.	Relative scale set through r_1 = 0.3117(22). The error in r_1 comes from the spread of different absolute scale determinations using f_π, f_K and the Υ splitting.
PACS-CS 11	[317]	2+1	0.09	Cutoff effects from the heavy-quark action estimated by naive power counting to be at the percent level.	Scale set through m_Ω.
HPQCD 10A	[318]	2+1	0.15, 0.12, 0.09, 0.06, 0.044	Chiral and continuum extrapolations performed simultaneously. Polynomials up to am_c^8 are kept (even powers only).	See the discussion for HPQCD 12A.
HPQCD/UKQCD 07	[157]	2+1	0.15, 0.12, 0.09	Combined chiral and continuum extrapolations using HMχPT at NLO augmented by second and third-order polynomial terms in m_q and terms up to a^4.	Scale set through r_1 obtained from the Υ spectrum using the non-relativistic QCD action for b quarks. Uncertainty propagated among the systematics.
FNAL/MILC 05	[319]	2+1	0.175, 0.121, 0.086	Most light-quark cutoff effects are removed through NLO HMχPT for rooted staggered quarks. Continuum values are then obtained by averaging the $a \approx 0.12$ and $a \approx 0.09$ fm results.	Scale set through r_1 obtained from the Υ spectrum using the non-relativistic QCD action for b quarks.
ETM 09, (ETM 11A)	[160, 320]	2	0.10, 0.085, 0.065, (0.054)	NLO SU(2) HMχPT supplemented by terms linear in a^2 and in $m_D a^2$ is used in the combined chiral/continuum extrapolation.	Scale set through f_π.

Table 67: Lattice spacings and description of actions used in determinations of the D and D_s meson decay constants.

Collab.	Ref.	N_f	Ren.	Description
FNAL/MILC 12B	[314]	2+1+1	–	The axial current is absolutely normalized.
HPQCD 12A	[315]	2+1	–	The axial current is absolutely normalized.
FNAL/MILC 11	[316]	2+1	mNPR	Two-loop and higher-order perturbative truncation errors estimated to be the full size of the one-loop term.
PACS-CS 11	[317]	2+1	PT1ℓ+NP	Mass dependent part of the renormalization constant of the axial current computed at one-loop; the NP contribution is added in the chiral limit.
HPQCD 10A	[318]	2+1	–	The axial current is absolutely normalized.
HPQCD/UKQCD 07	[157]	2+1	–	The axial current is absolutely normalized.
FNAL/MILC 05	[319]	2+1	mNPR	Errors due to higher order corrections in the perturbative part are estimated to be 1.3%.
ETM 09, (ETM 11A)	[160, 320]	2	–	The axial current is absolutely normalized.

Table 68: Operator renormalization in determinations of the D and D_s meson decay constants.

Collab.	Ref.	N_f	Action	Description
FNAL/MILC 12B	[314]	2+1+1	HISQ (on HISQ)	$0.29 < am_c < 0.7$. Discretization errors estimated using different fit ansätze to be $\approx 1.5\%$ for $f_{D_{(s)}}$.
HPQCD 12A	[315]	2+1	HISQ	$0.41 < am_c < 0.62$. Heavy-quark discretization errors estimated using different fit ansätze to be $\approx$ 1.2%.
FNAL/MILC 11	[316]	2+1	Fermilab	Discretization errors from charm quark estimated through a combination of Heavy Quark and Symanzik Effective Theories to be around 3% for $f_{D_{(s)}}$ and negligible for the ratio.
PACS-CS 11	[317]	2+1	Tsukuba	$am_c \approx 0.57$. Heavy-quark discretization errors estimated to be at the percent level by power counting.
HPQCD 10A	[318]	2+1	HISQ	$0.193 < am_c < 0.825$. Heavy-quark discretization errors estimated by changing the fit-inputs to be $\approx$ 0.4%.
HPQCD/UKQCD 07	[157]	2+1	HISQ	$0.43 < am_c < 0.85$. Heavy-quark discretization errors estimated from the chiral/continuum fits to be $\approx$ 0.5%. $\delta(a_{\rm min})$ slightly >1 for f_{D_s}.
FNAL/MILC 05	[319]	2+1	Fermilab	Discretization errors from charm quark estimated via heavy-quark power-counting at 4.2% for $f_{D_{(s)}}$ and 0.5% for the ratio.
ETM 09, (ETM 11A)	[160, 320]	2	tmWil	$0.16 < am_c < 0.23$. $D(a_{\rm min}) \approx 5\%$ in ETM 09.

Table 69: Heavy quark treatment in determinations of the D and D_s meson decay constants.

B.5.2 $D \to \pi \ell \nu$ and $D \to K \ell \nu$ form factors

Collab.	Ref.	N_f	a [fm]	Continuum extrapolation	Scale setting
HPQCD 10B, 11	[321, 323]	2+1	0.09, 0.12	Modified z-expansion fit combining the continuum and chiral extrapolations and the momentum transfer dependence. Leading discretization errors from $(am_c)^n$ charm-mass effects (see Table 74). Subleading $(aE)^n$ discretization corrections estimated to be 1.0% for both $D \to \pi$ and $D \to K$.	Relative scale r_1/a set from the static-quark potential. Absolute scale r_1 set from several quantities including f_π, f_K, and Υ $2S - 1S$ splitting c.f. HPQCD 09B [175]. Scale uncertainty estimated to be 0.7% in $D \to \pi$ and and 0.2% in $D \to K$.
FNAL/MILC 04	[330]	2+1	0.12	Discretization effects from light-quark sector estimated to be 4% by power counting. Discretization effects from final-state pion and kaon energies estimated to be 5%.	Scale set through Υ $2S - 1S$ splitting c.f. HPQCD 03 [569]. Error in a^{-1} estimated to be 1.2%, but scale error in dimensionless form factor negligible compared to other uncertainties.
ETM 11B	[326]	2	0.068, 0.086, 0.102	Discretization errors estimated to be 5% for $D \to \pi$ and 3% for $D \to K$ from comparison of results in the continuum limit to those at the finest lattice spacing.	Scale set through f_π c.f. ETM 07A [560] and ETM 09C [230].

Table 70: Continuum extrapolations/estimation of lattice artifacts in determinations of the $D \to \pi \ell \nu$ and $D \to K \ell \nu$ form factors.

Collab.	Ref.	N_f	$M_{\pi,\text{min}}$ [MeV]	Description
HPQCD 10B, 11	[321, 323]	2+1	390, 390	Modified z-expansion fit combining the continuum and chiral extrapolations and the momentum transfer dependence. Contributions to error budget from light valence and sea-quark mass dependence estimated to be 2.0% for $D \to \pi$ and 1.0% for $D \to K$.
FNAL/MILC 04	[330]	2+1	510	Fit to SχPT, combined with the Becirevic-Kaidalov ansatz for the momentum transfer dependence of form factors. Error estimated to be 3% for $D \to \pi$ and 2% for $D \to K$ by comparing fits with and without one extra analytic term.
ETM 11B	[326]	2	270	$SU(2)$ tmHMχPT plus Becirevic-Kaidalov ansatz for fits to the momentum transfer dependence of form factors. Fit uncertainty estimated to be 7% for $D \to \pi$ and 5% for $D \to K$ by considering fits with and without NNLO corrections of order $\mathcal{O}(m_\pi^4)$ and/or higher-order terms through E^5, and by excluding data with $E \gtrsim 1$ GeV.

Table 71: Chiral extrapolation/minimum pion mass in determinations of the $D \to \pi\ell\nu$ and $D \to K\ell\nu$ form factors. For actions with multiple species of pions, masses quoted are the RMS pion masses. The different $M_{\pi,\text{min}}$ entries correspond to the different lattice spacings.

Collab.	Ref.	N_f	L [fm]	$M_{\pi,\text{min}}L$	Description
HPQCD 10B, 11	[321, 323]	2+1	2.4, 2.4/2.9	$\gtrsim 3.8$	Finite volume effects estimated to be 0.04% for $D \to \pi$ and 0.01% for $D \to K$ by comparing the "$m_\pi^2 \log(m_\pi^2)$" term in infinite and finite volume.
FNAL/MILC 04	[330]	2+1	2.4/2.9	$\gtrsim 3.8$	No explicit estimate of FV error, but expected to be small for simulation masses and volumes.
ETM 11B	[326]	2	2.2, 2.1/2.8, 2.4	$\gtrsim 3.7$	Finite volume uncertainty estimated to be at most 2% by considering fits with and without the lightest pion mass point at $m_\pi L \approx 3.7$.

Table 72: Finite volume effects in determinations of the $D \to \pi\ell\nu$ and $D \to K\ell\nu$ form factors. Each L-entry corresponds to a different lattice spacing, with multiple spatial volumes at some lattice spacings. For actions with multiple species of pions, the lightest pion masses are quoted.

Collab.	Ref.	N_f	Ren.	Description
HPQCD 10B, 11	[321, 323]	2+1	—	Form factor extracted from absolutely normalised scalar-current matrix element then using kinematic constraint at zero momentum-transfer $f_+(0) = f_0(0)$.
FNAL/MILC 04	[330]	2+1	mNPR	Size of two-loop correction to current renormalization factor assumed to be negligible.
ETM 11B	[326]	2	—	Form factors extracted from double ratios insensitive to current normalization.

Table 73: Operator renormalization in determinations of the $D \to \pi\ell\nu$ and $D \to K\ell\nu$ form factors.

Collab.	Ref.	N_f	Action	Description
HPQCD 10B, 11	[321, 323]	2+1	HISQ	Bare charm-quark mass $am_c \sim 0.41$–0.63. Errors of $(am_c)^n$ estimated within modified z-expansion to be 1.4% for $D \to K$ and 2.0% for $D \to \pi$. Consistent with expected size of dominant one-loop cutoff effects on the finest lattice spacing, $\mathcal{O}(\alpha_S(am_c)^2(v/c)) \sim 1.6\%$.
FNAL/MILC 04	[330]	2+1	Fermilab	Discretization errors from charm quark estimated via heavy-quark power-counting to be 7%.
ETM 11B	[326]	2	tmWil	Bare charm-quark mass $am_c \sim 0.17$–0.30. Expected size of $\mathcal{O}((am_c)^2)$ cutoff effects on the finest lattice spacing consistent with quoted 5% continuum-extrapolation uncertainty.

Table 74: Heavy quark treatment in determinations of the $D \to \pi\ell\nu$ and $D \to K\ell\nu$ form factors.

B.6 Notes to section 8 on B-meson decay constants, mixing parameters, and form factors

In the following, we summarize the characteristics (lattice actions, pion masses, lattice spacings, etc.) of the recent $N_f = 2+1$ and $N_f = 2$ runs. We also provide brief descriptions of how systematic errors are estimated by the various authors. We focus on calculations with either preliminary or published quantitative results.

B.6.1 $B_{(s)}$-meson decay constants

Collab.	Ref.	N_f	a [fm]	Continuum extrapolation	Scale setting
ALPHA 11/12A	[337, 342]	2	0.075, 0.065, 0.048	Combined continuum and chiral extrapolation with linear in a^2 term. Continuum extrapolation errors estimated to be 5 MeV in ALPHA 11.	Relative scale set from r_0. Absolute scale set from f_K. Scale setting uncertainty included in combined statistical and extrapolation error.
ETM 11A/12B	[320, 365]	2	0.098, 0.085, 0.067, 0.054	Combined continuum and chiral extrapolation, with a term linear in a^2. ETM 12 includes a heavier mass than ETM 11A. Discretization error included in combined statistical and systematic error, estimated by dropping the data at the coarsest lattice spacing as $\sim 0.5-1\%$.	Scale set from f_π. Scale setting uncertainty included in combined statistical and systematic error.
ETM 09D	[364]	2	0.098, 0.085, 0.067	Combined continuum and chiral extrapolation, keeping only a term linear in a^2.	Scale set from f_π. Scale setting uncertainty included in combined statistical and systematic error.

Table 75: Continuum extrapolations/estimation of lattice artifacts in determinations of the B and B_s meson decay constants for $N_f = 2$ simulations.

Collab.	Ref.	N_f	a [fm]	Continuum extrapolation	Scale setting
HPQCD 13	[371]	2+1+1	0.15, 0.12, 0.09	Combined continuum and chiral extrapolation. Continuum extrapolation errors estimated to be 0.7%.	Scale set from Υ(2S-1S) splitting, see Ref. [355]. Scale uncertainty included in statistical error.
HPQCD 12	[372]	2+1	0.12, 0.09	Combined continuum and chiral extrapolation. Continuum extrapolation errors estimated to be 0.9%.	Relative scale r_1/a from the static-quark potential. Absolute scale r_1 from f_π, f_K, and Υ(2S-1S) splitting. Scale uncertainty estimated to be 1.1%.
HPQCD 11A	[338]	2+1	0.15, 0.12, 0.09, 0.06, 0.045	$am_Q \approx 0.2 - 0.85$. Combined continuum and HQET fit. Continuum extrapolation error estimated by varying the fit ansatz and the included data points to be 0.63%. Discretization errors appear to decrease with increasing heavy-meson mass.	Relative scale r_1/a from the static-quark potential. Absolute scale r_1 from f_π, f_K, and Υ(2S-1S) splitting. Scale uncertainty estimated to be 0.74%.
FNAL/MILC 11	[316]	2+1	0.15, 0.12, 0.09	Combined continuum and chiral extrapolation. Continuum extrapolation errors estimated to be 1.3%.	Relative scale r_1/a from the static-quark potential. Absolute scale r_1 from f_π, f_K, and Υ(2S-1S) splitting. Scale uncertainty estimated to be 1 MeV.
RBC/UKQCD 10C	[374]	2+1	0.11	One lattice spacing with discretization errors estimated by power counting as 3%.	Scale set by the Ω baryon mass. Combined scale and mass tuning uncertainties on f_{B_s}/f_B estimated as 1%
HPQCD 09	[373]	2+1	0.12, 0.09	Combined continuum and chiral extrapolation. Continuum extrapolation errors estimated to be 3%.	Relative scale r_1/a from the static-quark potential. Absolute scale r_1 from the Υ(2S-1S) splitting. Scale uncertainty estimated to be 2.3%.

Table 76: Continuum extrapolations/estimation of lattice artifacts in determinations of the B and B_s meson decay constants for $N_f = 2+1+1$ and $N_f = 2+1$ simulations.

Collab.	Ref.	N_f	$M_{\pi,\text{min}}$ [MeV]	Description
HPQCD 13	[371]	2+1+1	310, 294, 173	Two or three pion masses at each lattice spacing, one each with a physical mass GB pion. NLO (full QCD) HMχPT supplemented by generic a^2 and a^4 terms is used to interpolate to the physical pion mass.
HPQCD 12	[372]	2+1	390, 390	Two or three pion masses at each lattice spacing. NLO (full QCD) HMχPT supplemented by NNLO analytic terms and generic a^2 and a^4 terms is used. The systematic error is estimated by varying the fit Ansatz, in particular for the NNLO analytic terms and the a^{2n} terms.
HPQCD 11A	[338]	2+1	?, 450?, 390, 330?, 330	One light sea quark mass only at each lattice spacing. The sea-quark mass dependence is assumed to be negligible, based on HPQCD 10's f_{D_s} analysis, where the sea quark extrapolation error was estimated as 0.34%.
FNAL/MILC 11	[316]	2+1	570, 440, 320	Three to five sea-quark masses per lattice spacing, and $9-12$ valence light quark masses per ensemble. NLO partially quenched HMrSχPT including $1/m$ terms and supplemented by NNLO analytic and $\alpha_s^2 a^2$ terms is used. The systematic error is estimated by varying the fit Ansatz, in particular the NNLO analytic terms and the chiral scale.
RBC/UKQCD 10C	[374]	2+1	430	Three light quark masses at one lattice spacing. NLO SU(2) χPT is used. The systematic error is estimated from the difference between NLO χPT and linear fits as $\sim 7\%$.
HPQCD 09	[373]	2+1	440, 400	Four or two pion masses per lattice spacing. NLO (full QCD) HMrSχPT supplemented by NNLO analytic terms and $\alpha_s a^2, a^4$ terms is used. The chiral fit error is estimated by varying the fit Ansatz, in particular, by adding or removing NNLO and discretization terms.
ETM 11A & 12B	[320, 365]	2	410, 275, 300, 270	$M_{\pi,\text{min}}$ refers to the charged pions. Linear and NLO (full QCD) HMχPT supplemented by an a^2 term is used.The chiral fit error is estimated from the difference between the NLO HMχPT and linear fits. For the static limit calculation, Φ_s^{stat} is extrapolated assuming a constant in light quark mass. The ratio $\Phi_s^{\text{stat}}/\Phi_\ell^{\text{stat}}$ is fit using three different chiral fit forms (NLO HMχPT, linear, and quadratic) to estimate the chiral fir error.
ETM 10B	[60]	2	410, 275, 300, 270	$M_{\pi,\text{min}}$ refers to the charged pions. **Ratio method:** Linear and NLO (full QCD) HMχPT is used. The final result given by the average of NLO HMChiPT and linear *Ansätze* $\pm$ half the difference). **Interpolation:** NLO HMChiPT or linear *Ansätze* always including O(a^2) are used in the continuum/chiral extrapolations. For the static limit calculation, NLO HMChiPT or linear *Ansätze* are used.
ALPHA 12A, ALPHA 11	[337, 342]	2	331, 190 [267], 268	LO and NLO HMChPT supplemented by a term linear in a^2 are used. The final result is an average between LO and NLO with half the difference used as estimate of the systematic error.

Table 77: Chiral extrapolation/minimum pion mass in determinations of the B and B_s meson decay constants. For actions with multiple species of pions, masses quoted are the RMS pion masses. The different $M_{\pi,\text{min}}$ entries correspond to the different lattice spacings.

Collab.	Ref.	N_f	L [fm]	$M_{\pi,\min}L$	Description
HPQCD 13	[371]	2+1+1	2.4/3.5/4.7, 2.9/3.8/5.8, 2.8/5.6	3.30, 3.88, 3.66	The analysis uses finite-volume χPT.
HPQCD 12	[372]	2+1	2.4/2.9, 2.5/3.6	3.84, 4.21	FV error is taken from Ref. [157] for HPQCD's D meson analysis, where it was estimated using finite volume χPT .
HPQCD 11A	[338]	2+1	2.4, 2.4, 2.5, 2.9, 2.9	3.93, 4.48, 4.14, 4.49, 4.54	FV error is assumed to negligible.
FNAL/MILC 11	[316]	2+1	2.4, 2.4/2.9, 2.5/3.6	3.93, 3.78, 4.14	FV error is estimated using finite-volume χPT.
RBC/UKQCD 10C	[374]	2+1	1.8	3.9	FV error estimated using finite-volume χPT to be 1% for SU(3) breaking ratios.
HPQCD 09	[373]	2+1	2.4/2.9, 2.5	3.78, 4.14	FV error is assumed to negligible.
ETM 11A/12B	[320, 365]	2	2.4, 2.0/2.7, 2.1, 1.7/2.6	5, 3.7, 3.3, 3.5	FV errors are found to be negligible by comparing results at $m_\pi L = 3.3$ and $m_\pi L = 4.3$ for $m_\pi \simeq 310$ MeV.
ALPHA 12A, ALPHA 11	[337, 342]	2	2.4, 2.1/4.2 [3.1], 2.3/3.1	$\gtrsim 4$	No explicit estimate of FV errors, but expected to be much smaller than other uncertainties.

Table 78: Finite volume effects in determinations of the B and B_s meson decay constants. Each L-entry corresponds to a different lattice spacing, with multiple spatial volumes at some lattice spacings.

Collab.	Ref.	N_f	Ren.	Description
HPQCD 13	[371]	2+1+1	PT1ℓ	The NRQD effective current is matched through $O(1/m)$ and renormalized using one-loop PT. Included are all terms though $O(\alpha_s)$, $O(\alpha_s\, a)$, $O(\Lambda_{\rm QCD}/M)$, $O(\alpha_s/aM)$, $O(\alpha_s\, \Lambda_{\rm QCD}/M)$. The dominant error is due unknown $O(\alpha_s^2)$ contributions to the current renormalization. The perturbation theory used in this work is the same as in HPQCD 09 and 12, but is rearranged to match the mNPR method. Using the fact that the heavy-heavy temporal vector current is normalized, and that the light-light HISQ vector current receives a small one-loop correction, the error is estimated as $\sim 1.4\%$.
HPQCD 12/09	[372, 373]	2+1	PT1ℓ	The NRQD effective current is matched through $O(1/m)$ and renormalized using one-loop PT. Included are all terms though $O(\alpha_s)$, $O(\alpha_s\, a)$, $O(\Lambda_{\rm QCD}/M)$, $O(\alpha_s/aM)$, $O(\alpha_s\, \Lambda_{\rm QCD}/M)$. The dominant error is due unknown $O(\alpha_s^2)$ contributions to the current renormalization. The authors take the perturbative error as $\sim 2\rho_0\, \alpha_s^2$, where ρ_0 is the coefficient of the one-loop correction to the leading term, which yields an error of $\sim 4\%$.
HPQCD 11A	[338]	2+1	–	This work uses PCAC together with an absolutely normalized current.
FNAL/MILC 11	[316]	2+1	mNPR	The authors' estimate of the perturbative errors is comparable in size to the actual one-loop corrections.
RBC/UKQCD 10C	[374]	2+1	PT1ℓ	The static-light current is matched through $O(\alpha_s a, \alpha_s)$ and renormalized using one-loop tadpole improved PT. For massless light quarks, the renormalization factors cancel in the ratio of decay constants.
ALPHA 11/12A	[337, 342]	2	NPR	The authors use the Schrd̈ingier functional for the NP matching.
ETM 11A/12B	[320, 365]	2	–, PT1ℓ	The current used for the relativistic decay constants is absolutely normalized. **Interpolation method:** The static limit current renormalization is calculated in one-loop mean field improved perturbation theory, there half the correction is used to estimate the error. **Ratio method:** The ratio is constructed from the relativistic decay constant data and the heavy-quark pole masses. Ratios of pole-to-$\overline{\rm MS}$ mass conversion factors are included at NLO in continuum perturbation theory.

Table 79: Description of the renormalization/matching procedure adopted in the determinations of the B and B_s meson decay constants.

Collab.	Ref.	N_f	Action	Description
HPQCD 13	[371]	2+1+1	NRQCD	HQ truncation effects estimated as in HPQCD 09 to be 1.0%
HPQCD 12	[372]	2+1	NRQCD	HQ truncation effects estimated as in HPQCD 09 to be 1.0%
HPQCD 11A	[338]	2+1	HISQ	The analysis uses a combined continuum and $1/m$ extrapolation.
FNAL/MILC 11	[316]	2+1	Fermilab	HQ discretization effects are included in the combined chiral and continuum fits, and are estimated by varying the fit Ansatz and excluding the data at the coarsest lattice spacing to be $\sim 2\%$, consistent with simple power counting estimates but larger than the residual discretization errors observed in the data.
RBC/UKQCD 10C	[374]	2+1	Static	Truncation effects of $\mathcal{O}(1/m_h)$ on the SU(3) breaking ratios are estimated by power counting to be 2%.
HPQCD 09	[373]	2+1	NRQCD	The leading HQ truncation effects are of $\mathcal{O}(\alpha_s \Lambda_{\rm QCD}/m_h)$ due to the tree-level coefficient of the $\boldsymbol{\sigma} \cdot \mathbf{B}$ term. The error is estimated by calculating the $B^* - B$ hyperfine splitting and comparing with experiment as 1%.
ALPHA 11/12A	[337, 342]	2	HQET	NP improved through $\mathcal{O}(1/m_h)$. Truncation errors of $\mathcal{O}(\Lambda_{\rm QCD}/m_h)^2$ are not included.
ETM 11A/12B	[320, 365]	2	tmWil	The estimate of the discretization effects is described in the continuum table. In both methods the relativistic data are matched to HQET using NLO continuum PT in an intermediate step, and converted back to QCD at the end. The error due to HQET matching (estimated by replacing the NLO expressions with LO) is a very small contribution to the systematic error due to the heavy quark mass dependence. The variation observed from adding heavier masses to their data and/or including $1/m_h^3$ terms is $0.4 - 1.3\%$.

Table 80: Heavy quark treatment in determinations of the B and B_s meson decay constants.

B.6.2 $B_{(s)}$-meson mixing matrix elements

Collab.	Ref.	N_f	a [fm]	Continuum extrapolation	Scale setting
FNAL/MILC 12	[382]	2+1	0.12, 0.09	Combined continuum and chiral extrapolation with NLO rHMSχPT, NNLO analytic and generic $\mathcal{O}(\alpha_s^2 a^2, a^4)$ terms. Combined statistical, chiral and light-quark discretization error is estimated, by examining the variation with different fit Ansätze to be 3.7% on ξ.	Relative scale r_1/a is set via static quark potential. Absolute scale $r_1 = 0.3117(22)$ fm is determined [316] through averaging the f_π input and the estimate of HPQCD collaboration [175]. The scale uncertainty on ξ is estimated as 0.2%.
FNAL/MILC 11A	[379]	2+1	0.12, 0.09, 0.06	Combined continuum and chiral extrapolation with NLO rHMSχPT, NNLO analytic and and generic $\mathcal{O}(\alpha_s^2 a^2, a^4)$ terms.	See above. The error in r_1 yields a 3% uncertainty on $f_B^2 B_B$.
RBC/UKQCD 10C	[374]	2+1	0.11	Only one lattice spacing is used. Discretization error is estimated to be 4% on ξ by power counting.	Scale is set using the Ω^- mass as input [79].The error on ξ due to the combined scale and light quark mass uncertainties is estimated as 1%.
HPQCD 09	[373]	2+1	0.12, 0.09	Combined continuum and chiral extrapolation with NLO rHMSχPT and NNLO analytic terms. Light-quark discretization error is estimated as 3, 2 and 0.3% for $f_B\sqrt{B_B}$, $f_{B_s}\sqrt{B_{B_s}}$ and ξ respectively.	Relative scale r_1/a is set via static quark potential. Absolute scale $r_1 = 0.321(5)$ fm is determined through Υ mass [352]. The error on $f_B\sqrt{B_B}$ due to the scale uncertainty is estimated as 2.3%.
HPQCD 06A	[380]	2+1	0.12	Only one lattice spacing is used. Light-quark discretization error on $f_{B_s}^2 B_{B_s}$ is estimated as 4% by power counting.	Scale is set using the Υ $2S - 1S$ splitting as input [352]. The error on $f_B^2 B_B$ due to the scale uncertainty is estimated as 5%.
ETM 12A,12B	[365, 381]	2	0.098, 0.085, 0.067	Combined chiral and continuum extrapolation, with a term linear in a^2. Discretization error included in combined statistical, chiral and continuum extrapolation error and estimated as 4.5%. The heavy-quark masses vary in the range $0.25 \lesssim am_h \lesssim 0.6$.	Relative scale r_0/a set from the static quark potential. Absolute scale set from f_π. Scale setting uncertainty included in combined statistical and systematic error.

Table 81: Continuum extrapolations/estimation of lattice artifacts in determinations of the neutral B-meson mixing matrix elements.

Collab.	Ref.	N_f	$M_{\pi,\text{min}}$ [MeV]	Description
FNAL/MILC 12	[382]	2+1	440, 320	Combined continuum and chiral extrapolation with NLO rHMSχPT and NNLO analytic terms. See the entry in Table 81. The omission of wrong-spin contributions [383] in the HMrSχPT is treated as a systematic error and estimated to be 3.2% for ξ.
FNAL/MILC 11A	[379]	2+1	440, 320, 250	Combined continuum and chiral extrapolation with NLO rHMSχPT and NNLO analytic terms.
RBC/UKQCD 10C	[374]	2+1	430	Linear fit matched with $SU(2)$ NLO HMχPT at the lightest ud mass point is used as the preferred fit. Many different fit Ansätze are considered. The systematic error is estimated from the difference between the $SU(2)$ HMχPT fit described above and a linear fit.
HPQCD 09	[373]	2+1	440, 400	Combined continuum and chiral extrapolation with NLO rHMSχPT and NNLO analytic terms.
HPQCD 06A	[380]	2+1	510	Two sea ud quark masses $m_{ud}/m_s = 0.25$ and 0.5 are used to calculate the matrix elemet for B_s meson at the predetermined value of the strange quark mass. No significant sea quark mass dependence is observed and the value at the lighter sea ud mass is taken as the result.
ETM 12A, 12B	[365, 381]	2	410, 275, 300	$M_{\pi,\text{min}}$ refers to the charged pions. Linear and NLO (full QCD) HMχPT supplemented by an a^2 term is used. The chiral fit error is estimated from the difference between the NLO HMχPT and linear fits.

Table 82: Chiral extrapolation/minimum pion mass in determinations of the neutral B-meson mixing matrix elements. For actions with multiple species of pions, masses quoted are the RMS pion masses. The different $M_{\pi,\text{min}}$ entries correspond to the different lattice spacings.

Collab.	Ref.	N_f	L [fm]	$M_{\pi,\min}L$	Description
FNAL/MILC 12	[382]	2+1	2.4/2.9, 2.5	$\gtrsim 3.8$	FV error is estimated to be less than 0.1% for $SU(3)$ breaking ratios from FV HMrSχPT.
FNAL/MILC 11A	[379]	2+1	2.4/2.9, 2.5/2.9/3.6, 3.8	$\gtrsim 3.8$	FV error on $f_B\sqrt{B_B}$ is estimated to be less than 1%, which is inferred from the study of the B-meson decay constant using FV HMχPT [316].
RBC/UKQCD 10C	[374]	2+1	1.8	$\gtrsim 3.9$	FV error estimated through FV HMχPT as 1% for $SU(3)$ breaking ratios.
HPQCD 09	[373]	2+1	2.4/2.9, 2.5	$\gtrsim 3.8$	No explicit estimate of FV error, but expected to be much smaller than other uncertainties.
HPQCD 06A	[380]	2+1	2.4	$\gtrsim 4.5$	No explicit estimate of FV error, but expected to be much smaller than other uncertainties.
ETM 12A, 12B	[365, 381]	2	2.4, 2.0/2.7, 2.1	$\gtrsim 3.2$	FV error is assumed to be negligible based on the study of D-meson decay constants in Ref. [160].

Table 83: Finite volume effects in determinations of the neutral B-meson mixing matrix elements. Each L-entry corresponds to a different lattice spacing, with multiple spatial volumes at some lattice spacings. For actions with multiple species of pions, the lightest masses are quoted.

Collab.	Ref.	N_f	Ren.	Description
FNAL/MILC 12	[382]	2+1	PT1l	One-loop mean-field improved PT is used to renormalize the four-quark operators with heavy quarks rotated to eliminate tree-level $O(a)$ errors. The error from neglecting higher order corrections is estimated to be 0.5% on ξ.
FNAL/MILC 11A	[379]	2+1	PT1l	One-loop mean-field improved PT is used to renormalize the four-quark operators with heavy quarks rotated to eliminate tree-level $O(a)$ errors. The error from neglected higher order corrections is estimated to be 4% on $f_B\sqrt{B_B}$.
RBC/UKQCD 10C	[374]	2+1	PT1l	Static-light four-quark operators are renormalized with one-loop mean field improved PT. The error due to neglected higher order effects is estimated to be 2.2% on ξ.
HPQCD 09	[373]	2+1	PT1l	Four-quark operators in lattice NRQCD are matched to QCD through order α_s, $\Lambda_{\rm QCD}/M$ and $\alpha_s/(aM)$ [570] using one-loop PT. The error due to neglected higher order effects is estimated to be 4% on $f_B\sqrt{B_B}$ and 0.7% on ξ.
HPQCD 06A	[380]	2+1	PT1l	Four-quark operators in lattice NRQCD are matched to full QCD through order α_s, $\Lambda_{\rm QCD}/M$ and $\alpha_s/(aM)$ [570]. The error is estimated as $\sim 1\cdot\alpha_s^2$ to be 9% on $f_{B_s}^2 B_{B_s}$
ETM 12A, 12B	[365, 381]	2	NPR	The bag parameters are nonperturbatively renormalized in the RI'-MOM scheme. They are calculated as functions of the ($\overline{\rm MS}$) heavy-quark mass (renormalized nonperturbatively in RI/MOM).

Table 84: Operator renormalization in determinations of the neutral B-meson mixing matrix elements.

Collab.	Ref.	N_f	Action	Description
FNAL/MILC 12	[382]	2+1	Fermilab	The heavy-quark discretization error on ξ is estimated to be 0.3 %. The error on ξ due to the uncertainty in the b-quark mass is are estimated to be 0.4 %.
FNAL/MILC 11A	[379]	2+1	Fermilab	The heavy-quark discretization error on $f_B\sqrt{B_B}$ is estimated as 4% using power-counting.
RBC/UKQCD 10C	[374]	2+1	Static	Two different static-quark actions with Ape and HYP smearings are used. The discretization error on ξ is estimated as $\sim 4\%$ and the error due to the missing $1/m_b$ corrections as $\sim 2\%$, both using power-counting.
HPQCD 09	[373]	2+1	NRQCD	Heavy-quark truncation errors due to relativistic corrections are estimated to be 2.5, 2.5 and 0.4 % for $f_B\sqrt{B_B}$, $f_{B_s}\sqrt{B_{B_s}}$ and ξ respectively.
HPQCD 06A	[380]	2+1	NRQCD	Heavy-quark truncation errors due to relativistic corrections are estimated to be 3% for $f^2_{B_s}B_{B_s}$.
ETM 12A, 12B	[365, 381]	2	tmWilson	The ratio method is used where ratios of bag parameters at a fixed ratio of heavy-quark mass are constructed such that they are equal to unity in the static limit. In an intermediate step, the ratios include HQET matching factors calculated at TL and LL in continuum PT, to aid with the interpolation to the physical b quark mass. The interpolation to the physical b-quark mass uses a linear or quadratic polynomial in the inverse quark-mass. The systematic errors are estimated from changing the interpolating polynomial as 2% and from changing the order of HQET matching factors as 3%

Table 85: Heavy-quark treatment in determinations of the neutral B-meson mixing matrix elements.

B.6.3 $B \to \pi \ell \nu$ form factor

Collab.	Ref.	N_f	a [fm]	Continuum extrapolation	Scale setting
FNAL/MILC 08	[397]	2+1	0.09, 0.12	Fit to rHMSχPT to remove light-quark discretization errors. Residual heavy-quark discretization errors estimated with power-counting to be 3.4%.	Relative scale r_1/a set from the static-quark potential. Absolute scale r_1 set through f_π cf. MILC 07 [561]; error in scale taken to be difference from scale set through Υ $2S-1S$ splitting c.f. HPQCD 05B [352]. Scale-uncertainty estimated at between 1% and 1.5% in the range of q^2 explored.
HPQCD 06	[396]	2+1	0.09,0.12	Central values obtained from data at $a = 0.12$ fm. Discretization errors observed to be within the statistical error by comparison with data at $a = 0.09$ fm.	Relative scale r_1/a set from the static-quark potential. Absolute scale r_1 set through Υ $2S-1S$ splitting c.f. HPQCD 05B [352].

Table 86: Continuum extrapolations/estimation of lattice artifacts in determinations of the $B \to \pi \ell \nu$ form factor.

Collab.	Ref.	N_f	$M_{\pi,\rm min}$ [MeV]	Description
FNAL/MILC 08	[397]	2+1	400, 440	Simultaneous chiral-continuum extrapolation and q^2 interpolation using $SU(3)$ rHMSχPT. Systematic error estimated by adding higher-order analytic terms and varying the B^*-B-π coupling.
HPQCD 06	[396]	2+1	400, 440	First interpolate data at fixed quark mass to fiducial values of E_π using the Becirevic-Kaidalov and Ball-Zwicky ansätze, then extrapolate data at fixed E_π to physical quark masses using $SU(3)$ rHMSχPT. Systematic error estimated by varying interpolation and extrapolation fit functions.

Table 87: Chiral extrapolation/minimum pion mass in determinations of the $B \to \pi \ell \nu$ form factor. For actions with multiple species of pions, masses quoted are the RMS pion masses. The different $M_{\pi,\rm min}$ entries correspond to the different lattice spacings.

Collab.	Ref.	N_f	L [fm]	$M_{\pi,\min}L$	Description
FNAL/MILC 08	[397]	2+1	2.4, 2.4/2.9	$\gtrsim 3.8$	Estimate FV error to be 0.5% using 1-loop rHMSχPT.
HPQCD 06	[396]	2+1	2.4/2.9	$\gtrsim 3.8$	No explicit estimate of FV error, but expected to be much smaller than other uncertainties.

Table 88: Finite volume effects in determinations of the $B \to \pi\ell\nu$ form factor. Each L-entry corresponds to a different lattice spacing, with multiple spatial volumes at some lattice spacings. For actions with multiple species of pions, the lightest masses are quoted.

Collab.	Ref.	N_f	Ren.	Description
FNAL/MILC 08	[397]	2+1	mNPR	Perturbative truncation error estimated at 3% with size of 1-loop correction on finer ensemble.
HPQCD 06	[396]	2+1	PT1ℓ	Currents included through $\mathcal{O}(\alpha_S\Lambda_{\rm QCD}/M$, $\alpha_S/(aM)$, $\alpha_S\, a\Lambda_{\rm QCD})$. Perturbative truncation error estimated from power-counting.

Table 89: Operator renormalization in determinations of the $B \to \pi\ell\nu$ form factor.

Collab.	Ref.	N_f	Action	Description
FNAL/MILC 08	[397]	2+1	Fermilab	Discretization errors in $f+(q^2)$ from heavy-quark action estimated to be 3.4% by heavy-quark power-counting.
HPQCD 06	[396]	2+1	NRQCD	Discretization errors in $f_+(q^2)$ estimated to be $\mathcal{O}(\alpha_s(a\Lambda_{\rm QCD})^2) \sim 3\%$. Relativistic errors estimated to be $\mathcal{O}((\Lambda_{\rm QCD}/M)^2) \sim 1\%$.

Table 90: Heavy quark treatment in determinations of the $B \to \pi\ell\nu$ form factor.

B.6.4 $B \to D\ell\nu$ and $B \to D^*\ell\nu$ form factors and $R(D)$

Collab.	Ref.	N_f	a [fm]	Continuum extrapolation	Scale setting
FNAL/MILC 12A	[415]	2+1	0.09, 0.12	Continuum extrapolation using rHMSχPT to remove light-quark discretization errors. Residual discretization errors estimated to be very small for the ratio of branching fractions $R(D)$ at 0.2%	See below.
FNAL/MILC 10	[408]	2+1	0.06, 0.09, 0.12, 0.15	Continuum extrapolation using rHMSχPT to remove light-quark discretization errors. Residual discretization errors estimated to be 1.0% from power-counting. Further, the data displays no observable trend with lattice spacing.	Relative scale r_1/a set from the static-quark potential. Absolute scale r_1 set through f_π c.f. MILC 09B [571]. Comparison with r_1 set via other quantities by HPQCD [175] shows negligible change.
FNAL/MILC 08A	[409]	2+1	0.09, 0.12, 0.15	Continuum extrapolation using rHMSχPT to remove light-quark discretization errors. Residual discretization errors estimated to be 1.5% from power-counting and by comparison of data at 0.12 and 0.09 fm.	Relative scale r_1/a set from the static-quark potential. Absolute scale r_1 set through f_π c.f. MILC 07 [561]. Comparison with scale set through Υ $2S-1S$ shows negligible change.
FNAL/MILC 04A	[413]	2+1	0.12	Central value obtained from data at a single lattice spacing. Comparison with quenched simulations at different lattice spacings interpreted as indication of small discretization effects.	Relative scale r_1/a set from the static-quark potential. Absolute scale r_1 set through Υ $2S-1S$ splitting c.f. HPQCD 03 [569].

Table 91: Continuum extrapolations/estimation of lattice artifacts in determinations of the $B \to D\ell\nu$ and $B \to D^*\ell\nu$ form factors and of $R(D)$.

Collab.	Ref.	N_f	$M_{\pi,\text{min}}$ [MeV]	Description
FNAL/MILC 12A	[415]	2+1	400, 440	See below.
FNAL/MILC 10	[408]	2+1	340, 320, 440, 570	See below.
FNAL/MILC 08A	[409]	2+1	320, 440, 570	Simultaneous chiral-continuum extrapolation using $SU(3)$ rHMSχPT. Systematic errors estimated by adding higher-order analytic terms and varying the D^*-D-π coupling.
FNAL/MILC 04A	[413]	2+1	510	Linear extrapolation in the light-quark mass.

Table 92: Chiral extrapolation/minimum pion mass in determinations of the $B \to D\ell\nu$ and $B \to D^*\ell\nu$ form factors and of $R(D)$. For actions with multiple species of pions, masses quoted are the RMS pion masses. The different $M_{\pi,\text{min}}$ entries correspond to the different lattice spacings.

Collab.	Ref.	N_f	L [fm]	$M_{\pi,\text{min}}L$	Description
FNAL/MILC 12A	[415]	2+1	2.5, 2.4	$\gtrsim 3.8$	FV error estimated to be negligible in [416].
FNAL/MILC 10	[408]	2+1	2.8, 2.4/3.4, 2.4/2.9, 2.4	$\gtrsim 3.8$	See below.
FNAL/MILC 08A	[409]	2+1	2.4/3.4, 2.4/2.9, 2.4	$\gtrsim 3.8$	Estimate FV error to be negligible using 1-loop rHMSχPT.
FNAL/MILC 04A	[413]	2+1	2.4/2.9	$\gtrsim 4.5$	No estimate of FV error quoted.

Table 93: Finite volume effects in determinations of the $B \to D\ell\nu$ and $B \to D^*\ell\nu$ form factors and of $R(D)$. Each L-entry corresponds to a different lattice spacing, with multiple spatial volumes at some lattice spacings. For actions with multiple species of pions, the lightest pion masses are quoted.

Collab.	Ref.	N_f	Ren.	Description
FNAL/MILC 12A	[415]	2+1	mNPR	Only the relative matching of the spatial and temporal components of currents is relevant for the ratio $R(D)$. Uncertainty for this is estimated to be 0.4%.
FNAL/MILC 10	[408]	2+1	mNPR	See below. A 0.3% perturbative truncation error is estimated.
FNAL/MILC 08A	[409]	2+1	mNPR	Majority of current renormalization factor cancels in double ratio of lattice correlation functions. Remaining correction calculated with 1-loop tadpole-improved lattice perturbation theory. 0.3% perturbative truncation error estimated from size of one-loop correction on finest ensemble.
FNAL/MILC 04A	[413]	2+1	mNPR	No explicit estimate of perturbative truncation error.

Table 94: Operator renormalization in determinations of the $B \to D\ell\nu$ and $B \to D^*\ell\nu$ form factors and of $R(D)$.

Collab.	Ref.	N_f	Action	Description
FNAL/MILC 12A	[415]	2+1	Fermilab	Discretization errors of form factors estimated via power counting which leads to negligible ($\sim$0.2%) errors in the ratio $R(D)$.
FNAL/MILC 10	[408]	2+1	Fermilab	Discretization errors from heavy quark action estimated to be 1.1% from power counting and a more detailed theory of cut-off effects.
FNAL/MILC 08A	[409]	2+1	Fermilab	Heavy-quark discretization errors estimated to be 1.5% from power counting and comparisons of data at different lattice spacings.
FNAL/MILC 04A	[413]	2+1	Fermilab	No explicit estimate of heavy-quark discretization errors.

Table 95: Heavy quark treatment in determinations of the $B \to D\ell\nu$ and $B \to D^*\ell\nu$ form factors and of $R(D)$.

References

[1] G. Colangelo, S. Dürr, A. Jüttner, L. Lellouch, H. Leutwyler *et al.*, *Review of lattice results concerning low energy particle physics*, *Eur.Phys.J.* **C71** (2011) 1695, [arXiv:1011.4408].

[2] J. Laiho, E. Lunghi and R. S. Van de Water, *Lattice QCD inputs to the CKM unitarity triangle analysis*, *Phys. Rev.* **D81** (2010) 034503, [arXiv:0910.2928].

[3] J. Laiho, E. Lunghi and R. Van de Water, *2+1 Flavor Lattice QCD Averages*, http://mypage.iu.edu/~elunghi/webpage/LatAves.

[4] [RBC 07A] D. J. Antonio *et al.*, *Localization and chiral symmetry in 3 flavor domain wall QCD*, *Phys. Rev.* **D77** (2008) 014509, [arXiv:0705.2340].

[5] [MILC 10] A. Bazavov *et al.*, *Topological susceptibility with the asqtad action*, *Phys. Rev.* **D81** (2010) 114501, [arXiv:1003.5695].

[6] [ALPHA 10C] S. Schaefer, R. Sommer and F. Virotta, *Critical slowing down and error analysis in lattice QCD simulations*, *Nucl.Phys.* **B845** (2011) 93–119, [arXiv:1009.5228].

[7] M. Lüscher, *Topology, the Wilson flow and the HMC algorithm*, *PoS* **LATTICE2010** (2010) 015, [arXiv:1009.5877].

[8] S. Schaefer, *Algorithms for lattice QCD: progress and challenges*, *AIP Conf.Proc.* **1343** (2011) 93–98, [arXiv:1011.5641].

[9] K. Symanzik, *Continuum limit and improved action in lattice theories. 1. Principles and ϕ^4 theory*, *Nucl. Phys.* **B226** (1983) 187.

[10] K. Symanzik, *Continuum limit and improved action in lattice theories. 2. O(N) nonlinear sigma model in perturbation theory*, *Nucl. Phys.* **B226** (1983) 205.

[11] S. Dürr, *Theoretical issues with staggered fermion simulations*, *PoS* **LAT2005** (2006) 021, [hep-lat/0509026].

[12] S. R. Sharpe, *Rooted staggered fermions: good, bad or ugly?*, *PoS* **LAT2006** (2006) 022, [hep-lat/0610094].

[13] A. S. Kronfeld, *Lattice gauge theory with staggered fermions: how, where, and why (not)*, *PoS* **LAT2007** (2007) 016, [arXiv:0711.0699].

[14] M. Golterman, *QCD with rooted staggered fermions*, *PoS* **CONFINEMENT8** (2008) 014, [arXiv:0812.3110].

[15] [MILC 09] A. Bazavov *et al.*, *Full nonperturbative QCD simulations with 2+1 flavors of improved staggered quarks*, *Rev. Mod. Phys.* **82** (2010) 1349–1417, [arXiv:0903.3598].

[16] M. Schmelling, *Averaging correlated data*, *Phys.Scripta* **51** (1995) 676–679.

[17] A. Manohar and C. T. Sachrajda, *Quark masses, in Review of Particle Physics*, *Phys.Rev.* **D86** (2012) 010001.

[18] M. Gell-Mann, R. J. Oakes and B. Renner, *Behavior of current divergences under SU(3)×SU(3)*, *Phys. Rev.* **175** (1968) 2195–2199.

[19] [PACS-CS 08] S. Aoki *et al.*, *2+1 flavor lattice QCD toward the physical point*, *Phys. Rev.* **D79** (2009) 034503, [arXiv:0807.1661].

[20] [PACS-CS 09] S. Aoki *et al.*, *Physical point simulation in 2+1 flavor lattice QCD*, *Phys. Rev.* **D81** (2010) 074503, [arXiv:0911.2561].

[21] [PACS-CS 10] S. Aoki *et al.*, *Non-perturbative renormalization of quark mass in $N_f = 2 + 1$ QCD with the Schrödinger functional scheme*, *JHEP* **1008** (2010) 101, [arXiv:1006.1164].

[22] [BMW 10A] S. Dürr, Z. Fodor, C. Hoelbling, S. Katz, S. Krieg *et al.*, *Lattice QCD at the physical point: light quark masses*, *Phys.Lett.* **B701** (2011) 265–268, [arXiv:1011.2403].

[23] [BMW 10B] S. Dürr, Z. Fodor, C. Hoelbling, S. Katz, S. Krieg *et al.*, *Lattice QCD at the physical point: simulation and analysis details*, *JHEP* **1108** (2011) 148, [arXiv:1011.2711].

[24] [MILC 11] A. Bazavov *et al.*, *Properties of light pseudoscalars from lattice QCD with HISQ ensembles*, *PoS* **LAT2011** (2011) 107, [arXiv:1111.4314].

[25] [RBC/UKQCD 12] R. Arthur *et al.*, *Domain wall QCD with near-physical pions*, *Phys.Rev.* **D87** (2013) 094514, [arXiv:1208.4412].

[26] B. Bloch-Devaux, *Results from NA48/2 on $\pi\pi$ scattering lengths measurements in $K^\pm \to \pi^+\pi^-e^\pm\nu$ and $K^\pm \to \pi^0\pi^0\pi^\pm$ decays*, *PoS* **CONFINEMENT8** (2008) 029.

[27] J. Gasser, A. Rusetsky and I. Scimemi, *Electromagnetic corrections in hadronic processes*, *Eur. Phys. J.* **C32** (2003) 97–114, [hep-ph/0305260].

[28] A. Rusetsky, *Isospin symmetry breaking*, *PoS* **CD09** (2009) 071, [arXiv:0910.5151].

[29] J. Gasser, *Theoretical progress on cusp effect and $K_{\ell 4}$ decays*, *PoS* **KAON07** (2008) 033, [arXiv:0710.3048].

[30] H. Leutwyler, *Light quark masses*, *PoS* **CD09** (2009) 005, [arXiv:0911.1416].

[31] R. F. Dashen, *Chiral SU(3)×SU(3) as a symmetry of the strong interactions*, *Phys. Rev.* **183** (1969) 1245–1260.

[32] T. Blum *et al.*, *Electromagnetic mass splittings of the low lying hadrons and quark masses from 2+1 flavor lattice QCD+QED*, *Phys. Rev.* **D82** (2010) 094508, [arXiv:1006.1311].

[33] A. Duncan, E. Eichten and H. Thacker, *Electromagnetic splittings and light quark masses in lattice QCD*, *Phys. Rev. Lett.* **76** (1996) 3894–3897, [hep-lat/9602005].

[34] [RBC 07] T. Blum, T. Doi, M. Hayakawa, T. Izubuchi and N. Yamada, *Determination of light quark masses from the electromagnetic splitting of pseudoscalar meson masses computed with two flavors of domain wall fermions*, *Phys. Rev.* **D76** (2007) 114508, [arXiv:0708.0484].

[35] [MILC 04A] C. Aubin *et al.*, *Results for light pseudoscalars from three-flavor simulations*, *Nucl. Phys. Proc. Suppl.* **140** (2005) 231–233, [hep-lat/0409041].

[36] [MILC 04] C. Aubin *et al.*, *Light pseudoscalar decay constants, quark masses and low energy constants from three-flavor lattice QCD*, *Phys. Rev.* **D70** (2004) 114501, [hep-lat/0407028].

[37] [MILC 09A] A. Bazavov *et al.*, *MILC results for light pseudoscalars*, *PoS* **CD09** (2009) 007, [arXiv:0910.2966].

[38] J. Bijnens and J. Prades, *Electromagnetic corrections for pions and kaons: masses and polarizabilities*, *Nucl. Phys.* **B490** (1997) 239–271, [hep-ph/9610360].

[39] J. F. Donoghue and A. F. Perez, *The electromagnetic mass differences of pions and kaons*, *Phys. Rev.* **D55** (1997) 7075–7092, [hep-ph/9611331].

[40] [MILC 08] S. Basak *et al.*, *Electromagnetic splittings of hadrons from improved staggered quarks in full QCD*, *PoS* **LAT2008** (2008) 127, [arXiv:0812.4486].

[41] [MILC 12A] S. Basak *et al.*, *Status of the MILC calculation of electromagnetic contributions to pseudoscalar masses*, *PoS* **LAT2012** (2012) 137, [arXiv:1210.8157].

[42] [MILC 13] S. Basak, A. Bazavov, C. Bernard, C. DeTar, E. Freeland *et al.*, *Electromagnetic contributions to pseudoscalar masses*, *PoS* **CD12** (2012) 030, [arXiv:1301.7137].

[43] [BMW 10C] A. Portelli *et al.*, *Electromagnetic corrections to light hadron masses*, *PoS* **LAT2010** (2010) 121, [arXiv:1011.4189].

[44] [BMW 12] A. Portelli, S. Dürr, Z. Fodor, J. Frison, C. Hoelbling *et al.*, *Systematic errors in partially-quenched QCD plus QED lattice simulations*, *PoS* **LAT2011** (2011) 136, [arXiv:1201.2787].

[45] [RM123 13] G. M. de Divitiis, R. Frezzotti, V. Lubicz, G. Martinelli, R. Petronzio *et al.*, *Leading isospin breaking effects on the lattice*, *Phys.Rev.* **D87** (2013) 114505, [arXiv:1303.4896].

[46] R. Urech, *Virtual photons in chiral perturbation theory*, *Nucl. Phys.* **B433** (1995) 234–254, [hep-ph/9405341].

[47] R. Baur and R. Urech, *On the corrections to Dashen's theorem*, *Phys. Rev.* **D53** (1996) 6552–6557, [hep-ph/9508393].

[48] R. Baur and R. Urech, *Resonance contributions to the electromagnetic low energy constants of chiral perturbation theory*, *Nucl. Phys.* **B499** (1997) 319–348, [hep-ph/9612328].

[49] B. Moussallam, *A sum rule approach to the violation of Dashen's theorem*, *Nucl. Phys.* **B504** (1997) 381–414, [hep-ph/9701400].

[50] L. Lellouch, *Light quarks and lattice QCD, plenary talk given at Quark Confinement and the Hadron Spectrum X, 8-12 October 2012*, http://www.confx.de.

[51] W. N. Cottingham, *The neutron proton mass difference and electron scattering experiments*, *Ann. of Phys.* **25** (1963) 424.

[52] R. H. Socolow, *Departures from the Eightfold Way. 3. Pseudoscalar-meson electromagnetic masses*, *Phys. Rev.* **137** (1965) B1221–B1228.

[53] D. J. Gross, S. B. Treiman and F. Wilczek, *Light quark masses and isospin violation*, *Phys. Rev.* **D19** (1979) 2188.

[54] J. Gasser and H. Leutwyler, *Quark masses*, *Phys. Rept.* **87** (1982) 77–169.

[55] T. Das, G. S. Guralnik, V. S. Mathur, F. E. Low and J. E. Young, *Electromagnetic mass difference of pions*, *Phys. Rev. Lett.* **18** (1967) 759–761.

[56] J. Gasser and H. Leutwyler, *Chiral perturbation theory: expansions in the mass of the strange quark*, *Nucl. Phys.* **B250** (1985) 465.

[57] G. Amoros, J. Bijnens and P. Talavera, *QCD isospin breaking in meson masses, decay constants and quark mass ratios*, *Nucl. Phys.* **B602** (2001) 87–108, [hep-ph/0101127].

[58] J. Gasser and H. Leutwyler, *Chiral perturbation theory to one loop*, *Ann. Phys.* **158** (1984) 142.

[59] [ALPHA 12] P. Fritzsch, F. Knechtli, B. Leder, M. Marinkovic, S. Schaefer *et al.*, *The strange quark mass and the Λ parameter of two flavor QCD*, *Nucl.Phys.* **B865** (2012) 397–429, [arXiv:1205.5380].

[60] [ETM 10B] B. Blossier *et al.*, *Average up/down, strange and charm quark masses with $N_f = 2$ twisted mass lattice QCD*, *Phys. Rev.* **D82** (2010) 114513, [arXiv:1010.3659].

[61] S. Dürr and G. Koutsou, *The ratio m_c/m_s with Wilson fermions*, *Phys.Rev.Lett.* **108** (2012) 122003, [arXiv:1108.1650].

[62] [ETM 07] B. Blossier *et al.*, *Light quark masses and pseudoscalar decay constants from $N_f = 2$ lattice QCD with twisted mass fermions*, *JHEP* **04** (2008) 020, [arXiv:0709.4574].

[63] [CP-PACS 01] A. Ali Khan *et al.*, *Light hadron spectroscopy with two flavors of dynamical quarks on the lattice*, *Phys. Rev.* **D65** (2002) 054505, [hep-lat/0105015]. Erratum: *Phys. Rev.* **D66** (2003) 059901.

[64] [ALPHA 05] M. Della Morte *et al.*, *Non-perturbative quark mass renormalization in two-flavor QCD*, *Nucl. Phys.* **B729** (2005) 117–134, [hep-lat/0507035].

[65] R. Sommer, *A new way to set the energy scale in lattice gauge theories and its applications to the static force and α_s in SU(2) Yang-Mills theory*, *Nucl. Phys.* **B411** (1994) 839–854, [hep-lat/9310022].

[66] [QCDSF/UKQCD 04] M. Göckeler *et al.*, *Determination of light and strange quark masses from full lattice QCD*, *Phys. Lett.* **B639** (2006) 307–311, [hep-ph/0409312].

[67] [JLQCD/TWQCD 08A] J. Noaki *et al.*, *Convergence of the chiral expansion in two-flavor lattice QCD*, *Phys. Rev. Lett.* **101** (2008) 202004, [arXiv:0806.0894].

[68] [QCDSF/UKQCD 06] M. Göckeler *et al.*, *Estimating the unquenched strange quark mass from the lattice axial Ward identity*, *Phys. Rev.* **D73** (2006) 054508, [hep-lat/0601004].

[69] [SPQcdR 05] D. Bećirević *et al.*, *Non-perturbatively renormalised light quark masses from a lattice simulation with $N_f = 2$*, *Nucl. Phys.* **B734** (2006) 138–155, [hep-lat/0510014].

[70] [JLQCD 02] S. Aoki *et al.*, *Light hadron spectroscopy with two flavors of $O(a)$-improved dynamical quarks*, *Phys. Rev.* **D68** (2003) 054502, [hep-lat/0212039].

[71] [ETM 10C] M. Constantinou *et al.*, *Non-perturbative renormalization of quark bilinear operators with $N_f = 2$ (tmQCD) Wilson fermions and the tree- level improved gauge action*, *JHEP* **08** (2010) 068, [arXiv:1004.1115].

[72] [HPQCD 10] C. McNeile, C. T. H. Davies, E. Follana, K. Hornbostel and G. P. Lepage, *High-precision c and b masses and QCD coupling from current-current correlators in lattice and continuum QCD*, *Phys. Rev.* **D82** (2010) 034512, [arXiv:1004.4285].

[73] [HPQCD 09A] C. T. H. Davies *et al.*, *Precise charm to strange mass ratio and light quark masses from full lattice QCD*, *Phys. Rev. Lett.* **104** (2010) 132003, [arXiv:0910.3102].

[74] [PDG 12] J. Beringer *et al.*, *Review of Particle Physics*, *Phys.Rev.* **D86** (2012) 010001.

[75] [MILC 10A] A. Bazavov *et al.*, *Staggered chiral perturbation theory in the two-flavor case and SU(2) analysis of the MILC data*, *PoS* **LAT2010** (2010) 083, [arXiv:1011.1792].

[76] [PACS-CS 12] S. Aoki, K.-I. Ishikawa, N. Ishizuka, K. Kanaya, Y. Kuramashi *et al.*, *1+1+1 flavor QCD + QED simulation at the physical point*, *Phys.Rev.* **D86** (2012) 034507, [arXiv:1205.2961].

[77] J. Laiho and R. S. Van de Water, *Pseudoscalar decay constants, light-quark masses and B_K from mixed-action lattice QCD*, *PoS* **LAT2011** (2011) 293, [arXiv:1112.4861].

[78] [RBC/UKQCD 10A] Y. Aoki *et al.*, *Continuum limit physics from 2+1 flavor domain wall QCD*, *Phys.Rev.* **D83** (2011) 074508, [arXiv:1011.0892].

[79] [RBC/UKQCD 08] C. Allton *et al.*, *Physical results from 2+1 flavor domain wall QCD and SU(2) chiral perturbation theory*, *Phys. Rev.* **D78** (2008) 114509, [arXiv:0804.0473].

[80] [CP-PACS/JLQCD 07] T. Ishikawa *et al.*, *Light quark masses from unquenched lattice QCD*, *Phys. Rev.* **D78** (2008) 011502, [arXiv:0704.1937].

[81] [HPQCD 05] Q. Mason, H. D. Trottier, R. Horgan, C. T. H. Davies and G. P. Lepage, *High-precision determination of the light-quark masses from realistic lattice QCD*, *Phys. Rev.* **D73** (2006) 114501, [hep-ph/0511160].

[82] [HPQCD/MILC/UKQCD 04] C. Aubin *et al.*, *First determination of the strange and light quark masses from full lattice QCD*, *Phys. Rev.* **D70** (2004) 031504, [hep-lat/0405022].

[83] T. van Ritbergen, J. A. M. Vermaseren and S. A. Larin, *The four-loop β-function in Quantum Chromodynamics*, *Phys. Lett.* **B400** (1997) 379–384, [hep-ph/9701390].

[84] K. G. Chetyrkin and A. Retey, *Renormalization and running of quark mass and field in the regularization invariant and $\overline{\rm MS}$ schemes at three and four loops*, *Nucl. Phys.* **B583** (2000) 3–34, [hep-ph/9910332].

[85] [HPQCD 08] I. Allison *et al.*, *High-precision charm-quark mass from current-current correlators in lattice and continuum QCD*, *Phys. Rev.* **D78** (2008) 054513, [arXiv:0805.2999].

[86] T. Ishikawa, T. Blum, M. Hayakawa, T. Izubuchi, C. Jung *et al.*, *Full QED+QCD low-energy constants through reweighting*, *Phys.Rev.Lett.* **109** (2012) 072002, [arXiv:1202.6018].

[87] M. Lüscher, R. Narayanan, P. Weisz and U. Wolff, *The Schrödinger functional: a renormalizable probe for non-abelian gauge theories*, *Nucl. Phys.* **B384** (1992) 168–228, [hep-lat/9207009].

[88] C. A. Dominguez, N. F. Nasrallah, R. Röntsch and K. Schilcher, *Light quark masses from QCD sum rules with minimal hadronic bias*, *Nucl. Phys. Proc. Suppl.* **186** (2009) 133–136, [arXiv:0808.3909].

[89] K. G. Chetyrkin and A. Khodjamirian, *Strange quark mass from pseudoscalar sum rule with $O(\alpha_s^4)$ accuracy*, *Eur. Phys. J.* **C46** (2006) 721–728, [hep-ph/0512295].

[90] M. Jamin, J. A. Oller and A. Pich, *Scalar $K\pi$ form factor and light quark masses*, *Phys. Rev.* **D74** (2006) 074009, [hep-ph/0605095].

[91] S. Narison, *Strange quark mass from e^+e^- revisited and present status of light quark masses*, *Phys. Rev.* **D74** (2006) 034013, [hep-ph/0510108].

[92] A. I. Vainshtein *et al.*, *Sum rules for light quarks in Quantum Chromodynamics*, *Sov. J. Nucl. Phys.* **27** (1978) 274.

[93] K. Maltman and J. Kambor, *$m_u + m_d$ from isovector pseudoscalar sum rules*, *Phys. Lett.* **B517** (2001) 332–338, [hep-ph/0107060].

[94] K. G. Chetyrkin, B. A. Kniehl and M. Steinhauser, *Strong coupling constant with flavour thresholds at four loops in the $\overline{\rm MS}$ scheme*, *Phys. Rev. Lett.* **79** (1997) 2184–2187, [hep-ph/9706430].

[95] S. Bethke, *The 2009 world average of $\alpha_s(M_Z)$*, *Eur. Phys. J.* **C64** (2009) 689–703, [arXiv:0908.1135].

[96] [ETM 10] R. Baron *et al.*, *Light hadrons from lattice QCD with light (u,d), strange and charm dynamical quarks*, *JHEP* **1006** (2010) 111, [arXiv:1004.5284].

[97] [BMW 08] S. Dürr *et al.*, *Ab-initio determination of light hadron masses*, *Science* **322** (2008) 1224–1227, [arXiv:0906.3599].

[98] S. Weinberg, *The problem of mass*, *Trans. New York Acad. Sci.* **38** (1977) 185–201.

[99] J. A. Oller and L. Roca, *Non-perturbative study of the light pseudoscalar masses in chiral dynamics*, *Eur. Phys. J.* **A34** (2007) 371–386, [hep-ph/0608290].

[100] R. Kaiser, *The η and the η' at large N_c, diploma work, University of Bern* (1997); H. Leutwyler, *On the 1/N-expansion in chiral perturbation theory*, *Nucl. Phys. Proc. Suppl.* **64** (1998) 223–231, [hep-ph/9709408].

[101] H. Leutwyler, *The ratios of the light quark masses*, *Phys. Lett.* **B378** (1996) 313–318, [hep-ph/9602366].

[102] [RM123 11] G. M. de Divitiis, P. Dimopoulos, R. Frezzotti, V. Lubicz, G. Martinelli *et al.*, *Isospin breaking effects due to the up-down mass difference in lattice QCD*, *JHEP* **1204** (2012) 124, [arXiv:1110.6294].

[103] J. Gasser and H. Leutwyler, *$\eta \to 3\pi$ to one loop*, *Nucl. Phys.* **B250** (1985) 539.

[104] J. Kambor, C. Wiesendanger and D. Wyler, *Final state interactions and Khuri-Treiman equations in $\eta \to 3\pi$ decays*, *Nucl. Phys.* **B465** (1996) 215–266, [hep-ph/9509374].

[105] A. V. Anisovich and H. Leutwyler, *Dispersive analysis of the decay $\eta \to 3\pi$*, *Phys. Lett.* **B375** (1996) 335–342, [hep-ph/9601237].

[106] C. Ditsche, B. Kubis and U.-G. Meissner, *Electromagnetic corrections in $\eta \to 3\pi$ decays*, *Eur. Phys. J.* **C60** (2009) 83–105, [arXiv:0812.0344].

[107] G. Colangelo, S. Lanz and E. Passemar, *A new dispersive analysis of $\eta \to 3\pi$*, *PoS* **CD09** (2009) 047, [arXiv:0910.0765].

[108] J. Bijnens and K. Ghorbani, *$\eta \to 3\pi$ at two loops in chiral perturbation theory*, *JHEP* **11** (2007) 030, [arXiv:0709.0230].

[109] M. Antonelli *et al.*, *An evaluation of $|V_{us}|$ and precise tests of the Standard Model from world data on leptonic and semileptonic kaon decays*, *Eur. Phys. J.* **C69** (2010) 399–424, [arXiv:1005.2323].

[110] J. Gasser and G. R. S. Zarnauskas, *On the pion decay constant*, *Phys. Lett.* **B693** (2010) 122–128, [arXiv:1008.3479].

[111] J. L. Rosner and S. Stone, *Leptonic decays of charged pseudoscalar mesons, in Review of Particle Physics*, *Phys.Rev.* **D86** (2012) 010001, [arXiv:1201.2401].

[112] J. C. Hardy and I. S. Towner, *Superallowed $0^+ \to 0^+$ nuclear β decays: A new survey with precision tests of the conserved vector current hypothesis and the Standard Model*, *Phys. Rev.* **C79** (2009) 055502, [arXiv:0812.1202].

[113] I. S. Towner and J. C. Hardy, *An improved calculation of the isospin-symmetry-breaking corrections to superallowed Fermi β decay*, *Phys. Rev.* **C77** (2008) 025501, [arXiv:0710.3181].

[114] G. A. Miller and A. Schwenk, *Isospin-symmetry-breaking corrections to superallowed Fermi β decay: formalism and schematic models*, *Phys. Rev.* **C78** (2008) 035501, [arXiv:0805.0603].

[115] N. Auerbach, *Coulomb corrections to superallowed β decay in nuclei*, *Phys. Rev.* **C79** (2009) 035502, [arXiv:0811.4742].

[116] H. Liang, N. Van Giai and J. Meng, *Isospin corrections for superallowed Fermi β decay in self-consistent relativistic random-phase approximation approaches*, *Phys. Rev.* **C79** (2009) 064316, [arXiv:0904.3673].

[117] G. A. Miller and A. Schwenk, *Isospin-symmetry-breaking corrections to superallowed Fermi β decay: radial excitations*, *Phys. Rev.* **C80** (2009) 064319, [arXiv:0910.2790].

[118] I. Towner and J. Hardy, *Comparative tests of isospin-symmetry-breaking corrections to superallowed $0^+ \to 0^+$ nuclear β decay*, *Phys.Rev.* **C82** (2010) 065501, [arXiv:1007.5343].

[119] E. Gamiz, M. Jamin, A. Pich, J. Prades and F. Schwab, *Determination of m_s and $|V_{us}|$ from hadronic τ decays*, *JHEP* **01** (2003) 060, [hep-ph/0212230].

[120] E. Gamiz, M. Jamin, A. Pich, J. Prades and F. Schwab, *V_{us} and m_s from hadronic τ decays*, *Phys. Rev. Lett.* **94** (2005) 011803, [hep-ph/0408044].

[121] K. Maltman, *A mixed τ-electroproduction sum rule for V_{us}*, *Phys. Lett.* **B672** (2009) 257–263, [arXiv:0811.1590].

[122] A. Pich and R. Kass, *talks given at CKM 2008*, http://ckm2008.roma1.infn.it.

[123] [HFAG 12] Y. Amhis *et al.*, *Averages of b-hadron, c-hadron and τ-lepton properties as of early 2012*, arXiv:1207.1158.

[124] K. Maltman, C. E. Wolfe, S. Banerjee, J. M. Roney and I. Nugent, *Status of the hadronic τ determination of V_{us}*, *Int. J. Mod. Phys.* **A23** (2008) 3191–3195, [arXiv:0807.3195].

[125] K. Maltman, C. E. Wolfe, S. Banerjee, I. M. Nugent and J. M. Roney, *Status of the hadronic τ decay determination of $|V_{us}|$*, *Nucl. Phys. Proc. Suppl.* **189** (2009) 175–180, [arXiv:0906.1386].

[126] E. Gamiz, M. Jamin, A. Pich, J. Prades and F. Schwab, *Theoretical progress on the V_{us} determination from τ decays*, *PoS* **KAON07** (2008) 008, [arXiv:0709.0282].

[127] E. Gamiz, *$|V_{us}|$ from hadronic τ decays, CKM 2012*, arXiv:1301.2206.

[128] M. Beneke and M. Jamin, *α_s and the τ hadronic width: fixed-order, contour-improved and higher-order perturbation theory*, *JHEP* **09** (2008) 044, [arXiv:0806.3156].

[129] I. Caprini and J. Fischer, *α_s from τ decays: contour-improved versus fixed-order summation in a new QCD perturbation expansion*, *Eur. Phys. J.* **C64** (2009) 35–45, [arXiv:0906.5211].

[130] S. Menke, *On the determination of α_s from hadronic τ decays with contour-improved, fixed order and renormalon-chain perturbation theory*, arXiv:0904.1796.

[131] P. Boyle, L. Del Debbio, N. Garron, R. Hudspith, E. Kerrane *et al.*, *New results from the lattice on the theoretical inputs to the hadronic τ determination of V_{us}*, *PoS* **ConfinementX** (2012) 100, [arXiv:1301.4930].

[132] T. Izubuchi, *Lattice QCD + QED - from Isospin breaking to g-2 light-by-light*, talk given at Lattice 2012, Cairns, Australia, http://www.physics.adelaide.edu.au/cssm/lattice2012.

[133] [MILC 12] A. Bazavov, C. Bernard, C. Bouchard, C. DeTar, D. Du *et al.*, *Kaon semileptonic vector form factor and determination of $|V_{us}|$ using staggered fermions*, *Phys.Rev.* **D87** (2013) 073012, [arXiv:1212.4993].

[134] [JLQCD 12] T. Kaneko *et al.*, *Chiral behavior of kaon semileptonic form factors in lattice QCD with exact chiral symmetry*, *PoS* **LAT2012** (2012) 111, [arXiv:1211.6180].

[135] [JLQCD 11] T. Kaneko *et al.*, *Kaon semileptonic form factors in QCD with exact chiral symmetry*, *PoS* **LAT2011** (2011) 284, [arXiv:1112.5259].

[136] [RBC/UKQCD 10] P. A. Boyle *et al.*, *$K \to \pi$ form factors with reduced model dependence*, *Eur.Phys.J.* **C69** (2010) 159–167, [arXiv:1004.0886].

[137] [RBC/UKQCD 07] P. A. Boyle, A. Jüttner, R. Kenway, C. Sachrajda, S. Sasaki *et al.*, *K_{l3} semileptonic form-factor from 2+1 flavour lattice QCD*, *Phys.Rev.Lett.* **100** (2008) 141601, [arXiv:0710.5136].

[138] [ETM 10D] V. Lubicz, F. Mescia, L. Orifici, S. Simula and C. Tarantino, *Improved analysis of the scalar and vector form factors of kaon semileptonic decays with $N_f = 2$ twisted-mass fermions*, *PoS* **LAT2010** (2010) 316, [arXiv:1012.3573].

[139] [ETM 09A] V. Lubicz, F. Mescia, S. Simula and C. Tarantino, *$K \to \pi \ell \nu$ semileptonic form factors from two-flavor lattice QCD*, *Phys. Rev.* **D80** (2009) 111502, [arXiv:0906.4728].

[140] [QCDSF 07] D. Brömmel *et al.*, *Kaon semileptonic decay form factors from $N_f = 2$ non-perturbatively $O(a)$-improved Wilson fermions*, *PoS* **LAT2007** (2007) 364, [arXiv:0710.2100].

[141] [RBC 06] C. Dawson, T. Izubuchi, T. Kaneko, S. Sasaki and A. Soni, *Vector form factor in K_{l3} semileptonic decay with two flavors of dynamical domain-wall quarks*, *Phys. Rev.* **D74** (2006) 114502, [hep-ph/0607162].

[142] [JLQCD 05] N. Tsutsui *et al.*, *Kaon semileptonic decay form factors in two-flavor QCD*, *PoS* **LAT2005** (2006) 357, [hep-lat/0510068].

[143] M. Ademollo and R. Gatto, *Nonrenormalization theorem for the strangeness violating vector currents*, *Phys. Rev. Lett.* **13** (1964) 264–265.

[144] G. Furlan, F. Lannoy, C. Rossetti and G. Segré, *Symmetry-breaking corrections to weak vector currents*, *Nuovo Cim.* **38** (1965) 1747.

[145] J. Gasser and H. Leutwyler, *Low-energy expansion of meson form factors*, *Nucl. Phys.* **B250** (1985) 517–538.

[146] D. Bećirević, G. Martinelli and G. Villadoro, *The Ademollo-Gatto theorem for lattice semileptonic decays*, *Phys. Lett.* **B633** (2006) 84–88, [hep-lat/0508013].

[147] [RBC 08] J. M. Flynn and C. T. Sachrajda, *SU(2) chiral perturbation theory for $K_{\ell 3}$ decay amplitudes*, *Nucl. Phys.* **B812** (2009) 64–80, [arXiv:0809.1229].

[148] [HPQCD 13A] R. Dowdall, C. Davies, G. Lepage and C. McNeile, *V_{us} from π and K decay constants in full lattice QCD with physical u, d, s and c quarks*, arXiv:1303.1670.

[149] [MILC 13A] A. Bazavov, C. Bernard, C. DeTar, J. Foley, W. Freeman *et al.*, *Leptonic decay-constant ratio f_{K^+}/f_{π^+} from lattice QCD with physical light quarks*, *Phys.Rev.Lett.* **110** (2013) 172003, [arXiv:1301.5855].

[150] [ETM 10E] F. Farchioni, G. Herdoiza, K. Jansen, M. Petschlies, C. Urbach *et al.*, *Pseudoscalar decay constants from $N_f = 2 + 1 + 1$ twisted mass lattice QCD*, *PoS* **LAT2010** (2010) 128, [arXiv:1012.0200].

[151] [MILC 10] A. Bazavov *et al.*, *Results for light pseudoscalar mesons*, *PoS* **LAT2010** (2010) 074, [arXiv:1012.0868].

[152] [JLQCD/TWQCD 10] J. Noaki *et al.*, *Chiral properties of light mesons in $N_f = 2 + 1$ overlap QCD*, *PoS* **LAT2010** (2010) 117.

[153] [BMW 10] S. Dürr, Z. Fodor, C. Hoelbling, S. Katz, S. Krieg *et al.*, *The ratio F_K/F_π in QCD*, *Phys.Rev.* **D81** (2010) 054507, [arXiv:1001.4692].

[154] [JLQCD/TWQCD 09A] J. Noaki *et al.*, *Chiral properties of light mesons with $N_f = 2 + 1$ overlap fermions*, *PoS* **LAT2009** (2009) 096, [arXiv:0910.5532].

[155] C. Aubin, J. Laiho and R. S. Van de Water, *Light pseudoscalar meson masses and decay constants from mixed action lattice QCD*, *PoS* **LAT2008** (2008) 105, [arXiv:0810.4328].

[156] [PACS-CS 08A] Y. Kuramashi, *PACS-CS results for 2+1 flavor lattice QCD simulation on and off the physical point*, *PoS* **LAT2008** (2008) 018, [arXiv:0811.2630].

[157] [HPQCD/UKQCD 07] E. Follana, C. T. H. Davies, G. P. Lepage and J. Shigemitsu, *High precision determination of the π, K, D and D_s decay constants from lattice QCD*, *Phys. Rev. Lett.* **100** (2008) 062002, [arXiv:0706.1726].

[158] [NPLQCD 06] S. R. Beane, P. F. Bedaque, K. Orginos and M. J. Savage, *f_K/f_π in full QCD with domain wall valence quarks*, *Phys. Rev.* **D75** (2007) 094501, [hep-lat/0606023].

[159] [BGR 11] G. P. Engel, C. Lang, M. Limmer, D. Mohler and A. Schäfer, *QCD with two light dynamical chirally improved quarks: mesons*, *Phys.Rev.* **D85** (2012) 034508, [arXiv:1112.1601].

[160] [ETM 09] B. Blossier *et al.*, *Pseudoscalar decay constants of kaon and D-mesons from $N_f = 2$ twisted mass lattice QCD*, *JHEP* **0907** (2009) 043, [arXiv:0904.0954].

[161] [QCDSF/UKQCD 07] G. Schierholz *et al.*, *Probing the chiral limit with clover fermions I: the meson sector, talk given at Lattice 2007, Regensburg, Germany*, PoS **LAT2007**, 133.

[162] A. Kastner and H. Neufeld, *The K_{l3} scalar form factors in the Standard Model*, *Eur. Phys. J.* **C57** (2008) 541–556, [arXiv:0805.2222].

[163] V. Cirigliano *et al.*, *The Green function and SU(3) breaking in K_{l3} decays*, *JHEP* **04** (2005) 006, [hep-ph/0503108].

[164] M. Jamin, J. A. Oller and A. Pich, *Order p^6 chiral couplings from the scalar $K\pi$ form factor*, *JHEP* **02** (2004) 047, [hep-ph/0401080].

[165] J. Bijnens and P. Talavera, *K_{l3} decays in chiral perturbation theory*, *Nucl. Phys.* **B669** (2003) 341–362, [hep-ph/0303103].

[166] H. Leutwyler and M. Roos, *Determination of the elements V_{us} and V_{ud} of the Kobayashi-Maskawa matrix*, *Z. Phys.* **C25** (1984) 91.

[167] P. Post and K. Schilcher, *K_{l3} form factors at order p^6 in chiral perturbation theory*, *Eur. Phys. J.* **C25** (2002) 427–443, [hep-ph/0112352].

[168] V. Cirigliano and H. Neufeld, *A note on isospin violation in $P_{\ell 2}(\gamma)$ decays*, *Phys.Lett.* **B700** (2011) 7–10, [arXiv:1102.0563].

[169] [FNAL/MILC 12D] E. Gamiz *et al.*, *Kaon semileptonic decay form factors with HISQ valence quarks*, *PoS* **LAT2012** (2012) 113, [arXiv:1211.0751].

[170] D. Guadagnoli, F. Mescia and S. Simula, *Lattice study of semileptonic form-factors with twisted boundary conditions*, *Phys.Rev.* **D73** (2006) 114504, [hep-lat/0512020].

[171] [UKQCD 07] P. A. Boyle, J. Flynn, A. Jüttner, C. Sachrajda and J. Zanotti, *Hadronic form factors in lattice QCD at small and vanishing momentum transfer*, *JHEP* **0705** (2007) 016, [hep-lat/0703005].

[172] [ETM 09F] S. Di Vita *et al.*, *Vector and scalar form factors for K- and D-meson semileptonic decays from twisted mass fermions with $N_f = 2$*, *PoS* **LAT2009** (2009) 257, [arXiv:0910.4845].

[173] [SPQcdR 04] D. Bećirević *et al.*, *The $K \to \pi$ vector form factor at zero momentum transfer on the lattice*, *Nucl. Phys.* **B705** (2005) 339–362, [hep-ph/0403217].

[174] [TWQCD 11] T.-W. Chiu, T.-H. Hsieh and Y.-Y. Mao, *Pseudoscalar meson in two flavors QCD with the optimal domain-wall fermion*, *Phys.Lett.* **B717** (2012) 420–424, [arXiv:1109.3675].

[175] [HPQCD 09B] C. T. H. Davies, E. Follana, I. Kendall, G. P. Lepage and C. McNeile, *Precise determination of the lattice spacing in full lattice QCD*, *Phys.Rev.* **D81** (2010) 034506, [arXiv:0910.1229].

[176] M. E. Fisher and V. Privman, *First-order transitions breaking O(n) symmetry: finite-size scaling*, *Phys. Rev.* **B32** (1985) 447–464.

[177] E. Brezin and J. Zinn-Justin, *Finite size effects in phase transitions*, *Nucl. Phys.* **B257** (1985) 867.

[178] J. Gasser and H. Leutwyler, *Light quarks at low temperatures*, *Phys. Lett.* **B184** (1987) 83.

[179] J. Gasser and H. Leutwyler, *Thermodynamics of chiral symmetry*, *Phys. Lett.* **B188** (1987) 477.

[180] J. Gasser and H. Leutwyler, *Spontaneously broken symmetries: effective Lagrangians at finite volume*, *Nucl. Phys.* **B307** (1988) 763.

[181] P. Hasenfratz and H. Leutwyler, *Goldstone boson related finite size effects in field theory and critical phenomena with O(N) symmetry*, *Nucl. Phys.* **B343** (1990) 241–284.

[182] G. Colangelo, J. Gasser and H. Leutwyler, *$\pi\pi$ scattering*, *Nucl. Phys.* **B603** (2001) 125–179, [hep-ph/0103088].

[183] F. C. Hansen, *Finite size effects in spontaneously broken SU(N)×SU(N) theories*, *Nucl. Phys.* **B345** (1990) 685–708.

[184] F. C. Hansen and H. Leutwyler, *Charge correlations and topological susceptibility in QCD*, *Nucl. Phys.* **B350** (1991) 201–227.

[185] L. Giusti, P. Hernandez, M. Laine, P. Weisz and H. Wittig, *Low-energy couplings of QCD from current correlators near the chiral limit*, *JHEP* **0404** (2004) 013, [hep-lat/0402002].

[186] H. Leutwyler and A. V. Smilga, *Spectrum of Dirac operator and role of winding number in QCD*, *Phys. Rev.* **D46** (1992) 5607–5632.

[187] P. H. Damgaard, M. C. Diamantini, P. Hernandez and K. Jansen, *Finite-size scaling of meson propagators*, *Nucl. Phys.* **B629** (2002) 445–478, [hep-lat/0112016].

[188] P. H. Damgaard, P. Hernandez, K. Jansen, M. Laine and L. Lellouch, *Finite-size scaling of vector and axial current correlators*, *Nucl. Phys.* **B656** (2003) 226–238, [hep-lat/0211020].

[189] S. Aoki and H. Fukaya, *Chiral perturbation theory in a θ vacuum*, *Phys. Rev.* **D81** (2010) 034022, [arXiv:0906.4852].

[190] F. Bernardoni, P. H. Damgaard, H. Fukaya and P. Hernandez, *Finite volume scaling of Pseudo Nambu-Goldstone Bosons in QCD*, *JHEP* **10** (2008) 008, [arXiv:0808.1986].

[191] P. Hernandez, S. Necco, C. Pena and G. Vulvert, $N_f = 2$ *chiral dynamics in the mixed chiral regime*, *PoS* **LAT2012** (2012) 204, [arXiv:1211.1488].

[192] P. H. Damgaard and H. Fukaya, *The chiral condensate in a finite volume*, *JHEP* **01** (2009) 052, [arXiv:0812.2797].

[193] S. Aoki and H. Fukaya, *Interpolation between the* ϵ*- and p-regimes*, *Phys.Rev.* **D84** (2011) 014501, [arXiv:1105.1606].

[194] H. Leutwyler, *Energy levels of light quarks confined to a box*, *Phys. Lett.* **B189** (1987) 197.

[195] P. Hasenfratz, *The QCD rotator in the chiral limit*, *Nucl. Phys.* **B828** (2010) 201–214, [arXiv:0909.3419].

[196] F. Niedermayer and C. Weiermann, *The rotator spectrum in the* δ*-regime of the* $O(n)$ *effective field theory in 3 and 4 dimensions*, *Nucl. Phys.* **B842** (2011) 248–263, [arXiv:1006.5855].

[197] M. Weingart, *The QCD rotator with a light quark mass*, arXiv:1006.5076.

[198] A. Hasenfratz, P. Hasenfratz, F. Niedermayer, D. Hierl and A. Schäfer, *First results in QCD with 2+1 light flavors using the fixed-point action*, *PoS* **LAT2006** (2006) 178, [hep-lat/0610096].

[199] [QCDSF 10] W. Bietenholz *et al.*, *Pion in a box*, *Phys. Lett.* **B687** (2010) 410–414, [arXiv:1002.1696].

[200] P. Di Vecchia and G. Veneziano, *Chiral dynamics in the large N limit*, *Nucl. Phys.* **B171** (1980) 253.

[201] [TWQCD 09] Y.-Y. Mao and T.-W. Chiu, *Topological susceptibility to the one-loop order in chiral perturbation theory*, *Phys. Rev.* **D80** (2009) 034502, [arXiv:0903.2146].

[202] V. Bernard, S. Descotes-Genon and G. Toucas, *Topological susceptibility on the lattice and the three-flavour quark condensate*, *JHEP* **1206** (2012) 051, [arXiv:1203.0508].

[203] V. Bernard, S. Descotes-Genon and G. Toucas, *Determining the chiral condensate from the distribution of the winding number beyond topological susceptibility*, arXiv:1209.4367.

[204] [CERN 08] L. Giusti and M. Lüscher, *Chiral symmetry breaking and the Banks–Casher relation in lattice QCD with Wilson quarks*, *JHEP* **03** (2009) 013, [arXiv:0812.3638].

[205] T. Banks and A. Casher, *Chiral symmetry breaking in confining theories*, *Nucl. Phys.* **B169** (1980) 103.

[206] [ETM 13] K. Cichy, E. Garcia-Ramos and K. Jansen, *Chiral condensate from the twisted mass Dirac operator spectrum*, arXiv:1303.1954.

[207] S. Necco and A. Shindler, *Corrections to the Banks-Casher relation with Wilson quarks*, *PoS* **CD12** (2012) 056, [arXiv:1302.5595].

[208] E. V. Shuryak and J. J. M. Verbaarschot, *Random matrix theory and spectral sum rules for the Dirac operator in QCD*, *Nucl. Phys.* **A560** (1993) 306–320, [hep-th/9212088].

[209] J. J. M. Verbaarschot and I. Zahed, *Spectral density of the QCD Dirac operator near zero virtuality*, *Phys. Rev. Lett.* **70** (1993) 3852–3855, [hep-th/9303012].

[210] J. J. M. Verbaarschot, *The spectrum of the QCD Dirac operator and chiral random matrix theory: the threefold way*, *Phys. Rev. Lett.* **72** (1994) 2531–2533, [hep-th/9401059].

[211] J. J. M. Verbaarschot and T. Wettig, *Random matrix theory and chiral symmetry in QCD*, *Ann. Rev. Nucl. Part. Sci.* **50** (2000) 343–410, [hep-ph/0003017].

[212] S. M. Nishigaki, P. H. Damgaard and T. Wettig, *Smallest Dirac eigenvalue distribution from random matrix theory*, *Phys. Rev.* **D58** (1998) 087704, [hep-th/9803007].

[213] P. H. Damgaard and S. M. Nishigaki, *Distribution of the k-th smallest Dirac operator eigenvalue*, *Phys. Rev.* **D63** (2001) 045012, [hep-th/0006111].

[214] F. Basile and G. Akemann, *Equivalence of QCD in the ϵ-regime and chiral random matrix theory with or without chemical potential*, *JHEP* **12** 043, [arXiv:0710.0376].

[215] M. Kieburg, J. J. M. Verbaarschot and S. Zafeiropoulos, *Random matrix models for the hermitian Wilson-Dirac operator of QCD-like theories*, *PoS* **LAT2012** (2012) 209, [arXiv:1303.3242].

[216] G. Akemann, P. H. Damgaard, J. C. Osborn and K. Splittorff, *A new chiral two-matrix theory for Dirac spectra with imaginary chemical potential*, *Nucl. Phys.* **B766** (2007) 34–67, [hep-th/0609059].

[217] C. Lehner, S. Hashimoto and T. Wettig, *The ϵ-expansion at next-to-next-to-leading order with small imaginary chemical potential*, *JHEP* **06** (2010) 028, [arXiv:1004.5584].

[218] C. Lehner, J. Bloch, S. Hashimoto and T. Wettig, *Geometry dependence of RMT-based methods to extract the low-energy constants Σ and F*, *JHEP* **1105** (2011) 115, [arXiv:1101.5576].

[219] [CERN-TOV 05] L. Del Debbio, L. Giusti, M. Lüscher, R. Petronzio and N. Tantalo, *Stability of lattice QCD simulations and the thermodynamic limit*, *JHEP* **02** (2006) 011, [hep-lat/0512021].

[220] [JLQCD/TWQCD 07B] H. Fukaya *et al.*, *Two-flavor lattice QCD in the ϵ-regime and chiral random matrix theory*, *Phys. Rev.* **D76** (2007) 054503, [arXiv:0705.3322].

[221] [BGR 06] C. B. Lang, P. Majumdar and W. Ortner, *The condensate for two dynamical chirally improved quarks in QCD*, *Phys. Lett.* **B649** (2007) 225–229, [hep-lat/0611010].

[222] T. DeGrand, Z. Liu and S. Schaefer, *Quark condensate in two-flavor QCD*, *Phys. Rev.* **D74** (2006) 094504, [hep-lat/0608019].

[223] P. Hasenfratz *et al.*, *2+1 flavor QCD simulated in the ϵ-regime in different topological sectors*, *JHEP* **11** (2009) 100, [arXiv:0707.0071].

[224] T. DeGrand and S. Schaefer, *Parameters of the lowest order chiral Lagrangian from fermion eigenvalues*, *Phys. Rev.* **D76** (2007) 094509, [arXiv:0708.1731].

[225] J. F. Donoghue, J. Gasser and H. Leutwyler, *The decay of a light Higgs boson*, *Nucl. Phys.* **B343** (1990) 341–368.

[226] J. Bijnens, G. Colangelo and P. Talavera, *The vector and scalar form factors of the pion to two loops*, *JHEP* **05** (1998) 014, [hep-ph/9805389].

[227] [ETM 08] R. Frezzotti, V. Lubicz and S. Simula, *Electromagnetic form factor of the pion from twisted-mass lattice QCD at $N_f = 2$*, *Phys. Rev.* **D79** (2009) 074506, [arXiv:0812.4042].

[228] [JLQCD/TWQCD 08] T. Kaneko *et al.*, *Pion vector and scalar form factors with dynamical overlap quarks*, *PoS* **LAT2008** (2008) 158, [arXiv:0810.2590].

[229] A. Jüttner, *Revisiting the pion's scalar form factor in chiral perturbation theory*, *JHEP* **1201** (2012) 007, [arXiv:1110.4859].

[230] [ETM 09C] R. Baron *et al.*, *Light meson physics from maximally twisted mass lattice QCD*, *JHEP* **08** (2010) 097, [arXiv:0911.5061].

[231] J. Gasser, C. Haefeli, M. A. Ivanov and M. Schmid, *Integrating out strange quarks in ChPT*, *Phys. Lett.* **B652** (2007) 21–26, [arXiv:0706.0955].

[232] J. Gasser, C. Haefeli, M. A. Ivanov and M. Schmid, *Integrating out strange quarks in ChPT: terms at order p^6*, *Phys. Lett.* **B675** (2009) 49–53, [arXiv:0903.0801].

[233] S. Dürr, *Convergence issues in ChPT: a lattice perspective*, *PoS* **KAON13** (2013) 027, [arXiv:1305.5758].

[234] G. Rupak and N. Shoresh, *Chiral perturbation theory for the Wilson lattice action*, *Phys. Rev.* **D66** (2002) 054503, [hep-lat/0201019].

[235] S. Aoki, *Chiral perturbation theory with Wilson-type fermions including a^2 effects: $N_f = 2$ degenerate case*, *Phys. Rev.* **D68** (2003) 054508, [hep-lat/0306027].

[236] O. Bär, G. Rupak and N. Shoresh, *Chiral perturbation theory at $O(a^2)$ for lattice QCD*, *Phys. Rev.* **D70** (2004) 034508, [hep-owat/0306021].

[237] [ETM 13A] G. Herdoiza, K. Jansen, C. Michael, K. Ottnad and C. Urbach, *Determination of low-energy constants of Wilson chiral perturbation theory*, *JHEP* **1305** (2013) 038, [arXiv:1303.3516].

[238] S. Borsanyi, S. Dürr, Z. Fodor, S. Krieg, A. Schäfer *et al.*, *SU(2) chiral perturbation theory low-energy constants from 2+1 flavor staggered lattice simulations*, *Phys.Rev.* **D88** (2013) 014513, [arXiv:1205.0788].

[239] [MILC 12B] A. Bazavov *et al.*, *Lattice QCD ensembles with four flavors of highly improved staggered quarks*, *Phys.Rev.* **D87** (2013) 054505, [arXiv:1212.4768].

[240] [JLQCD 09] H. Fukaya *et al.*, *Determination of the chiral condensate from 2+1-flavor lattice QCD*, *Phys. Rev. Lett.* **104** (2010) 122002, [arXiv:0911.5555].

[241] [JLQCD/TWQCD 10A] H. Fukaya *et al.*, *Determination of the chiral condensate from QCD Dirac spectrum on the lattice*, *Phys. Rev.* **D83** (2011) 074501, [arXiv:1012.4052].

[242] [RBC/UKQCD 08A] P. A. Boyle *et al.*, *The pion's electromagnetic form factor at small momentum transfer in full lattice QCD*, *JHEP* **07** (2008) 112, [arXiv:0804.3971].

[243] [TWQCD 08] T.-W. Chiu, T.-H. Hsieh and P.-K. Tseng, *Topological susceptibility in 2+1 flavors lattice QCD with domain-wall fermions*, *Phys. Lett.* **B671** (2009) 135–138, [arXiv:0810.3406].

[244] [JLQCD/TWQCD 08B] T.-W. Chiu *et al.*, *Topological susceptibility in (2+1)-flavor lattice QCD with overlap fermion*, *PoS* **LAT2008** (2008) 072, [arXiv:0810.0085].

[245] [ETM 12] F. Burger, V. Lubicz, M. Muller-Preussker, S. Simula and C. Urbach, *Quark mass and chiral condensate from the Wilson twisted mass lattice quark propagator*, *Phys.Rev.* **D87** (2013) 034514, [arXiv:1210.0838].

[246] F. Bernardoni, N. Garron, P. Hernandez, S. Necco and C. Pena, *Light quark correlators in a mixed-action setup*, *PoS* **LAT2011** (2011) 109, [arXiv:1110.0922].

[247] [TWQCD 11A] T.-W. Chiu, T. H. Hsieh and Y. Y. Mao, *Topological susceptibility in two flavors lattice QCD with the optimal domain-wall fermion*, *Phys.Lett.* **B702** (2011) 131–134, [arXiv:1105.4414].

[248] F. Bernardoni, P. Hernandez, N. Garron, S. Necco and C. Pena, *Probing the chiral regime of $N_f = 2$ QCD with mixed actions*, *Phys. Rev.* **D83** (2011) 054503, [arXiv:1008.1870].

[249] [JLQCD/TWQCD 07A] S. Aoki *et al.*, *Topological susceptibility in two-flavor lattice QCD with exact chiral symmetry*, *Phys. Lett.* **B665** (2008) 294–297, [arXiv:0710.1130].

[250] [ETM 09B] K. Jansen and A. Shindler, *The ϵ-regime of chiral perturbation theory with Wilson-type fermions*, *PoS* **LAT2009** (2009) 070, [arXiv:0911.1931].

[251] A. Hasenfratz, R. Hoffmann and S. Schaefer, *Low energy chiral constants from ϵ-regime simulations with improved Wilson fermions*, *Phys. Rev.* **D78** (2008) 054511, [arXiv:0806.4586].

[252] [JLQCD/TWQCD 07] H. Fukaya *et al.*, *Lattice study of meson correlators in the ϵ-regime of two-flavor QCD*, *Phys. Rev.* **D77** (2008) 074503, [arXiv:0711.4965].

[253] [ETM 11] R. Baron *et al.*, *Light hadrons from $N_f = 2 + 1 + 1$ dynamical twisted mass fermions*, *PoS* **LAT2010** (2010) 123, [arXiv:1101.0518].

[254] [NPLQCD 11] S. R. Beane, W. Detmold, P. Junnarkar, T. Luu, K. Orginos *et al.*, *SU(2) low-energy constants from mixed-action lattice QCD*, *Phys.Rev.* **D86** (2012) 094509, [arXiv:1108.1380].

[255] [QCDSF 13] R. Horsley, Y. Nakamura, A. Nobile, P. Rakow, G. Schierholz *et al.*, *Nucleon axial charge and pion decay constant from two-flavor lattice QCD*, arXiv:1302.2233.

[256] G. Colangelo and S. Dürr, *The pion mass in finite volume*, *Eur. Phys. J.* **C33** (2004) 543–553, [hep-lat/0311023].

[257] [JLQCD/TWQCD 09] S. Aoki *et al.*, *Pion form factors from two-flavor lattice QCD with exact chiral symmetry*, *Phys. Rev.* **D80** (2009) 034508, [arXiv:0905.2465].

[258] [CERN-TOV 06] L. Del Debbio, L. Giusti, M. Lüscher, R. Petronzio and N. Tantalo, *QCD with light Wilson quarks on fine lattices (I): first experiences and physics results*, *JHEP* **02** (2007) 056, [hep-lat/0610059].

[259] O. Bär, *Chiral logs in twisted mass lattice QCD with large isospin breaking*, *Phys.Rev.* **D82** (2010) 094505, [arXiv:1008.0784].

[260] G. Colangelo, U. Wenger and J. M. S. Wu, *Twisted mass finite volume effects*, *Phys. Rev.* **D82** (2010) 034502, [arXiv:1003.0847].

[261] [LHP 04] F. D. R. Bonnet, R. G. Edwards, G. T. Fleming, R. Lewis and D. G. Richards, *Lattice computations of the pion form factor*, *Phys. Rev.* **D72** (2005) 054506, [hep-lat/0411028].

[262] [QCDSF/UKQCD 06A] D. Brömmel *et al.*, *The pion form factor from lattice QCD with two dynamical flavours*, *Eur. Phys. J.* **C51** (2007) 335–345, [hep-lat/0608021].

[263] S. R. Amendolia *et al.*, *A measurement of the space-like pion electromagnetic form factor*, *Nucl. Phys.* **B277** (1986) 168.

[264] S. Dürr, *M_π^2 versus m_q: comparing CP-PACS and UKQCD data to chiral perturbation theory*, *Eur. Phys. J.* **C29** (2003) 383–395, [hep-lat/0208051].

[265] N. H. Fuchs, H. Sazdjian and J. Stern, *How to probe the scale of $\bar{q}q$ in chiral perturbation theory*, *Phys. Lett.* **B269** (1991) 183–188.

[266] J. Stern, H. Sazdjian and N. H. Fuchs, *What π-π scattering tells us about chiral perturbation theory*, *Phys. Rev.* **D47** (1993) 3814–3838, [hep-ph/9301244].

[267] S. Descotes-Genon, L. Girlanda and J. Stern, *Paramagnetic effect of light quark loops on chiral symmetry breaking*, *JHEP* **01** (2000) 041, [hep-ph/9910537].

[268] V. Bernard, S. Descotes-Genon and G. Toucas, *Chiral dynamics with strange quarks in the light of recent lattice simulations*, *JHEP* **1101** (2011) 107, [arXiv:1009.5066].

[269] J. Bijnens, N. Danielsson and T. A. Lähde, *Three-flavor partially quenched chiral perturbation theory at NNLO for meson masses and decay constants*, *Phys. Rev.* **D73** (2006) 074509, [hep-lat/0602003].

[270] J. Bijnens and I. Jemos, *A new global fit of the L_i^r at next-to-next-to-leading order in chiral perturbation theory*, *Nucl.Phys.* **B854** (2012) 631–665, [arXiv:1103.5945].

[271] C. Bernard and M. Golterman, *On the foundations of partially quenched chiral perturbation theory*, *Phys.Rev.* **D88** (2013) 014004, [arXiv:1304.1948].

[272] [JLQCD 08A] E. Shintani *et al.*, *S-parameter and pseudo-Nambu-Goldstone boson mass from lattice QCD*, *Phys. Rev. Lett.* **101** (2008) 242001, [arXiv:0806.4222].

[273] RBC Collaborations, UKQCD Collaborations Collaboration, P. A. Boyle, L. Del Debbio, J. Wennekers and J. M. Zanotti, *The S Parameter in QCD from Domain Wall Fermions*, *Phys.Rev.* **D81** (2010) 014504, [arXiv:0909.4931].

[274] J. Bijnens and P. Talavera, *Pion and kaon electromagnetic form-factors*, *JHEP* **0203** (2002) 046, [hep-ph/0203049].

[275] M. Davier, L. Girlanda, A. Hocker and J. Stern, *Finite energy chiral sum rules and tau spectral functions*, *Phys.Rev.* **D58** (1998) 096014, [hep-ph/9802447].

[276] C. Jung, *Status of dynamical ensemble generation*, *PoS* **LAT2009** (2009) 002, [arXiv:1001.0941].

[277] G. C. Branco, L. Lavoura and J. P. Silva, *CP violation*, *Int. Ser. Monogr. Phys.* **103** (1999) 1–536.

[278] G. Buchalla, A. J. Buras and M. E. Lautenbacher, *Weak decays beyond leading logarithms*, *Rev. Mod. Phys.* **68** (1996) 1125–1144, [hep-ph/9512380].

[279] A. J. Buras, *Weak Hamiltonian, CP violation and rare decays*, hep-ph/9806471. Published in *Les Houches 1997, Probing the standard model of particle interactions*, Pt. 1, 281-539.

[280] T. Inami and C. S. Lim, *Effects of superheavy quarks and leptons in low-energy weak processes $K_L \to \mu\bar{\mu}$, $K^+ \to \pi^+\nu\bar{\nu}$ and $K^0 \leftrightarrow \bar{K}^0$*, *Prog. Theor. Phys.* **65** (1981) 297.

[281] J. Brod and M. Gorbahn, *Next-to-next-to-leading-order charm-quark contribution to the CP violation parameter ϵ_K and ΔM_K*, *Phys.Rev.Lett.* **108** (2012) 121801, [arXiv:1108.2036].

[282] J. Brod and M. Gorbahn, *ϵ_K at next-to-next-to-leading order: the charm-top-quark contribution*, *Phys. Rev.* **D82** (2010) 094026, [arXiv:1007.0684].

[283] G. Martinelli, C. Pittori, C. T. Sachrajda, M. Testa and A. Vladikas, *A general method for nonperturbative renormalization of lattice operators*, *Nucl. Phys.* **B445** (1995) 81–108, [hep-lat/9411010].

[284] C. Aubin, J. Laiho and R. S. Van de Water, *The neutral kaon mixing parameter B_K from unquenched mixed-action lattice QCD*, *Phys. Rev.* **D81** (2010) 014507, [arXiv:0905.3947].

[285] [SWME 11] J. Kim, C. Jung, H.-J. Kim, W. Lee and S. R. Sharpe, *Finite volume effects in B_K with improved staggered fermions*, *Phys.Rev.* **D83** (2011) 117501, [arXiv:1101.2685].

[286] [SWME 11A] T. Bae *et al.*, *Kaon B-parameter from improved staggered fermions in $N_f = 2+1$ QCD*, *Phys.Rev.Lett.* **109** (2012) 041601, [arXiv:1111.5698].

[287] [BMW 11] S. Dürr, Z. Fodor, C. Hoelbling, S. Katz, S. Krieg *et al.*, *Precision computation of the kaon bag parameter*, *Phys.Lett.* **B705** (2011) 477–481, [arXiv:1106.3230].

[288] [ALPHA 07A] P. Dimopoulos *et al.*, *Non-perturbative renormalisation of $\Delta F = 2$ four-fermion operators in two-flavour QCD*, *JHEP* **0805** (2008) 065, [arXiv:0712.2429].

[289] K. Anikeev *et al.*, *B physics at the Tevatron: Run II and beyond*, hep-ph/0201071.

[290] U. Nierste, *Three lectures on meson mixing and CKM phenomenology, published in Dubna 2008, Heavy Quark Physics (HQP08), pp. 1-39*, arXiv:0904.1869.

[291] A. J. Buras, D. Guadagnoli and G. Isidori, *On ϵ_K beyond lowest order in the operator product expansion*, *Phys. Lett.* **B688** (2010) 309–313, [arXiv:1002.3612].

[292] A. J. Buras and D. Guadagnoli, *Correlations among new CP violating effects in $\Delta F = 2$ observables*, *Phys. Rev.* **D78** (2008) 033005, [arXiv:0805.3887].

[293] [RBC/UKQCD 11A] T. Blum, P. Boyle, N. Christ, N. Garron, E. Goode *et al.*, *The $K \to (\pi\pi)_{I=2}$ decay amplitude from lattice QCD*, *Phys. Rev. Lett.* **108** (2012) 141601, [arXiv:1111.1699].

[294] [RBC/UKQCD 12D] T. Blum, P. Boyle, N. Christ, N. Garron, E. Goode *et al.*, *Lattice determination of the $K \to (\pi\pi)_{I=2}$ decay amplitude A_2*, *Phys. Rev.* **D86** (2012) 074513, [arXiv:1206.5142].

[295] D. Bećirević *et al.*, *$K^0\bar{K}^0$ mixing with Wilson fermions without subtractions*, *Phys. Lett.* **B487** (2000) 74–80, [hep-lat/0005013].

[296] [ALPHA 01] R. Frezzotti, P. A. Grassi, S. Sint and P. Weisz, *Lattice QCD with a chirally twisted mass term*, *JHEP* **08** (2001) 058, [hep-lat/0101001].

[297] [ALPHA 06] P. Dimopoulos *et al.*, *A precise determination of B_K in quenched QCD*, *Nucl. Phys.* **B749** (2006) 69–108, [hep-ph/0601002].

[298] P. H. Ginsparg and K. G. Wilson, *A remnant of chiral symmetry on the lattice*, *Phys. Rev.* **D25** (1982) 2649.

[299] [RBC 04] Y. Aoki *et al.*, *Lattice QCD with two dynamical flavors of domain wall fermions*, *Phys. Rev.* **D72** (2005) 114505, [hep-lat/0411006].

[300] [ETM 10A] M. Constantinou *et al.*, *BK-parameter from $N_f = 2$ twisted mass lattice QCD*, *Phys. Rev.* **D83** (2011) 014505, [arXiv:1009.5606].

[301] [RBC/UKQCD 10B] Y. Aoki *et al.*, *Continuum limit of B_K from 2+1 flavor domain wall QCD*, *Phys.Rev.* **D84** (2011) 014503, [arXiv:1012.4178].

[302] [SWME 10] T. Bae *et al.*, *B_K using HYP-smeared staggered fermions in $N_f = 2+1$ unquenched QCD*, *Phys. Rev.* **D82** (2010) 114509, [arXiv:1008.5179].

[303] [RBC/UKQCD 07A] D. J. Antonio *et al.*, *Neutral kaon mixing from 2+1 flavor domain wall QCD*, *Phys. Rev. Lett.* **100** (2008) 032001, [hep-ph/0702042].

[304] [HPQCD/UKQCD 06] E. Gamiz *et al.*, *Unquenched determination of the kaon parameter B_K from improved staggered fermions*, *Phys. Rev.* **D73** (2006) 114502, [hep-lat/0603023].

[305] [JLQCD 08] S. Aoki *et al.*, *B_K with two flavors of dynamical overlap fermions*, *Phys. Rev.* **D77** (2008) 094503, [arXiv:0801.4186].

[306] [UKQCD 04] J. M. Flynn, F. Mescia and A. S. B. Tariq, *Sea quark effects in B_K from $N_f = 2$ clover-improved Wilson fermions*, *JHEP* **11** (2004) 049, [hep-lat/0406013].

[307] [ETM 11E] N. Carrasco, V. Gimenez, P. Dimopoulos, R. Frezzotti, D. Palao *et al.*, *$K^0\bar{K}^0$ mixing in the Standard Model from $N_f = 2+1+1$ twisted mass lattice QCD*, *PoS* **LAT2011** (2011) 276, [arXiv:1111.1262].

[308] J. Kim, T. Bae, H.-J. Kim, J. Kim, K. Kim *et al.*, *Determination of B_K using improved staggered fermions (IV) One-loop matching*, *PoS* **LAT2009** (2009) 264, [arXiv:0910.5583].

[309] P. M. Vranas, *Domain wall fermions in vector theories, Dubna, 1999*, hep-lat/0001006.

[310] P. M. Vranas, *Gap domain wall fermions*, *Phys. Rev.* **D74** (2006) 034512, [hep-lat/0606014].

[311] [JLQCD 06] H. Fukaya *et al.*, *Lattice gauge action suppressing near-zero modes of H_W*, *Phys.Rev.* **D74** (2006) 094505, [hep-lat/0607020].

[312] D. Renfrew, T. Blum, N. Christ, R. Mawhinney and P. Vranas, *Controlling residual chiral symmetry breaking in domain wall fermion simulations*, *PoS* **LAT2008** (2008) 048, [arXiv:0902.2587].

[313] [RBC/UKQCD 07C] Y. Aoki *et al.*, *Non-perturbative renormalization of quark bilinear operators and B_K using domain wall fermions*, *Phys. Rev.* **D78** (2008) 054510, [arXiv:0712.1061].

[314] [FNAL/MILC 12B] A. Bazavov *et al.*, *Pseudoscalar meson physics with four dynamical quarks*, *PoS* **LAT2012** (2012) 159, [arXiv:1210.8431].

[315] [HPQCD 12A] H. Na, C. T. Davies, E. Follana, G. P. Lepage and J. Shigemitsu, *$|V_{cd}|$ from D meson leptonic decays*, *Phys.Rev.* **D86** (2012) 054510, [arXiv:1206.4936].

[316] [FNAL/MILC 11] A. Bazavov *et al.*, *B- and D-meson decay constants from three-flavor lattice QCD*, *Phys.Rev.* **D85** (2012) 114506, [arXiv:1112.3051].

[317] [PACS-CS 11] Y. Namekawa *et al.*, *Charm quark system at the physical point of 2+1 flavor lattice QCD*, *Phys.Rev.* **D84** (2011) 074505, [arXiv:1104.4600].

[318] [HPQCD 10A] C. T. H. Davies, C. McNeile, E. Follana, G. Lepage, H. Na *et al.*, *Update: precision D_s decay constant from full lattice QCD using very fine lattices*, *Phys.Rev.* **D82** (2010) 114504, [arXiv:1008.4018].

[319] [FNAL/MILC 05] C. Aubin, C. Bernard, C. E. DeTar, M. Di Pierro, E. D. Freeland *et al.*, *Charmed meson decay constants in three-flavor lattice QCD*, *Phys.Rev.Lett.* **95** (2005) 122002, [hep-lat/0506030].

[320] [ETM 11A] P. Dimopoulos *et al.*, *Lattice QCD determination of m_b, f_B and f_{B_s} with twisted mass Wilson fermions*, *JHEP* **1201** (2012) 046, [arXiv:1107.1441].

[321] [HPQCD 11] H. Na *et al.*, *$D \to \pi\ell\nu$ semileptonic decays, $|V_{cd}|$ and 2^{nd} row unitarity from lattice QCD*, *Phys.Rev.* **D84** (2011) 114505, [arXiv:1109.1501].

[322] D. Bećirević, B. Haas and F. Mescia, *Semileptonic D-decays and lattice QCD*, *PoS* **LAT2007** (2007) 355, [arXiv:0710.1741].

[323] [HPQCD 10B] H. Na, C. T. Davies, E. Follana, G. P. Lepage and J. Shigemitsu, *The $D \to K\ell\nu$ semileptonic decay scalar form factor and $|V_{cs}|$ from lattice QCD*, *Phys.Rev.* **D82** (2010) 114506, [arXiv:1008.4562].

[324] P. F. Bedaque, *Aharonov-Bohm effect and nucleon nucleon phase shifts on the lattice*, *Phys.Lett.* **B593** (2004) 82–88, [nucl-th/0402051].

[325] C. Sachrajda and G. Villadoro, *Twisted boundary conditions in lattice simulations*, *Phys.Lett.* **B609** (2005) 73–85, [hep-lat/0411033].

[326] [ETM 11B] S. Di Vita *et al.*, *Form factors of the $D \to \pi$ and $D \to K$ semileptonic decays with $N_f = 2$ twisted mass lattice QCD*, *PoS* **LAT2010** (2010) [arXiv:1104.0869].

[327] [HPQCD 11C] J. Koponen *et al.*, *The D to K and D to π semileptonic decay form factors from lattice QCD*, *PoS* **LAT2011** (2011) 286, [arXiv:1111.0225].

[328] [HPQCD 12B] J. Koponen, C. Davies and G. Donald, *D to K and D to π semileptonic form factors from lattice QCD*, *Charm 2012*, arXiv:1208.6242.

[329] D. Bećirević and A. B. Kaidalov, *Comment on the heavy $\to$ light form-factors*, *Phys.Lett.* **B478** (2000) 417–423, [hep-ph/9904490].

[330] [FNAL/MILC 04] C. Aubin *et al.*, *Semileptonic decays of D mesons in three-flavor lattice QCD*, *Phys.Rev.Lett.* **94** (2005) 011601, [hep-ph/0408306].

[331] FOCUS Collaboration, J. Link *et al.*, *Measurements of the q^2 dependence of the $D^0 \to K^-\mu^+\nu$ and $D^0 \to \pi^-\mu^+\nu$ form factors*, *Phys.Lett.* **B607** (2005) 233–242, [hep-ex/0410037].

[332] Belle Collaboration, K. Abe *et al.*, *Measurement of $D^0 \to \pi l\nu(Kl\nu)$ and their form-factors*, hep-ex/0510003.

[333] [FNAL/MILC 12G] J. A. Bailey *et al.*, *Charm semileptonic decays and $|V_{cs(d)}|$ from heavy clover quarks and 2+1 flavor asqtad staggered ensembles*, *PoS* **LAT2012** (2012) 272, [arXiv:1211.4964].

[334] P. F. Bedaque and J.-W. Chen, *Twisted valence quarks and hadron interactions on the lattice*, *Phys.Lett.* **B616** (2005) 208–214, [hep-lat/0412023].

[335] [FNAL/MILC 10A] C. Bernard *et al.*, *Tuning Fermilab Heavy Quarks in 2+1 Flavor Lattice QCD with Application to Hyperfine Splittings*, *Phys.Rev.* **D83** (2011) 034503, [arXiv:1003.1937].

[336] [HPQCD 10C] E. B. Gregory *et al.*, *Precise B, B_s and B_c meson spectroscopy from full lattice QCD*, *Phys.Rev.* **D83** (2011) 014506, [arXiv:1010.3848].

[337] [ALPHA 11] B. Blossier, J. Bulava, M. Della Morte, M. Donnellan, P. Fritzsch *et al.*, *M_b and f_B from non-perturbatively renormalized HQET with $N_f = 2$ light quarks*, *PoS* **LAT2011** (2011) 280, [arXiv:1112.6175].

[338] [HPQCD 11A] C. McNeile, C. Davies, E. Follana, K. Hornbostel and G. Lepage, *High-precision f_{B_s} and HQET from relativistic lattice QCD*, *Phys.Rev.* **D85** (2012) 031503, [arXiv:1110.4510].

[339] G. Bali, S. Collins, S. Dürr, Z. Fodor, R. Horsley *et al.*, *Spectra of heavy-light and heavy-heavy mesons containing charm quarks, including higher spin states for $N_f = 2 + 1$*, *PoS* **LATTICE2011** (2011) 135, [arXiv:1108.6147].

[340] D. Mohler and R. Woloshyn, *D and D_s meson spectroscopy*, *Phys.Rev.* **D84** (2011) 054505, [arXiv:1103.5506].

[341] [HPQCD 12F] R.J. Dowdall, C. Davies, T. Hammant and R. Horgan, *Precise heavy-light meson masses and hyperfine splittings from lattice QCD including charm quarks in the sea*, *Phys.Rev.* **D86** (2012) 094510, [arXiv:1207.5149].

[342] [ALPHA 12A] F. Bernardoni, B. Blossier, J. Bulava, M. Della Morte, P. Fritzsch *et al.*, *B-physics from HQET in two-flavour lattice QCD*, *PoS* **LAT2012** (2012) 273, [arXiv:1210.7932].

[343] S. Basak, S. Datta, M. Padmanath, P. Majumdar and N. Mathur, *Charm and strange hadron spectra from overlap fermions on HISQ gauge configurations*, *PoS* **LATTICE2012** (2012) 141, [arXiv:1211.6277].

[344] G. Bali, S. Collins and P. Perez-Rubio, *Charmed hadron spectroscopy on the lattice for $N_f = 2 + 1$ flavours*, *J.Phys.Conf.Ser.* **426** (2013) 012017, [arXiv:1212.0565].

[345] G. Moir, M. Peardon, S. M. Ryan, C. E. Thomas and L. Liu, *Excited spectroscopy of charmed mesons from lattice QCD*, *JHEP* **1305** (2013) 021, [arXiv:1301.7670].

[346] M. Kalinowski and M. Wagner, *Masses of mesons with charm valence quarks from 2+1+1 flavor twisted mass lattice QCD*, *Acta Phys.Polon.Supp.* **B6** (2013) 991, [arXiv:1304.7974].

[347] [FNAL/MILC 09A] T. Burch, C. DeTar, M. Di Pierro, A. El-Khadra, E. Freeland *et al.*, *Quarkonium mass splittings in three-flavor lattice QCD*, *Phys.Rev.* **D81** (2010) 034508, [arXiv:0912.2701].

[348] [FNAL/MILC 12H] C. DeTar, A. Kronfeld, S.-H. Lee, L. Levkova, D. Mohler *et al.*, *Charmonium mass splittings at the physical point*, *PoS* **LATTICE2012** (2012) 257, [arXiv:1211.2253].

[349] [HPQCD 12G] G.C. Donald, C. Davies, R. Dowdall, E. Follana, K. Hornbostel *et al.*, *Precision tests of the J/ψ from full lattice QCD: mass, leptonic width and radiative decay rate to η_c*, *Phys.Rev.* **D86** (2012) 094501, [arXiv:1208.2855].

[350] F. Sanfilippo and D. Becirevic, *Radiative decays of charmonia on the lattice*, *PoS* **ConfinementX** (2012) 134, [arXiv:1301.5204].

[351] [HS 12] L. Liu *et al.*, *Excited and exotic charmonium spectroscopy from lattice QCD*, *JHEP* **1207** (2012) 126, [arXiv:1204.5425].

[352] [HPQCD 05B] A. Gray *et al.*, *The upsilon spectrum and m_b from full lattice QCD*, *Phys.Rev.* **D72** (2005) 094507, [hep-lat/0507013].

[353] S. Meinel, *The Bottomonium spectrum from lattice QCD with 2+1 flavors of domain wall fermions*, *Phys.Rev.* **D79** (2009) 094501, [arXiv:0903.3224].

[354] S. Meinel, *Bottomonium spectrum at order v^6 from domain-wall lattice QCD: Precise results for hyperfine splittings*, *Phys.Rev.* **D82** (2010) 114502, [arXiv:1007.3966].

[355] [HPQCD 11B] R. J. Dowdall *et al.*, *The upsilon spectrum and the determination of the lattice spacing from lattice QCD including charm quarks in the sea*, *Phys.Rev.* **D85** (2012) 054509, [arXiv:1110.6887].

[356] [HPQCD 11D] J.O. Daldrop, C. Davies and R. Dowdall, *Prediction of the bottomonium D-wave spectrum from full lattice QCD*, *Phys.Rev.Lett.* **108** (2012) 102003, [arXiv:1112.2590].

[357] [RBC/UKQCD 12A] Y. Aoki *et al.*, *Nonperturbative tuning of an improved relativistic heavy-quark action with application to bottom spectroscopy*, *Phys.Rev.* **D86** (2012) 116003, [arXiv:1206.2554].

[358] R. Lewis and R. Woloshyn, *Higher angular momentum states of bottomonium in lattice NRQCD*, *Phys.Rev.* **D85** (2012) 114509, [arXiv:1204.4675].

[359] [HPQCD 04A] I. Allison *et al.*, *Mass of the B/c meson in three-flavor lattice QCD*, *Phys. Rev. Lett.* **94** (2005) 172001, [hep-lat/0411027].

[360] [HPQCD 09C] E.B. Gregory, C. Davies, E. Follana, E. Gamiz, I. Kendall *et al.*, *A Prediction of the B*(c) mass in full lattice QCD*, *Phys.Rev.Lett.* **104** (2010) 022001, [arXiv:0909.4462].

[361] [HPQCD 12E] C. McNeile, C. Davies, E. Follana, K. Hornbostel and G. Lepage, *Heavy meson masses and decay constants from relativistic heavy quarks in full lattice QCD*, *Phys.Rev.* **D86** (2012) 074503, [arXiv:1207.0994].

[362] [ALPHA 10] B. Blossier *et al.*, *HQET at order 1/m: III. Decay constants in the quenched approximation*, *JHEP* **1012** (2010) 039, [arXiv:1006.5816].

[363] [ALPHA 04A] J. Heitger, A. Jüttner, R. Sommer and J. Wennekers, *Non-perturbative tests of heavy quark effective theory*, *JHEP* **0411** (2004) 048, [hep-ph/0407227].

[364] [ETM 09D] B. Blossier *et al.*, *A proposal for B-physics on current lattices*, *JHEP* **1004** (2010) 049, [arXiv:0909.3187].

[365] [ETM 12B] N. Carrasco, P. Dimopoulos, R. Frezzotti, V. Gimenez, G. Herdoiza *et al.*, *B-physics from the ratio method with Wilson twisted mass fermions*, *PoS* **LAT2012** (2012) 104, [arXiv:1211.0568].

[366] [HPQCD 13B] A.J. Lee *et al.*, *The mass of the b-quark from lattice NRQCD and lattice perturbation theory*, *Phys.Rev.* **D87** (2013) 074018, [arXiv:1302.3739].

[367] [ETM 11F] K. Jansen, M. Petschlies and C. Urbach, *Charm Current-Current Correlators in Twisted Mass Lattice QCD*, *PoS* **LATTICE2011** (2011) 234, [arXiv:1111.5252].

[368] S. Dürr and G. Koutsou, *m_c/m_s with Brillouin fermions*, *PoS* **LATTICE2011** (2011) 230, [arXiv:1111.2577].

[369] G. Buchalla and A. J. Buras, *QCD corrections to rare K and B decays for arbitrary top quark mass*, *Nucl.Phys.* **B400** (1993) 225–239.

[370] LHCb Collaboration, R. Aaij *et al.*, *First evidence for the decay $B_s \to \mu^+\mu^-$*, *Phys.Rev.Lett.* **110** (2013) 021801, [arXiv:1211.2674].

[371] [HPQCD 13] R. J. Dowdall, C. Davies, R. Horgan, C. Monahan and J. Shigemitsu, *B-meson decay constants from improved lattice NRQCD and physical u, d, s and c sea quarks*, *Phys.Rev.Lett.* **110** (2013) 222003, [arXiv:1302.2644].

[372] [HPQCD 12] H. Na, C. J. Monahan, C. T. Davies, R. Horgan, G. P. Lepage *et al.*, *The B and B_s meson decay constants from lattice QCD*, *Phys.Rev.* **D86** (2012) 034506, [arXiv:1202.4914].

[373] [HPQCD 09] E. Gamiz, C. T. Davies, G. P. Lepage, J. Shigemitsu and M. Wingate, *Neutral B meson mixing in unquenched lattice QCD*, *Phys.Rev.* **D80** (2009) 014503, [arXiv:0902.1815].

[374] [RBC/UKQCD 10C] C. Albertus *et al.*, *Neutral B-meson mixing from unquenched lattice QCD with domain-wall light quarks and static b-quarks*, *Phys.Rev.* **D82** (2010) 014505, [arXiv:1001.2023].

[375] [FNAL/MILC 11B] E. T. Neil *et al.*, *B and D meson decay constants from $2+1$ flavor improved staggered simulations*, *PoS* **LAT2011** (2011) 320, [arXiv:1112.3978].

[376] O. Witzel, *Calculating B-meson decay constants using domain-wall light quarks and nonperturbatively tuned relativistic b-quarks*, *PoS* **LAT2012** (2012) 103, [arXiv:1211.3180].

[377] A. Lenz and U. Nierste, *Theoretical update of $B_s - \bar{B}_s$ mixing*, *JHEP* **0706** (2007) 072, [hep-ph/0612167].

[378] M. Beneke, G. Buchalla and I. Dunietz, *Width difference in the $B_s - \bar{B}_s$ system*, *Phys.Rev.* **D54** (1996) 4419–4431, [hep-ph/9605259].

[379] [FNAL/MILC 11A] C. M. Bouchard, E. Freeland, C. Bernard, A. El-Khadra, E. Gamiz *et al.*, *Neutral B mixing from $2+1$ flavor lattice-QCD: the Standard Model and beyond*, *PoS* **LAT2011** (2011) 274, [arXiv:1112.5642].

[380] [HPQCD 06A] E. Dalgic, A. Gray, E. Gamiz, C. T. Davies, G. P. Lepage *et al.*, *$B_s^0 - \bar{B}_s^0$ mixing parameters from unquenched lattice QCD*, *Phys.Rev.* **D76** (2007) 011501, [hep-lat/0610104].

[381] [ETM 12A] N. Carrasco *et al.*, *Neutral meson oscillations in the Standard Model and beyond from $N_f = 2$ twisted mass lattice QCD*, *PoS* **LAT2012** (2012) 105, [arXiv:1211.0565].

[382] [FNAL/MILC 12] A. Bazavov, C. Bernard, C. Bouchard, C. DeTar, M. Di Pierro *et al.*, *Neutral B-meson mixing from three-flavor lattice QCD: determination of the SU(3)-breaking ratio ξ*, *Phys.Rev.* **D86** (2012) 034503, [arXiv:1205.7013].

[383] [MILC 13B] C. Bernard, *Neutral B mixing in staggered chiral perturbation theory*, *Phys.Rev.* **D87** (2013) 114503, [arXiv:1303.0435].

[384] M. Della Morte, B. Jäger, T. Rae and H. Wittig, *Improved interpolating fields for hadrons at non-zero momentum*, *Eur.Phys.J.* **A48** (2012) 139, [arXiv:1208.0189].

[385] P. Ball and R. Zwicky, *New results on $B \to \pi, K, \eta$ decay form factors from light-cone sum rules*, *Phys.Rev.* **D71** (2005) 014015, [hep-ph/0406232].

[386] R. J. Hill, *Heavy-to-light meson form-factors at large recoil*, *Phys.Rev.* **D73** (2006) 014012, [hep-ph/0505129].

[387] G. P. Lepage and S. J. Brodsky, *Exclusive processes in perturbative Quantum Chromodynamics*, *Phys.Rev.* **D22** (1980) 2157.

[388] R. Akhoury, G. F. Sterman and Y. Yao, *Exclusive semileptonic decays of B mesons into light mesons*, *Phys.Rev.* **D50** (1994) 358–372.

[389] L. Lellouch, *Lattice constrained unitarity bounds for $\bar{B}^0 \to \pi^+ \ell\, \bar{\nu}_l$ decays*, *Nucl.Phys.* **B479** (1996) 353–391, [hep-ph/9509358].

[390] C. Bourrely, I. Caprini and L. Lellouch, *Model-independent description of $B \to \pi \ell \nu$ decays and a determination of $|V_{ub}|$*, *Phys.Rev.* **D79** (2009) 013008, [arXiv:0807.2722].

[391] C. Bourrely, B. Machet and E. de Rafael, *Semileptonic decays of pseudoscalar particles ($M \to M' \ell \nu_\ell$) and short distance behavior of Quantum Chromodynamics*, *Nucl. Phys.* **B189** (1981) 157.

[392] C. G. Boyd, B. Grinstein and R. F. Lebed, *Constraints on form-factors for exclusive semileptonic heavy to light meson decays*, *Phys.Rev.Lett.* **74** (1995) 4603–4606, [hep-ph/9412324].

[393] C. G. Boyd and M. J. Savage, *Analyticity, shapes of semileptonic form-factors, and $\bar{B} \to \pi \ell \bar{\nu}$*, *Phys.Rev.* **D56** (1997) 303–311, [hep-ph/9702300].

[394] M. C. Arnesen, B. Grinstein, I. Z. Rothstein and I. W. Stewart, *A precision model independent determination of $|V_{ub}|$ from $B \to \pi e \nu$*, *Phys.Rev.Lett.* **95** (2005) 071802, [hep-ph/0504209].

[395] T. Becher and R. J. Hill, *Comment on form-factor shape and extraction of $|V_{ub}|$ from $B \to \pi l \nu$*, *Phys.Lett.* **B633** (2006) 61–69, [hep-ph/0509090].

[396] [HPQCD 06] E. Dalgic *et al.*, *B meson semileptonic form-factors from unquenched lattice QCD*, *Phys.Rev.* **D73** (2006) 074502, [hep-lat/0601021].

[397] [FNAL/MILC 08A] J. A. Bailey *et al.*, *The $B \to \pi \ell \nu$ semileptonic form factor from three-flavor lattice QCD: a model-independent determination of $|V_{ub}|$*, *Phys.Rev.* **D79** (2009) 054507, [arXiv:0811.3640].

[398] [ALPHA 12B] F. Bahr *et al.*, *$B \to \pi$ form factor with 2 flavours of $O(a)$ improved Wilson quarks*, *PoS* **LAT2012** (2012) 110, [arXiv:1210.3478].

[399] [ALPHA 12C] F. Bahr *et al.*, *$|V_{ub}|$ determination in lattice QCD*, *PoS* **ICHEP2012** (2013) 424, [arXiv:1211.6327].

[400] [FNAL/MILC 12E] R. Zhou *et al.*, *Form factors for semi-leptonic B decays*, *PoS* **LAT2012** (2012) 120, [arXiv:1211.1390].

[401] [HPQCD 12C] C. M. Bouchard, G. P. Lepage, C. J. Monahan, H. Na and J. Shigemitsu, *Form factors for B and B_s semileptonic decays with NRQCD/HISQ quarks*, *PoS* **LAT2012** (2012) 118, [arXiv:1210.6992].

[402] [RBC/UKQCD 12B] T. Kawanai, R. S. Van de Water and O. Witzel, *The $B \to \pi \ell \nu$ form factor from unquenched lattice QCD with domain-wall light quarks and relativistic b-quarks*, *PoS* **LAT2012** (2012) 109, [arXiv:1211.0956].

[403] [FNAL/MILC 09] C. Bernard, C. DeTar, M. Di Pierro, A. El-Khadra, R. Evans *et al.*, *Visualization of semileptonic form factors from lattice QCD*, *Phys.Rev.* **D80** (2009) 034026, [arXiv:0906.2498].

[404] M. Antonelli *et al.*, *Flavor physics in the quark sector*, *Phys.Rept.* **494** (2010) 197–414, [arXiv:0907.5386].

[405] Z. Liu *et al.*, *Form factors for rare B decays: strategy, methodology, and numerical study*, *PoS* **LAT2009** (2009) 242, [arXiv:0911.2370].

[406] Z. Liu *et al.*, *A lattice calculation of $B \to K^{(*)}$ form factors, CKM 2010*, arXiv:1101.2726.

[407] A. Sirlin, *Large m_W, m_Z behavior of the $O(\alpha)$ corrections to semileptonic processes mediated by W*, *Nucl.Phys.* **B196** (1982) 83.

[408] [FNAL/MILC 10] J. A. Bailey *et al.*, *$B \to D^* \ell \nu$ at zero recoil: an update*, *PoS* **LAT2010** (2010) 311, [arXiv:1011.2166].

[409] [FNAL/MILC 08] C. Bernard *et al.*, *The $\bar{B} \to D^* \ell \bar{\nu}$ form factor at zero recoil from three-flavor lattice QCD: a model independent determination of $|V_{cb}|$*, *Phys.Rev.* **D79** (2009) 014506, [arXiv:0808.2519].

[410] L. Randall and M. B. Wise, *Chiral perturbation theory for $B \to D^*$ and $B \to D$ semileptonic transition matrix elements at zero recoil*, *Phys.Lett.* **B303** (1993) 135–139, [hep-ph/9212315].

[411] M. J. Savage, *Heavy meson observables at one loop in partially quenched chiral perturbation theory*, *Phys.Rev.* **D65** (2002) 034014, [hep-ph/0109190].

[412] S. Hashimoto, A. S. Kronfeld, P. B. Mackenzie, S. M. Ryan and J. N. Simone, *Lattice calculation of the zero recoil form-factor of $\bar{B} \to D^* \ell \bar{\nu}$: toward a model independent determination of $|V_{cb}|$*, *Phys.Rev.* **D66** (2002) 014503, [hep-ph/0110253].

[413] [FNAL/MILC 04A] M. Okamoto *et al.*, *Semileptonic $D \to \pi/K$ and $B \to \pi/D$ decays in 2+1 flavor lattice QCD*, *Nucl.Phys.Proc.Suppl.* **140** (2005) 461–463, [hep-lat/0409116].

[414] [FNAL/MILC 12F] S.-W. Qiu *et al.*, *Semileptonic B to D decays at nonzero recoil with 2+1 flavors of improved staggered quarks. An update*, *PoS* **LAT2012** (2012) 119, [arXiv:1211.2247].

[415] [FNAL/MILC 12A] J. A. Bailey *et al.*, *Refining new-physics searches in $B \to D\tau\nu$ decay with lattice QCD*, *Phys.Rev.Lett.* **109** (2012) 071802, [arXiv:1206.4992].

[416] [FNAL/MILC 12C] J. A. Bailey *et al.*, *$B_s \to D_s/B \to D$ semileptonic form-factor ratios and their application to BR($B_s^0 \to \mu^+\mu^-$)*, *Phys.Rev.* **D85** (2012) 114502, [arXiv:1202.6346].

[417] Babar Collaboration, B. Aubert *et al.*, *A search for $B^+ \to \ell^+\nu_\ell$ recoiling against $B^- \to D^0\ell^-\bar{\nu}X$*, *Phys.Rev.* **D81** (2010) 051101, [arXiv:0912.2453].

[418] Belle Collaboration, K. Hara *et al.*, *Evidence for $B^- \to \tau^-\bar{\nu}$ with a semileptonic tagging method*, *Phys.Rev.* **D82** (2010) 071101, [arXiv:1006.4201].

[419] Babar Collaboration, J. Lees *et al.*, *Evidence of $B \to \tau\nu$ decays with hadronic B tags*, *Phys.Rev.* **D88** (2013) 031102, [arXiv:1207.0698].

[420] Belle Collaboration, I. Adachi *et al.*, *Measurement of $B^- \to \tau^-\bar{\nu}_\tau$ with a hadronic tagging method using the full data sample of Belle*, *Phys. Rev. Lett.* **110** (2013) 131801, [arXiv:1208.4678].

[421] Babar Collaboration, J. Lees *et al.*, *Branching fraction and form-factor shape measurements of exclusive charmless semileptonic B decays, and determination of $|V_{ub}|$*, *Phys.Rev.* **D86** (2012) 092004, [arXiv:1208.1253].

[422] Belle Collaboration, H. Ha *et al.*, *Measurement of the decay $B^0 \to \pi^-\ell^+\nu$ and determination of $|V_{ub}|$*, *Phys.Rev.* **D83** (2011) 071101, [arXiv:1012.0090].

[423] C. W. Bauer, Z. Ligeti and M. E. Luke, *Precision determination of $|V_{ub}|$ from inclusive decays*, *Phys.Rev.* **D64** (2001) 113004, [hep-ph/0107074].

[424] B. O. Lange, M. Neubert and G. Paz, *Theory of charmless inclusive B decays and the extraction of V_{ub}*, *Phys.Rev.* **D72** (2005) 073006, [hep-ph/0504071].

[425] J. R. Andersen and E. Gardi, *Inclusive spectra in charmless semileptonic B decays by dressed gluon exponentiation*, *JHEP* **0601** (2006) 097, [hep-ph/0509360].

[426] E. Gardi, *On the determination of $|V_{ub}|$ from inclusive semileptonic B decays, La Thuile 2008*, arXiv:0806.4524.

[427] P. Gambino, P. Giordano, G. Ossola and N. Uraltsev, *Inclusive semileptonic B decays and the determination of $|V_{ub}|$*, *JHEP* **0710** (2007) 058, [arXiv:0707.2493].

[428] U. Aglietti, F. Di Lodovico, G. Ferrera and G. Ricciardi, *Inclusive measure of $|V_{ub}|$ with the analytic coupling model*, *Eur.Phys.J.* **C59** (2009) 831–840, [arXiv:0711.0860].

[429] Heavy Flavor Averaging Group, http://www.slac.stanford.edu/xorg/hfag/semi/EndOfYear11/home.shtml.

[430] P. Gambino and C. Schwanda, *Inclusive semileptonic fits, heavy quark masses, and V_{cb}*, arXiv:1307.4551.

[431] K. G. Wilson, *Confinement of quarks*, *Phys. Rev.* **D10** (1974) 2445–2459.

[432] M. Lüscher and P. Weisz, *On-shell improved lattice gauge theories*, *Commun. Math. Phys.* **97** (1985) 59.

[433] Y. Iwasaki, *Renormalization group analysis of lattice theories and improved lattice action: two-dimensional nonlinear O(N) sigma model*, *Nucl. Phys.* **B258** (1985) 141–156.

[434] T. Takaishi, *Heavy quark potential and effective actions on blocked configurations*, *Phys. Rev.* **D54** (1996) 1050–1053.

[435] P. de Forcrand *et al.*, *Renormalization group flow of SU(3) lattice gauge theory: numerical studies in a two coupling space*, *Nucl. Phys.* **B577** (2000) 263–278, [hep-lat/9911033].

[436] K. G. Wilson, *Quarks and strings on a lattice*, in *New Phenomena in Subnuclear Physics, part A. Proceedings of the first half of the 1975 International School of Subnuclear Physics, Erice, Sicily, July 11 - August 1, 1975, ed. A. Zichichi, Plenum Press, New York, 1977, p. 69, CLNS-321.*

[437] L. H. Karsten and J. Smit, *Lattice fermions: species doubling, chiral invariance, and the triangle anomaly*, *Nucl.Phys.* **B183** (1981) 103.

[438] M. Bochicchio, L. Maiani, G. Martinelli, G. C. Rossi and M. Testa, *Chiral symmetry on the lattice with Wilson fermions*, *Nucl.Phys.* **B262** (1985) 331.

[439] M. Lüscher, S. Sint, R. Sommer and P. Weisz, *Chiral symmetry and O(a) improvement in lattice QCD*, *Nucl. Phys.* **B478** (1996) 365–400, [hep-lat/9605038].

[440] G. P. Lepage and P. B. Mackenzie, *On the viability of lattice perturbation theory*, *Phys.Rev.* **D48** (1993) 2250–2264, [hep-lat/9209022].

[441] M. Lüscher, S. Sint, R. Sommer, P. Weisz and U. Wolff, *Non-perturbative O(a) improvement of lattice QCD*, *Nucl. Phys.* **B491** (1997) 323–343, [hep-lat/9609035].

[442] R. Frezzotti and G. C. Rossi, *Chirally improving Wilson fermions. I: O(a) improvement*, *JHEP* **08** (2004) 007, [hep-lat/0306014].

[443] J. B. Kogut and L. Susskind, *Hamiltonian formulation of Wilson's lattice gauge theories*, *Phys. Rev.* **D11** (1975) 395.

[444] T. Banks, L. Susskind and J. B. Kogut, *Strong coupling calculations of lattice gauge theories: (1+1)-dimensional exercises*, *Phys. Rev.* **D13** (1976) 1043.

[445] Cornell-Oxford-Tel Aviv-Yeshiva Collaboration, T. Banks *et al.*, *Strong coupling calculations of the hadron spectrum of Quantum Chromodynamics*, *Phys. Rev.* **D15** (1977) 1111.

[446] L. Susskind, *Lattice fermions*, *Phys. Rev.* **D16** (1977) 3031–3039.

[447] E. Marinari, G. Parisi and C. Rebbi, *Monte Carlo simulation of the massive Schwinger model*, *Nucl. Phys.* **B190** (1981) 734.

[448] C. Bernard, M. Golterman and Y. Shamir, *Observations on staggered fermions at non-zero lattice spacing*, *Phys. Rev.* **D73** (2006) 114511, [hep-lat/0604017].

[449] S. Prelovsek, *Effects of staggered fermions and mixed actions on the scalar correlator*, *Phys. Rev.* **D73** (2006) 014506, [hep-lat/0510080].

[450] C. Bernard, *Staggered chiral perturbation theory and the fourth-root trick*, *Phys. Rev.* **D73** (2006) 114503, [hep-lat/0603011].

[451] C. Bernard, C. E. DeTar, Z. Fu and S. Prelovsek, *Scalar meson spectroscopy with lattice staggered fermions*, *Phys. Rev.* **D76** (2007) 094504, [arXiv:0707.2402].

[452] C. Aubin, J. Laiho and R. S. Van de Water, *Discretization effects and the scalar meson correlator in mixed-action lattice simulations*, *Phys. Rev.* **D77** (2008) 114501, [arXiv:0803.0129].

[453] Y. Shamir, *Locality of the fourth root of the staggered-fermion determinant: renormalization-group approach*, *Phys. Rev.* **D71** (2005) 034509, [hep-lat/0412014].

[454] Y. Shamir, *Renormalization-group analysis of the validity of staggered-fermion QCD with the fourth-root recipe*, *Phys. Rev.* **D75** (2007) 054503, [hep-lat/0607007].

[455] W.-J. Lee and S. R. Sharpe, *Partial flavor symmetry restoration for chiral staggered fermions*, *Phys. Rev.* **D60** (1999) 114503, [hep-lat/9905023].

[456] C. Aubin and C. Bernard, *Pion and kaon masses in staggered chiral perturbation theory*, *Phys. Rev.* **D68** (2003) 034014, [hep-lat/0304014].

[457] S. R. Sharpe and R. S. Van de Water, *Staggered chiral perturbation theory at next-to-leading order*, *Phys. Rev.* **D71** (2005) 114505, [hep-lat/0409018].

[458] C. Bernard, M. Golterman and Y. Shamir, *Effective field theories for QCD with rooted staggered fermions*, *Phys. Rev.* **D77** (2008) 074505, [arXiv:0712.2560].

[459] C. Aubin and C. Bernard, *Staggered chiral perturbation theory for heavy-light mesons*, *Phys. Rev.* **D73** (2006) 014515, [hep-lat/0510088].

[460] J. Komijani and C. Bernard, *Staggered chiral perturbation theory for all-staggered heavy-light mesons*, *PoS* **LAT2012** (2012) 199, [arXiv:1211.0785].

[461] C. Bernard and J. Komijani, *Chiral Perturbation Theory for All-Staggered Heavy-Light Mesons*, arXiv:1309.4533.

[462] J. A. Bailey, *Staggered heavy baryon chiral perturbation theory*, *Phys.Rev.* **D77** (2008) 054504, [arXiv:0704.1490].

[463] O. Bär, C. Bernard, G. Rupak and N. Shoresh, *Chiral perturbation theory for staggered sea quarks and Ginsparg-Wilson valence quarks*, *Phys. Rev.* **D72** (2005) 054502, [hep-lat/0503009].

[464] S. Dürr and C. Hoelbling, *Staggered versus overlap fermions: a study in the Schwinger model with $N_f = 0, 1, 2$*, *Phys. Rev.* **D69** (2004) 034503, [hep-lat/0311002].

[465] S. Dürr and C. Hoelbling, *Scaling tests with dynamical overlap and rooted staggered fermions*, *Phys. Rev.* **D71** (2005) 054501, [hep-lat/0411022].

[466] S. Dürr and C. Hoelbling, *Lattice fermions with complex mass*, *Phys. Rev.* **D74** (2006) 014513, [hep-lat/0604005].

[467] [HPQCD 04] E. Follana, A. Hart and C. T. H. Davies, *The index theorem and universality properties of the low-lying eigenvalues of improved staggered quarks*, *Phys. Rev. Lett.* **93** (2004) 241601, [hep-lat/0406010].

[468] S. Dürr, C. Hoelbling and U. Wenger, *Staggered eigenvalue mimicry*, *Phys. Rev.* **D70** (2004) 094502, [hep-lat/0406027].

[469] K. Y. Wong and R. Woloshyn, *Systematics of staggered fermion spectral properties and topology*, *Phys.Rev.* **D71** (2005) 094508, [hep-lat/0412001].

[470] [HPQCD/FNAL 11] G. C. Donald, C. T. Davies, E. Follana and A. S. Kronfeld, *Staggered fermions, zero modes, and flavor-singlet mesons*, *Phys.Rev.* **D84** (2011) 054504, [arXiv:1106.2412].

[471] M. Creutz, *Flavor extrapolations and staggered fermions*, hep-lat/0603020.

[472] M. Creutz, *Diseases with rooted staggered quarks*, *PoS* **LAT2006** (2006) 208, [hep-lat/0608020].

[473] M. Creutz, *The evil that is rooting*, *Phys. Lett.* **B649** (2007) 230–234, [hep-lat/0701018].

[474] M. Creutz, *The author replies. (Chiral anomalies and rooted staggered fermions)*, *Phys. Lett.* **B649** (2007) 241–242, [arXiv:0704.2016].

[475] M. Creutz, *Why rooting fails*, *PoS* **LAT2007** (2007) 007, [arXiv:0708.1295].

[476] M. Creutz, *Comment on "'t Hooft vertices, partial quenching, and rooted staggered QCD"*, *Phys. Rev.* **D78** (2008) 078501, [arXiv:0805.1350].

[477] M. Creutz, *Comments on staggered fermions/Panel discussion*, *PoS* **CONFINEMENT8** (2008) 016, [arXiv:0810.4526].

[478] C. Bernard, M. Golterman, Y. Shamir and S. R. Sharpe, *Comment on 'chiral anomalies and rooted staggered fermions'*, *Phys. Lett.* **B649** (2007) 235–240, [hep-lat/0603027].

[479] C. Bernard, M. Golterman, Y. Shamir and S. R. Sharpe, *'t Hooft vertices, partial quenching, and rooted staggered QCD*, *Phys. Rev.* **D77** (2008) 114504, [arXiv:0711.0696].

[480] C. Bernard, M. Golterman, Y. Shamir and S. R. Sharpe, *Reply to: Comment on 't Hooft vertices, partial quenching, and rooted staggered QCD*, *Phys. Rev.* **D78** (2008) 078502, [arXiv:0808.2056].

[481] D. H. Adams, *The rooting issue for a lattice fermion formulation similar to staggered fermions but without taste mixing*, *Phys. Rev.* **D77** (2008) 105024, [arXiv:0802.3029].

[482] G. 't Hooft, *Symmetry breaking through Bell-Jackiw anomalies*, *Phys.Rev.Lett.* **37** (1976) 8–11.

[483] G. 't Hooft, *Computation of the quantum effects due to a four-dimensional pseudoparticle*, *Phys.Rev.* **D14** (1976) 3432–3450.

[484] [MILC 99] K. Orginos, D. Toussaint and R. L. Sugar, *Variants of fattening and flavor symmetry restoration*, *Phys. Rev.* **D60** (1999) 054503, [hep-lat/9903032].

[485] [HPQCD 06B] E. Follana *et al.*, *Highly improved staggered quarks on the lattice, with applications to charm physics*, *Phys. Rev.* **D75** (2007) 054502, [hep-lat/0610092].

[486] Y. Aoki, Z. Fodor, S. Katz and K. Szabo, *The equation of state in lattice QCD: with physical quark masses towards the continuum limit*, *JHEP* **0601** (2006) 089, [hep-lat/0510084].

[487] A. Hasenfratz and F. Knechtli, *Flavor symmetry and the static potential with hypercubic blocking*, *Phys.Rev.* **D64** (2001) 034504, [hep-lat/0103029].

[488] S. Naik, *On-shell improved lattice action for QCD with Susskind fermions and asymptotic freedom scale*, *Nucl. Phys.* **B316** (1989) 238.

[489] G. P. Lepage, *Flavor-symmetry restoration and Symanzik improvement for staggered quarks*, *Phys. Rev.* **D59** (1999) 074502, [hep-lat/9809157].

[490] P. Hasenfratz, *Lattice QCD without tuning, mixing and current renormalization*, *Nucl.Phys.* **B525** (1998) 401–409, [hep-lat/9802007].

[491] P. Hasenfratz, V. Laliena and F. Niedermayer, *The index theorem in QCD with a finite cut-off*, *Phys. Lett.* **B427** (1998) 125–131, [hep-lat/9801021].

[492] M. Lüscher, *Exact chiral symmetry on the lattice and the Ginsparg-Wilson relation*, *Phys. Lett.* **B428** (1998) 342–345, [hep-lat/9802011].

[493] H. B. Nielsen and M. Ninomiya, *No go theorem for regularizing chiral fermions*, *Phys. Lett.* **B105** (1981) 219.

[494] H. Neuberger, *Exactly massless quarks on the lattice*, *Phys. Lett.* **B417** (1998) 141–144, [hep-lat/9707022].

[495] D. B. Kaplan, *A method for simulating chiral fermions on the lattice*, *Phys. Lett.* **B288** (1992) 342–347, [hep-lat/9206013].

[496] Y. Shamir, *Chiral fermions from lattice boundaries*, *Nucl. Phys.* **B406** (1993) 90–106, [hep-lat/9303005].

[497] V. Furman and Y. Shamir, *Axial symmetries in lattice QCD with Kaplan fermions*, *Nucl. Phys.* **B439** (1995) 54–78, [hep-lat/9405004].

[498] T. Blum and A. Soni, *QCD with domain wall quarks*, *Phys.Rev.* **D56** (1997) 174–178, [hep-lat/9611030].

[499] S. R. Sharpe, *Future of Chiral Extrapolations with Domain Wall Fermions*, arXiv:0706.0218.

[500] A. Borici, *Truncated overlap fermions*, *Nucl.Phys.Proc.Suppl.* **83** (2000) 771–773, [hep-lat/9909057].

[501] A. Borici, *Truncated overlap fermions: The link between overlap and domain wall fermions*, hep-lat/9912040. In: Lattice fermions and structure of the vacuum, eds. V. Mitrjushkin and G. Schierholz (Kluwer Academic Publishers, 2000) p. 41.

[502] W. Bietenholz and U. Wiese, *Perfect lattice actions for quarks and gluons*, *Nucl.Phys.* **B464** (1996) 319–352, [hep-lat/9510026].

[503] P. Hasenfratz *et al.*, *The construction of generalized Dirac operators on the lattice*, *Int. J. Mod. Phys.* **C12** (2001) 691–708, [hep-lat/0003013].

[504] P. Hasenfratz, S. Hauswirth, T. Jörg, F. Niedermayer and K. Holland, *Testing the fixed-point QCD action and the construction of chiral currents*, *Nucl. Phys.* **B643** (2002) 280–320, [hep-lat/0205010].

[505] C. Gattringer, *A new approach to Ginsparg-Wilson fermions*, *Phys. Rev.* **D63** (2001) 114501, [hep-lat/0003005].

[506] A. Hasenfratz, R. Hoffmann and S. Schaefer, *Hypercubic smeared links for dynamical fermions*, *JHEP* **05** (2007) 029, [hep-lat/0702028].

[507] C. Morningstar and M. J. Peardon, *Analytic smearing of SU(3) link variables in lattice QCD*, *Phys. Rev.* **D69** (2004) 054501, [hep-lat/0311018].

[508] [BMW 08A] S. Dürr *et al.*, *Scaling study of dynamical smeared-link clover fermions*, *Phys. Rev.* **D79** (2009) 014501, [arXiv:0802.2706].

[509] S. Capitani, S. Dürr and C. Hoelbling, *Rationale for UV-filtered clover fermions*, *JHEP* **11** (2006) 028, [hep-lat/0607006].

[510] N. Isgur and M. B. Wise, *Weak decays of heavy mesons in the static quark approximation*, *Phys.Lett.* **B232** (1989) 113.

[511] E. Eichten and B. R. Hill, *An effective field theory for the calculation of matrix elements involving heavy quarks*, *Phys.Lett.* **B234** (1990) 511.

[512] N. Isgur and M. B. Wise, *Weak transition form-factors between heavy mesons*, *Phys.Lett.* **B237** (1990) 527.

[513] W. E. Caswell and G. P. Lepage, *Effective Lagrangians for bound state problems in QED, QCD and other field fheories*, *Phys. Lett.* **B167** (1986) 437.

[514] G. T. Bodwin, E. Braaten and G. P. Lepage, *Rigorous QCD analysis of inclusive annihilation and production of heavy quarkonium*, *Phys.Rev.* **D51** (1995) 1125–1171, [hep-ph/9407339].

[515] [ALPHA 03] J. Heitger and R. Sommer, *Nonperturbative heavy quark effective theory*, *JHEP* **0402** (2004) 022, [hep-lat/0310035].

[516] B. Thacker and G. P. Lepage, *Heavy quark bound states in lattice QCD*, *Phys.Rev.* **D43** (1991) 196–208.

[517] G. P. Lepage, L. Magnea, C. Nakhleh, U. Magnea and K. Hornbostel, *Improved nonrelativistic QCD for heavy quark physics*, *Phys.Rev.* **D46** (1992) 4052–4067, [hep-lat/9205007].

[518] A. X. El-Khadra, A. S. Kronfeld and P. B. Mackenzie, *Massive fermions in lattice gauge theory*, *Phys.Rev.* **D55** (1997) 3933–3957, [hep-lat/9604004].

[519] N. H. Christ, M. Li and H.-W. Lin, *Relativistic heavy quark effective action*, *Phys.Rev.* **D76** (2007) 074505, [hep-lat/0608006].

[520] S. Aoki, Y. Kuramashi and S.-i. Tominaga, *Relativistic heavy quarks on the lattice*, *Prog.Theor.Phys.* **109** (2003) 383–413, [hep-lat/0107009].

[521] T. Ishikawa, Y. Aoki, J. M. Flynn, T. Izubuchi and O. Loktik, *One-loop operator matching in the static heavy and domain-wall light quark system with $O(a)$ improvement*, *JHEP* **1105** (2011) 040, [arXiv:1101.1072].

[522] B. Blossier, *Lattice renormalisation of $O(a)$ improved heavy-light operators: an addendum*, *Phys.Rev.* **D84** (2011) 097501, [arXiv:1106.2132].

[523] [ALPHA 10B] B. Blossier, M. Della Morte, N. Garron and R. Sommer, *HQET at order $1/m$: I. Non-perturbative parameters in the quenched approximation*, *JHEP* **1006** (2010) 002, [arXiv:1001.4783].

[524] R. Sommer, *Non-perturbative QCD: renormalization, $O(a)$-improvement and matching to heavy quark effective theory, Nara, Japan, 2005*, hep-lat/0611020.

[525] M. Della Morte, *Standard Model parameters and heavy quarks on the lattice*, *PoS* **LAT2007** (2007) 008, [arXiv:0711.3160].

[526] [ALPHA 12D] B. Blossier *et al.*, *Parameters of heavy quark effective theory from $N_f = 2$ lattice QCD*, *JHEP* **1209** (2012) 132, [arXiv:1203.6516].

[527] [ALPHA 05A] M. Della Morte, A. Shindler and R. Sommer, *On lattice actions for static quarks*, *JHEP* **0508** (2005) 051, [hep-lat/0506008].

[528] C. J. Morningstar, *Radiative corrections to the kinetic couplings in nonrelativistic lattice QCD*, *Phys.Rev.* **D50** (1994) 5902–5911, [hep-lat/9406002].

[529] T. Hammant, A. Hart, G. von Hippel, R. Horgan and C. Monahan, *Radiative improvement of the lattice NRQCD action using the background field method and application to the hyperfine splitting of quarkonium states*, *Phys.Rev.Lett.* **107** (2011) 112002, [arXiv:1105.5309].

[530] [HPQCD 12D] C. Monahan, J. Shigemitsu and R. Horgan, *Matching lattice and continuum axial-vector and vector currents with NRQCD and HISQ quarks*, *Phys.Rev.* **D87** (2013) 034017, [arXiv:1211.6966].

[531] [HPQCD 10D] J. Koponen *et al.*, *Heavy-light current-current correlators*, *PoS* **LAT2010** (2010) 231, [arXiv:1011.1208].

[532] J. Harada, S. Hashimoto, K.-I. Ishikawa, A. S. Kronfeld, T. Onogi *et al.*, *Application of heavy-quark effective theory to lattice QCD. 2. Radiative corrections to heavy-light currents*, *Phys.Rev.* **D65** (2002) 094513, [hep-lat/0112044].

[533] B. Sheikholeslami and R. Wohlert, *Improved continuum limit lattice action for QCD with Wilson fermions*, *Nucl. Phys.* **B259** (1985) 572.

[534] A. S. Kronfeld, *Application of heavy quark effective theory to lattice QCD. 1. Power corrections*, *Phys.Rev.* **D62** (2000) 014505, [hep-lat/0002008].

[535] J. Harada, S. Hashimoto, A. S. Kronfeld and T. Onogi, *Application of heavy-quark effective theory to lattice QCD. 3. Radiative corrections to heavy-heavy currents*, *Phys.Rev.* **D65** (2002) 094514, [hep-lat/0112045].

[536] A. X. El-Khadra, A. S. Kronfeld, P. B. Mackenzie, S. M. Ryan and J. N. Simone, *The semileptonic decays $B \to \pi \ell \nu$ and $D \to \pi \ell \nu$ from lattice QCD*, *Phys.Rev.* **D64** (2001) 014502, [hep-ph/0101023].

[537] C. Lehner, *Automated lattice perturbation theory and relativistic heavy quarks in the Columbia formulation*, *PoS* **LAT2012** (2012) 126, [arXiv:1211.4013].

[538] [CP-PACS/JLQCD 05] S. Aoki *et al.*, *Nonperturbative $O(a)$ improvement of the Wilson quark action with the RG-improved gauge action using the Schrödinger functional method*, *Phys.Rev.* **D73** (2006) 034501, [hep-lat/0508031].

[539] S. Aoki, Y. Kayaba and Y. Kuramashi, *A perturbative determination of mass dependent $O(a)$ improvement coefficients in a relativistic heavy quark action*, *Nucl.Phys.* **B697** (2004) 271–301, [hep-lat/0309161].

[540] [CP-PACS/JLQCD/ALPHA 07] T. Kaneko *et al.*, *Non-perturbative improvement of the axial current with three dynamical flavors and the Iwasaki gauge action*, *JHEP* **0704** (2007) 092, [hep-lat/0703006].

[541] S. Aoki, Y. Kayaba and Y. Kuramashi, *Perturbative determination of mass dependent O(a) improvement coefficients for the vector and axial vector currents with a relativistic heavy quark action*, *Nucl.Phys.* **B689** (2004) 127–156, [hep-lat/0401030].

[542] D. Guazzini, R. Sommer and N. Tantalo, *m_b and f_{B_s} from a combination of HQET and QCD*, *PoS* **LAT2006** (2006) 084, [hep-lat/0609065].

[543] [ETM 09E] B. Blossier *et al.*, *f_B and f_{B_s} with maximally twisted Wilson fermions*, *PoS* **LAT2009** (2009) 151, [arXiv:0911.3757].

[544] C. W. Bernard *et al.*, *The static quark potential in three flavor QCD*, *Phys. Rev.* **D62** (2000) 034503, [hep-lat/0002028].

[545] [RBC 10] R. Arthur and P. A. Boyle, *Step scaling with off-shell renormalisation*, *Phys.Rev.* **D83** (2011) 114511, [arXiv:1006.0422].

[546] A. X. El-Khadra, E. Gamiz, A. S. Kronfeld and M. A. Nobes, *Perturbative matching of heavy-light currents at one-loop*, *PoS* **LAT2007** (2007) 242, [arXiv:0710.1437].

[547] C. Aubin and C. Bernard, *Pseudoscalar decay constants in staggered chiral perturbation theory*, *Phys. Rev.* **D68** (2003) 074011, [hep-lat/0306026].

[548] S. R. Sharpe and R. L. Singleton, Jr, *Spontaneous flavor and parity breaking with Wilson fermions*, *Phys. Rev.* **D58** (1998) 074501, [hep-lat/9804028].

[549] S. R. Sharpe and J. M. S. Wu, *Twisted mass chiral perturbation theory at next-to-leading order*, *Phys. Rev.* **D71** (2005) 074501, [hep-lat/0411021].

[550] S. Aoki and O. Bär, *Twisted-mass QCD, O(a) improvement and Wilson chiral perturbation theory*, *Phys. Rev.* **D70** (2004) 116011, [hep-lat/0409006].

[551] C. W. Bernard and M. F. L. Golterman, *Partially quenched gauge theories and an application to staggered fermions*, *Phys. Rev.* **D49** (1994) 486–494, [hep-lat/9306005].

[552] M. F. L. Golterman and K.-C. Leung, *Applications of partially quenched chiral perturbation theory*, *Phys. Rev.* **D57** (1998) 5703–5710, [hep-lat/9711033].

[553] S. R. Sharpe, *Enhanced chiral logarithms in partially quenched QCD*, *Phys. Rev.* **D56** (1997) 7052–7058, [hep-lat/9707018]. Erratum: *Phys. Rev.* **D62** (2000) 099901.

[554] S. R. Sharpe and N. Shoresh, *Physical results from unphysical simulations*, *Phys. Rev.* **D62** (2000) 094503, [hep-lat/0006017].

[555] O. Bär, G. Rupak and N. Shoresh, *Simulations with different lattice Dirac operators for valence and sea quarks*, *Phys. Rev.* **D67** (2003) 114505, [hep-lat/0210050].

[556] M. Golterman, T. Izubuchi and Y. Shamir, *The role of the double pole in lattice QCD with mixed actions*, *Phys. Rev.* **D71** (2005) 114508, [hep-lat/0504013].

[557] J.-W. Chen, D. O'Connell and A. Walker-Loud, *Two meson systems with Ginsparg-Wilson valence quarks*, *Phys. Rev.* **D75** (2007) 054501, [hep-lat/0611003].

[558] J.-W. Chen, D. O'Connell and A. Walker-Loud, *Universality of mixed action extrapolation formulae*, *JHEP* **04** (2009) 090, [arXiv:0706.0035].

[559] J.-W. Chen, M. Golterman, D. O'Connell and A. Walker-Loud, *Mixed action effective field theory: an addendum*, *Phys. Rev.* **D79** (2009) 117502, [arXiv:0905.2566].

[560] [ETM 07A] Ph. Boucaud *et al.*, *Dynamical twisted mass fermions with light quarks*, *Phys.Lett.* **B650** (2007) 304–311, [hep-lat/0701012].

[561] [MILC 07] C. Bernard *et al.*, *Status of the MILC light pseudoscalar meson project*, *PoS* **LAT2007** (2007) 090, [arXiv:0710.1118].

[562] [RBC/UKQCD 11] C. Kelly, *Continuum results for light hadronic quantities using domain wall fermions with the Iwasaki and DSDR gauge actions*, *PoS* **LAT2011** (2011) 285, [arXiv:1201.0706].

[563] G. Colangelo, S. Dürr and C. Haefeli, *Finite volume effects for meson masses and decay constants*, *Nucl. Phys.* **B721** (2005) 136–174, [hep-lat/0503014].

[564] G. Herdoiza, *private communication* (2011).

[565] R. Brower, S. Chandrasekharan, J. W. Negele and U. Wiese, *QCD at fixed topology*, *Phys.Lett.* **B560** (2003) 64–74, [hep-lat/0302005].

[566] O. Bär, S. Necco and S. Schaefer, *The ϵ-regime with Wilson fermions*, *JHEP* **03** (2009) 006, [arXiv:0812.2403].

[567] S. Aoki, H. Fukaya, S. Hashimoto and T. Onogi, *Finite volume QCD at fixed topological charge*, *Phys. Rev.* **D76** (2007) 054508, [arXiv:0707.0396].

[568] T. Bunton, F.-J. Jiang and B. Tiburzi, *Extrapolations of lattice meson form factors*, *Phys.Rev.* **D74** (2006) 034514, [hep-lat/0607001].

[569] [HPQCD 03] M. Wingate, C. T. Davies, A. Gray, G. P. Lepage and J. Shigemitsu, *The B_s and D_s decay constants in three flavor lattice QCD*, *Phys.Rev.Lett.* **92** (2004) 162001, [hep-ph/0311130].

[570] [HPQCD 08B] E. Gamiz, J. Shigemitsu and H. Trottier, *Four fermion operator matching with NRQCD heavy and AsqTad light quarks*, *Phys.Rev.* **D77** (2008) 114505, [arXiv:0804.1557].

[571] [MILC 09B] A. Bazavov *et al.*, *Results from the MILC collaboration's SU(3) chiral perturbation theory analysis*, *PoS* **LAT2009** (2009) 079, [arXiv:0910.3618].